Coherent Emission Mechanisms in Radio Pulsars

Thesis by

Maxim Lyutikov

In Partial Fulfillment of the Requirements

for the Degree of

Doctor of Philosophy

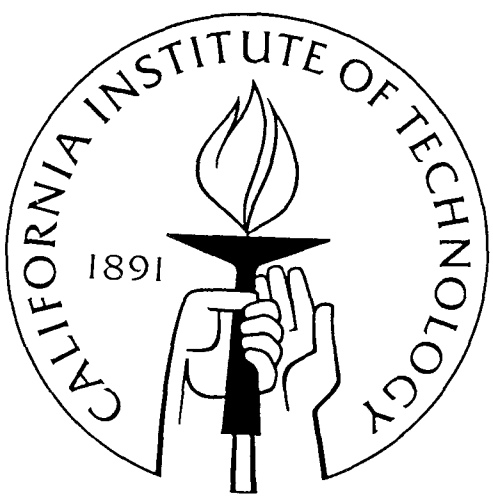

California Institute of Technology

Pasadena, California

1998

(Submitted March 11, 1998)

Abstract

In this work we investigate some possible mechanisms for pulsar radio emission. First we analyze the normal modes of a strongly magnetized electron-positron plasma taking into account a possible difference in the distribution functions of electrons and positrons. The dispersion relations, polarization properties and various regimes of beam instabilities in pair plasma are considered. We argue that kinetic instabilities of electromagnetic modes are more promising candidates for the pulsar radio emission mechanism than electrostatic instabilities (which occur in the hydrodynamic regime). We elucidate the microphysical processes underlying cyclotron-Cherenkov and Cherenkov-drift emission, stressing the importance of collective plasma effects involving all the particles of a medium. We show that cyclotron-Cherenkov emission at the anomalous Doppler effect can account for various observed phenomena of the "core" emission. Cherenkov-drift emission is a likely candidate for the "cone" emission.

We developed a new description that treats Cherenkov-drift emission in cylindrical coordinates. This approach describes consistently the resonant wave-particle interaction and provides a link between the Cherenkov, curvature and drift emission mechanisms recovering them as a limiting cases of the Cherenkov-drift emission process.

We also consider two possible nonlinear stages of the development of the cyclotron-Cherenkov instability: quasilinear diffusion and induced Raman scattering. We calculate the asymptotic particle distribution and emerging spectra for the cyclotron-Cherenkov instability and also show that induced Raman scattering may be important for the wave propagation and nonlinear saturation of electromagnetic instabilities. Finally, we considered the escape of waves from a pulsar magnetosphere taking into account cyclotron, Cherenkov and Cherenkov-drift absorption processes.

О сколько нам отрытий чудных
Готовит просвещенья дух,
И опыт - сын ошибок трудных,
И гений - парадоксов друг,
И случай - Бог изобретатель.

А.С. Пушкин

O how many miraculous discoveries
The spirit of enlightening prepares
And experience - a son of mistakes difficult,
And genius - a friend of paradoxes,
And chance - God inventor.

A.S. Pushkin

Как землю нам больше небес не любить?
Нам небесное счастье темно;
Хоть счастье земное и меньше в сто раз
Но мы знаем, какое оно.

Земля и небо, М.Ю. Лермонтов

Whoever needs Heaven when earth is so near?
Heaven's light is a promise at best;
Though the joys of our earth are deplorably few,
They are something that people can test.

Earth and Heaven, M.Yu. Lermontov

List of Frequently Used Symbols

Primes signs near the physical quantities denote pulsar frame, and primes near the functions denote derivative with respect to argument.

$A_\alpha^\pm$	(5.29)
$\mathbf{B}$,B	magnetic field
B_{PFF}	magnetic field at the pair formation front
c	speed of light
d	(5.70)
F	flux
F_ν	energy flux per unit frequency
$G(r, r_0, \lambda, \nu, k_x)$	eigenfunction expansion of scalar Green's function
$\mathcal{G}_E(\mathbf{r}, \mathbf{r}_0)$, $\mathcal{G}_B(\mathbf{r}, \mathbf{r}_0)$	electric and magnetic dyadic Green's functions
$\hbar$	Plank constant
I	moment of inertia of the neutron star
$I(\theta, \omega, n)$	(5.119)
j_b	current due to the primary beam
j_p	current due to each plasma component
K	(5.98)
$K(\omega, \mathbf{k})$	(5.41)
$\mathbf{k}$, k	wave vector
k_o	cross-over wave vector
L	luminosity
$\mathbf{L}, \mathbf{M}, \mathbf{N}$	cylindrical vector eigenfunctions
m_e	mass of an electron
n	refractive index
n_b	beam density
n_{GJ}	Goldreich-Julian density
n_p	plasma density
$n_\pm$	density of the fast/slow component
n_α	density of species α
$n(\mathbf{k})$, $n(k)$	photon distribution functions

P	period of neutron star rotation
$\dot{P}$	derivative of pulsar period
p_T	scatter in moments of the plasma particles
q	charge
R_L	light cylinder
R_B	radius of curvature
R_{NS}	neutron star radius
r_e	classical radius of electron
r_L	Larmor radius
$\mathbf{r}_0(t)$	unperturbed trajectory of a particle
T	(5.98)
T_p	temperature of plasma in units $m_e c^2$
u_d, u_α	drift velocity
v_b	velocity of the beam
v_p	plasma velocity in the pulsar frame
$v_\pm$	velocity of the fast and slow component
z	Eq. (6.24)
W, X, Y, Z	(5.49)
α	Eq. (9.11)
α^*	page 199
β	temperature parameter
β_o	velocity difference between fast and slow component
β_R	Eq. (9.10)
β_T	thermal velocity of plasma particles
Γ	growth rate
γ	Lorentz factor
γ_b	Lorentz factor of the primary beam
γ_p	average Lorentz factor of plasma
γ_T	scatter in Lorentz factors of the plasma particles
γ_t	Lorentz factor of the tail of the distribution function
γ_o	Lorentz factor of relative streaming
$\Delta\gamma$	scatter in Lorentz factors of the resonant particles
δ, $\delta^{(1)}$	difference of refractive index from unity
δ_{lm}	Kroneker symbol
ϵ	dielectric constant
ϵ_{lm}	dielectric tensor

η	(5.43), (5.76)
$\eta(\omega)$	spectral emissivity
λ	multiplicity factor
λ^*	critical multiplicity factor
μ	unit vector along the magnetic moment of the star
μ	resonance parameter (7.12)
ν	order of the Bessel functions, frequency of the wave
Ω	angular frequency of neutron star rotation
$\Omega_\alpha^\pm$	(5.29)
Ω_ϕ	angular frequency of particle rotation
ω_B	nonrelativistic positive cyclotron frequency
ω_b	plasma frequency of the beam
ω	angular frequency of the wave
ω_o	cross-over frequency
ω_p	plasma frequency
$\hat{\omega}$, $\hat{\hat{\omega}}$	definition after Eq. (7.31)
$\hat{\omega}_i$	definition after Eq. (9.60)
ρ	ratio of ion and electron masses
Ψ	electric potential
θ	angle of propagation with respect to magnetic field
θ_c	critical angle of propagation near the cross-over point
	Subscripts:
$_A$	Alfven wave
$_{SA}$	slow Alfven wave
$_O$	ordinary wave
$_{ft}$	fast transverse
$_{st}$	slow transverse

Contents

List of Figures

List of Tables

Chapter 1 Introduction

Открылась бездна звезд полна,
Звездам нет счета, бездне - дна.

М.В. Ломоносов

An abyss opened, full of stars,
Stars have no count, abyss - no bound.

M.V. Lomonosov

A thesis opened, full of equations,
Equations have no count, thesis - no bound.

R.B. Blandford

Pulsars rank among the most interesting objects in the Universe. Physicists from a variety of fields have been attracted by the extreme conditions which prevail in pulsars and their magnetospheres and which are characterized by (Michel 1991): (i)$\sim 10^8 - 10^{12}$ G surface magnetic field, (ii) nuclear density of the neutron stars themselves; (iii) superfluid and superconducting phases in the interior of the neutron star; (iv) relativistic electron-positron plasmas, and so on. Pulsars appear to be ideal laboratories for investigating physical extremes, unapproachable on Earth.

Not only are pulsars "laboratories" (Hewish et al. 1992), they have also turned out to be excellent sources used for many different types of astrophysical investigation. The modulated pulse arrival time from binary pulsars has been used to detect the effect of gravitational radiation and provide a 10^{-3} quantitative test of general relativity (Taylor 1994), an accomplishment which, like the original discovery of pulsars itself, garnered a Nobel prize. The single millisecond pulsars provide excellent clocks which challenge the best trapped ion clocks available and have been used to set impressive limits on the cosmic gravitation radiation energy density. Another pulsar produced the first detection of extrasolar planets (Wolszczan 1996). The high brightness radio emission is allowing unique wave propagation experiments that probe the properties of turbulent interstellar plasma (e.g., Armstrong, Rickett & Spangler 1995).

The last decade of pulsar research has been marked by exciting new discoveries (millisecond pulsars, pulsars in globular clusters and new binary pulsars), further developments in theoretical understanding of pulsar electrodynamics, properties of relativistic pair plasmas, interior structure of neutron stars and a rapid progress in observational techniques like coherent dedispersion and high temporal resolution monitoring.

An important part of these activities is the need to understand the actual radio emission mechanisms and here, it must be acknowledged there is no consensus as to its true nature (Melrose 1995). Indeed lack of understanding of the basic character of the emission process is a major limitation to the further development of "applied" pulsar physics.

At the present time, there are about a dozen competing theories of pulsar radio emission generation which differ both in the physical effects responsible for the radiation and in the locations where they operate (Melrose 1995). Probably the only point of agreement between all these theories is the association of pulsars with magnetized rotating neutron stars. By contrast, there is so much observational data available that none of the existing theories can explain all the *main* observational facts.

To date, the most widely discussed theory attributes the emission to coherent curvature emission by bunches of particles. Though this theory can explain a broad range of observed pulsar properties by the careful arrangement of the magnetic field geometry and of the form and size of bunches, thirty years of theoretical efforts have failed to explain the origin of these bunches (Melrose 1995). This theory also fails to explain some fundamental observational facts, namely the existence of two orthogonal polarizations in pulsar radio emission, the observed correlations across the pulse profile and a large coherent size of the emitting region (see Chapter 2).

In this work we discuss an alternative theory of pulsar radio emission developed by Machabeli & Usov 1989, Kazbegi et al. 1991b, Kazbegi et al. 1991c, Lyutikov 1997a, Lyutikov, Blandford & Machabeli 1997, Lyutikov & Machabeli 1997, Lyutikov, Machabeli & Blandford 1997a. The pulsar radiation is generated by the instabilities developing in the outflowing plasma on the open field lines in the outer regions of the pulsar magnetosphere. Radiation is generated by two kinds of *electromagnetic* plasma instabilities – cyclotron-Cherenkov and Cherenkov-drift instabilities. The cyclotron-Cherenkov instability is responsible for the generation of the core-type emission and the Cherenkov-drift instability is responsible for the generation of the cone-type emission (Rankin 1992). The waves generated by these instabilities are vacuum-like electromagnetic waves so that they can leave the magnetosphere directly.

Both instabilities occur in the outer parts of magnetosphere at radii comparable to the light cylinder radius. The location of the emission region is determined by the corresponding resonant condition for the cyclotron-Cherenkov and Cherenkov-drift instabilities. Instabilities develop in a limited region on the open field lines. The size of the emission region is determined by the curvature of the magnetic field lines, which limits the length of the resonant wave-particle interaction. The location of the cyclotron-Cherenkov instability is limited to the field lines with large curvature, while the Cherenkov-drift instability occurs on the field lines with the radius of curvature limited both from above and from below. Thus, both instabilities produce narrow pulses, though they operate at radii where the opening angle of the open field lines is large.

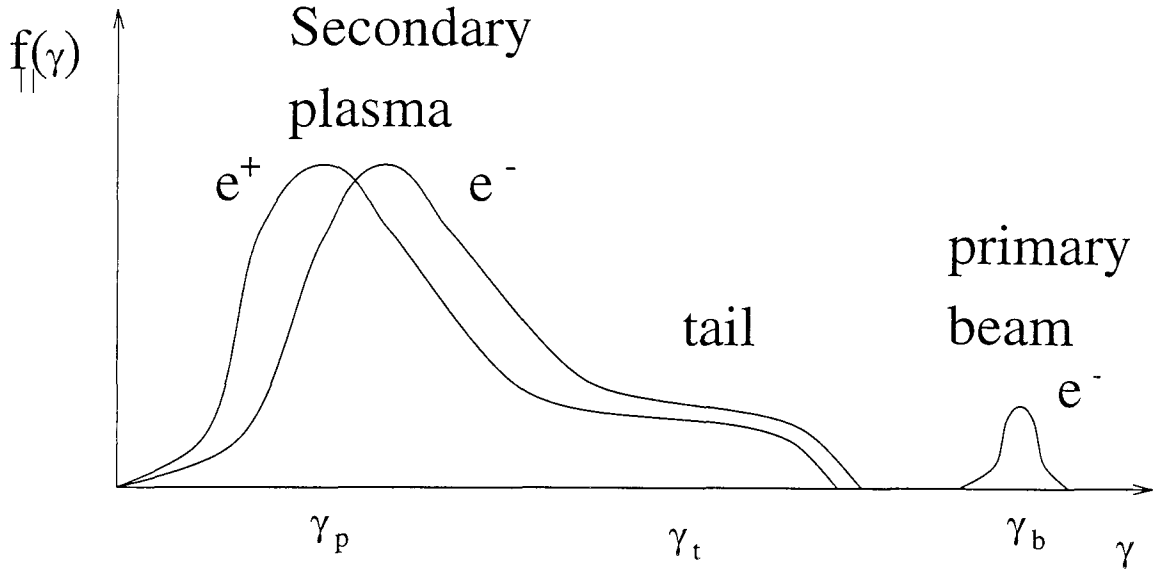

Figure 1.1: Distribution function for a one-dimensional electron-positron plasma of pulsar magnetosphere.

Apart from the association of pulsars with rotating, strongly magnetized neutron stars, the *only* other assumption required for the development of these instabilities is that a rotating neutron star generates a steady mildly relativistic, dense flow of electron-positron pairs penetrated by a highly relativistic electron beam. At this point we know only the general features of the distribution function of the particles in a pulsar magnetosphere (Tademaru 1973,Arons 1981b, Daugherty & Harding 1983, Chapter 4). It comprises (see Fig. 1.1) (i) a highly relativistic primary beam with the Lorentz factor $\gamma_b \approx 10^7$ and density of the order of Goldreich-Julian density $n_{GJ} = \Omega \cdot \mathbf{B}/(2\pi e c)$, (ii) a secondary electron positron plasma with a bulk streaming Lorentz factor $\gamma_p \approx 10 - 1000$, a similar scatter in energy $T_p \approx \gamma_p$ and a density much larger than the beam density $n_p \approx \lambda n_{GJ} = 10^3 - 10^6 n_{GJ}$, (iii) a tail of plasma distribution with the energy up to $\gamma_t = 10^4 - 10^5$.

The choice of a particular distribution function (Fig. 1.1) is very important. All the following is predicated on this choice. In particular, in our model the primary beam is composed of electrons or positrons. We show in Appendix K that both cyclotron-Cherenkov and Cherenkov-drift instabilities do not develop on ion beam.

The *electromagnetic* cyclotron-Cherenkov and Cherenkov-drift instabilities are the strongest instabilities in the pulsar magnetosphere (Lyutikov 1997c, Chapter 7). This differs from the more common case of a nonrelativistic plasma, where *electrostatic* Cherenkov-type instabilities (i.e., those that result in emission of electrostatic Langmuir-type waves) are generally stronger than electromagnetic instabilities. In addition, for a *one-dimensional plasma* streaming along the magnetic field, the effective parallel mass is considerably increased by relativistic effects. For the particles in the primary beam, which contribute to the development of the instability, the effective parallel

mass is $m_{eff\parallel} = \gamma_b^3 m \approx 10^{21}\, m$ (m is a mass of a particle). This suppresses the development of the electrostatic instabilities. In contrast, the effective transverse mass, $m_{eff\perp} = \gamma_b m$, is less affected by the large parallel momentum. Thus, the relativistic velocities and one-dimensionality of the distribution function result in a strong suppression of the electrostatic instabilities and strengthen the electromagnetic instabilities.

Cyclotron-Cherenkov generation of wave by fast particles is not new in astrophysics. For example, cosmic rays in the interstellar medium and in the supernova shock generate Alfvén waves by a similar mechanism. In the case of Alfvén waves in the nonrelativistic electron-ion plasma, the frequency of the waves ω can be much smaller than the kv term and can be neglected in the resonance condition. The important difference between these applications and cyclotron-Cherenkov instability in pulsar magnetosphere is that the generated waves belong not to the hydromagnetic Alfvẽn waves, that cannot leave plasma, but to the almost vacuum electromagnetic waves.

We should also mention that a cyclotron-Cherenkov instability of an electron beam propagating along a magnetic field is known in the laboratory as a very effective source of the high frequency microwave radio emission (Galuzo et al. 1982, Didenko et al. 1983, Nusinovich et al. 1995). The so called slow-wave electron cyclotron masers (ECM) provides a high efficiency and high power microwave source. Though there are no commercial slow-wave ECM available now, they are believed to be very promising devices due to their better control of the beam quality and potentially more compact design than the cyclotron autoresonance masers. Thus, pulsars can be regarded as cosmic slow-wave ECMs.

In this work we also develop a new look at the theory of amplification of curvature radiation. We argue that a new, Cherenkov-drift instability may be operational in the pulsar magnetosphere. The Cherenkov-drift emission combines the features of both Cherenkov and curvature emission processes. This instability is similar to the drift instabilities of the inhomogeneous plasma. The striking feature is that, unlike the nonrelativistic laboratory plasma, where drift instabilities develop on the low frequency waves with the wave length on the order of the inhomogeneity size, in the strong relativistic plasma drift instabilities can produce high frequency waves.

We develop an approach that treat Cherenkov and curvature emission consistently in cylindrical coordinates. The choice of cylindrical coordinates allows one to consider curvature emission as a resonant emission process. In the former approaches the wave-particles interaction length was very limited, that precluded a strong amplification under all circumstances. Another important difference in this work is the proper account of the dispersion and polarization of the normal modes. We show that Cherenkov-drift instability develops only in a medium which supports subluminous waves.

The outline of the thesis is the following. In Chapter 2, we review the observational properties of pulsar radio emission. In Chapter 3, we review the current theories of pulsar radio emission generation. In Chapter 4, we discuss the adopted parameters of the pulsar plasma. In Chapter 5,

we investigate in detail the properties of the normal modes in a strongly magnetized, hot electron-positron plasma taking into account the possible difference in distribution functions of electrons and positron. To calculate the dispersion relations of the normal modes in curved magnetic field, we discuss the properties of the dielectric response in cylindrical coordinates. In curvilinear coordinates the electric displacement is related to the electric field via the dielectric tensor operator, which is nonlocal in nature - it involves derivatives with respect to the radial coordinate. The operator relations between electric field and electric induction can be simplified to give algebraic relations in two different limits: (i) for the nonresonant particles, when we can use the WKB approximation for the wave-particle interaction, (ii) in a particular limit $z \gg 1$ (Section 6.2.1 and Appendix C for the definition of z) for the resonant interaction of subluminous waves with particles having velocity larger than the phase speed of the waves. Assuming that these two limits apply for nonresonant and resonant wave-particle interaction, we calculate the dielectric tensor in cylindrical coordinates taking into account the curvature drift of particles. From that dielectric tensor we find wave dispersions and polarizations for relativistic pair plasma with different distribution functions. In Chapter 6, we discuss the elementary emission process for the cyclotron-Cherenkov and Cherenkov-drift instabilities. Following the ideas of Schwinger et al. 1976, that cyclotron-Cherenkov emission is a synergetic process that combines the features of both cyclotron and Cherenkov emission processes, we suggest that, similarly, Cherenkov-drift emission is a synergetic emission process that combines the features of both curvature and Cherenkov emission processes. In Chapter 7 we discuss a theory of beam instabilities in a magnetized pair plasma. We distinguish two regimes of Cherenkov and cyclotron instabilities: hydrodynamic and kinetic. In a hydrodynamic regime all the particles resonate with a given wave which grows coherently. In a kinetic regime different particles resonate with different waves which grow incoherently. Kinetic and hydrodynamic instabilities can be thought of as two limiting regimes of a single instability. We give the simplified calculations of the various Cherenkov and cyclotron growth rates in both hydrodynamic and kinetic regimes. We argue that cyclotron-Cherenkov and Cherenkov-drift instabilities are the strongest instabilities in the pulsar magnetosphere. In Chapter 8 we outline the general features of our model of pulsar radio emission and show how various observational facts can be explained in the frame work of the cyclotron-Cherenkov and Cherenkov-drift instabilities. In Chapter 9 we first discuss nonlinear process that can saturate cyclotron-Cherenkov instability, namely quasilinear diffusion of the resonant particles and induced Raman scattering. We calculate the observed intensities that these two nonlinear processesproduce and argue that both these processes can be important in pulsar magnetosphere. Then we discuss the escape of the generated radiation from the pulsar magnetosphere. Finally, in Chapter 10 we present the conclusions of this work.

Chapter 2 Review of the Observational Data and Phenomenological Theory of Pulsar Radio Emission

2.1 Core and Cone Emission

In this section we will summarize the most important observational facts about pulsars. The available database on pulsar radio emission is enormous and the range of pulsar properties is equally large. Therefore, the observational properties will be presented in the framework of a phenomenological theory of pulsar radio emission (Rankin 1992). The main feature of this model is the division of emission into two main components called "core" and "cone" (there are two cones of emission in the most general case). In each pulsar, the averaged profile may be a combination of core and/or cone emissions (Fig. 2.1).

2.1.1 Properties of the Core Emission

The majority of pulsars (about 70%) show core-type emission. In combination with the cone-type emission, core pulsars are divided into three groups – core singles, triplets and five-components. The typical core emission has the following features: (a) the profile has a single component at 400 MHz but might develop conal (sometimes nonsymmetrical) outriders above 1400 MHz which can dominate at higher frequencies; in such pulsars the core component might arrive a little earlier than conal emission, (b) core emission has a steeper spectrum than conal emission, (c) moderate circular polarization (up to 60%); the sense of which may reverse in the middle of the pulse (Fig. 2.1), if the cone component is present, the sense of circular polarization in the core correlates with the swing of the position angle of the linear polarization in the cone, (d) linear polarization varies from nearly 100% to unpolarized, in most cases the radiation may be split into two orthogonally polarized modes (Stinebring et al. 1984), (e) the size of the beam seems to follow a simple relation, which is independent of radio frequency $W = 2.^o45/P^{1/2}$, where P is the period of the pulsar.

2.1.2 Properties of the Cone Emission

About 30% of all pulsars show pure conal emission and they are divided into two main groups – cone singles and cone doubles which are believed to be closely connected, the only difference being

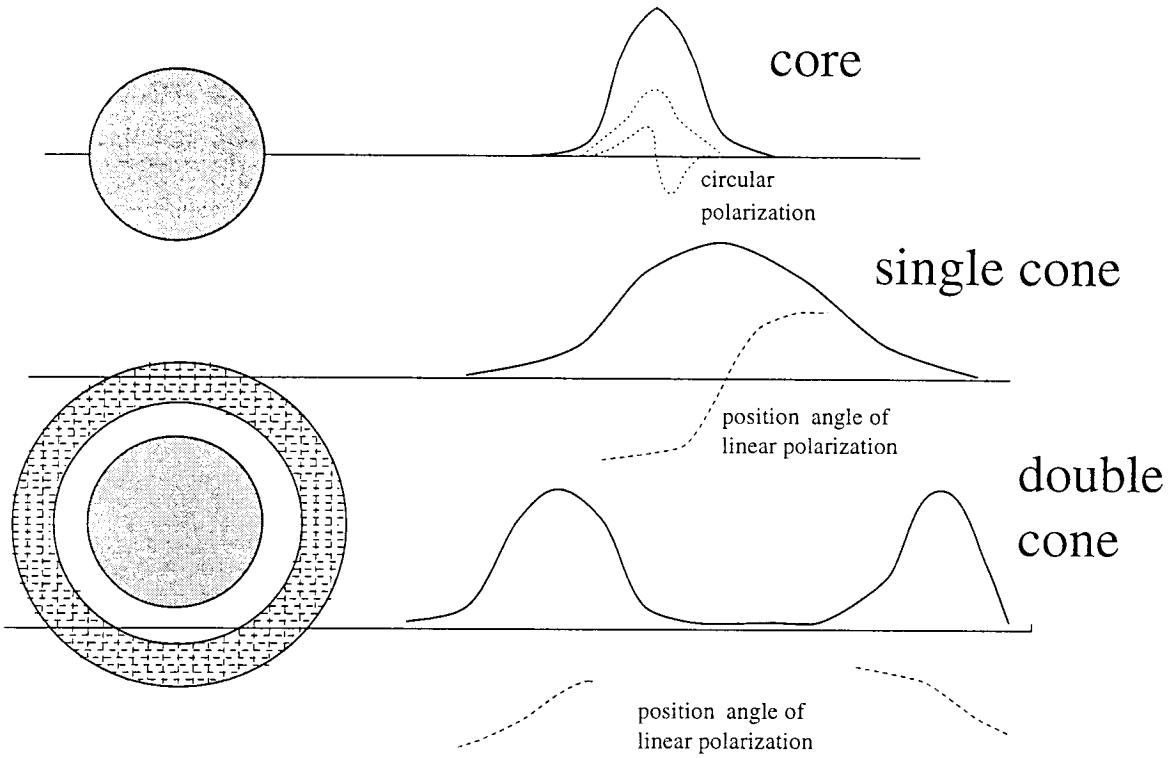

Figure 2.1: Example of emission geometry that produces core and cone profiles.

the geometrical path of the line of sight through the emission region. The typical features of conal emission are (e.g., Rankin 1992):

(a) the profiles can have up to four components, corresponding to two cones; at high frequencies the cone might merge forming a smooth emission pattern,

(b) the cone component has a harder spectrum than the core emission,

(c) circular polarization is small and unsystematic,

(d) linear polarization is moderate to virtually unpolarized; if the core emission is present, the swing of a position angle is strongly correlated with the sense of circular polarization in the core with a large (near 180^o) total swing, otherwise (in the absence of the core emission) the swing of position angle is less ($\sim 90^o$); similarly to the core emission, the radiation may be split into two orthogonally polarized modes (Stinebring et al. 1984) with changing intensities resulting in a sudden change of position angle by $\pm\pi/2$; the frequency dependence of linear polarization shows great variety – in most cases it is a constant or slightly decreasing function of frequency, but occasionally it has a maximum or increases with frequency, (e) the geometry of the beam corresponds to the cones with angles $4.^o3P^{-1/2}$ and $5.^o9P^{-1/2}$; in contrast to the core emission where the width is independent of frequency, for conal emission the width changes with frequency as $\nu^{-0.6}$, and seems to reach a plateau at high frequencies, (f) a few pulsars with conal profiles show drifting subpulses, some pulsars change between three different drift rates, (g) the nulling effect - sudden (on time scales less

than 2 microseconds (Deich et al. 1986) disappearance of pulses for an interval much longer than the pulsar's rotation period; in pulsars which exhibit both drifting subpulses and nulling, the drift path recovers from a null according to the length of the null (Lyne & Ashworth 1983), mean drift rate during the null decreases with the null length, (h) mode switching – a spontaneous change of the averaged pulse between two or several different profiles; mode switching conserves the number and position of the emission components but changes their relative strength, mode switching and nulling tend to take place in pulsars with low $\dot{P}$, (i) microstructure – noise like spikes of emission on the time scale of microseconds, microstructure is more prominent at low frequencies and occurs in pulsars with low $\dot{P}$.

2.2 Other Properties of Pulsar Radio Emission

An important feature of the conal emission is that the cone components show correlations of intensity, while the core component, if present, is not correlated with the cone (Kazbegi et al. 1991a). In a recent work Gwinn (Gwinn et al. 1997) have measured the coherent emission size of Vela pulsar using the refractive scintillations from the supernova remnant. Their result - 500 km - strongly suggests that the emission region is located in the outer parts of the magnetosphere. The thickness of emitting region is harder to determine since if the emitting particles move almost with the speed of light and emit in the direction of their motion, the time delay between two different emitted pulses would be Lorentz-contracted. So far no motion of emitters in the magnetosphere has been detected, the upper bound for the time delay is about 1 μs.

The radio spectra of pulsars are well represented by a power law (Lorimer et al. 1995) with mean value of spectral indices of -1.6 and varying from 0.5 to 3. Young pulsars have predominantly flatter spectra. Sometimes a break is observed with high frequencies having a steeper spectrum.

There have been many attempts to determine observationally the emission altitude. Unfortunately, most of the techniques for determining emission altitudes rely on the accepted emission model (e.g., Thorsett 1992), thus giving contradictory results. In most studies the results are interpreted in such a way that the emission is coming from low altitudes. Sometime too low: the results of Cordes et al. 1990 imply emission height of 3 km. The assumptions of dipolar geometry, radius to frequency mapping and an assumption of a particular emission mechanism are essential to many estimates. Contrary to these conclusions the results of Gwinn et al. 1997, analyses of Gil & Kijak 1993 and the interpretation of (Manchester 1996) of the "wide beam geometry" (highly-polarized, wide-spaced pulses observed in some pulsars) provides an example of the emission originated at a considerable fraction of light cylinder.

2.3 Temporal Structure of Pulses

Temporal variations in pulsar radio emission occur on three different time scales subject to scaling with the pulsar's period: 1-100 milliseconds for the main pulse, 0.1- 10 milliseconds for subpulses and 1-2000 microseconds for the micropulses (in any given pulsar micropulse time scale is shorter than subpulse time scale). The average pulse seems to be a superposition of different subpulses plus amorphous emission, but there is a distinct physical difference between micropulses and subpulses. Micropulses (see Fig. 2.2) have a broader emission band and frequency independent longitudes whereas subpulses appear at different longitudes at different frequencies. In addition, micropulses have a steeper spectrum than subpulses and the main pulse. They are much more pronounced at low frequencies and become undetectable at frequencies above ≈ 1 GHz. The polarization angle is fairly constant inside a micropulse (although it changes slightly at the edges) whereas it changes inside a subpulse.

This raises the question as to whether micropulses reflect the properties of the emission generation or propagation in the pulsar magnetosphere. In the former case, subpulses and micropulses may be due to the two independent emission mechanisms or they can reflect different spatial or temporal structures in the pulsar magnetosphere. One possibility is that small scale beams cause subpulses and temporal modulations cause micropulses (Cordes 1981). Alternatively, micropulses may be due to the self-focusing of radio emission as it propagates in pulsar magnetosphere.

If microstructure is inherent to the emission generation, then each microspike may not represent elementary emitters. They may be an incoherent superposition of coherent emitters (see Rickett 1975, Cordes 1981, Zhuravlev & Popov 1990). This conclusion follows from the observation that average autocorrelation function of micropulses is well represented by amplitude modulated white Gaussian noise. The characteristic variation time for the elementary coherent emitters is approximately the reciprocal of the typical bandwidth (1 GHz), i.e., $\tau = 1/\nu \approx 10^{-9}$ s. Thus, each micropulse of a temporal length $t \approx 10^{-6}$ s would contain a contribution from about 10^3 independent coherent emitters.

Another insight into the physical nature of microstructure involves the temporal auto-correlation function of micropulses which show quasi-periodicity with two different times scales: a short time scale of less than 0.5 milliseconds and long time scale of about 0.5-3 milliseconds (Soglasnov, Popov & Kuz'min 1983). The number of observed quasiperiods (5-10) implies that the structures that generate micropulses come in bunches or arrays and that the process that creates these arrays is a low Q process.

One of the fundamental questions concerning pulsar emission is whether it is broad- or narrow-band. Multifrequency observations of microstructure show that long duration microstructure (longer than 500 μs) preserves correlation both in broad- and narrow-band filters at frequencies up to 1GHz

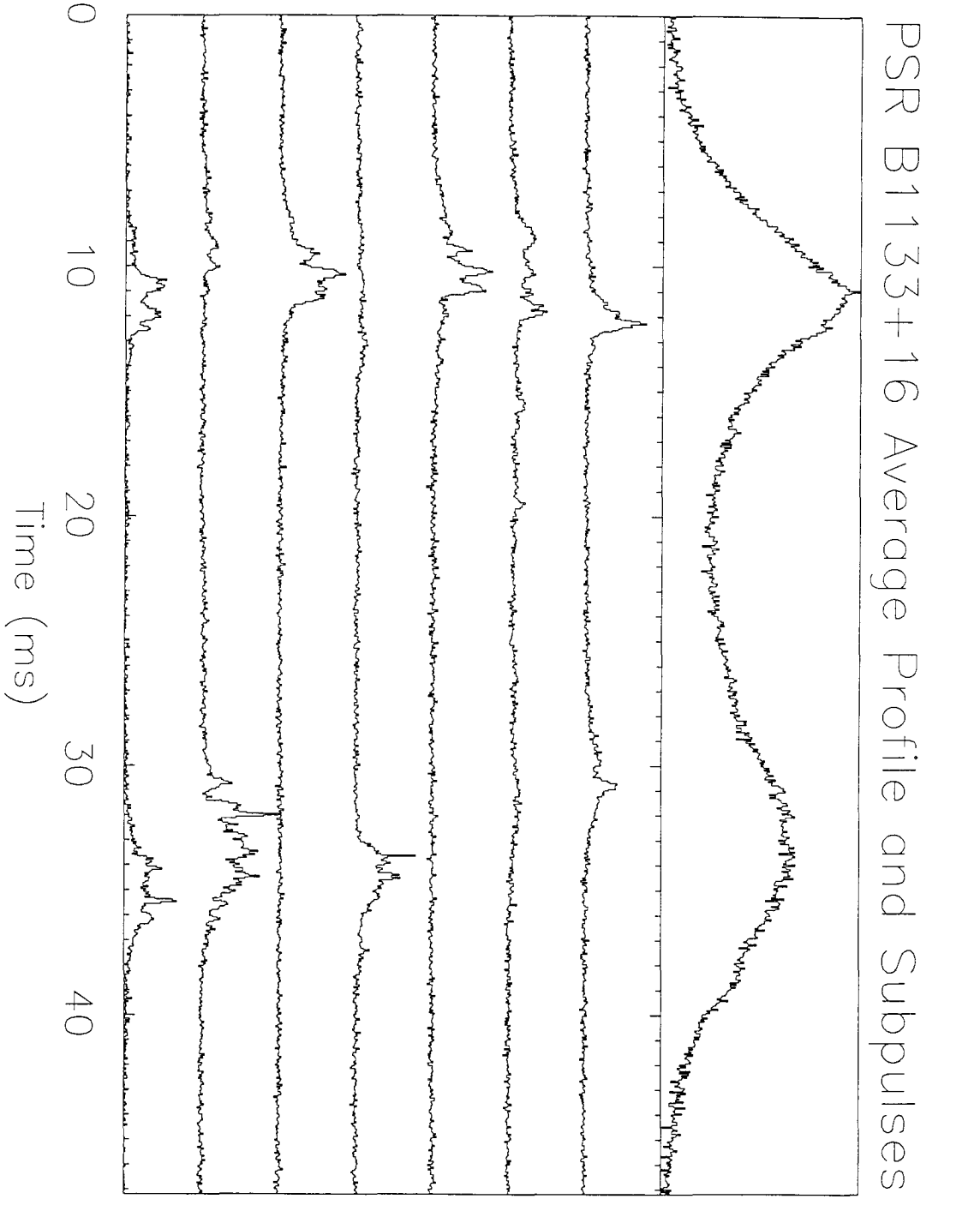

Figure 2.2: An example of microstructure. The first graph shows an average pulse (Jenet & Prince 1997).

apart. On the other hand, short scale microstructure (shorter than 500 μs) when observed in narrow band filters showed no correlation between frequencies 50 kHz apart (Gurvits et al. 1987). The statistical interpretation of long time scale microstructures in the framework of amplitude modulated noise theory (Rickett 1975) is a broad-band (white) noise modulated by some stochastic process. Physically, this could correspond either to the broad-band noise radiated in a thin layer or to the narrow-band noise with the emitting frequency scanning a wide range of frequencies in, for example, radius to frequency mapping. For short time scale noise, the characteristic time of fluctuations of the modulating function approaches the shot noise structure of micropulses and that gives the decorrelation in narrow bands. The existence of a spectral break at about 100 MHz might also be a reflection of two existing mechanisms (soft broad-band and hard narrow-band) with different spectral features.

Chapter 3 Review of the Theory

3.1 Introduction

In this Chapter we review the most promising theories of pulsar radio emission. A common feature of all of them is that they attribute emission to some kind of instability in relativistic plasma flowing along the open field lines in the magnetosphere of the rotating neutron star.

The most important constraints which a possible radiation mechanism should satisfy are: (a) it should be operational in a very broad range of pulsar periods – from 1.5 millisecond to more than 5 seconds, more than three orders of magnitude, (b) it should combine long time stability of the average pulse profile with small time scale variations, (c) it must explain high brightness of observed radio emission and its complicated polarization properties.

We assume that those theories based on the polar cap model deserve most attention. In these models the rotation of the neutron star generates a dense outflow of mildly relativistic electron-positron pairs penetrated by highly relativistic electron or positron beam along the open field lines (Fig. 3.1). Due to the very strong magnetic field near the neutron star, the spontaneous synchrotron decay times are very short and all the leptons quickly loose their transverse moments and stay in the lowest Landau level throughout the inner magnetosphere.

It is generally believed now that the pulsar radio emission is generated by some *collective plasma processes* in which the energy is put into the local plasma normal mode. A study of collective instabilities in plasma involves several stages. Initially it is necessary to identify the normal modes of the medium, their dispersion relations and their polarization. Next, one should investigate the stability of these modes due to both resonant or nonresonant interactions with plasma particles. Collective plasma instabilities due to the nonresonant interactions of the normal modes with the plasma particles are called hydrodynamic instabilities (e.g., firehose instability) and plasma instabilities due to the resonant interactions of the normal modes with the plasma particles are called kinetic instabilities. For the discussion of various regimes of plasma instabilities in the pulsar magnetosphere, see Chapter 7.2.

3.2 Single Stage and Two Stage Theories

The various plasma theories of the pulsar radio emission can be classified according to criteria whether or not the originally unstable waves have to be nonlinearly converted into radiation that can

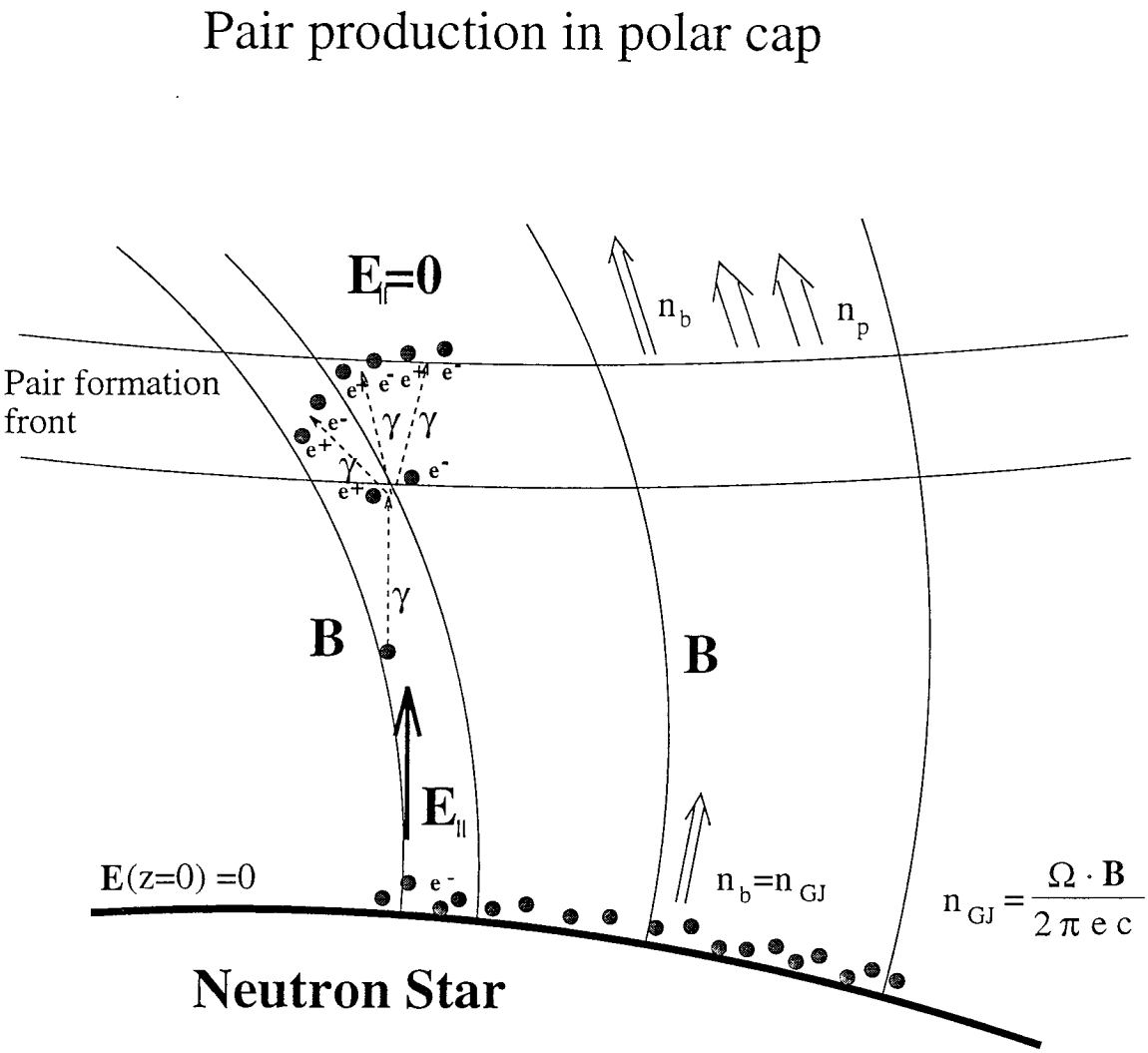

Figure 3.1: Pair production near the neutron star polar caps (after Arons 1983). In a thin inertial layer near the surface of the star (≈ 1 cm) a primary beam with a density $n_b = n_{GJ}$ is accelerated to relativistic velocities screening the parallel electric field. As the flow propagates outward, the density of the beam changes with radius with a different radial dependence than n_{GJ} due to the curvature of field lines or due to the Lense-Thirring precession. The resulting electric field accelerate the charges to energies $E \approx 10^{13}$ eV. The primary particles emit curvature photons, which in turn produces electron-positron pairs. The pairs are born at excited Landau levels. The secondary synchrotron photons produce more pairs in an avalanche-like process.

propagate directly in vacuum. The former approach includes two stages in generating the observed radio emission: in the first stage emission is generated on the waves that cannot leave magnetosphere and in the second stage they are converted into escaping modes (Ruderman & Sutherland 1975).

Conventionally, the two stage models are based on the development of the electrostatic instabilities (Ruderman & Sutherland 1975, Cheng & Ruderman 1977). In the two stage models the conversion may be linear or nonlinear in the amplitudes of the electrostatic waves. The nonlinear conversion is due to the interaction of the nonlinear waves, for example a decay of the electrostatic into two electromagnetic waves. The linear conversion is due to the propagation effects in the inhomogeneous curved magnetic field of pulsar magnetosphere. Asseo, Pellat & Rosado 1980 have argued that in the curved magnetic field it is possible to emit electromagnetic waves directly through the conventional Cherenkov two-stream instability. In fact, this can be considered as a propagation effect, when the original electrostatic wave is emitted along the magnetic field and acquires electromagnetic components as it propagates in the presence of a curved magnetic field. The fact that this is a linear conversion process occurring well in the adiabatic approximation (when the wave length is much smaller than the radius of the inhomogeneity, which is the local radius of curvature of the magnetic field lines), suggests that as the wave propagates in the plasma, it always stays on the same branch of the dispersion relation. As the wave moves along the particular branch of the dispersion relation, its polarization may change from longitudinal to transverse.

An important fact, omitted in many works that considered propagation of waves along the magnetic field, is that the electrostatic plasma waves propagating along magnetic field lines are the limiting cases of the two branches of ordinary and Alfvén waves that intersect only in the degenerate case of the parallel propagation (see Fig. 5.3). For oblique propagation the ordinary and Alfvén waves do not have intersection points. Thus, the linear evolution of the longitudinal plasma wave, emitted originally along the field line, will drastically depend on which branch (ordinary or Alfvén) the wave actually belongs to.

The propagation of ordinary and Alfvén waves in the inhomogeneous plasma of a pulsar magnetosphere differs considerably (Arons & Barnard 1986, Barnard & Arons 1986, Lyutikov & Machabeli 1997, Section 9.3). Alfvén waves cannot escape directly from plasma into vacuum, while ordinary waves may become superluminous and can escape from magnetosphere. Consequently, if the emitted quasilongitudinal plasma wave belongs to the Alfvén branch, it will not be able to escape from magnetosphere and will have to be nonlinearly converted into the escaping mode, even though it has a transverse electromagnetic component.

A very important problem with the two-stream instability model is the low growth rate on the resonance with the primary beam (Benford & Bushauer 1977) and the strong sensitivity to the plasma distribution function for the two stream instability due to the relative streaming of plasma components (Hinata 1976, Bushauer & Benford 1977). In Section 7.9 we shall show that two-stream

instability involving primary beam occurs in a hydrodynamic regime and is strongly suppressed by the large relativistic γ-factor of the beam.

The fact that Alfvén waves cannot leave magnetosphere is very important. This means that electromagnetic cyclotron-type instabilities involving Alfvén waves (Tsytovich & Kaplan 1972, Hardee & Rose 1978) should be classified as two stage process. The growth rates of the electromagnetic cyclotron type instabilities can be very large, but all the complications of the nonlinear wave conversion and Alfvén wave absorption in the outflowing plasma put the model based on the Alfvén wave excitation as disadvantage.

Another type of pulsar radio emission generation models is based on the instabilities on the waves that can leave magnetosphere directly (Kazbegi et al. 1991a, Kazbegi et al. 1991b, Zheleznyakov & Shaposhnikov 1979, Lyutikov, Blandford & Machabeli 1997). The advantages of this approach are obvious: the basic emission mechanism does not rely on the numerous complicated nonlinear wave processes. In this work we show that electromagnetic cyclotron-Cherenkov and Cherenkov-drift instabilities on the high frequency vacuum-like ordinary and extraordinary waves in the pulsar magnetosphere may constitute a possible source of the pulsar radio emission.

An important factor in the development of the electromagnetic instabilities is that, unlike the electrostatic Cherenkov instabilities, in the pulsar magnetosphere they occur in the kinetic regime and are not subject to the relativistic suppression by the large parallel momentum of the resonant particles.

3.3 Review of the Theories

3.3.1 Coherent Emission by Bunches

Chronologically, the oldest surviving theory of radio emission is the "bunching theory." In this theory the emitting particles somehow form bunches and all the particles in a bunch emit coherent curvature radiation.

There has been a long discussion of a possible force that can result in the formation of bunches. Ruderman & Sutherland 1975 and Cheng & Ruderman 1977 have proposed that two stream instability due to the excitation of Langmiur waves by the primary beam or by the relative velocity of the secondary components. Development of the two-stream instability may lead to the formation of Langmuir solitons with charge separation (Pataraya & Melikidze 1980) that play a role of bunches. Alternatively, Goldreich & Keeley 1971 proposed a radiative instability of a monoenergetic beam in a curved magnetic field as a possible mechanism for the formation of bunches. Development of the two-stream instability can reach nonlinear phase forming a lattice of Langmuir solitons (Pataraya & Melikidze 1980) which emit radiation by three possible mechanisms: direct radiation when perturbed by curved magnetic field in transverse direction, curvature radiation due to the movement

along dipole magnetic field and by scattering the particles of the primary beam which in the case of inhomogeneous beam may produce coherent radiation (Asseo, Pelletier & Sol 1990).

Unfortunately, the theories of bunch formations has faced some fundamental problems in creating and maintaining the bunches (Melrose 1995). The main factors that destroy bunching are velocity dispersion and radiation reaction of the coherent emission which tend to disperse bunches on a short time scales. These two effects work in tandem in a sense that even if the original velocity dispersion were small, the growth of the instability would increase it and suppress the instability itself. Another disrupting effect is the curvature of magnetic field lines which misaligns a coherence axis of pancake-like bunches with the direction of the magnetic field.

Though the phenomenological theory of coherent emission by bunches could explain a broad range of observed pulsar properties by the careful arrangement of the magnetic field geometry and of the form and size of bunches, it failed to explain the observed correlations across the pulse profile (Kazbegi et al. 1991a, Gwinn et al. 1997) and existence of the two orthogonal polarizations. The spectra in the bunching theory is due exclusively to the geometrical properties of the emitting region which fails to explain a great variety of observed spectra (Mamradze, Machabeli & Melikidze 1980).

The two-stream instability model has been criticized by (Bushauer & Benford 1977, Hinata 1976). Two stream instability on the primary beam has a very low growth rate due to the high rigidity of the beam ($\gamma_b \approx 10^7$), while the two stream instability due to the relative velocity of the secondary plasma is easily suppressed by the relatively low thermal scatter of plasma particles (Hinata 1976, see though Weatherall 1994). In both cases the instability growth rate is constant in a very small angle which limits the growth length in the curved magnetic field (Lyutikov 1997c). An additional complication in these theories comes from the fact that in the lower regions of the pulsar magnetosphere, where these mechanisms are supposed to operate, the Cherenkov streaming instabilities occur on the Alfvén branch which cannot leave magnetosphere. The waves have to be nonlinearly converted into escaping modes.

3.3.2 Shear Instabilities

In a series of papers (Asseo, Pellat & Rosado 1980, Asseo, Pellat & Sol, Asseo, Pelletier & Sol 1990, Asseo 1995) it has been shown that the radiative Goldreich-Keeley and two-stream instabilities may be treated as two limiting cases of a general instability of an inhomogeneous (finite transverse size) beam propagating in curved magnetic field lines and bounded by the stationary plasma. The radiative Goldreich-Keeley is then obtained as a limiting case of a very thin beam and the two-stream instabilities may be obtained in the case of a very large transverse size of a beam. In the infinite plasma in constant curved magnetic field, the Goldreich-Keeley instability of a monoenergetic beam does not develop. If there is a considerable shear in the flow, then the generalized Goldreich-Keeley radiative instability can develop. It is argued (Asseo, Pelletier & Sol 1990) that the instability can

evolve into the nonlinear regime resulting in a soliton formation.

The initial conditions for the development of the shear instabilities, i.e., the presence of the large shear and small spread in particle moments, are the weakest points of this theory. It is expected that the flow of the secondary plasma above the pair formation front is relatively homogeneous, has a considerable spread in the moments of the particles and occurs in a region with large transverse dimensions.

3.3.3 Growth of a Curvature Wave

In the theory by Beskin et.al (Beskin, Gurevich & Istomin 1983, Beskin, Gurevich & Istomin 1986 Beskin, Gurevich & Istomin 1993) it is argued that an Alfvén-type curvature mode can become unstable in the infinitely strong curved magnetic field. In their theory an Alfvén wave splits into three waves in the curved magnetic field, one of which becomes unstable. The observed radiation results from nonlinear conversion of this wave.

In spite of some success of the theory, it is very fundamental ideas have been seriously criticized (Machabeli 1995, Nambu 1989, Larroche & Pellat 1988). The dispersion relations of the curvature-Alfvén waves are intrinsically non-local and cannot be derived by conventional perturbative methods. One of the main objections is that the unstable wave grows coherently even in the case of infinite magnetic field which contradicts the mentioned proof of the impossibility of a maser action in this limit (Blandford 1975, Melrose 1978a).

3.3.4 Curvature Maser

Until recently, the works that considered a possibility of a curvature maser, i.e., the amplification of the curvature radiation due to the interaction with particles (Blandford 1975, Melrose 1978a, Zheleznyakov & Shaposhnikov 1979, Chugunov & Shaposhnikov 1981, Luo & Melrose 1992a) were treating the curvature emission process as an analog of the synchrotron radiation in vacuum. It has been shown that the coherent curvature emission is impossible (Blandford 1975, Melrose 1978a) in this limit in the case of infinitely strong curved magnetic field. This proof, though, allows for a loophole if the magnetic field is finite. Then, the particles streaming along the curved magnetic field lines experience a curvature drift perpendicular to the plane of the curved field line allowing for the possibility of the wave excitation (Zheleznyakov & Shaposhnikov 1979, Chugunov & Shaposhnikov 1981, Luo & Melrose 1992a). Drift velocities for the bulk plasma are negligible and only the particles from the primary beam or from the tail of the distribution could undergo masing action. Curvature maser, in a way considered by (Zheleznyakov & Shaposhnikov 1979, Chugunov & Shaposhnikov 1981, Luo & Melrose 1992a, Lyutikov, Machabeli & Blandford 1997a) is a plausible mechanism of the pulsar radio emission generation. It will be considered in more details in Section 6.2. The most

important difference in our approach is that we take correctly into account the influence of the medium on the resonant wave-particle interaction. What one finds, then, is that the modes emitted by the charged particle streaming along the curved magnetic field *in plasma* are substantially different from the vacuum modes, so that the emission process resemble more the collective Cherenkov-type emission than the single particle cyclotron emission.

We believe that the Cherenkov-drift instability may produce the observed radio waves. It may be responsible for the "cone" emission (Chapter 8). We will discuss the physics of the cyclotron-Cherenkov instability in more details in Chapter 6 and show in Appendix H that the conditions for the development of the cyclotron-Cherenkov instability are satisfied in the magnetosphere of a typical pulsar.

3.3.5 Cyclotron-Cherenkov Instability

Near the light cylinder the magnetic field strength falls considerably which allows for synchrotron excitation of transverse motion of particle. At a distance 10^9 cm from the neutron star, an anomalous Doppler resonance could be fulfilled for the particles of the primary beam and for the fast particles in the tail of the plasma distribution. The emitting particle undergoes a transition to the higher Landau level and emits a cyclotron photon; the free energy is supplied by the parallel motion. The wave becomes kinetically unstable and has features which could explain a broad variety of spectral and polarization characteristics of observed core type emission. We believe that cyclotron-Cherenkov instability is a possible mechanism of pulsar radio emission and may be responsible for the "core" emission (Chapter 8). We will discuss the physics of the cyclotron-Cherenkov instability in more details in Chapter 6 and show in Appendix F that the conditions for the development of the cyclotron-Cherenkov instability are satisfied in the magnetosphere of a typical pulsar.

Chapter 4 Parameters of the Pulsar Magnetospheric Plasma

The primary purpose of this Chapter is to define the fiducial parameters for the pulsar magnetospheric plasma. Unfortunately, the current poor understanding of the general magnetospheric structure and the complicated physics of the pair production process still allows a very broad range of plasma parameters. Undoubtedly, the plasma parameters change from pulsar to pulsar and also experience strong temporal variations in a given pulsar. As a first step in approaching the problem we will assume the plasma parameters are stationary, thus neglecting a broad variety of transient and secular events in pulsar phenomenology. The numerical estimates will be done for a "typical" pulsar (see Section 4.1.1).

4.1 Structure of Pulsar Magnetosphere

Rotating, strongly magnetized neutron stars induce strong electric fields that pull the charges from their surfaces. Inside the closed field lines of the neutron star magnetosphere, a steady charge distribution established, compensating the induced electric field. On the open field lines, the neutron star generates a dense flow of relativistic electron-positron pairs penetrated by a highly relativistic electron or positron beam (Fig. 4.1). The density of the primary beam is roughly equal to the Goldreich-Julian density $n_{GJ} = \Omega \cdot \mathbf{B}/(2\,\pi\,q\,c)$. We will normalize the density of the pair plasma to the Goldreich-Julian density.

$$n_\alpha = \lambda\, n_{GJ} = 10^3 - 10^6 n_{GJ}, \qquad \omega_p^2 = \lambda\omega_b^2 = 2\lambda\omega_B\Omega \tag{4.1}$$

where λ is the multiplicity factor which is the number of pairs produced by each primary particle (subscript α in Eq. (4.1) refers to the electrons and positrons of the bulk plasma). Secondary pairs are born with almost the same energy in the avalanche-like process above in the polar cap (Arons 1983). The pair creation front in the polar cap region is expected to be very thin so we can in the first approximation neglect the residual electric field in the front that could lead to the reversed current and different initial energies and densities of secondary particles.

The combination of the pair plasma and primary beam is expected to screen the rotationally induced electric field so that the flow is force-free. This can be seen from the following reasoning. The Poisson equation in the frame rotating with the neutron star reads

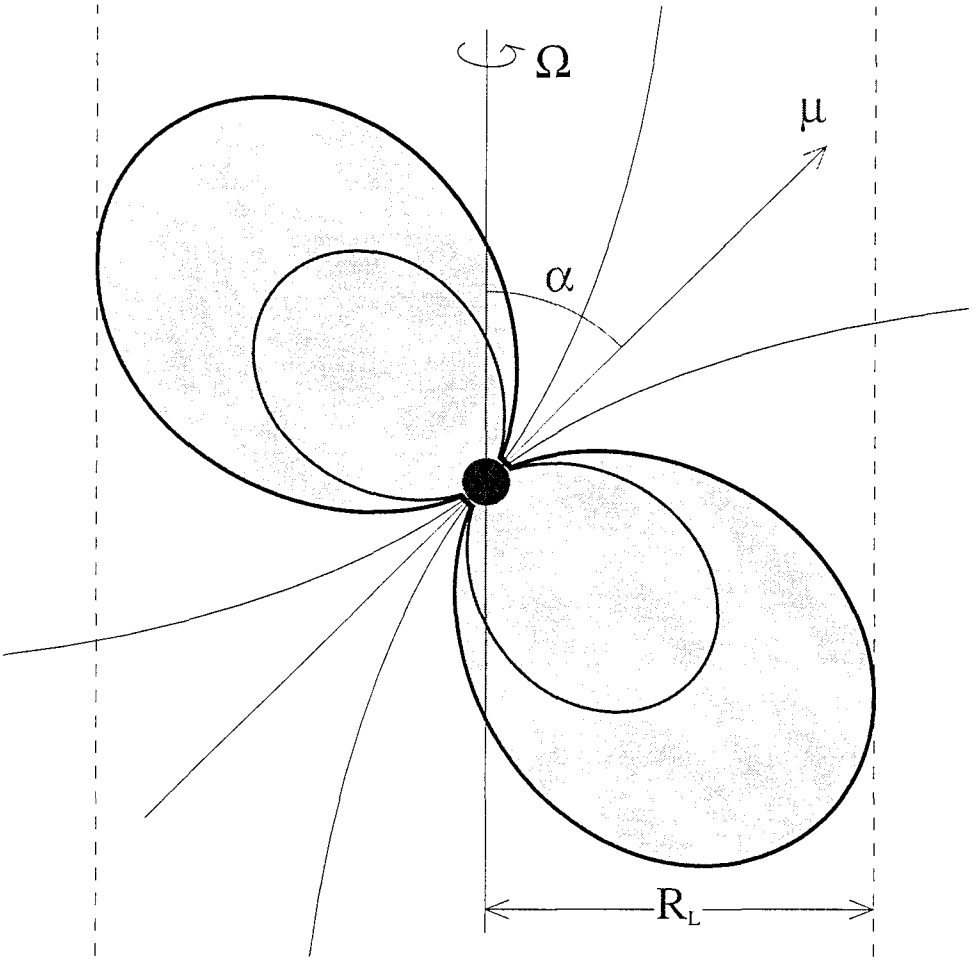

Figure 4.1: Pulsar magnetosphere. $\mathbf{\Omega}$ is the rotation frequency, μ is a unit vector along the direction of the magnetic moment, α is the angle between $\mathbf{\Omega}$ and μ, R_L is the light cylinder radius.

$$\frac{\partial^2 \Psi}{\partial \mathbf{r}^2} = -4\,\pi\, q(n_+ - n_- - n_b + n_{GJ}) \tag{4.2}$$

Here $n_\pm$ are the densities of secondary plasma particles, n_b is the beam density and Ψ is electric potential. This equation and the current conservation for all three components,

$$\frac{q\, n_\pm\, v_\pm}{B} = \pm \frac{j_p}{B_{PFF}}, \qquad\qquad \frac{q\, n_b\, v_b}{B} = \frac{j_b}{B_{PFF}} \tag{4.3}$$

determine the charge densities and currents throughout the pulsar magnetosphere. In (4.3) the current density components, j_p and j_b, are constants determined by the general magnetospheric conditions and B_{PPF} is the magnetic field at the pair formation front.

If the beam density at the pair formation front is equal to the local Goldreich-Julian density, then, from (4.2) and (4.3), it follows that the densities and energies of both components of the secondary plasma are equal. As the flows propagate along the dipolar magnetic field, the primary beam can no longer screen the rotationally induced electric field since, for the relativistic flow along the open magnetic field lines, $n_b \propto B$ and $n_{GJ} \propto B\cos\theta$, where θ is the angle between the local magnetic field and the rotation axis.

Since we have an ample supply of particles, the electric field that could result from this deviation of the beam density from the Goldreich-Julian density will be screened by accelerating one kind of the secondary particles and decelerating the other so that in every point the relation

$$j_p \left(\frac{1}{v_+} - \frac{1}{v_-}\right) - \frac{j_b}{v_b} + q\, n_{GJ}\, \frac{B_{PFF}}{B} = 0 \tag{4.4}$$

holds.

Another relation between the parameters of the plasma and the beam comes from the energy argument that the primary particles stop producing the pairs when the energy in the pair plasma becomes equal to the energy in the primary beam:

$$2 < \gamma >_\pm^{(0)} \lambda \approx \gamma_b, \qquad\qquad \text{at the pair formation front} \tag{4.5}$$

where it was assumed that the initial densities, temperatures and velocities of the plasma components are equal. For cold components $< \gamma >_\pm^{(0)} = \gamma_p$ while for the relativistic components with a temperature T_p, the average energy is $< \gamma >_\pm^{(0)} = 2\,\gamma_p\, T_p$. The assumption of equipartition (4.5) is a very approximate one, but it allows considerable simplification of numerical estimates. If, for some reason, this would turn out to be an incorrect assumption, the corresponding formula can be adjusted by changing the scaling.

As an estimate of the densities of the particles from the tail of plasma distribution, we will use

the assumption that the energy in the tail is approximately equal to the energy in the plasma (and in the beam):

$$\gamma_t n_t \approx \gamma_b^{(0)} n_b \tag{4.6}$$

where γ_t and n_t are the typical energy and the density of the tail particles.

Solutions of (4.4), (4.5) and $n_+ = n_-$ with given values for j_p, j_b and n_{GJ} at the pair formation front determine average energies of each component in every point in the magnetosphere. There are two qualitatively different possibilities: (a) the relative streaming in the center-of-momentum frame is nonrelativistic, (b) the relative streaming in the center-of-momentum frame is relativistic. In the case of nonrelativistic relative streaming, both components contribute approximately equally to the dielectric tensor in the pulsar frame, while in the case of relativistic relative streaming, the contribution of the slower component may dominate due to the relativistic effects.

For the nonrelativistic relative streaming of the hot components, the maximum relative velocity β_o (in units of c) measured in the plasma frame may be estimated from (4.4) and (4.5)

$$\beta_o = \frac{\gamma_p^2}{2\lambda} = \frac{\gamma_b^2}{32\,\lambda^3\,(1+2T_p)^2} \tag{4.7}$$

while for the relativistic relative streaming, the γ-factor of the hot plasma components in the center-of-momentum frame are

$$\gamma_o \approx \frac{\gamma_p}{\sqrt{2\,\lambda}} = \frac{\gamma_b}{2^{5/2}\,\lambda^{3/2}\,(1+2T_p)} \tag{4.8}$$

The critical value for the parameter λ at which the relative velocity of the particles become relativistic may be estimated as $\lambda^* = (\gamma_b/T_p)^{2/3}$. For the larger λ the relative velocity of the plasma components is nonrelativistic; for smaller values it is relativistic. For the characteristic beam energy $\gamma_b \approx 10^7$ this gives $\lambda^* \approx 10^4$. With the present uncertainty in the multiplicity factor $\lambda \approx 10^3 - 10^6$ and the temperatures of the plasma $T_p \approx 0.1 - 10$, the actual relative flow may be either nonrelativistic or strongly relativistic.

4.1.1 Typical Pulsar

In this work we will make numerical estimates for the "typical" pulsar with the following parameters:

(i) Magnetic field is assumed to be dipole with the magnetic field strength at the surface of neutron star $B_{NS} = 10^{12} G$.

(ii) Rotational period of the star $P = 0.5$ s (light cylinder radius $R_{LS} = 2.4 \times 10^9$ cm).

(iii) Average streaming energy of the plasma components $\gamma_p = 10$.

(iv) Temperature of the plasma components $T_p = 10$.

(v) Initial energy of the primary beam at the pair formation front $\gamma_b = 6 \times 10^7$.

The energy of the beam will decrease due to the curvature radiation reaction force (Section

J). Then at the light cylinder, where the instabilities occur, the beam will decelerate due to the curvature radiation reaction to $\gamma_b = 2 \times 10^6$.

For a given period and magnetic field Eq. (4.5) reduces the number of free parameters for the plasma to two: the plasma temperature and the bulk streaming energy γ_p (or temperature and the multiplicity factor λ). We chose a strongly relativistic plasma with the invariant temperature $T_p = 10$. The multiplicity factor λ corresponding to these parameters follows from Eq. (4.5): $\lambda = 3 \times 10^5$. The average energy of the tail particles is assumed to be $\gamma_t = 10^5$. An important factor that determines the growth rate of the instabilities is the energy scatter of the resonant particles. In estimating the growth rates of the cyclotron-Cherenkov and Cherenkov-drift instabilities on the primary beam, we will also assume that the scatter in Lorentz factors of the primary particles in the pulsar frame $\Delta\gamma = 10^2$. This assumes that the beam has cooled considerably due to the curvature radiation and lost about 10 percent of its energy.

Two points are important in our choice of parameters. First, we use a relatively low plasma streaming γ-factor (and respectively high multiplicity factor λ). In the polar cap models (Arons 1981, Arons 1983), the pulsar plasma will have a low streaming γ-factor if the magnetic field near the surface differs considerably from the dipole field thus reducing the radius of curvature (Machabeli & Usov 1989). Secondly, the required scatter in energy of the primary beam particles ($\Delta\gamma = 10^2$) is very small. This is due to the effects of curvature radiation reaction on the primary beam during its propagation through the dipole pulsar magnetosphere. The highly nonlinear damping rate due to the emission of curvature radiation by the primary beam result in an effective cooling of the beam (see Appendix J).

We will use two types of the particle distribution function to calculate the relevant moments: water bag and relativistic Maxwellian (see Section 5.6). For the case of relativistic Maxwellian distribution function, the strongly relativistic temperature $T_p = 10$ implies that, formally, there are many backward streaming particles. We note, though, that the backward streaming particles do not contribute significantly to any of the relevant moments of the distribution function, so that we can regard the strongly relativistic streaming Maxwellian distribution as a fair approximation to the relatively unknown, but definitely very hot, real distribution function.

The location of our typical pulsar on the $P - \dot{E}$ diagram is shown on Fig. 4.2.

The corresponding plasma densities and frequencies are given in Tables 4.1 and 4.2 for the two locations (near the stellar surface and at the emission region $R \approx 10^9$ cm in the pulsar and plasma reference frames).

The radius dependence of the parameters is assumed to follow the dipole geometry of the magnetic field:

$$\omega_B(r) = \omega_B(R_{NS}) \left(\frac{R_{NS}}{r} \right)^3 ,$$

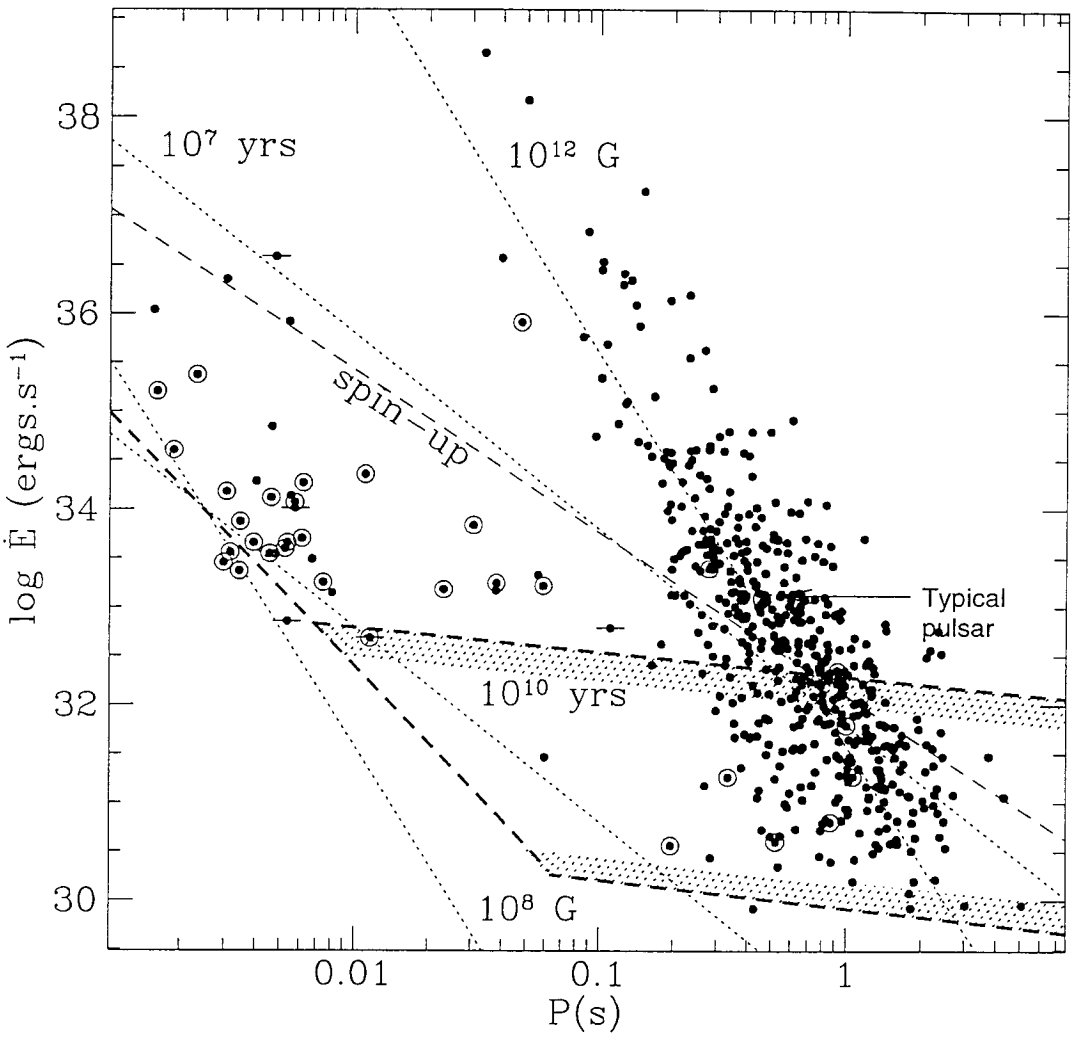

Figure 4.2: The dotted lines show constant spin down ages and magnetic fields. There is also a dashed line for the equilibrium period spin-up line. The heavy dashed curves and shading illustrate several death lines from the literature (see Hansen 1997 for references). The circles indicate binary pulsars and those points with horizontal lines through them are in globular clusters with apparently negative $\dot{E}$ (they are contaminated by cluster accelerations).

	Pulsar frame	Plasma frame
Magnetic field, G	10^{12}	10^{12}
Cyclotron frequency $\omega_B{}^{\star}$, $(rad\,s^{-1})$,	1.8×10^{19}	1.8×10^{19}
Beam density, cm^{-3}	$n'_{GJ} = \Omega B/(2\,\pi\,e\,c) = 1.4 \times 10^{11}$	$n_{GJ} = \Omega B/(2\,\pi\,e\,c\gamma_p) = 1.4 \times 10^{10}$
Beam plasma frequency, $rad\,s^{-1}$	$\omega'_{GJ} = \sqrt{\frac{4\,\pi\,q^2\,n^2_{GJ}}{m}} = \sqrt{2\Omega\omega_B} = 2 \times 10^{10}$	$\omega_{GJ} = \frac{\omega'_{GJ}}{\sqrt{\gamma_p}} = \sqrt{\frac{2\Omega\omega_B}{\gamma_p}} = 6.3 \times 10^9$
Beam energy	$\gamma'_b = 6 \times 10^7$	$\gamma_b = \frac{\gamma'_b}{2\gamma_p} = 3 \times 10^6$
Plasma density, cm^{-3}	$n'_p = \frac{\lambda\,\Omega\,B}{2\,\pi\,e\,c} = 4 \times 10^{16}$	$n_p, = \frac{\lambda\,\Omega B}{2\,\pi\,e\,c\gamma_p} = 4 \times 10^{15}$
Plasma frequency, $rad\,s^{-1}$	$\omega'_p = \sqrt{2\,\omega_B\,\Omega\,\lambda} = 1.2 \times 10^{13}$	$\omega_p = \sqrt{\frac{2\,\omega_B\,\Omega\,\lambda}{\gamma_p}} = 4 \times 10^{12}$
$1 - \beta_X$, β_X- phase speed of X mode	$\delta' = \frac{\omega'^2_p T_p}{4\gamma_p^3\omega_B^2} = \frac{\lambda\Omega T_p}{2\gamma_p^3\omega_B} = 10^{-15}$	$\delta = \frac{\omega_p^2 T_p}{\gamma_p\omega_B^2} = \frac{2\lambda\Omega T_p}{\gamma_p\omega_B} = 4 \times 10^{-13}$

Table 4.1: Plasma parameters at the surface of the neutron star

	Pulsar frame	Plasma frame
Magnetic field, G	10^3	10^3
Cyclotron frequency $\omega_B{}^*$, $(rad\,s^{-1})$,	1.8×10^{10}	1.8×10^{10}
Beam density, cm^{-3}	$n'_{GJ} = \Omega B/(2\,\pi\,e\,c) = 1.4 \times 10^2$	$n_{GJ} = \Omega B/(2\,\pi\,e\,c\gamma_p) = 14$
Beam plasma frequency, $rad\,s^{-1}$	$\omega'_{GJ} = \sqrt{\frac{4\,\pi\,q^2\,n^2_{GJ}}{m}} = 6 \times 10^5$	$\omega_{GJ} = \frac{\omega'_{GJ}}{\sqrt{\gamma_p}} = 3 \times 10^5$
Beam energy	$\gamma'_b \approx \times 10^6$	$\gamma_b = \frac{\gamma'_b}{2\gamma_p} = 5 \times 10^4$
Plasma density, cm^{-3}	$n'_p = \frac{\lambda\,\Omega\,B}{2\,\pi\,e\,c} = 4 \times 10^7$	$n_p, = \frac{\lambda\,\Omega B}{2\,\pi\,e\,c\gamma_p} = 4 \times 10^6$
Plasma frequency, $rad\,s^{-1}$	$\omega'_p = \sqrt{2\,\omega_B\,\Omega\,\lambda} = 4 \times 10^8$	$\omega_p = \sqrt{\frac{2\,\omega_B\,\Omega\,\lambda}{\gamma_p}} = 1.2 \times 10^8$
$1-\beta_X$,β_X phase speed of X mode	$\delta' = \frac{\omega_p^2 T_p}{4\gamma_p^3\omega_B^2} = \frac{\lambda\Omega T_p}{2\gamma_p^3\omega_B} = 5 \times 10^{-7}$	$\delta = \frac{\omega_p^2 T_p}{\gamma_p\omega_B^2} = \frac{2\lambda\Omega T_p}{\gamma_p\omega_B} = 1.2 \times 10^{-4}$
Typical frequency, $rad\,s^{-1}$	$\omega' = 5 \times 10^9$	$\omega = \frac{\omega'}{2\gamma_p} = 2.5 \times 10^8$

Table 4.2: Plasma parameters at the emission region $R \approx 10^9$ cm

$$\omega_p(r) = \omega_p(R_{NS}) \left(\frac{R_{NS}}{r} \right)^{3/2} . \tag{4.9}$$

4.1.2 Electromagnetic Parameters

Next let us estimate the parameters of the electromagnetic radiation in the pulsar magnetosphere. The typical observed fluxes are of the order of 1 Jy (1 Jy $= 10^{-23}\mathrm{erg\,s^{-1}cm^{-2}Hz^{-1}}$) at a frequency around 1 GHz. For the typical distance to the pulsar of $d = 1$ kpc, this translates in the magnetospheric flux of $F_\nu = 1Jy(d/R)^2 = 10^2\mathrm{erg\,s^{-1}cm^{-2}}R_9^{-2}$ at the distance of $R \approx 10^9$ cm from the stellar surface. Taking the bandwidth of the emission $\delta\nu = 10^9$ Hz, we find a typical radiative energy flux in the pulsar magnetosphere:

$$F = 10^{11} R_9^{-2} \mathrm{erg\,s^{-1}cm^{-2}} \tag{4.10}$$

which gives a total radio luminosity around

$$L \approx \pi R^2 F = 3 \times 10^{29} \mathrm{erg\,s^{-1}} \tag{4.11}$$

We note that the radio luminosity is just a small fraction of the particle energy flux:

$$E_{prtcl} \approx \gamma_b \, n_{GJ} m \, c^3 R^2 = 10^{32} \mathrm{erg\,s^{-1}} \tag{4.12}$$

which, in turn, constitutes a small fraction of the total energy loss of the rotating neutron star

$$E_{NS} = I\Omega\dot{\Omega} \approx 10^{33} \, \dot{P}_{15} \mathrm{erg\,s^{-1}} \tag{4.13}$$

We can also estimate the one dimension photon density (see Eq. (9.17). We find:

$$n(k) = \frac{F_\nu}{\hbar\omega} \approx 10^{19} \, \frac{1}{\mathrm{cm}^2} \tag{4.14}$$

4.2 Transformation of Physical Quantities

In this section we will give the rules of transformation of various quantities from the pulsar frame to the plasma frame. We will give simple examples, assuming in most cases that the velocities of particles and wave vectors are directed along the field lines. The transformations of some parameters are given in Tables 4.1, 4.2 and 4.3.

The typical observed frequency of $\omega' = 5\times10^9 \mathrm{rad\,sec}^{-1}$ ($\nu \approx 1\,\mathrm{GHz}$) corresponds to the frequency in the plasma frame $\omega = \omega'/(2\gamma_p) \approx 2.5 \times 10^8$. This can be compared with the characteristic frequencies of plasma in the plasma frame at the presumed emission site of $R = 10^9\mathrm{cm}$ (Table 4.2). More precisely, we should compare the wave frequency with the frequency of plasma oscillations at small wave number $\omega(k \ll \omega_p/c) = \sqrt{2/T_p}\omega_p$ and with the cross-over frequency $\omega_o = \sqrt{2T}\omega_p$. We find that the emission frequency is much larger than the frequency of plasma oscillations at small wave number: $\omega \gg \omega(k \ll \omega_p/c)$, but may be comparable to the cross-over frequency: $\omega \geq \omega_o$.

When making transformation of the refractive index, we assumed that $\gamma_p^2\delta \ll 1$ and $\gamma_p^2\delta^{(1)}/kc \ll 1$ ($\delta + \delta^{(1)}/kc$ is the difference of the phase speed of transverse waves from the speed of light. In physical terms this implies that the velocity of the plasma frame with respect to the pulsar frame is less than the phase velocity of the transverse waves. So that if a wave travels in the negative direction in the plasma frame, it will also be traveling in the negative direction in the pulsar frame. The above conditions are well satisfied in pulsar magnetopsheres, where $\gamma_p \approx 10 - 100$ and $\delta \leq 10^{-6}$ in the outer regions.

Quantity	Plasma frame	Pulsar Frame
Frequency of vacuum-like waves	$\omega(k)$	$\begin{cases} 2\gamma_p\omega & k>0 \\ \frac{\omega}{2\gamma_p} & k<0 \end{cases}$
Refractive index of vacuum-like waves	$n = 1+\delta+\delta^{(1)}/kc$	$n' = \frac{n+\beta_p}{1+n\beta_p} \approx \begin{cases} 1+\frac{\delta}{4\gamma_p^2}+\frac{\delta^{(1)}}{2\gamma_p k'c} & k>0 \\ -(1+4\gamma_p^2\delta-\frac{2\delta^{(1)}\gamma_p}{k'c}) & k<0 \end{cases}$
Angle of propagation	θ	$\begin{cases} \frac{\theta}{2\gamma_p} & \text{if } \theta \approx 0 \\ 2\gamma_p\theta & \text{if } \theta \approx \pi \end{cases}$
Occupation number	$n(\mathbf{k})$	$n(\mathbf{k}')$
One-dimensional flux	$F(\nu)$	$F(\nu')\frac{\nu}{\nu'}$

Table 4.3: Transformation of various quantities from pulsar to the plasma frame

Chapter 5 Waves in Magnetized Pair Plasma

5.1 Outline of the Chapter

In this Chapter we first derive the dielectric tensor in cylindrical coordinates. Generally, in cylindrical coordinates the electric induction is related to electric field through a linear dielectric tensor *operator*, which involves derivatives of the electric field with respect to radius. In two particular cases this *operator* relation can be simplified to *algebraic* relations: for the nonresonant wave (this will correspond to the WKB approximation) and for resonant *subluminous* waves in the limit $z \gg 1$ (see Section 6.2.1). In Appendix A, we discuss the properties of electromagnetic waves and wave-particle interaction in vacuum when described in cylindrical coordinates and show when the *nonresonant* terms of the dielectric tensor operator can be reduced to *algebraic* relations, i.e., to the dielectric tensor. In Appendix B we calculate the dyadic Green's function for a particle executing a circular motion in cylindrical coordinates, and show how the conventional expressions for the curvature emissivity can be obtained using our approach. In Appendix C we show when the *resonant* terms of the dielectric tensor operator can be described by more simple *algebraic* relations, i.e., by the dielectric tensor.

Next we discuss the properties of linear waves in a strongly magnetized electron-positron plasma streaming along the magnetic field. The particles are assumed to be in their ground gyrational state so that the plasma is one-dimensional. Properties of a one-dimensional pair plasma are considerably different from the properties of a well studied electron-ion plasma. In this chapter we present the most thorough consideration available of the properties of the waves in pair plasma taking into account possible relativistic temperatures and relative streaming of the plasma components. Another complication in considering the wave modes in a pulsar magnetosphere comes from the large bulk streaming of plasma which does not allow a simple Lorentz transformation from the plasma rest frame to the observer frame.

5.2 Response Tensor for a One-Dimensional Plasma

We will calculat the response tensor of a one-dimensional plasma in cylindrical coordinates using the analogy of the forward-scattering method (see, e.g., Melrose 1986) adopted to cylindrical coordinates. We introduce cylindrical coordinates x, r, ϕ with r along the radius of curvature of the field line, x perpendicular to the plane of the curved field line and ϕ the azimuthal coordinate (Fig. 5.1).

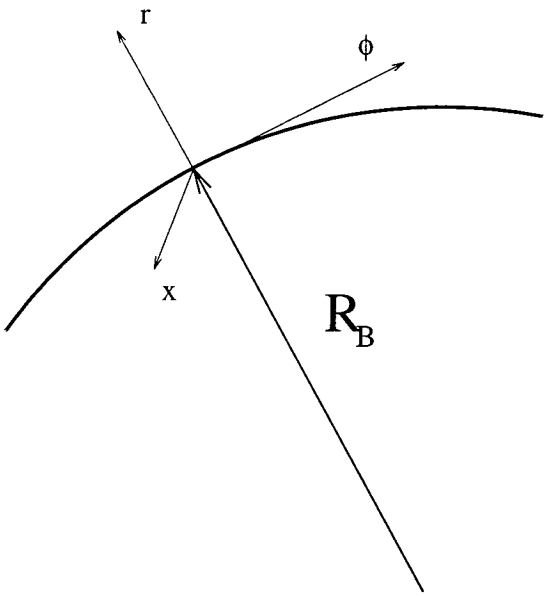

Figure 5.1: System of coordinates.

Torsion is neglected and the radius of curvature is assumed to be constant.

We represent the current as a sum of currents due to each single particle moving along its trajectory $\mathbf{r}^0(t)$:

$$\mathbf{j}(\mathbf{r},t) = \int d\mathbf{r}^0 d\mathbf{p}\, \mathbf{j}_{sp}(\mathbf{r},t) f(\mathbf{p},\mathbf{r}^0(t)) \tag{5.1}$$

We expand the single particle current (denoted by the subscript sp)

$$\mathbf{j}_{sp}(\mathbf{r},t) = q\dot{\mathbf{r}}\,\delta(\mathbf{r}-\mathbf{r}^0(t)) \tag{5.2}$$

in Fourier amplitudes in time, x and ϕ and in Hankel amplitudes in r

$$\begin{aligned}\mathbf{j}_{sp}(r,m,k_x,\omega) &= \int dt \exp\{-i\omega t\} \int dx \exp\{ik_x x\} \int d\phi \exp\{i\nu\phi\}\, \mathbf{j}_{sp}(\mathbf{r},t) \\ &= \int dt \exp\{i(\nu\phi^0(t) + k_x x_0(t) - \omega t)\}\dot{\mathbf{r}} \int \xi d\xi J_\nu(\xi r) J_\nu(\xi r^0(t))\end{aligned} \tag{5.3}$$

where we used a Hankel transform of the delta function

$$\int \xi d\xi J_\nu(\xi r) J_\nu(\xi r^0) = \frac{\delta(r-r^0)}{r} \tag{5.4}$$

1

[1] A Hankel transform is defined as $F(x) = \int_0^\infty J_\nu(\xi x)\xi d\xi \int_0^\infty y dy J_\nu(\xi y) F(y)$

We expand the orbit of the particle in powers of wave amplitudes:

$$\mathbf{r}(t) = \mathbf{r}^0(t) + \mathbf{r}^{(1)}(t) \tag{5.5}$$

where $\mathbf{r}^0(t)$ is the unperturbed trajectory of a particle, when no wave is present and $\mathbf{r}^{(1)}(t)$ is first order purturbations.

The first order Fourier transform of the single particle current is then

$$\mathbf{j}^{(1)}_{sp}(r, m, k_x, \omega) = q \int dt \exp\{i(\nu\phi^0(t) + k_x x_0(t) - \omega t\} \int \xi d\xi J_\nu(\xi r)$$
$$\times \left[\dot{\mathbf{r}}^{(1)} J_\nu(\xi r^0(t)) + \mathbf{r}^0(t) \left(\left(i\nu\phi^{(1)}(t) + ik_x x^{(1)}(t) \right) J_\nu(\xi r^0(t)) + \frac{\partial J_\nu(\xi r^0(t))}{\partial r^0} r^{(1)}(t) \right) \right] \tag{5.6}$$

The orbit of a particle is found by solving the equation of motion

$$\frac{d\mathbf{p}}{dt} = \mathbf{F}^0(t, \mathbf{r}, \mathbf{v}) + \mathbf{F}^{(1)}(t, \mathbf{r}, \mathbf{v}) \tag{5.7}$$

where $\mathbf{F}^0(t, \mathbf{r}, \mathbf{v})$ is a force acting on a particle when no wave is present and $\mathbf{F}^{(1)}(t, \mathbf{r}, \mathbf{v})$, i.e., a force acting on a particle due to the presence of a waves. Expanding Eq. (5.7) in powers of waves amplitudes we find

$$\frac{d\mathbf{p}^0(t)}{dt} = \mathbf{F}^0(t, \mathbf{r}^0, \mathbf{v}^0) \tag{5.8}$$
$$\frac{d\mathbf{p}^{(1)}(t)}{dt} = \mathbf{F}^{(1)}(t, \mathbf{r}^0, \mathbf{v}^0) \tag{5.9}$$

The force $\mathbf{F}^{(1)}(t, \mathbf{r}^0, \mathbf{v}^0)$ also can be expanded in Fourier amplitudes in t, x and ϕ.

$$\mathbf{F}^{(1)}(t, \mathbf{r}^0, \mathbf{v}^0) = \sum_{\nu'} \int d\omega' dk'_x \exp\{-i(\omega' t - k'_x x^0(t) - \nu'\phi^0(t)) \mathbf{F}^{(1)}(\omega, m, k_x, r^0(t), t) \tag{5.10}$$

Equation (5.9) can be solved for the first order velocity perturbation $\dot{\mathbf{r}}^{(1)}(t)$ and first order trajectory perturbations $x^{(1)}(t)$, $\phi^{(1)}(t)$ and $r^{(1)}(t)$:

$$\begin{pmatrix} \dot{\mathbf{r}}^{(1)}(t) \\ x^{(1)}(t) \\ \phi^{(1)}(t) \\ r^{(1)}(t) \end{pmatrix} = \sum_{\nu'} \int d\omega' dk'_x \exp\{-i(\omega' t - k'_x x^0(t) - \nu'\phi^0(t)) \begin{pmatrix} \tilde{\mathbf{V}}(\omega', \nu', k'_x, r^0(t), t) \\ \tilde{x}^{(1)}(\omega', \nu', k'_x, r^0(t), t) \\ \tilde{\phi}^{(1)}(\omega', \nu', k'_x, r^0(t), t) \\ \tilde{r}^{(1)}(\omega', \nu', k'_x, r^0(t), t) \end{pmatrix} \tag{5.11}$$

where tilde denotes Fourier transforms.

The first order single particle current then becomes

$$\mathbf{j}_{sp}^{(1)}(r,m,k_x,\omega) = q\sum_{\nu'}\int d\omega' dk_x' \int dt e^{\{i\left((\omega-\omega')t-(k_x-k_x')x^0(t)-(\nu-\nu')\phi^0(t)\right)\}} \int \xi d\xi J_\nu(\xi r)$$
$$\left[\tilde{\mathbf{V}}J_\nu(\xi r^0(t)) + \mathbf{r}^0(t)\left(\left(i\nu\tilde{\phi}^{(1)} + ik_x\tilde{x}^{(1)}\right)J_\nu(\xi r^0(t)) + \frac{\partial J_\nu(\xi r^0(t))}{\partial r^0}\tilde{r}^{(1)}\right)\right] \tag{5.12}$$

Using this single particle current we can calculate the current (5.1). In the general case, current (5.12) may be related to the electric field of the perturbing wave through a generalized dielectric tensor *operator*:

$$\mathbf{j}(r,m,k_x,\omega) = \mathcal{E}(r,m,k_x,\omega)\cdot\mathbf{E}(r,m,k_x,\omega) \tag{5.13}$$

where $\mathcal{E}$ is a dielectric tensor operator which involves a Hankel transform of the external current and partial derivatives with respect to r. This is different from Cartesian coordinates, where the electric induction is related to electric field through a dielectric tensor. [2] To simplify the calculations we find when the radial dependence of both the Hankel transform of the external current and of the perturbing electric field can be approximated by the plane wave form. For the nonresonant term in the dielectric tensor operator this is justified in the WKB limit, while for the resonant terms this is justified for subluminous waves in the limit $\delta\nu^{2/3} \gg 1$ (ν is the order of the Bessel function).

Thus, in the Hankel transform of the external current and in the derivatives of the perturbing electric field we can identify

$$\frac{\partial}{\partial r^0} \to ik_{r_0}, \qquad \frac{\partial}{\partial r} \to ik_r \tag{5.14}$$

In this approximation the Hankel transform of the external current will reduce to the Fourier transform in r and the derivatives of the perturbing electric field are replaced by ik_r. The dielectric tensor operator $\mathcal{E}$ then becomes a conventional tensor.

The integration of the induced current over $d\phi^0 dx^0$ then gives delta-functions $\delta(\nu-\nu')\,\delta(k_x-k_x')$ that are subsequently removed by the corresponding integrations. For $r_0 = \text{const}$, the time and $d\omega'$ integrations insure that only secular terms are retained. The integration over $d\xi$ and dr^0 are removed using relation (5.4).

5.2.1 Perturbed Trajectory

The equations of motions for a particle in a circular magnetic field when the Larmor radius is much smaller than the radius of curvature are the following:

$$\frac{dp_r}{dt} = eE_r(\mathbf{r}^0) + \frac{q}{c}\left((B_\phi(\mathbf{r}^0)+B_0)v_x - v_\phi B_x(\mathbf{r}^0)\right) \tag{5.15}$$

[2] Mathematically, the difference is that dielectric tensor acts in a space tangent to the vector field at some point, while dielectric tensor operator acts on a vector field itself.

$$\frac{dp_x}{dt} = eE_x(\mathbf{r}^0) + \frac{q}{c}\left(B_r(\mathbf{r}^0)v_\phi - v_r(B_\phi(\mathbf{r}^0) + B_0)\right) \tag{5.16}$$

$$\frac{dp_\phi}{dt} = eE_\phi(\mathbf{r}^0) + \frac{q}{c}\left(B_x(\mathbf{r}^0)v_r - v_x B_r(\mathbf{r}^0)\right) \tag{5.17}$$

We solve Eqs. (5.15- 5.17) by expanding in powers of waves amplitudes. We assume that initially the particles are in the ground gyration state. Then in the zeroth order we find: $v_r^0 = 0$, $\phi^0 = \Omega t = v_\phi t/r$, $v_x^0 = u_d$, with $u_d = \frac{\gamma v_\phi^2}{R_B \omega_B}$. The first order in wave amplitudes gives

$$\frac{dv_r^{(1)}}{dt} = \frac{q}{\gamma m_e c}\left(E_r(\mathbf{r}^0) - \frac{v_\phi}{c}B_x(\mathbf{r}^0) + \frac{u_d}{c}B_\phi(\mathbf{r}^0)\right) + \frac{\omega_B}{\gamma}v_x^{(1)} \tag{5.18}$$

$$\frac{dv_x^{(1)}}{dt} = \frac{q}{\gamma m_e c}\left(E_x(\mathbf{r}^0) + \frac{v_\phi}{c}B_r(\mathbf{r}^0) - \frac{u_d(v_\phi E_\phi(\mathbf{r}^0) + u_d E_x(\mathbf{r}^0))}{c^2}\right) + \frac{\omega_B}{\gamma}v_r^{(1)} \tag{5.19}$$

$$\frac{dv_\phi^{(1)}}{dt} = \frac{q}{\gamma m_e c}\left(E_\phi(\mathbf{r}^0) - \frac{u_d}{c}B_r(\mathbf{r}^0) - \frac{v_\phi(v_\phi E_\phi(\mathbf{r}^0) + u_d E_x(\mathbf{r}^0))}{c^2}\right) \tag{5.20}$$

Expanding Eqs. (5.18 - 5.20) in Fourier amplitudes, we find the solutions:

$$\tilde{v}_r^{(1)} = \frac{q}{m_e c\gamma(\omega_B^2/\gamma^2 - \Omega^{0\,2})}\left(i\Omega^0\left(E_r + \frac{B_\phi u_d - B_x v_\phi}{c}\right)\right.$$
$$\left. + \frac{\omega_B}{\gamma}\left(E_x + \frac{v_\phi B_r}{c} - \frac{u_d(v_\phi E_\phi + u_d E_x)}{c^2}\right)\right) \tag{5.21}$$

$$\tilde{v}_x^{(1)} = \frac{q}{m_e c\gamma(\omega_B^2/\gamma^2 - \Omega^{0,2})}\left(i\Omega^0\left(E_x + \frac{v_\phi B_r}{c} - \frac{u_d((v_\phi E_\phi + u_d E_x)}{c^2}\right)\right.$$
$$\left. - \frac{\omega_B}{\gamma}\left(E_r + \frac{B_\phi u_d - B_x v_\phi}{c}\right)\right) \tag{5.22}$$

$$\tilde{v}_\phi^{(1)} = i\frac{q}{m_e \Omega^0 \gamma}\left(-\left(E_\phi - \frac{u_d}{c}B_r\right) + \frac{v_\phi(v_\phi E_\phi + u_d E_x)}{c^2}\right) \tag{5.23}$$

where $\Omega^0 = \omega - k_\phi v_\phi - k_x u_d$, $k_\phi = m/r$.

The first order variations in trajectory are

$$x^{(1)} = \frac{v_x^{(1)}}{i\Omega^0}, \qquad \phi^{(1)} = \frac{v_\phi^{(1)}}{i\Omega^0 r}, \qquad r^{(1)} = \frac{r^{(1)}}{i\Omega^0} \tag{5.24}$$

In a wave magnetic field is related to the electric field:

$$\mathbf{B} = -\frac{ic}{\omega}\mathbf{curl}\,\mathbf{E} \tag{5.25}$$

In cylindrical coordinates we have

$$B_r = \frac{k_x c}{\omega}E_\phi - \frac{k_\phi c}{\omega}E_x$$
$$B_\phi = -\frac{k_x c}{\omega}E_r - i\frac{c\partial E_x}{\omega \partial r}$$

$$B_x = \frac{k_\phi c}{\omega} E_r + i \frac{c}{\omega r} \frac{\partial}{\partial r} (r E_\phi) \tag{5.26}$$

5.2.2 Simplified Response Tensor

Using Eqs. (5.21 - 5.26) we can find the dielectric tensor operator $\mathcal{E}$. In Appendix A it is shown that in some particular cases the operator relations between electric field and electric displacement can be simplified to algebraic relations. This is possible in the WKB limit for the nonresonant particles and in the limit $z \gg 1$ for the resonant particles (see Appendix A). In these limits it is possible to change all the radial derivative $\partial_r \to i k_r$. The relations between magnetic and electric field then simplify

$$\begin{aligned} B_\phi &\approx -\frac{k_x c}{\omega} E_r + \frac{k_r c}{\omega} E_x \\ B_x &\approx \frac{k_\phi c}{\omega} E_r - \frac{k_r c}{\omega} E_\phi \end{aligned} \tag{5.27}$$

The resulting dielectric tensor is still complicated. It can be simplified according to the following procedure: (i) for the nonresonant parts, the drift velocity is small and can be neglected, (ii) for Cherenkov-type resonance (resonances that do not involve ω_B) , we retain all the terms, (iii) for cyclotron-type resonances (resonances that do involve ω_B) we assume that $k_x/k_\phi \approx u_d/c$, $u_d/c \gg 1/\gamma$ and expand in small drift velocity retaining only the first terms in u_d and k_x. Implicit in this expansion in small u_d is the assumption that $\gamma\omega^2 \gg \omega_B^2 u_d^2/c^2$. In this limit, in the cyclotron-type resonant terms involving drift velocity we can approximate $v_\phi \approx c$. The dielectric tensor is then

$$\begin{aligned}
\epsilon_{xx} &= 1 - \frac{1}{2}\sum_\alpha \frac{\omega_{p\alpha}^2}{\omega^2} \int \frac{dp_\phi}{\gamma} \left((\omega - k_\phi v_\phi) A_\alpha^+ f_\alpha \right) - \sum_\alpha \omega_{p\alpha}^2 \int \frac{dp_\phi}{\gamma} \frac{f_\alpha}{\Omega_\alpha^{o\,2}} \frac{k_\phi^2 u_\alpha^2}{\omega^2} \left(1 - \frac{\omega v_\phi}{k_\phi c^2} \right) \\
\epsilon_{rr} &= 1 - \frac{1}{2}\sum_\alpha \frac{\omega_{p\alpha}^2}{\omega^2} \int \frac{dp_\phi}{\gamma} (\omega - k_\phi v_\phi - k_x u_\alpha) A_\alpha^+ f_\alpha \\
\epsilon_{\phi\phi} &= 1 - \sum_\alpha \omega_{p\alpha}^2 \int \frac{dp_\phi}{\gamma} \frac{f_\alpha}{\Omega_\alpha^{o\,2}} \left((1 - \frac{k_x u_\alpha}{\omega}) \left((1 - \frac{k_x u_\alpha}{\omega}) - \frac{v_\phi^2}{c^2} \right) \right) \\
&\quad - \sum_\alpha \frac{\omega_{p\alpha}^2}{\omega^2} \int \frac{dp_\phi}{\gamma} f_\alpha \frac{(k_x^2 + k_r^2) v_\phi^2}{\Omega_\alpha^+ \Omega_\alpha^-} - \frac{1}{2}\sum_\alpha \frac{\omega_{p\alpha}^2}{\omega^2} \int \frac{dp_\phi}{\gamma} k_r u_\alpha A_\alpha^- f_\alpha \\
\epsilon_{xr} &= -\frac{i}{2}\sum_\alpha \frac{\omega_{p\alpha}^2}{\omega^2} \int \frac{dp_\phi}{\gamma} \left((\omega - k_\phi v_\phi) A_\alpha^- + i k_r u_d A_\alpha^+ \right) f_\alpha \\
\epsilon_{rx} &= \frac{i}{2}\sum_\alpha \frac{\omega_{p\alpha}^2}{\omega^2} \int \frac{dp_\phi}{\gamma} \left((\omega - k_\phi v_\phi) A_\alpha^- - i k_r u_\alpha A_\alpha^+ \right) f_\alpha \\
\epsilon_{x\phi} &= -\frac{1}{2}\sum_\alpha \frac{\omega_{p\alpha}^2}{\omega^2} \int \frac{dp_\phi}{\gamma} v_\phi \left(\left(k_x - \frac{\omega u_\alpha}{c^2} \right) A_\alpha^+ + i k_r A_\alpha^- \right) f_\alpha \\
&\quad - \sum_\alpha \frac{\omega_{p\alpha}^2}{\omega^2} \int \frac{dp_\phi}{\gamma} v_\phi u_\alpha \frac{(k_x^2 + k_r^2)}{\Omega_\alpha^+ \Omega_\alpha^-} f_\alpha
\end{aligned}$$

$$
\begin{aligned}
& -\sum_\alpha \omega_{p\alpha}^2 \int \frac{dp_\phi}{\gamma} \frac{f_\alpha}{\Omega_\alpha^{o\,2}} \frac{k_\phi u_\alpha}{\omega} \left((1 - \frac{k_x u_\alpha}{\omega}) - \frac{v_\phi^2}{c^2} \right) \\
\epsilon_{\phi x} \quad & = \frac{1}{2} \sum_\alpha \frac{\omega_{p\alpha}^2}{\omega^2} \int \frac{dp_\phi}{\gamma} v_\phi \left(k_x A_\alpha^+ - i k_r A_\alpha^- \right) f_\alpha \\
& -\sum_\alpha \omega_{p\alpha}^2 \int \frac{dp_\phi}{\gamma} \frac{f_\alpha}{\Omega_\alpha^{o\,2}} \frac{k_\phi u_\alpha}{\omega} \left(1 - \frac{k_x u_\alpha}{\omega} \right) \left(1 - \frac{\omega v_\phi}{k_\phi c^2} \right) \\
\epsilon_{r\phi} \quad & = -\frac{1}{2} \sum_\alpha \frac{\omega_{p\alpha}^2}{\omega^2} \int \frac{dp_\phi}{\gamma} \frac{v_\phi}{c} \left(k_r A_\alpha^+ - i \left(k_x c - \frac{\omega u_\alpha}{c} \right) A_\alpha^- \right) f_\alpha \\
\epsilon_{\phi r} \quad & = -\frac{1}{2} \sum_\alpha \frac{\omega_{p\alpha}^2}{\omega^2} \int \frac{dp_\phi}{\gamma} \frac{v_\phi}{c} \left(k_r A_\alpha^+ + i k_x A_\alpha^- \right) f_\alpha
\end{aligned}
\tag{5.28}
$$

Here

$$
A_\alpha^+ = \left(\frac{1}{\Omega_\alpha^+} + \frac{1}{\Omega_\alpha^-} \right), \quad A_\alpha^- = \left(\frac{1}{\Omega_\alpha^-} - \frac{1}{\Omega_\alpha^+} \right), \quad \Omega_\alpha^\pm = \omega - k_\phi v_\phi - k_x u_\alpha \pm \omega_B \gamma^{-1}, \quad \Omega_\alpha^o = \omega - k_\phi v_\phi - k_x u_\alpha,
\tag{5.29}
$$

where f_α are one-dimensional distribution functions of the components α.

This dielectric tensor reduces to the dielectric tensor for plasma in straight magnetic fields for $u_\alpha = 0$. It takes correct account of the Cherenkov-curvature emission and gives the drift corrections to the cyclotron emission. We also note that this dielectric tensor is nonhermitian, since k_r is not a Killing vector.

It can be shown that for the typical parameters in the pulsar magnetosphere, the drift velocity of plasma particles due to the curvature of magnetic field lines could be neglected in the calculations of the real part of the dielectric tensor unless the curvature of field lines satisfies the condition $R_B \ll \gamma_p^2 r_L$ (here γ_p is the average streaming energy of plasma particles in the pulsar frame and $r_L = c/\omega_B$- Larmor radius). This follows from the assumption of a nonrelativistic transverse motion and the transformation of the radius of curvature seen in the center of gyration frame $R_{B,cg} = R_B/\gamma^2$. This condition is well satisfied inside the pulsar magnetosphere for the plasma streaming energy $\gamma_p < 10^4$. By contrast, the drift velocity is very important for the high energy resonant particles.

The use of the simplified response tensor, which assumes a plane wave approximation to the normal modes of a medium, implies that we effectively have spatially uniform medium. Thus the use of cylindrical coordinates allows one to eliminate the only inhomogeneity present in the problem, the weak inhomogeneity of magnetic field, by choosing the cylindrical system of coordinates. For stationary and spatially uniform plasma we can use Fourier analysis which reduces the problem to the following system of equations for the perturbations in the electric field:

$$
\Lambda_{\alpha\beta} E_\beta(\omega, \mathbf{k}) = 0
\tag{5.30}
$$

where $\epsilon_{\alpha\beta}(\omega, \mathbf{k})$ is the dielectric tensor of the medium and

$$\Lambda_{\alpha\beta} = k_\alpha k_\beta - k^2 c^2 \delta_{\alpha\beta} + \omega^2 \epsilon_{\alpha\beta}(\omega, \mathbf{k}) \tag{5.31}$$

The normal modes satisfy a dispersion relation

$$Det\,|\Lambda_{\alpha\beta}| = 0 \tag{5.32}$$

whose roots determine the time behavior of the perturbations.

5.3 Waves in Cold Pair Plasma with Identical Distributions of Electrons and Positrons

In this section we will consider the wave propagation in a cold magnetized electron-positron plasma with equal densities. Though the pulsar plasma is probably hot, the simpler case of cold plasma is more easily understood and in many cases may serve as a good first order approximation. The assumption of equal densities of electrons and positrons needs some justification since, in reality, the pulsar plasma is nonneutral due to the presence of the primary beam with density of the order of the Goldreich-Julian density and a γ-factor $\gamma_b \approx 10^7$. As we will see the diagonal term in the dielectric tensor are proportional to the total densities of the plasma components which are larger than the Goldreich-Julian density by a factor $\lambda \gg 1$ and thus almost unaffected by the presence of the beam. The most important nondiagonal terms, like ϵ_{xy}, are proportional to the difference of the bulk velocities of the plasma components. For exactly parallel propagation and in the region $n \approx 1$ (n is the refractive index), the condition that the terms associated with the nonneutrality of the plasma are much less than the terms associated with the different bulk streaming of plasma components is $\beta_o' \lambda \gamma_b \gg 1$ (β_o' is the velocity difference (in units of c) of the plasma components in the pulsar frame). From (4.4) we may estimate $\beta_o' \leq 1/\lambda$ so that the terms associated with the nonneutrality of the plasma are $1/\gamma_b$ times smaller than the terms associated with the different velocities of the plasma components.

5.4 Plasma Frame

In this section we consider waves in a cold, strongly magnetized, electron-positron plasma in its rest frame. The drift velocity for the bulk plasma is ignored. In this first approximation we neglect the influence of the beam on the properties of the modes propagating in the medium. This can be done provided that the beam density is much smaller than the plasma density. If the average velocities of the electrons and positrons of the secondary plasma are the same, then retaining only nonresonant terms we find from Eq. (5.28) the dielectric tensor for cold pair plasma with coincident distribution functions:

$$\begin{aligned} \epsilon_{xx} &= 1 + \frac{2\,\omega_p^2}{\omega_B^2 - \omega^2} = \epsilon_{rr} \\ \epsilon_{\phi\phi} &= 1 - \frac{2\,{\omega_p}^2}{\omega^2} \\ \epsilon_{xr} &= \epsilon_{rx} = \epsilon_{x\phi} = \epsilon_{\phi x} = \epsilon_{r\phi} = \epsilon_{\phi r} = 0 \end{aligned} \tag{5.33}$$

where $\omega_p^2 = 4\,\pi n_p q^2/m$ is the plasma frequency, and $\omega_B = |q|B/mc$ is the nonrelativistic cyclotron frequency.

5.4.1 Waves in Cold Pair Plasma

Equation (5.32) with the dielectric tensor (5.33) factorizes giving the three wave branches: extraordinary and two coupled ordinary and Alfvén branches:

$$n^2 = 1 - \frac{2\,{\omega_p}^2}{\omega^2 - {\omega_B}^2} \qquad \text{X mode} \tag{5.34}$$

$$n^2 = \frac{\left(\omega^2 - 2\,{\omega_p}^2\right)\left(\omega^2 - {\omega_B}^2 - 2\,{\omega_p}^2\right)}{\omega^4 - \omega^2\,{\omega_B}^2 - 2\,\omega^2\,{\omega_p}^2 + 2\,{\omega_B}^2\,{\omega_p}^2\cos^2\theta} \qquad \text{Alfvén and O mode} \tag{5.35}$$

(see Figs. 5.2 and 5.3).

Equation (5.34) describes the transverse extraordinary wave with the electric vector perpendicular to the **k-B** plane and Eq. (5.35) describes the coupled longitudinal-transverse wave which has two branches: ordinary quasi-transverse wave with the electric vector in the **k-B** plane and quasi-longitudinal Alfvén wave with the electric vector along **B**.

The normal modes of the plasma for the parallel propagation are given by

$$\omega_l = \sqrt{2}\,\omega_p \tag{5.36}$$

$$n_t^2 = 1 + \frac{2\,\omega_p^2}{\omega_B^2 - \omega_t^2} \tag{5.37}$$

(subscripts $_l$ and $_t$ refer to longitudinal and transverse polarizations of waves).

For exactly parallel propagation, the dispersion curves for the ordinary mode and Alfvén mode intersect at

$$\omega^* = \sqrt{2}\omega_p \qquad k^* c \approx \sqrt{2}\omega_p\left(1 + \omega_p^2/{\omega_B}^2\right) \tag{5.38}$$

This intersection occurs only for the parallel propagation, for oblique the dispersion curves for ordinary, extraordinary and Alfvén modes are well separated. It follows that Eq. (5.36) describes the ordinary mode for $k < k^*$ and the Alfvén mode for $k > k^*$, while Eq. (5.37) describes the extraordinary mode for all frequencies and the Alfvén mode for $k < k^*$ and the ordinary mode for $k > k^*$.

In the pulsar magnetosphere the waves that may be important for the generation of the observed radio emission have frequencies much less than the gyrofrequency. In what follows, we will often use the low frequency approximation when all the relevant frequencies are much less than the gyrofrequency. In the cold plasma in its rest frame this implies: $\omega \ll \omega_B$. The solution of Eq. (5.34) in the low frequency limit describes a *subluminous* transverse electromagnetic wave:

$$\omega^2 = k^2 c^2\left(1 - \frac{2\omega_p^2}{\omega_B^2}\right), \qquad \omega \ll \omega_B, \qquad \text{X mode} \tag{5.39}$$

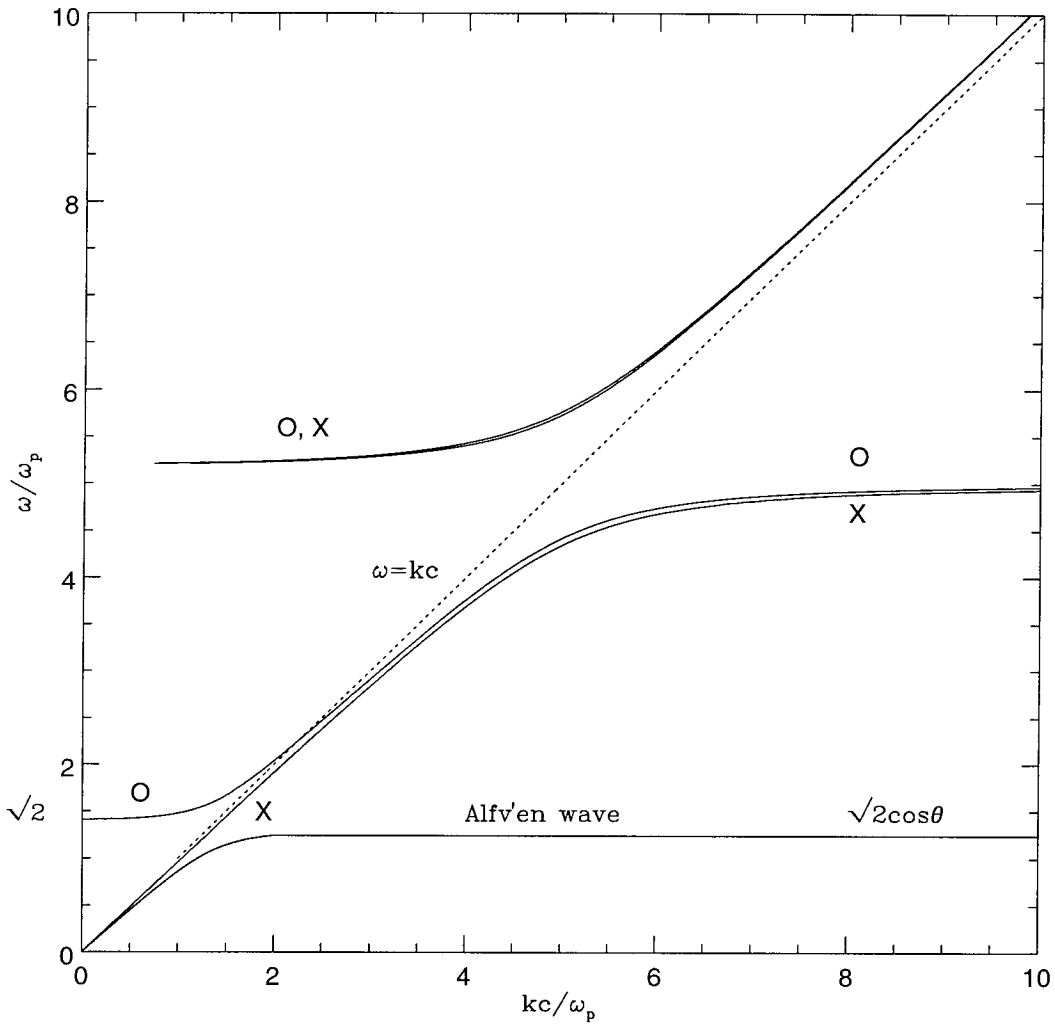

Figure 5.2: Dispersion curves for the waves in a cold electron-positron plasma in the plasma frame for oblique propagation ($\theta = 0.5$). There are three modes: Ordinary (O), Extraordinary (X) and Alfvén. For graphic purposes gyrofrequency was chosen to be $\omega_B = 5\omega_p$. In the high frequency regime $\omega \gg \omega_B$ there are two subluminous waves with the dispersion relation $\omega^2 \approx k^2c^2 + 2\omega_p^2$ for the X and O modes. Both X and O modes have resonances at $\omega = \omega_B$ and Alfvén has a resonance at $\omega = \sqrt{2}\cos\theta\omega_p$. O mode has a cutoff at $\omega = \sqrt{2}\omega_p$. O mode crosses the vacuum dispersion relation at $\omega^2 = 2\omega_p^2 + \omega_B^2 \sin\theta^2$.

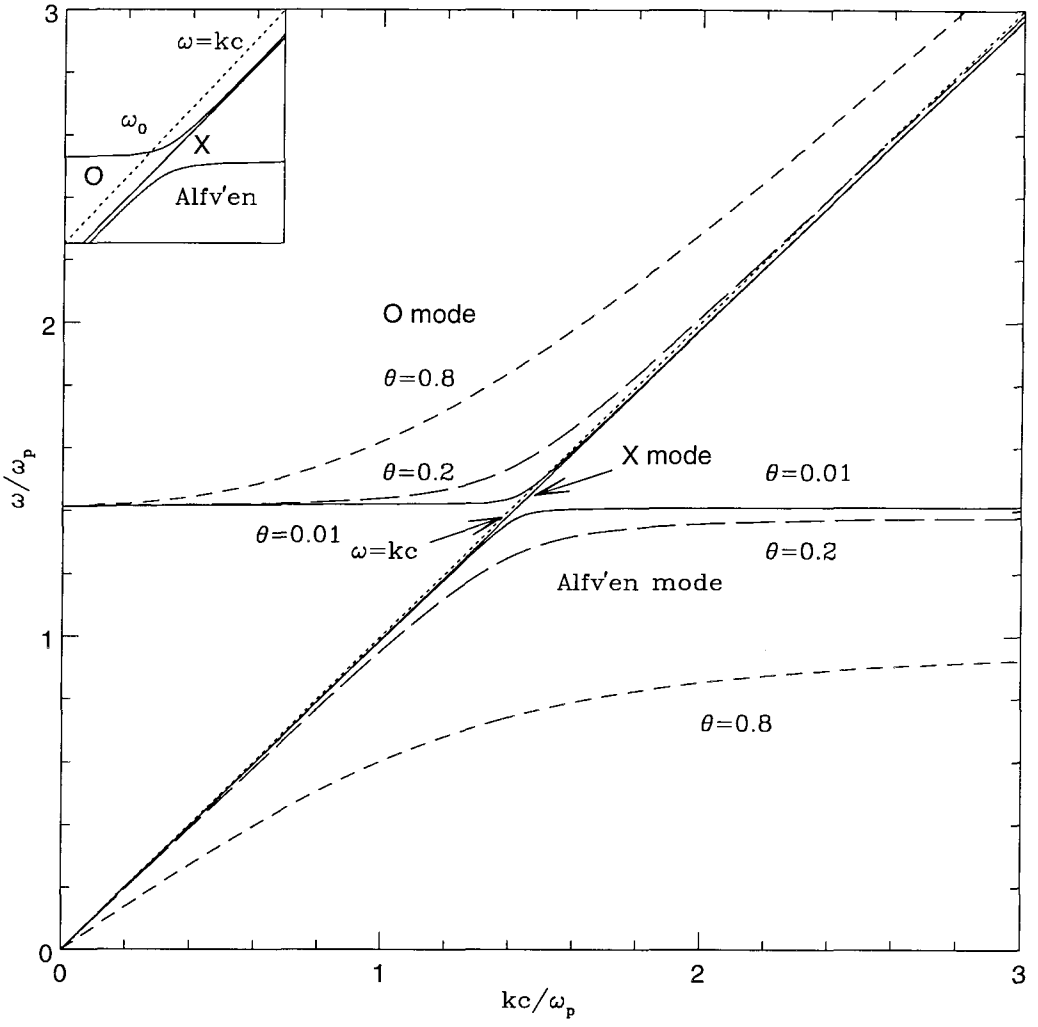

Figure 5.3: Dispersion curves for the waves in a cold electron-positron plasma in the plasma frame in the limit $\omega_p \ll \omega_B$. There are three modes represented by the dashed (ordinary mode), solid (extraordinary mode) and long dashed (Alfvén mode). The dotted line represents the vacuum dispersion relation. For the exact parallel propagation, the dispersion curves for the ordinary mode and Alfvén mode intersect. The insert in the upper left corner shows the region near the cross-over point ω_0.

Solutions of Eq. (5.35) are more complicated. The simple form for the dispersion relation may be obtained near the cross-over point, where the dispersion relation of the ordinary mode crosses the vacuum dispersion relation or in the asymptotic regimes far from the cross-over point.

Solving (5.35) with the refractive index set to unity we find the cross-over point for the ordinary wave.

$$\omega_0^2 = k_0^2 c^2 = 2\omega_p{}^2 + \omega_B{}^2 \sin^2\theta \tag{5.40}$$

Near the cross-over point, the approximate dispersion relation for the ordinary mode may be found using the relation

$$\omega - \omega_0 = -\left(\frac{\partial K(\omega,\mathbf{k})}{\partial \mathbf{k}}\right) \Big/ \left(\frac{\partial K(\omega,\mathbf{k})}{\partial \omega}\right) d\mathbf{k} \tag{5.41}$$

where $K(\omega,\mathbf{k}) = 0$ is the dispersion Eq. for $\omega(\mathbf{k})$.

From Eq. (5.35) we find

$$\omega = k_0\, c + \eta(k - k_0)c \tag{5.42}$$

where

$$\begin{aligned}\eta = \frac{1}{c}\left.\frac{\partial\omega}{\partial k}\right|_{k=k_0} &= \frac{\omega_B{}^4 \cos^2\theta \sin^2\theta}{4\omega_p{}^4 + 2\omega_B{}^2\omega_p{}^2 \sin^2\theta + \omega_B{}^4 \cos^2\theta \sin^2\theta} \\ &\approx 1 - \frac{4\omega_p{}^4}{4\omega_p{}^4 + \omega_B{}^4 \cos^2\theta \sin^2\theta}\end{aligned} \tag{5.43}$$

where we used the assumption $\omega_B \gg \omega_p$. From (5.43) it follows that the behavior of the dispersion relation of the ordinary wave near the cross-over point shows a very sensitive dependence on the angle of propagation. There exists a critical angle $\theta_c = 2\omega_p^2/\omega_B^2$ at which the dispersion relation changes:

$$\begin{aligned}\omega &= \sqrt{2}\,\omega_p + \tfrac{\omega_B{}^4}{2\omega_p^4}(k - k_0)c, \qquad k_0^2 \approx 2\omega_p^2/c^2 \qquad \text{if } \theta \ll 2\omega_p^2/\omega_B{}^2 \\ \omega &= kc - \tfrac{4(k-k_o)c\,\omega_p{}^4}{\sin^2\theta\cos^2\theta}\omega_B{}^4, \quad k_0^2c^2 = 2\omega_p^2 + \omega_B{}^2 \sin^2\theta \quad \text{if } 2\omega_p^2/\omega_B{}^2 \ll \theta\end{aligned} \tag{5.44}$$

For angles smaller than θ_c, we can generally use the approximation of parallel propagation when considering the dispersion relations of the waves, while for larger angles we must take into account the effects of oblique propagation.

The other limits when the dispersion relations for the ordinary and Alfvén waves may be obtained in closed form are the asymptotic limits far from the cross-over point. Then the large and small

wave vector asymptotic solutions are

$$\omega^2 = \begin{cases} k^2c^2\left(1-\frac{2\,{\omega_p}^2\cos^2\theta}{{\omega_B}^2}\right)+2\,{\omega_p}^2\sin^2\theta & \text{ordinary wave} \\ & \text{if } kc \gg \omega_p \\ 2\,{\omega_p}^2\cos^2\theta\left(1-\frac{2\,{\omega_p}^2\sin^2\theta}{k^2c^2}-\frac{2\,{\omega_p}^2\sin^2\theta}{{\omega_B}^2}\right) & \text{Alfvén wave} \end{cases} \tag{5.45}$$

$$\omega^2 = \begin{cases} 2\,{\omega_p}^2+k^2c^2\left(1-\frac{k^2c^2\cos^2\theta}{{\omega_p}^2}\right)\sin^2\theta & \text{ordinary wave} \\ & \text{if } kc \ll \omega_p \\ k^2c^2\cos^2\theta\left(1-\frac{2\,{\omega_p}^2}{{\omega_B}^2}-\frac{k^2c^2\sin^2\theta}{2\,{\omega_p}^2}\right) & \text{Alfvén wave} \end{cases} \tag{5.46}$$

From (5.45) and (5.46) it follows that for Alfvén waves in the limit $kc \gg \omega_p$ and for the ordinary mode in the opposite limit $kc \ll \omega_p$ we can always set the magnetic field to infinity, while for the ordinary mode in the limit $kc \gg \omega_p$ and for the Alfvén waves in the limit $kc \ll \omega_p$ we may set the magnetic field equal to infinity for the angles of propagation larger than some characteristic angle:

$$\begin{aligned} \theta &> \tfrac{kc}{\omega_B} \quad \text{if } kc \gg \omega_p \\ \theta &> \tfrac{\omega_p}{\omega_B} \quad \text{if } kc \ll \omega_p \end{aligned} \tag{5.47}$$

In the limit of infinitely strong magnetic field the dispersion relations for the ordinary (plus sign) and Alfvén modes (minus sign) are (Arons & Barnard 1986)

$$\omega^2 = \frac{k^2c^2}{2}+{\omega_p}^2 \pm \frac{\sqrt{k^4c^4+4\,{\omega_p}^4-4\,k^2\,c^2{\omega_p}^2\,\cos(2\,\theta)}}{2} \tag{5.48}$$

The short and long wave length asymptotics are then given by (5.45) and (5.46) with the magnetic field set to infinity.

An important point in considering the wave excitation in the superstrong magnetic field is that we *cannot* neglect the very large but finite magnetic field. In the approximation of the infinitely strong magnetic field the ordinary mode is always superluminous and thus cannot be excited by the Cherenkov-type resonant wave-particle interaction. In this limit any instability would occur on the Alfvén waves which are strongly damped as they propagate out in the pulsar magnetosphere. When the finite magnetic field is taken into account, ordinary wave becomes subluminous for the small angles of propagation and can be resonantly excited by the Cherenkov, cyclotron or Cherenkov-drift interaction with the fast particles.

5.4.2 CMA Diagram for Cold Pair Plasma

CMA diagrams (e.g., Budden 1985) are useful tools in considering wave propagation. It is a plot of the refractive index versus some functions of wave, plasma and cyclotron frequencies. We chose the following coordinates for CMA diagram:

$$W = \frac{1}{Y^2} = \left(\frac{\omega}{\omega_B}\right)^2, \qquad Z = \frac{X}{Y^2} = \left(\frac{\omega_p}{\omega_B}\right)^2 \tag{5.49}$$

where Y and X are the standard quantities in the magnetosonic theory. With this choice of coordinates, the lines of constant Z are the lines of constant density and are independent of wave frequency. The lines of constant W are the lines of constant wave frequency and are independent of the density. The regions on the CMA diagram are separated by the resonance, where $n \to \infty$ and cutoffs, where $n \to 0$.

Using Eqs (5.34) and (5.35) we find resonance

$$W = 1 \qquad \text{X modes} \tag{5.50}$$

$$W = \tfrac{1}{2} + Z \pm \sqrt{\left(\tfrac{1}{2} + Z\right)^2 - 2Z\cos^2\theta} \qquad \text{O \& Alfvén modes} \tag{5.51}$$

and reflection points

$$W = 1 + 2Z \qquad \text{X modes} \tag{5.52}$$

$$\begin{cases} W = 1 + 2Z \\ W = 2Z \end{cases} \qquad \text{O \& Alfvén modes} \tag{5.53}$$

For the X wave the curve $n = 1$ corresponds to $Z = 0$ (vacuum case). For the ordinary mode $n = 1$ at $W = 2Z + \sin^2\theta$ (cross-over point) and $Z = 0$ (vacuum case). Other useful relations for the resonances of the coupled ordinary and Alfvén modes are

$$\tfrac{1}{2} + Z + \sqrt{\left(\tfrac{1}{2} + Z\right)^2 - 2Z\cos^2\theta} = \begin{cases} 1 & \theta = 0 \\ 1 + 2Z & \theta = \pi/2 \\ 1 + 2Z\sin^2\theta & Z \ll 1 \\ 2Z + \sin^2\theta & Z \gg 1 \end{cases}$$

$$\tfrac{1}{2} + Z - \sqrt{\left(\tfrac{1}{2} + Z\right)^2 - 2Z\cos^2\theta} = \begin{cases} 2Z & \theta = 0 \\ 0 & \theta = \pi/2 \\ 2Z\cos^2\theta & Z \ll 1 \\ \cos^2\theta & Z \gg 1 \end{cases} \tag{5.54}$$

The CMA diagrams are plotted in Figs. 5.4 and 5.5.

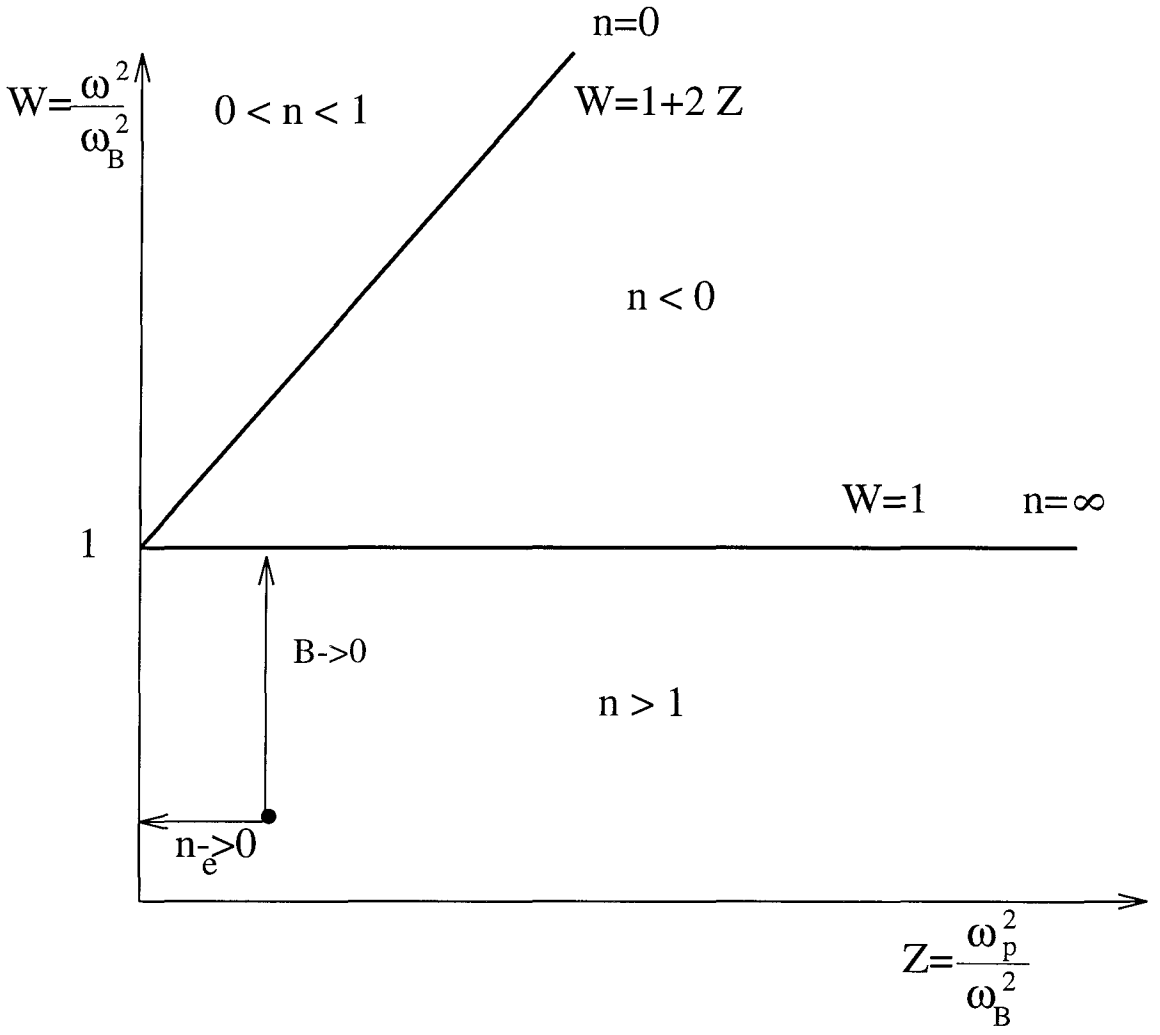

Figure 5.4: CMA diagram for the X mode.The vacuum case corresponds to $Z = 0$. On the axis $W = 0$ refractive index is $n = 1$. Resonance occurs at $W = 1$ ($n = \infty$) and reflection occurs at $W = 1 + 2Z$. Typical X waves in the pulsar magnetosphere have $Z \ll 1$, $W \ll 1$ and $n > 1$ deep in the magnetosphere. Arrows indicate the adiabatic tracks for the constant density and decreasing magnetic field ($B \to 0$) and constant magnetic field and decreasing density ($n \to 0$).

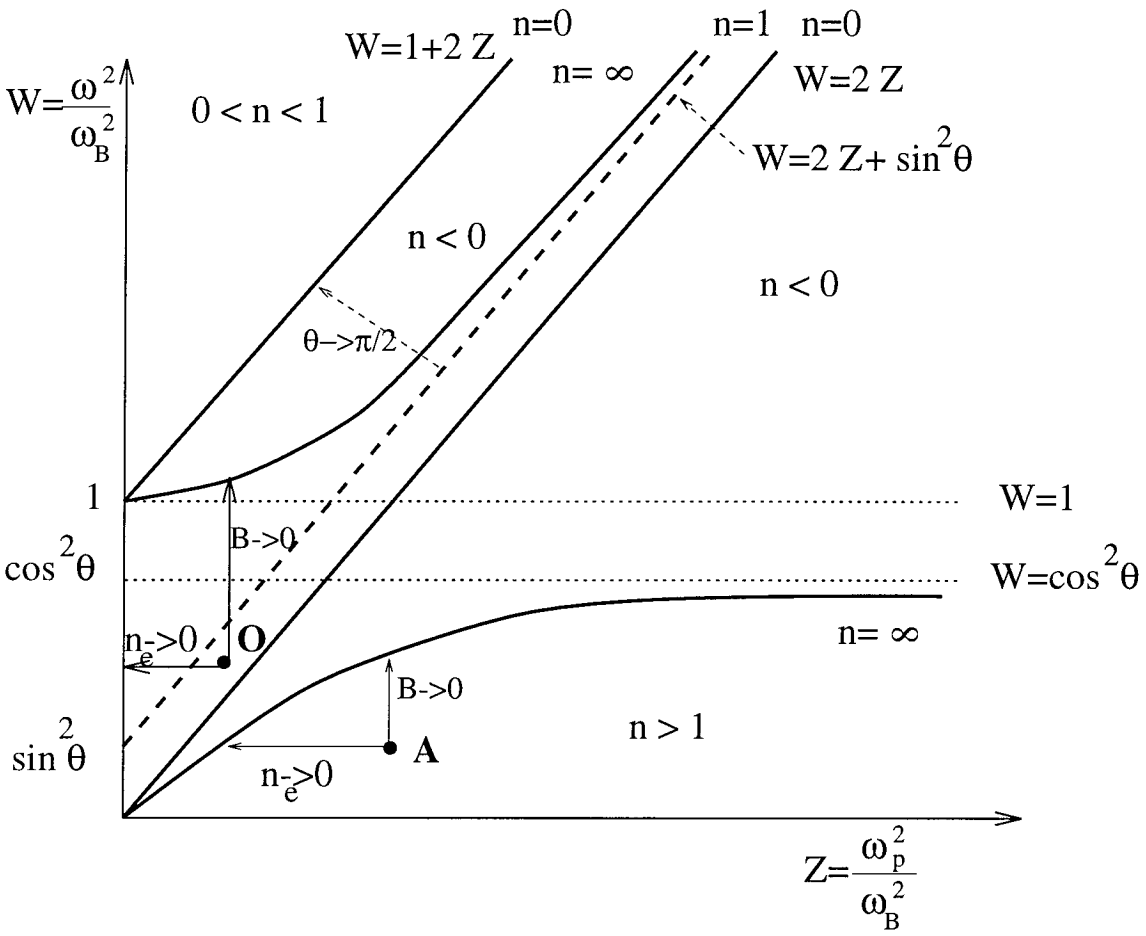

Figure 5.5: CMA diagram for the O and Alfvén modes. Vacuum case corresponds to $Z = 0$. On the axis $W = 0$ refractive index is $n = 1$. Resonances occur at $n = \infty$ and reflections occur at $W = 1 + 2Z$ and $W = 2Z$ ($n = 0$). The curve $W = 1 + 2Z$ corresponds to the upper hybrid wave $\omega^2 = \omega_B^2 + 2\omega_p^2$ and the curve $W = 2Z$ corresponds to the plasma wave $\omega^2 = 2\omega_p^2$. Typical O waves (denotes by **O**) in the pulsar magnetosphere have $Z \ll 1$, $2Z < W \ll 1$. Typical Alfvén modes (denotes by **A**) in the pulsar magnetosphere have $W \ll 1$ and $n > 1$. The arrows $B \to 0$, $n \to 0$ and $\theta \to \pi/2$ indicate correspondingly adiabatic tracks for constant density and decreasing magnetic field, constant magnetic field and decreasing density and increasing angle of propagation.

5.4.3 Polarization of Waves in Cold Plasma

To find the polarizations of the waves, we construct a matrix of cofactors of Λ (Melrose 1978c):

$$\lambda_{\alpha\beta} = n^4 k_\alpha k_\beta - n^2 \left(k_\alpha k_\beta \epsilon_{\gamma\gamma} + \delta_{\alpha\beta} k_\gamma k_\eta \epsilon_{\gamma\eta} - k_\alpha k_\gamma \epsilon_{\gamma\beta} - k_\beta k_\gamma \epsilon_{\alpha\gamma}\right) + \frac{1}{2}\delta_{\alpha\beta}\left(\epsilon_{\gamma\gamma}^2 - \epsilon_{\gamma\eta}\epsilon_{\eta\gamma}\right) + \epsilon_{\alpha\gamma}\epsilon_{\gamma\beta} - \epsilon_{\gamma\gamma}\epsilon_{\alpha\beta} \tag{5.55}$$

Then the polarization vectors may be chosen as columns of $\lambda_{\alpha\beta}$.

For the cold plasma the elements of $\lambda_{\alpha\beta}$ are

$$\begin{aligned}
\lambda_{xx} &= \left(-1 + n^2 - \frac{2\omega_p^2}{-\omega^2 + {\omega_B}^2}\right)\left(-1 + \frac{2\omega_p^2}{\omega^2} + n^2 \sin^2\theta\right) \\
\lambda_{x\phi} &= n^2\left(-1 + n^2 + \frac{2\omega_p^2}{\omega^2 - {\omega_B}^2}\right)\cos\theta\,\sin\theta = \lambda_{zx} \\
\lambda_{rr} &= -\left(\left(-1 + n^2 + \frac{2\omega_p^2}{\omega^2}\right)\left(1 + \frac{2\omega_p^2}{-\omega^2 + {\omega_B}^2}\right)\right) + \frac{2n^2 {\omega_B}^2 \omega_p^2 \cos^2\theta}{\omega^2\left(-\omega^2 + {\omega_B}^2\right)} \\
\lambda_{\phi\phi} &= \left(1 - n^2 + \frac{2\omega_p^2}{-\omega^2 + {\omega_B}^2}\right)\left(1 + \frac{2\omega_p^2}{-\omega^2 + {\omega_B}^2} - n^2\cos^2\theta\right)
\end{aligned} \tag{5.56}$$

We note that these relations are exact in frequency.

For the extraordinary mode using (5.34) for the refractive index in (5.56), we find the polarization vector for the extraordinary mode $e_X = (0, 1, 0)$. For the ordinary and Alfvén modes using (5.35) for the refractive index in (5.56), we obtain the ratio of the electric field components in the wave:

$$\frac{E_x}{E_z} = -\frac{\left(\omega^2 - {\omega_B}^2\right)\left(\omega^2 - 2\omega_p^2\right)\cot\theta}{\omega^2\left(\omega^2 - {\omega_B}^2 - 2\omega_p^2\right)} \tag{5.57}$$

For the points far from the cross-over point, we can use the approximation of a very strong magnetic field to find

$$\frac{E_x}{E_z} = \left(-1 + \frac{2\omega_p^2}{\omega^2}\right)\left(1 - 2\frac{\omega_p^2}{\omega_B^2}\right)\cot\theta \tag{5.58}$$

Using the relation (5.57) we can estimate the polarization of the ordinary wave at the cross-over point. We find that

$$\frac{E_x}{E_z} \approx \frac{2{\omega_p}^2\theta}{{\omega_B}^2} \tag{5.59}$$

For the angles smaller than $\frac{\omega_p^2}{\omega_B^2}$, the ordinary wave is quasi-longitudinal at the cross-over point and for larger angles it is quasi-transverse.

Relations (5.58) and (5.59) allow us to find the normalized polarization vectors:

$$e_O = \begin{cases} \left\{\cos\theta\left(1-\frac{2\omega_p{}^2\sin^2\theta}{\omega^2}\right), 0, \left(1+\frac{2\omega_p{}^2\cos^2\theta}{\omega^2}\right)\sin\theta\right\} + O\left(\frac{\omega_p^2}{k^2c^2}\right) & kc \gg \omega_p \\ \left\{\frac{-\left(k^2\sin(2\theta)\right)}{4\omega_p^2}, 0, 1\right\} + O\left(\frac{k^2c^2}{\omega_p^2}\right) & kc \ll \omega_p \end{cases} \tag{5.60}$$

$$e_O = \left\{ \begin{array}{ll} \left\{\frac{\omega_B{}^2\theta}{\omega_0{}^2}, 0, -1\right\} & \theta \ll \frac{2\omega_p^2}{\omega_B^2} \\ \left\{1, 0, -\frac{\omega_0{}^2\csc\theta\sec\theta}{\omega_B{}^2}\right\} & \theta \gg \frac{2\omega_p^2}{\omega_B^2} \end{array} \right| \quad \omega \approx \omega_0 \tag{5.61}$$

$$e_A = \begin{cases} \left\{\left(1+\frac{2\omega_p{}^2\cos^2\theta}{k^2}\right)\sin\theta, 0, \cos\theta\left(1-\frac{2\omega_p{}^2\sin^2\theta}{k^2}\right)\right\} + O\left(\frac{\omega_p^2}{k^2}\right) & kc \gg \omega_p \\ \left\{1, 0, \frac{\omega^2\tan\theta}{2\omega_p^2}\right\} + O\left(\frac{k^2c^2}{\omega_p^2}\right) & kc \ll \omega_p \end{cases} \tag{5.62}$$

which are accurate to $O\left(\frac{\omega_p^2}{\omega_b{}^2}\right)$.

5.5 Pulsar Frame

The dispersion relations in the pulsar frame are complicated even for the case of a cold plasma. The waves propagating in different directions have different dispersion relations. So that the dispersion equation for the X mode becomes a fourth order equation for $\omega(\mathbf{k})$. To simplify the consideration we will use the low frequency approximation from the very beginning, i.e., we expand all the relevant relations in $1/\omega_B$.

First we consider forward propagating waves which in the plasma frame had $\theta \ll 1$. We obtain

$$\omega'_X = k'c(1 - \frac{\omega_p'^2}{4\gamma_p^3\omega_B^2})$$

$$\omega'_O = \begin{cases} k'c\left(1 - \frac{\omega_p'^2}{4\gamma_p^2\omega_B^2} + \frac{\gamma_p\omega_p'^2\sin^2\theta'}{c^2k'^2}\right) & \text{if } k'c \gg \gamma_p\omega'_p \\ v_pk' + \frac{\sqrt{2}\omega'_p}{\gamma_p^{3/2}} & \text{if } k'c \ll \gamma_p\omega'_p \end{cases}$$

$$\omega'_A = \begin{cases} k'c\cos\theta'\left(1 - \frac{\omega_p'^2}{4\gamma_p^3\omega_B^2} - \frac{c^2k'^2\sin^2\theta'}{4\gamma_p\omega_p'^2}\right) & \text{if } k'c \ll \gamma_p\omega'_p \\ v_pk' + \frac{\sqrt{2}\omega'_p\cos\theta'}{\gamma_p^{3/2}} & \text{if } k'c \gg \gamma_p\omega'_p \end{cases} \tag{5.63}$$

(we remind that $\omega'_p = \omega_p/\sqrt{\gamma_p}$).

The cross-over point is

$$\omega_o'^2 = \frac{2\omega_p'^2}{\gamma_p} + 4\gamma_p^2\omega_B^2\theta'^2 \tag{5.64}$$

For the waves propagating backwards in the plasma frame we give only relations for parallel propagation.

$$\omega_t' = -k'c\left(1 - \frac{4\gamma_p\omega_p'^2}{\omega_B^2}\right) \tag{5.65}$$

$$\omega_l' = -v_p k' + \frac{\sqrt{2}\omega_p'}{\gamma_p^{3/2}} \tag{5.66}$$

5.6 Waves in a Relativistic Pair Plasma with Identical Distributions of Electrons and Positrons

5.6.1 Effects of Thermal Motion on Wave Dispersion

In this section we consider wave propagation in the relativistic, strongly magnetized electron-positron plasma. The thermal motion of the plasma particles changes the dispersion relations of the waves, thus changing the conditions for the wave excitation. The thermal motion of plasma particles affects considerably the dispersion of the Alfvén mode at frequencies $\omega \geq \omega_p$ and the dispersion of the ordinary mode frequencies $\omega \leq \omega_p$. The corresponding dispersion relations are qualitatively different from the cold case. Another important *quantitative* modification is in the dispersion relation of the extraordinary mode. The difference of the phase speed of the extraordinary mode (parameter δ) is roughly proportional to $< 1/\gamma^3 >$ (Eq. 5.86), e.g., δ is decreased considerably by the bulk streaming of the plasma. In the relativistic streaming plasma there are many particles with low Lorentz factors. This results in an increase of δ which relaxes the conditions for the development of the cyclotron and curvature drift instabilities.

5.6.2 Distribution Functions

To estimate the thermal effects on the plasma mode, we use the two kinds of distribution functions: (i) waterbag distribution

$$f(p_z) = \begin{cases} \frac{n_p}{2p_T}, & \text{if } -p_T < p_z < p_T \\ 0, & \text{otherwise} \end{cases} \tag{5.67}$$

(here $p_T \approx mc\gamma_T$ is the scatter in moments) and (ii) relativistic Maxwellian distribution (see also Appendices D and E for the calculations of the relevant moments of the distribution)

$$f(p_z) = \frac{n_p}{2K_1(\beta_T)} \exp\{-\beta_T p_\mu U^\mu\} \tag{5.68}$$

Both these distributions are "fast falling" at large moments. This is an important factor for the dispersion relation of plasma waves (see below). The advantage of the water bag distribution is that the various moments of the distribution can be easily calculated. The relativistic Maxwellian distribution is explicitly Lorentz-invariant (see Appendix D for details of Lorentz transformation).

The relevant moments of the distributions are summarized in Table 5.1 for the water bag distribution (in the plasma frame only) and in Table D.1 for the relativistic Maxwellian distribution (in both plasma and pulsar frame).

In what follows we identify $2\gamma_T \equiv T_p$ to consolidate the average energies for the case of two distributions.

$<\gamma>$	$\gamma_T/2$
$<pv>$	$\gamma_T/2$
$<\frac{1}{\gamma}>$	$\frac{\log\gamma_T}{\gamma_T}$
$<\frac{1}{\gamma^3}>$	$\frac{1}{\gamma_T}$

Table 5.1: Relevant moments of the water bag distribution in its rest frame (dimensionless units). It is assumed that $p_T/m_ec \approx \gamma_T \gg 1$.

The water bag distribution is generally a good approximation for the account of the thermal motion of the particles. Its major drawback is the absence of a tail of high energy particles that can resonate with the waves in the plasma. The Cherenkov resonance on the tail particles will result in a strong damping of the waves. The cyclotron resonance on the tail particles may result in a wave excitation if the distribution function is asymmetric with a long high energy tail. The condition, that the Cherenkov resonance is unimportant, is that the phase speed of the waves in plasma is much larger than the thermal velocity of the particles. In the case of the idealized water bag distribution, this condition has to be put in by hand. Whenever the phase speed of the wave becomes comparable to the thermal velocity, the waves should be considered strongly damped and nonexistent. Therefore, we expect that the high frequency branch of the Alfvén wave, which in the limit of cold plasma had a very low phase velocity, will be strongly damped.

Here, we should also mention a long standing controversy about the dispersion of the longitudinal waves and the possibility of the two stream instabilities in the relativistic plasma. In the initial work (Silin 1960) and later works (Suvorov & Chugunov 1975), it was stated that the relativistic plasma does not support subluminous longitudinal waves. This problem has been considered anew by Tsytovich & Kaplan 1972 who found subluminous waves. The controversy has been resolved by Lominadze & Mikhailovskii 1978, who demonstrated the existence of the subluminous waves in the range $0 < n - 1 < 1/ <\gamma>^2$ ($n \approx 1$), provided that the third moment of the distribution ($<\gamma^3>$) is finite (here n is the refractive index and $<\gamma> \gg 1$ is the average Lorentz factor of the plasma particles). Thus, when the distribution function falls off at large momenta slower than $\frac{1}{\gamma^4}$ subluminous plasma waves do not exist.

For the water bag distribution, the dispersion of the plasma waves for the parallel propagation is given by Eq. (5.78). We find that $n - 1$ becomes larger than $1/T_p^2$ for $\omega >$ several times ω_o. For larger frequencies the longitudinal plasma waves are either strongly damped or do not exist at all (Silin 1960).

5.6.3 Dispersion Relations in Relativistic Pair Plasma

To simplify the analysis we will use the low frequency approximation $\omega \ll \omega_B$ and the assumption of a very strong magnetic field $\frac{T_p \omega_p^2}{\omega_B{}^2} \ll 1$ from the very beginning. The dielectric tensor is then given by

$$\begin{aligned} \epsilon_{xx} &= 1 + d\, T_p \left(1 + n^2\, \beta_T^2\, \cos^2\theta\right) = \epsilon_{yy} \\ \epsilon_{\phi\phi} &= 1 - \frac{2\, n^2\, \omega_p^2}{T_p\, \left(1 - n^2\, \beta_T^2\, \cos^2\theta\right)} + d\, T_p\, n^2 \sin^2\theta \\ \epsilon_{xr} &== \epsilon_{rx} = \epsilon_{x\phi} = \epsilon_{\phi x} = \epsilon_{r\phi} = \epsilon_{\phi r} \end{aligned} \tag{5.69}$$

where

$$d = \frac{\omega_p^2}{\omega_B^2} \tag{5.70}$$

The normal modes of a hot plasma are given by the solution of (5.32) with the dielectric tensor (5.69). Similarly to the cold case, Eq.(5.69) factorizes into a dispersion relation for the extraordinary mode

$$\omega^2 = k^2 c^2 \left(1 - d T_p \left(1 + \beta_T^2\, \cos^2\theta\right)\right) \tag{5.71}$$

and a dispersion relation for the coupled ordinary and Alfvén modes (not given here). This equation may be solved in the approximation of infinitely strong magnetic field:

$$\begin{aligned} n^2 = \frac{1}{\left(4\,\omega_p^2 + 2\, T_p\, k^2 c^2\, \beta_T^2\right)\, \cos^2\theta} \Bigg(& T_p\, k^2 c^2 + 2\,\omega_p^2 + T_p\, k^2 c^2\, \beta_T^2\, \cos^2\theta \\ & \pm \Big(\left(T_p\, k^2 c^2 + 2\,\omega_p^2\right)^2 - 2\, T_p\, k^2\, c^2 \left(T_p\, k^2 c^2\, {\beta_T}^2 - 2\,\omega_p^2\, \left(-2 + \beta_T^2\right)\right) \cos^2\theta \\ & + T_p^2\, k^4 c^4\, \beta_T^4\, \cos\theta^4 \Big)^{1/2} \Bigg) \end{aligned} \tag{5.72}$$

where the plus sign corresponds to an Alfvén wave and minus to an O wave. The dispersion relations for the ordinary and Alfvén waves in a hot pair plasma are plotted in Fig. 5.6. It is also possible to obtain the asymptotic expansion of the dispersion relation of Alfvén and ordinary modes in the limits of very small and very large wave vectors. In the limit $kc \gg \sqrt{T_p}\omega_p$ we have

$$\omega^2 = \begin{cases} c^2\, k^2\, \beta_T^2\, \cos^2\theta \left(1 - \frac{2\,\omega_p^2}{c^2\, T_p^3\, k^2\, \beta_T^2 \left(-1 + \beta_T^2\, \cos^2\theta\right)}\right) & \text{Alfvén wave} \\ c^2\, k^2 \left(1 - d\, T_p \left(1 + \beta_T^2\, \cos^2\theta\right)\right) \left(1 - \frac{2\,\omega_p^2\, \sin^2\theta}{c^2\, T_p\, k^2 \left(-1 + \beta_T^2\, \cos^2\theta\right)}\right) & \text{O-wave} \end{cases} \tag{5.73}$$

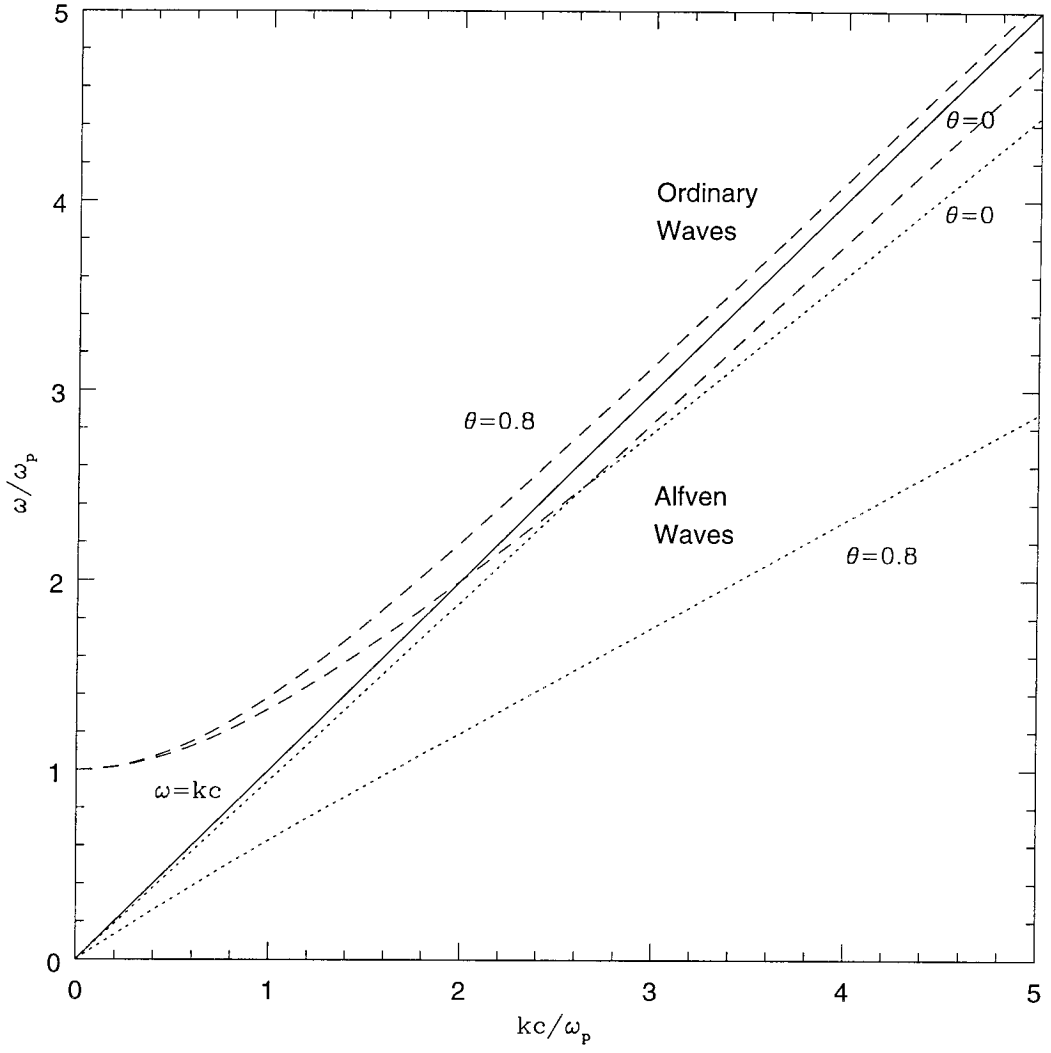

Figure 5.6: Dispersion curves for the waves in a hot electron-positron plasma in the plasma frame in the limit $\omega \ll \omega_B$. Only Alfvén (dotted) and ordinary (dashed) modes are shown. The dispersion curve for the extraordinary mode is very similar to the cold case. For the illustrative purposes we have chosen $T_p = 2$. The dispersion curves of the ordinary and Alfvén modes intersect only for parallel propagation.

while in the opposite limit $kc \ll \sqrt{T_p}\omega_p$

$$\omega^2 = \begin{cases} c^2\,k^2\,\cos^2\theta\,\left(1 - d\,T_p\,\left(1+\beta_T^2\,\cos^2\theta\right)\right)\left(1 - \frac{c^2\,k^2\sin^2\theta}{2\,T_p\,\omega_p^2}\right) & \text{Alfvén wave} \\ \frac{2\,\omega_p^2}{T_p} + c^2\,k^2\,\left(\beta_T^2\,\cos^2\theta + \sin^2\theta\right) & \text{O-wave} \end{cases} \tag{5.74}$$

We will give here also the relevant phase speed of the waves in the limit of small angles of propagation.

$$\begin{aligned} v_X^{ph} &= c\left(1 - \frac{\omega_p^2 T_p}{\omega_B^2}\right) && \text{X mode} \\ v_O^{ph} &= c\left(1 - \frac{\omega_p^2 T_p}{\omega_B^2} + \frac{\omega_p^2 T_p \sin^2\theta}{k^2c^2}\right) && \text{O-wave, } kc \gg \sqrt{T_p}\omega_p \\ v_A^{ph} &= c\,\cos\theta\left(1 - \frac{\omega_p^2 T_p}{\omega_B^2} - \frac{k^2c^2\sin^2\theta}{4\omega_p^2 T_p}\right) && \text{Alfvén wave} \end{aligned} \tag{5.75}$$

The X mode is always superluminous and the Alfvén mode is always subluminous. The ordinary mode is superluminous for small small vectors $kc \ll \sqrt{T_p}\omega_p$ and may become subluminous for very small angles of propagation $\theta \ll \sqrt{T_p}\omega_p/\omega_B$.

The cross-over point (where the phase speed of the ordinary mode become equal to the speed of light) is now $\omega_o^2 = k_o^2c^2 \approx 2\,T_p\omega_p^2 + {\omega_B}^2\sin^2\theta$. Using relation (5.41) we can approximate the dispersion relation near the cross-over point as

$$\omega = kc - \eta(k - k_0), \qquad \eta = \frac{1}{T^2} - \frac{(\omega_B^4 + 4T_p^3\omega_B^2\omega_p^2)\theta^2}{16T_p^6\omega_p^4} \tag{5.76}$$

Another analytical solution to the dispersion relation we can obtain for the parallel propagation. Then we have two transverse wavs with the dispersion

$$\omega^2 = k^2\,c^2\left(1 - d\,T_p(1+\beta_T^2)\right) \tag{5.77}$$

and a plasma wave

$$\omega^2 = \frac{2\,\omega_p^2}{T_p} + k^2c^2\beta_T^2 \tag{5.78}$$

It is also useful to represent the dispersion relations for the plasma waves near the cross-over point in the form (5.42). For the relativistic plasma components, we find

$$\begin{aligned} &\left(\frac{\partial K(\omega,k)}{\partial k}\right)\Big/\left(\frac{\partial K(\omega,k)}{\partial \omega}\right) = \left(1 - \frac{<\gamma(1+v)^2>}{<\gamma^3(1+v)^3>}\right) \\ &\omega \approx kc - \frac{1}{T^2}(k - k_0) \end{aligned} \tag{5.79}$$

The phase speed for the high frequency asymptotic of the plasma wave (5.78) approaches the

phase speed of the thermal particles $c\beta_T$. For the more realistic distribution function, these parts of the dispersion relation will be strongly damped on the Cherenkov resonance with the thermal tail particles. The high frequency asymptotic of the plasma wave belongs to the Alfvén wave. From this we make a conclusion that the high frequency ($kc \geq T_p\omega_p$) part of the Alfvén wave is strongly damped and does not propagate.

In most of the calculations to follow we will assume that the plasma is very hot: $p_T/mc \gg 1$ and $T_p = \sqrt{p_T^2/(mc)^2 + 1} \gg 1$.

Polarization of waves in a hot plasma

In the case of a hot plasma the matrix of cofactors $\lambda_{\alpha\beta}^{(h)}$ is quite complicated and is not given here. Simple relations may be obtained in the limit $\omega_B = \infty$ and near the cross-over point for the ordinary wave. In the limit $\omega_B = \infty$ we find the elements of the matrix $\lambda_{\alpha\beta}^{(h)}$

$$\begin{aligned}
\lambda_{xx}^{(h)} &= \left(-1+n^2\right)\left(-1-\frac{2\,\omega_p^2}{T_p\,\omega^2\,\left(-1+n^2\,v_o^2\,\cos^2\theta\right)}+n^2\sin^2\theta\right)\\
\lambda_{xz}^{(h)} &= n^2\,\left(-1+n^2\right)\cos\theta\,\sin\theta = \lambda_{zx}^{(h)}\\
\lambda_{yy}^{(h)} &= 1-n^2-\frac{2\,\omega_p^2\,\left(-1+n^2\,\cos^2\theta\right)}{T_p\,\omega^2\,\left(-1+n^2\,v_o^2\,\cos^2\theta\right)}\\
\lambda_{zz}^{(h)} &= \left(-1+n^2\right)\,\left(-1+n^2\,\cos^2\theta\right)
\end{aligned} \tag{5.80}$$

For the extraordinary mode we find that the polarization vector is $e_X = (0,1,0)$, while for the ordinary mode

$$\frac{E_x}{E_z} = \frac{n^2\,\cos\theta\,\sin\theta}{-1+n^2\,\cos^2\theta} \tag{5.81}$$

These relations are valid for the points not close to the cross-over point of the ordinary wave, where the approximation $\omega_B = \infty$ is applicable. Near the cross-over point, $n = 1$, we find

$$\frac{E_x}{E_z} = -\frac{{\omega_B}^2\theta}{4T_p^3{\omega_p}^2} \tag{5.82}$$

For oblique propagation the behavior of the ordinary mode at the cross-over point changes at

$$\theta \approx 4T_p^3 d \tag{5.83}$$

For smaller angles the ordinary mode is quasiparallel at the cross-over point while, for large angles, it is quasitransverse.

The polarization vectors for the ordinary and Alfvén modes are then given by

$$e_O^{(h)} = \begin{cases} \left\{\cos\theta\left(1-\frac{2\,T_p\,\omega_p^2\sin^2\theta}{c^2k^2}\right), 0, -\left(\left(1+\frac{2\,T_p\,\omega_p^2\cos^2\theta}{c^2k^2}\right)\sin\theta\right)\right\}, & kc \gg \omega_p \\ \left\{\frac{{\omega_B}^2\theta}{{\omega_0}^2}, 0, -1\right\} & \theta \ll \frac{2\,T_p\omega_p^2}{\omega_B^2},\ \omega = \omega_0^{(h)} \\ \left\{1, 0, -\frac{{\omega_0}^2}{\sin\theta\cos\theta{\omega_B}^2}\right\} & \theta \gg \frac{2\,T_p\omega_p^2}{\omega_B^2},\ \omega = \omega_0^{(h)} \end{cases} \tag{5.84}$$

$$e_A^{(h)} = \left\{1, 0, \frac{\omega^2\,\tan\theta}{2\,T_p\,\omega_p^2}\right\} \qquad kc \ll \omega_p \tag{5.85}$$

5.6.4 Dispersion Relation for Hot Pair Plasma in Pulsar Frame

The dispersion relations for the forward propagating modes in the pulsar frame in the limit $\omega' \ll \omega_B$ are

$$\begin{aligned} \omega'_X &= k'c\left(1-\frac{{\omega'_p}^2T_p}{4\,\omega_B^2\,\gamma_p^3}\right) \\ \hat{\omega}_O &= k'c\left(1-\frac{{\omega'_p}^2\,T_p}{4\,\gamma_p^3\,\omega_B^2}+\frac{\gamma_p\,{\omega_p}'^2T_p\sin^2\theta'}{c^2\,k^2}\right) \qquad \text{if } k'c \gg \sqrt{T_p}\,\gamma_p\omega'_p \text{ and } \theta' < 1/T_p \\ \hat{\omega}_A &= k'c\cos\theta'\left(1-\frac{{\omega'_p}^2\,T_p}{2\,\gamma_p^3\,\omega_B^2}-\frac{c^2\,{k'}^2\sin^2\theta'}{2\,T_p\,\gamma_p\,{\omega_p}'^2}\right) \qquad \text{if } kc \ll \sqrt{T_p}\,\gamma_p\omega_p \end{aligned} \tag{5.86}$$

These relationships are valid for the frequencies satisfying the inequality

$$\omega \ll \gamma_p\,\omega_B/T_p \tag{5.87}$$

This is a condition that in the reference frame of the plasma the frequency of the waves is much smaller that the typical cyclotron frequency of the particles ω_B/T_p.

The cross-over point is

$$\omega_o'^2 = \frac{2\omega_p'^2T_p}{\gamma_p} + 4\gamma_p^2\omega_B^2\theta'^2 \tag{5.88}$$

5.7 Waves in a Pair Plasma with Different Distributions of Electrons and Positrons

5.7.1 Response Tensor for Hot Pair Plasma with Streaming Distributions

We first derive the dielectric tensor for a cold, one-dimensional electron-positron plasma with equal densities and different average energies of electrons and positrons. In this case all nine components of the dielectric tensor are nonzero. We assume that the fast component of the plasma consists of positrons. If the charges of the fast and slow components are interchanged, then all the results of this section will be valid provided that the circular component of the polarization of the natural modes is reversed.

We assume that though the distribution may be ultrarelativistic, the contribution to the anti-hermitian part of the dielectric tensor from the cyclotron resonance is negligible so that we can use a frame invariant "low frequency approximation" $\omega_B^2/\gamma^2 \gg (\omega - k_\phi v_\phi)^2$.

Though it is expected that the relaxation time of the plasma present on the open lines in the neutron star magnetosphere due to the Coulomb collisions is much longer than the dynamical time, we still expect a large initial spread in the moments of the plasma particles (Arons 1981). As an approximation to the poorly constrained distribution, we use a relativistic streaming, one-dimensional Maxwell distribution:

$$f(p_\phi)_\alpha = \frac{n_\alpha}{2\,\gamma_\alpha K_1(\frac{1}{T_\alpha})} \exp\{\frac{-p_\mu U_\alpha^\mu}{T_\alpha}\} \tag{5.89}$$

Here T_α are the temperatures of the electrons and positrons of the plasma in the units of $m_e\,c^2$, p_μ is the 4-momentum of a particle and $U_\alpha^\mu = (\gamma_\alpha,\, \gamma_\alpha\beta_\alpha)$ is the 4-velocity, γ_α is the γ-factor and $\beta_\alpha = \mathbf{v}_\alpha/c$ is the three velocity of the system of reference where the particular component is at rest.

The calculations of the components of the dielectric tensor are outlined in the Appendix M. The resulting expressions are

$$\begin{aligned}
\epsilon_{xx} &= 1 + d\sum_\alpha \gamma_\alpha \left(\frac{K_0+K_2}{2K_1}\,(1 - n\,\cos\theta\,\beta_\alpha)^2 \,+\, T_\alpha\,(\beta_\alpha - n\,\cos\theta)^2 \right) = \epsilon_{rr} \\
\epsilon_{xr} &= i\,d\sum_\alpha \frac{\omega_B}{\omega}\, sign_\alpha\,(1\, - n\,\cos\theta\,\beta_\alpha) = -\epsilon_{rx} \\
\epsilon_{x\phi} &= d\sin\theta n \sum_\alpha \gamma_\alpha \left(\frac{K_0+K_2}{2K_1}\,\beta_\alpha\,(1 - n\,\cos\theta\,\beta_\alpha) \,+ T_\alpha(\beta_\alpha - n\,\cos\theta) \right) = \epsilon_{\phi x} \\
\epsilon_{r\phi} &= i\,d\,n\,\sin\theta\,\frac{\omega_B}{\omega}\sum_\alpha\, sign_\alpha\,\beta_\alpha = -\epsilon_{\phi r} \\
\epsilon_{\phi\phi} &= 1 - \sum_\alpha I_\alpha(\theta,\omega,n) + d\,n^2\,\sin^2\theta\,\sum_\alpha \gamma_\alpha \left(T_\alpha + \beta_\alpha^2\,\frac{K_0+K_2}{2K_1} \right)
\end{aligned} \tag{5.90}$$

where $d = \omega_p^2/\omega_B^2$, $\omega_p^2 = 4\pi n_\alpha e_\alpha^2/m_\alpha$ is the plasma frequency expressed in terms of the density n_α measured in the laboratory frame, e_α is the charge of species α (charge of an electron is $-e$), $n = kc/\omega$ is the refractive index, $K_s(1/T_\alpha)$ is the modified MacDonald functions, $sign_\alpha$ is the sign of the charge α, and we define

$$I_\alpha(\theta,\omega,n) = \frac{4\pi e_\alpha^2}{m_\alpha}\int \frac{dp_\phi}{\gamma^3} f_\alpha \frac{1}{(\omega - k_\phi v_\phi)^2} \tag{5.91}$$

We note that the temperatures T_α, cyclotron frequency ω_B and the quantities I_α are frame invariant. The frame invariance of I_α follows from the frame invariance of dp_ϕ/γ , f_α and $\gamma(\omega - k_\phi v_\phi)$ (the latter is the product of the wave and momentum four vectors).

I is a very sensitive function of the wavelength, distribution functions and angles of propagation with respect to the magnetic field. For the propagation of the quasi-transverse waves with a near vacuum dispersion $n \approx 1$ and for the wave vectors not in the vicinity of the cross-over points (where the dispersion relations for the quasi-longitudinal and quasi-transverse waves intersect) [3], the refractive index n in the expressions for I may be set to unity, but even in that case the angle and distribution function dependence of $\epsilon_{\phi\phi}$ is very complicated. Generally, for the frequencies much larger than the cross over frequency $I \ll 1$, and for frequencies much smaller than than the cross over frequency $I \gg 1$. We will give the forms of I separately for the each case considered.

We would like to stress that we use a noninvariant $\omega_p = \sqrt{4\pi n_p' q^2/m_e}$, i.e., expressed in terms of the density in the laboratory frame. It is equal to $\omega_p\sqrt{\gamma_\alpha}$, where ω_p is the invariant plasma frequency in the rest frame of the particular component and γ_α is the γ-factor of the component's rest frame with respect to the laboratory frame. We also should note that, in the case of relativistic plasma, the actual frequency of Langmuir oscillation measured in the component's rest frame will be $\omega_p\sqrt{K_0/K_1}$, i.e., it will decrease due to thermal effects.

The dispersion relations look much simpler in the center-of-momentum reference frame so we first discuss in details the properties of the waves in that frame. The general Lorentz transformations to the pulsar frame from the center-of-momentum frame is very complicated and, as it turns out, it is simpler to solve the dispersion relations in pulsar frame independently. We will denote the quantities measured in the pulsar frame by the primes.

[3] The cross-over point for the ordinary wave is given by solving $\epsilon_{\phi\phi} = 0$ with n, the refractive index, set to unity.

5.8 Waves in a Cold Plasma with Streaming Components. Center-of-momentum Frame

5.8.1 Dielectric Tensor for the Cold Plasma in the Center-of-momentum Frame

In the cold plasma approximation we expand (5.90) for $T_\alpha \ll 1$. In the center-of-momentum frame the distribution functions are $f_\alpha = n_\alpha \, \delta(p_\phi \pm \gamma_o \, \beta_o m_\alpha c)$ and we have $v_\alpha = \pm \beta_o c$ and $\gamma_\alpha = \gamma_o = 1/\sqrt{1-\beta_o^2}$.

The dielectric permittivity is then given by

$$\begin{aligned}
\epsilon_{\phi\phi} &= \epsilon_{yy} = 1 + 2\,d\,\gamma_o\,\left(1 + n^2\,\beta_o^2\cos^2\theta\right) \\
\epsilon_{\phi\phi} &= 1 - \frac{2\,{\omega_p}^2\,\left(1 + n^2\,\beta_o^2\cos^2\theta\right)}{\omega^2\,{\gamma_o}^3\,\left(1 - n^2\,\beta_o^2\cos^2\theta\right)^2} + 2\,dn^2\,\sin^2\theta\,\beta_o^2\gamma_o^2 \\
\epsilon_{xr} &= -\epsilon_{rx} = 2\,i\,\sqrt{d}\,n^2\,\frac{\omega_p}{kc}\,\beta_o\,\cos\theta \\
\epsilon_{x\phi} &= \epsilon_{\phi x} = -2\,d\,n^2\,\gamma_o^2\,\beta_o\,\sin\theta\,\cos\theta \\
\epsilon_{r\phi} &= -\epsilon_{\phi r} = 2\,i\,\sqrt{d}\,n^2\,\frac{\omega_p}{kc}\,\beta_o\,\sin\theta
\end{aligned} \tag{5.92}$$

5.8.2 Dispersion Relations for Exactly Parallel and Perpendicular Propagation

For parallel propagation $\theta = 0$ the dispersion relation splits in two for the longitudinal plasma modes:

$$\epsilon_{\phi\phi} = 0 \tag{5.93}$$

and for the two transverse waves:

$$(n^2 - \epsilon_{\phi\phi})^2 + \epsilon_{rx}^2 = 0. \tag{5.94}$$

Eq. (5.93) describes plasma waves with the electric field of the wave parallel to the wave vector and (5.94) describes transverse waves. Using (5.92) we arrive at the following solutions for the plasma waves:

$$\omega^2 = \frac{{\omega_p}^2}{{\gamma_o}^3} + k^2c^2\,{\beta_o}^2 \pm \frac{\omega_p\,\sqrt{{\omega_p}^2 + 4\,{\gamma_o}^3\,k^2c^2\,{\beta_o}^2}}{{\gamma_o}^3} \tag{5.95}$$

One pair of solutions of (5.95), corresponding to the minus sign, will be called a slow branch. The other pair of solutions of (5.95), corresponding to the plus sign, consists of three parts belonging to the ordinary, extraordinary and Alfvén modes. The dispersion curves for these modes intersect

only for parallel propagation. In the case of oblique propagation the modes are always distinct. For parallel propagation we will distinguish longitudinal plasma modes, described by equation (5.93) and transverse modes, described by equation (5.94). We stress that, except for the slow Alfvén wave, which stays separate for any angle of propagation, the longitudinal plasma modes and the transverse modes are composed of the parts of ordinary, extraordinary and Alfvén branches (see Fig. 5.7).

For large wave vectors $kc \gg \omega_p/{\gamma_o}^{3/2}$, Eq. (5.95) gives four modes corresponding to the Langmuir waves in each component propagating in each direction:

$$\omega = \pm kc\beta_o \pm \frac{\omega_p}{\gamma_o^{3/2}} \tag{5.96}$$

For small wave vectors $kc < \omega_p/\gamma_o^{3/2}$, the ordinary branch gives the conventional Langmuir plasma waves with $\omega = \pm\sqrt{2}\,\omega_p/\gamma_o^{3/2}$ propagating in a positive and negative direction and the slow wave becomes unstable for $k < \sqrt{2}\,\omega_p/\gamma_o^{3/2}\,\beta_o$ corresponding to the conventional two-stream instability (see Fig. 5.7). The maximum growth rate of this instability is $Im(\omega)_{max} = \omega_p/({\gamma_o}^{3/2}\,\beta_o)$.

The slow branch, which is unstable at low frequencies, is always subluminous and the ordinary branch becomes subluminous at $kc > \sqrt{2}\,\gamma_o\,\omega_p\,\sqrt{1+\beta_o^2}$.

The solutions of Eq. (5.94) for the transverse waves in the plasma frame are

$$\omega^2 = \frac{kc\left(kc \pm 2\sqrt{d}\,\omega_p\,\beta_o - 2\,d\,\gamma_o\,kc\,{\beta_o}^2\right)}{1+2\,d\,\gamma_o} \tag{5.97}$$

In the low frequency approximation, the minus sign in (5.97) corresponds to the extraordinary mode and the plus sign corresponds to Alfvén mode, while in the high frequency approximation, the minus sign corresponds to the ordinary mode and the plus sign corresponds to extraordinary mode. (see Fig. 5.7). For parallel propagation we will call these modes fast (plus sign in (5.97)) and slow (minus sign in (5.97)) transverse waves.

The polarization of the fundamental modes is given by quantities K and T of Melrose 1978c:

$$\begin{aligned}
K &= \frac{i}{-{\epsilon_{x\phi}}^2 + \epsilon_{\phi\phi}\,\epsilon_{\phi\phi} - A\,n^2}\Bigg(\quad \epsilon_{\phi\phi}\,\epsilon_{yz}\,\cos\theta - \epsilon_{xr}\,\epsilon_{\phi\phi}\,\sin\theta \\
&\qquad\qquad + n^2\,\left(-\left(\epsilon_{yz}\,\cos\theta\right) + \epsilon_{xr}\,\sin\theta\right) + \epsilon_{x\phi}\,\left(\epsilon_{xr}\,\cos\theta - \epsilon_{yz}\,\sin\theta\right)\Bigg) \\
T &= \frac{i\,\left(\left(\epsilon_{x\phi}\,\epsilon_{yz} + \epsilon_{xr}\,\epsilon_{\phi\phi}\right)\,\cos\theta + \left(\epsilon_{xr}\,\epsilon_{x\phi} + \epsilon_{\phi\phi}\,\epsilon_{yz}\right)\,\sin\theta\right)}{-{\epsilon_{x\phi}}^2 + \epsilon_{\phi\phi}\,\epsilon_{\phi\phi} - A\,n^2} \\
&\text{where } A = \epsilon_{\phi\phi}\cos^2\theta + 2\,\epsilon_{x\phi}\,\cos\theta\,\sin\theta + \epsilon_{\phi\phi}\sin^2\theta
\end{aligned} \tag{5.98}$$

The waves are quasi-transverse for $K \approx 0$, circularly polarized for $T = \pm 1$ and linearly polarized

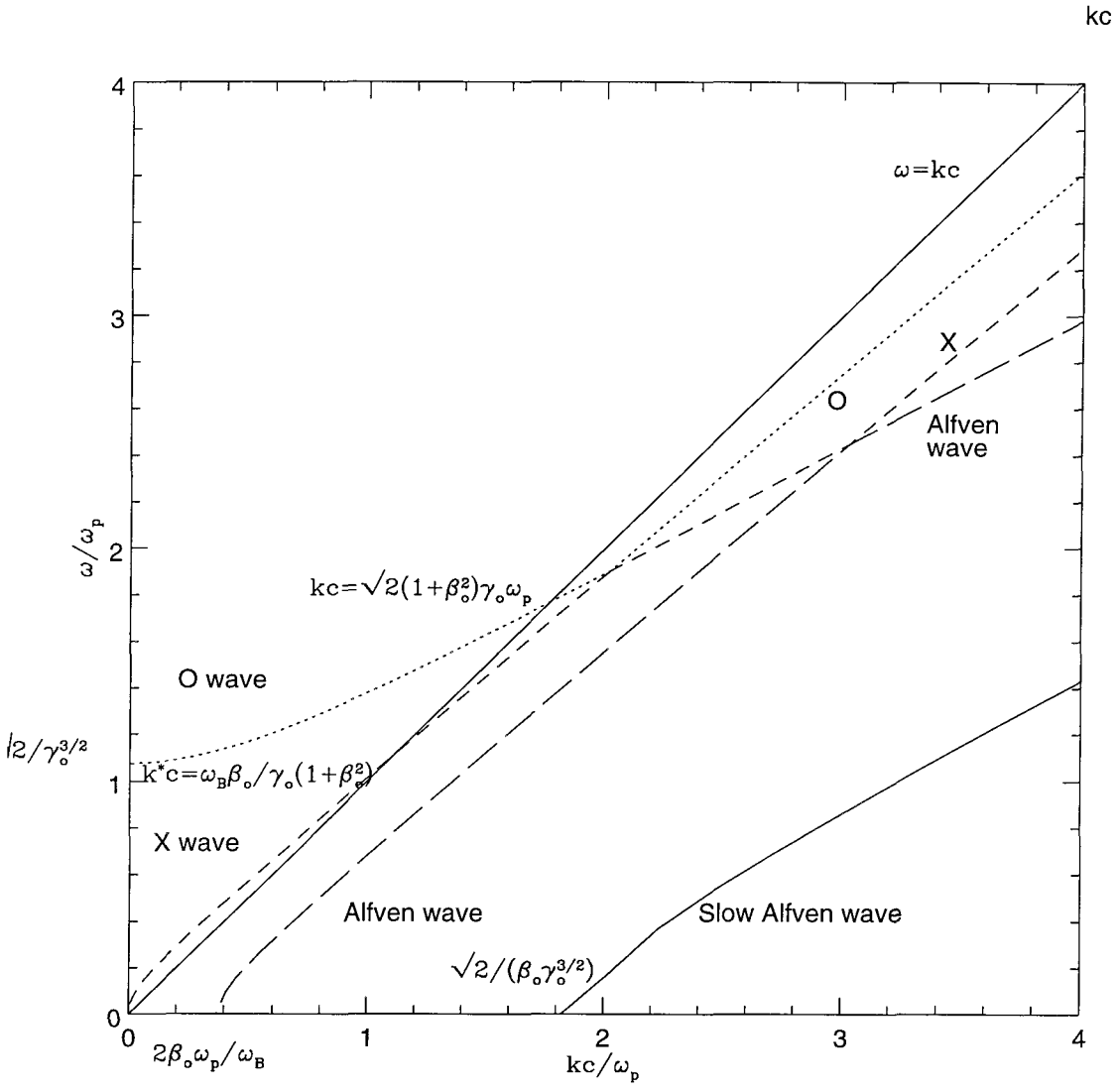

Figure 5.7: Dispersion curves in the center-of-momentum frame for the case of relative streaming of electrons and positrons for exactly parallel propagation with cutoff and cross-over points shown. The Lorentz factor of the relative flow is $\gamma_0 = 1.5$. There are four modes represented by the dotted (O mode), dashed (X mode), long dashed (Alfvén mode) and solid lines (slow Alfvén mode). The waves are subluminous if the dispersion curve lies below the vacuum dispersion $\omega = kc$. $kc/\omega_p = 2\beta_o\omega_p/\omega_B$ denotes the onset of cyclotron two-stream instability, $kc/\omega_p = 2^{1/2}/\beta_o\,\gamma_o$ denotes the onset of conventional two-stream instability, $k^*c = \omega_B\beta_o/\gamma_o(1+\beta_o^2)$ is a point when a fast transverse wave becomes subluminous and $kc = \left(2\,\gamma_o^3\,(1+\beta_o^2)\right)^{1/2}\omega_p$ is the point where the ordinary wave becomes subluminous. The ordinary branch has a cutoff at $\omega = \frac{2^{1/2}\omega_p}{\gamma_o}$.

for $T = 0$ or $T = \infty$. Using (5.97) we obtain

$$K_{ft} = 0, \qquad T_{ft} = -1,$$
$$K_{st} = 0, \qquad T_{st} = 1 \tag{5.99}$$

where ft stands for fast transverse and st for slow transverse mode. The waves are circularly polarized. The fast transverse wave propagating in the positive direction has a right circular polarization or negative helicity and slow transverse wave propagating in the positive direction has left circular polarization or positive helicity. This sense of polarization is determined by our choice of the sign of the charge of the ordinary component, which is, in turn, determined by the general structure of the pulsar magnetosphere (the product $\mathbf{\Omega}.\mathbf{B}$ at a given point in the magnetosphere). The appearance of the circular polarization in a plasma with the different charges having the same masses is due to the relative streaming of the plasma components.

The fact that the normal modes are circularly polarized for the parallel propagation may be seen as contradictory to our notions of ordinary and extraordinary modes, since in the magnetosonic theory the ordinary and extraordinary modes are defined as having linear polarization in the $\mathbf{k} \cdot \mathbf{B}$ plane and perpendicular to it. As we will see later, for oblique propagation the normal modes become linearly polarized which allows an identification with the conventional ordinary and extraordinary modes.

Eq. (5.97) shows two possible hydrodynamic instabilities for these branches:

(1) Firehose instability for $2\,d\,\gamma_o\,{\beta_o}^2 > 1$ for both modes

(2) Two-stream cyclotron instability for the slow transverse mode for $2\sqrt{d}\,\omega_p\,\beta_o\,/\,kc > 1$.

If the magnetic field is strong enough so that $2\,d\,\gamma_o\,{\beta_o}^2 \ll 1$ (this excludes the firehose instability), then for large wave numbers $kc \gg 2\sqrt{d}\,\omega_p\,\beta_o/\gamma_o$ (so we are far from the two-stream cyclotron instability) the asymptotic solutions are

$$\omega = \pm \left(kc \pm \sqrt{d}\,\omega_p\,\beta_o - d\,\gamma_o\,kc\,(1 + {\beta_o}^2) + d\frac{\omega_p^2\,\beta_o^2\,\gamma_o}{2\,k^2c^2} \right) \tag{5.100}$$

which describe two pairs of transverse waves propagating in each direction in the plasma frame. Slow transverse wave always stays subluminous while fast transverse wave is superluminous for $kc < \omega_B\,\beta_o\gamma_o\,\left(1 + \beta_o^2\right)$ and subluminous for larger wave vector. The dispersion curves for exactly parallel propagation are plotted in Fig. 5.7 for $\gamma_o = 1.2$, $d = \omega_p^2/\omega_B^2 = 1/10$ (the numerical values for the parameters were chosen only for the sake of graphically clarity).

For perpendicular propagation $\theta = \pi/2$ in the plasma frame the dispersion relations of the natural modes and their polarization vectors are (in the limit of strong magnetic field $d \ll 1$):

$$\omega_1^2(\theta=\pi/2)=k^2c^2(1-2d\gamma_o\,(1+\gamma_o^2\,\beta_o^2)) \qquad \mathbf{E}=\{0,\,E_y,\,-E_y\,i\,\gamma_o^3\,kc\,\beta_o\,/\omega_B\}$$
$$\omega_2^2(\theta=\pi/2)=k^2c^2+\frac{2\omega_p^2}{\gamma_o^3} \qquad \mathbf{E}=\{0,\,E_y,\,E_y\,i\,\omega_B/\,(\gamma_o^3\,\beta_o\,kc)\} \tag{5.101}$$

So we have two transverse elliptically polarized waves.

5.8.3 Waves in the Infinitely Strong Magnetic Field

For the infinitely strong magnetic field, the dispersion relation splits in two:

$$\begin{aligned} n^2&=1, && \mathbf{E}=\{0,E_y,0\}\\ (n^2\cos\theta^2-\epsilon_{\phi\phi})(n^2\sin\theta^2-\epsilon_{\phi\phi})-(n^2\cos\theta\sin\theta-\epsilon_{x\phi})^2&=0, && \mathbf{E}=\{E_x,\,0,\,E_\phi\}\end{aligned} \tag{5.102}$$

The vacuum dispersion relation corresponds to the linearly polarized wave whose electric vector is perpendicular to the **k-B** plane. This is the extraordinary mode. The second equation is for the mixed longitudinal- transverse wave. In the most general case it has three coupled branches corresponding to the ordinary, Alfvén and slow Alfven branches.

Setting $d=0$ in (5.92), the dispersion relation for the longitudinal- transverse wave in the plasma frame takes the form:

$$-1+n^2+\frac{2\,n^2\,{\omega_p}^2\,\left(1-n^2\cos\theta^2\right)\,\left(1+n^2\,\beta_o^2\cos\theta^2\right)}{c^2\,k^2\,{\gamma_o}^3\,\left(1-n^2\,\beta_o^2\cos\theta^2\right)^2}=0 \tag{5.103}$$

Eq. (5.103) is a cubic equation in n^2 and can be solved analytically. The solutions of (5.103) together with the vacuum solution for the t-wave are plotted on Fig. 5.8 for $\gamma_o=1.5$ and $\theta=0.5$.

In the case of oblique propagation in the infinitely strong magnetic field, the ordinary branch is always superluminous, while the Alfvén and slow Alfvén waves are always subluminous.

We will give here long and short wavelength asymptotic dispersion relations. For $kc\gg\sqrt{2}\omega_p/\gamma_o^{3/2}$ we have:

$$\begin{aligned} n_O^2&=1-\frac{2\left(\frac{\omega_p}{kc}\right)^2\,\left(1+\beta_o^2\cos\theta^2\right)\,\sin\theta^2}{{\gamma_o}^3\,\left(1-\beta_o^2\cos\theta^2\right)^2},\\ n_{SA}^2&=\frac{\sec\theta^2}{\beta_o^2}\left(1+\frac{2\,\frac{\omega_p}{kc}}{{\gamma_o}^3\,\beta_o^3\,\sqrt{1-\beta_o^2\cos\theta^2}}\right),\\ n_A^2&=\frac{\sec\theta^2}{\beta_o^2}\left(1-\frac{2\,\frac{\omega_p}{kc}}{{\gamma_o}^3\,\beta_o^3\,\sqrt{1-\beta_o^2\cos\theta^2}}\right),\end{aligned} \tag{5.104}$$

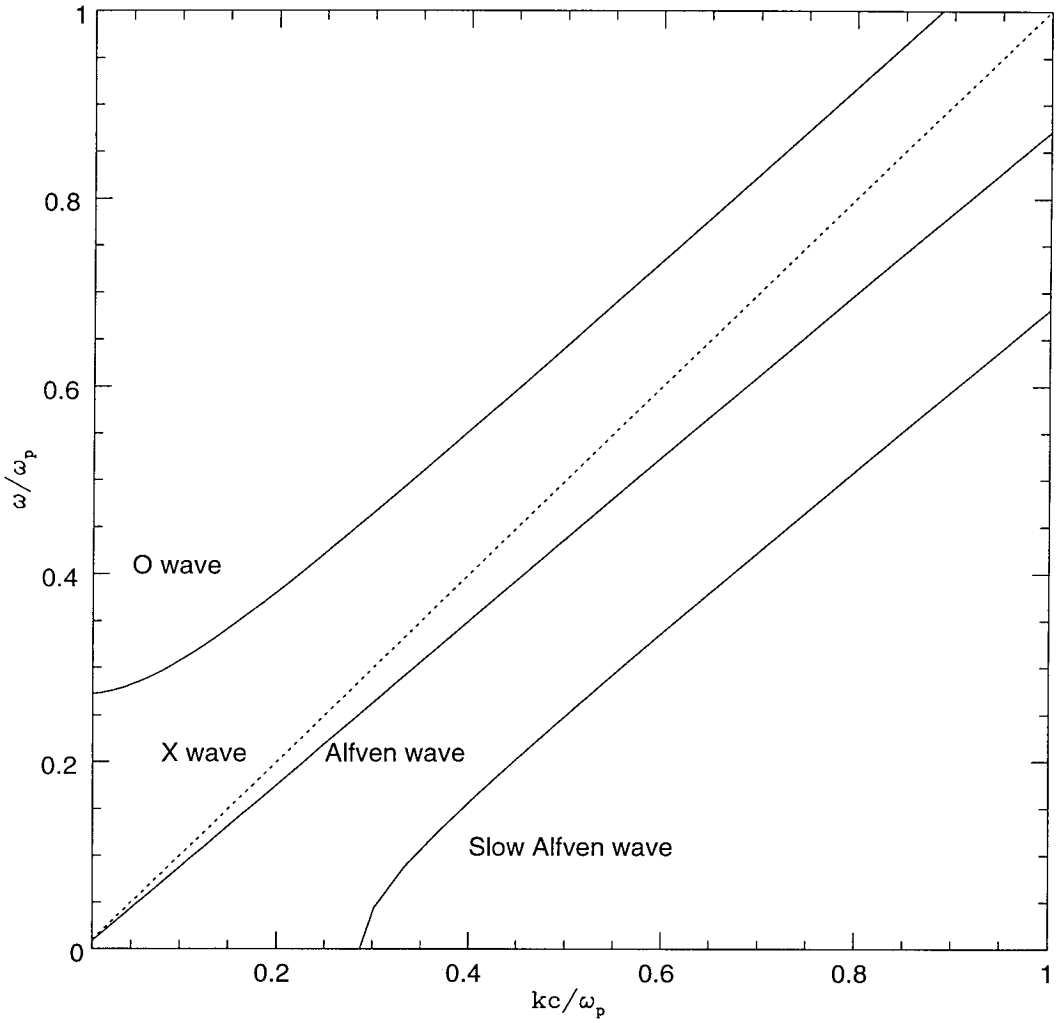

Fig. 2

Figure 5.8: Dispersion curves in the plasma frame for the infinitely strong magnetic field. Solid lines give the dispersion curves for the propagation along magnetic field, dashed lines give the dispersion curves for oblique propagation. X mode has a vacuum dispersion relation.

where the notations O, SA and A stand for ordinary, slow Alfven and Alfvén modes. The ratio of the longitudinal component of the electric field in the wave to the transverse are

$$\begin{aligned}
\frac{E_\parallel}{E_\perp}_O &= \begin{cases} \frac{2\gamma_o{}^3\,\omega_p{}^2\left(1+\beta_o{}^2\right)\sin\theta^2}{k^2c^2} \ll 1 & \text{if } \theta\gamma_o \ll 1 \\ \frac{4\,\omega_p{}^2}{\gamma_o{}^3\,k^2c^2\,\theta^3} \ll 1 & \text{if } \theta\gamma_o \gg 1 \end{cases} \\
\frac{E_\parallel}{E_\perp}_{A,SA} &= \begin{cases} -\frac{1}{\gamma_o{}^2\,\theta\,\beta_o{}^2} \gg 1 & \text{if } \theta\gamma_o \ll 1 \\ -\tan\theta \ll 1 & \text{if } \theta\gamma_o \gg 1 \end{cases}
\end{aligned} \tag{5.105}$$

This implies that for small angles of propagation $\theta\gamma_o \ll 1$ the ordinary wave is quasi-transverse and both plasma waves are quasi-longitudinal while for larger angles $\theta\gamma_o \gg 1$ all three waves (one of which is two-stream unstable) are quasi-transverse. This provides an interesting example when a conventional two stream instability produces quasi-transverse waves only.

The asymptotic dispersion relation for the ordinary wave may be obtained in the low density approximation of Melrose 1978a, but dispersion relations for Alfvén and slow Alfvén waves, which are quasi-transverse for $\theta > 1/\gamma_o$, cannot be derived in that limit.

In the small wave vectors limit ($kc \ll \sqrt{2}\omega_p/\gamma_o^{3/2}$) the asymptotic solutions are

$$\begin{aligned}
\omega_O^2 &= \frac{2\,\omega_p^2}{\gamma_o^3} + (kc)^2\left(3\,\beta_o\cos^2\theta + \sin^2\theta\right) & \frac{E_\perp}{E_\parallel}_O &= 2\,\gamma_o\,\frac{\omega_p{}^2}{k^2c^2}\left(1+\beta_o{}^2\right)\tan\theta \\
\omega_A &= kc\,\cos\theta\left(1 - \frac{(kc)^2\,\sin^2\theta}{4\,\gamma_o(1+\beta_o^2)\omega_p^2}\right) & \frac{E_\perp}{E_\parallel}_A &= \cot\theta\left(1 + \frac{3\,\gamma_o{}^3\,\beta_o{}^2\cot\theta^2k^2c^2}{2\,\omega_p{}^2}\right)
\end{aligned} \tag{5.106}$$

5.9 Waves in a Cold Plasma with Streaming Components in the Pulsar Frame

As mentioned above, the Lorentz transformation of the dispersion relations is too cumbersome to be carried out for arbitrary angle of propagation and it is easier to solve Eq. (5.32) in the pulsar frame. Since the components of the dielectric tensor strongly depend on the γ-factors of the plasma species, we will consider separately two cases: (i) nonrelativistic relative streaming, when the velocity of each plasma components in the *center-of-momentum* frame is small $\beta_o \ll 1$ (then both kinds of plasma particles contribute approximately equally to the dielectric tensor) and (ii) relativistic relative streaming, when the energy of each plasma components *in the center-of-momentum* frame is much larger than unity $\gamma_o \gg 1$ (some components of the dielectric tensor are dominated by one kind of particle).

In what follows we denote the velocity and the γ-factor of the center-of-momentum frame in the pulsar frame as β_p and γ_p, keeping the notations β_o and γ_o for the absolute value of velocity and energy in the center-of-momentum frame.

For the waves propagating forward (in the direction of the motion of the plasma frame) in the pulsar frame, the energies of the plasma components are

$$\begin{aligned}
\gamma_{faster} &= \gamma_p\gamma_o + \sqrt{\gamma_p^2-1}\sqrt{\gamma_o^2-1} = \quad \begin{cases} 2\,\gamma_p\gamma_o & \text{if } \gamma_p \gg \gamma_o \gg 1 \\ \gamma_p\,(1+\beta_p\,\beta_o) & \text{if } \gamma_p \gg 1,\ \beta_o \ll 1 \end{cases} \\
\gamma_{slower} &= \gamma_p\gamma_o - \sqrt{\gamma_p^2-1}\sqrt{\gamma_o^2-1} = \quad \begin{cases} \gamma_p/2\gamma_o & \text{if } \gamma_p \gg \gamma_o \gg 1 \\ \gamma_p\,(1-\beta_p\,\beta_o) & \text{if } \gamma_p \gg 1,\ \beta_o \ll 1 \end{cases}
\end{aligned} \tag{5.107}$$

and the velocities

$$\begin{aligned}
v_{faster} &= \frac{\beta_p+\beta_o}{1+\beta_p\,\beta_o} = \quad \begin{cases} 1-1/(8\,\gamma_p^2\,\gamma_o^2) & \text{if } \gamma_p \gg \gamma_o \gg 1 \\ \beta_p+\beta_o/\gamma_p^2 & \text{if } \gamma_p \gg 1,\ \beta_o \ll 1 \end{cases} \\
v_{slower} &= \frac{\beta_p-\beta_o}{1-\beta_p\,\beta_o} = \quad \begin{cases} 1-2\,\gamma_o^2/\gamma_p^2 & \text{if } \gamma_p \gg \gamma_o \gg 1 \\ \beta_p-\beta_o/\gamma_p^2 & \text{if } \gamma_p \gg 1,\ \beta_o \ll 1 \end{cases}
\end{aligned} \tag{5.108}$$

We will always assume that $\gamma_p \gg 1$, then the velocity difference in the pulsar frame is $\delta\beta = 2\,\beta_o/\gamma_p^2$.

5.9.1 Nonrelativistic Relative Streaming

We first derive the dielectric tensor for the cold electron-positron plasma in the pulsar frame when the relative velocity of the plasma components is nonrelativistic. Expanding (5.90) for $T_\alpha \ll 1$ and keeping only first term in the $\beta_o \ll 1$ limit of (5.107) (5.108), we have

$$\begin{aligned}
\epsilon'_{\phi\phi} &= 1+2\,d\,\gamma_p^2\,(1-n'\,\beta_p\,\cos\theta')^2 = \epsilon'_{yy} \\
\epsilon'_{\phi\phi} &= 1-\frac{2\,{\omega_p}^2}{{\omega'}^2\,{\gamma_p}^2\,(1-n'\,\beta_p\,\cos\theta')^2}+2\,d\,\gamma_p^2\,\beta_p^2\,{n'}^2\sin^2\theta' \\
\epsilon'_{xr} &= \frac{-2\,i\,n\,{\omega_p}^2\,\beta_o\,\gamma_p}{k'c\,\omega_B}\,(\beta_p-n'\,\cos\theta') = -\epsilon'_{rx} \\
\epsilon'_{x\phi} &= \epsilon'_{\phi x} = 0 \\
\epsilon'_{yz} &= \frac{-2\,i\,{n'}^2\,{\omega_p}^2\,\beta_o\,\sin\theta'\,\gamma_p}{k'c\,\omega_B} = -\epsilon'_{zy}
\end{aligned} \tag{5.109}$$

Parallel Propagation

For the case of exactly parallel propagation and in the limit $\beta_o \ll 1$, the solution of the Eq. (5.93) (which describes longitudinal plasma waves) may be approximated as

$$\omega' = k'c\beta_p \pm \sqrt{\frac{{\omega_p}^2}{{\gamma_p}^2 {k'}^2 c^2} + {\beta_o}^2 \pm \frac{\omega_p \sqrt{{\omega_p}^2 + 4{\gamma_p}^2 {k'}^2 c^2 {\beta_o}^2}}{{\gamma_p}^2 {k'}^2 c^2}} \tag{5.110}$$

which gives in the long wavelength limit $k'c \gg \omega_p/2\beta_o$ two pairs of waves propagating in each component

$$\omega' = k'\beta_p c \pm \frac{\omega_p}{\gamma_p} \tag{5.111}$$

while for smaller wavelength we have two Langmuir waves with $\omega' = k'c\beta_p \pm \sqrt{2}\omega_p/\gamma_p$ and two two-stream unstable waves.

For the transverse waves the refractive indices are

$$\begin{aligned} n'_{1,2} &= \frac{2\sqrt{\omega_B k'c\,({\omega_B}^2 + 2{\omega_p}^2)\,(\omega_B k'c \pm 2\gamma_p {\omega_p}^2 \beta_o)} + 2\gamma_p {\omega_p}^2\,(-2\gamma_p k'c \pm \omega_B \beta_o)\,\beta_p}{2\left({\omega_B}^2 k'c \pm 2\gamma_p \omega_B {\omega_p}^2 \beta_o - 2{\gamma_p}^2 {\omega_p}^2 {\beta_p}^2 k'c\right)} \\ n'_{3,4} &= \frac{-2\sqrt{\omega_B k'c\,({\omega_B}^2 + 2{\omega_p}^2)\,(\omega_B k'c \pm 2\gamma_p {\omega_p}^2 \beta_o)} + 2\gamma_p {\omega_p}^2\,(-2\gamma_p k'c \pm \omega_B \beta_o)\,\beta_p}{2\left({\omega_B}^2 k'c \pm 2\gamma_p \omega_B {\omega_p}^2 \beta_o - 2{\gamma_p}^2 {\omega_p}^2 k'c{\beta_p}^2\right)} \end{aligned} \tag{5.112}$$

which shows a cyclotron two-stream instability for $k'_c c < 2{\omega_p}^2 \beta_o \gamma_p/\omega_B$ with maximum growth rate $Im(\omega')_{max} = {\omega_p}^2 \beta_o \gamma_p/\omega_B$. For $k' > k'_c$ the solutions (5.112) may be approximated as

$$\begin{aligned} n'_{1,2} &= 1 \pm \frac{\sqrt{d}\,\omega_p \beta_o}{2\gamma_p k'c} + \frac{d}{4{\gamma_p}^2} \\ n'_{3,4} &= -1 \pm \frac{2\sqrt{d}\,\omega_p \beta_o \gamma_p}{k'c} - 4d\gamma_p^2 \end{aligned} \tag{5.113}$$

The fast transverse wave traveling in the positive direction (minus sign in $n'_{1,2}$) is superluminous for $k'c < 4\omega_B \gamma_p \beta_o$ and subluminous for larger wave vectors.

Solving Eq. $\epsilon'_{\phi\phi} = 0$ with the refractive index set to unity, we find the point where the ordinary wave becomes subluminous: $k' > 2\sqrt{2}\,\gamma_p\,\omega_p/c$

5.9.2 Relativistic Relative Streaming

In this section we assume that the streaming of electrons *relative* to positrons is relativistic meaning that their relative velocity in the *center-of-momentum* reference frame is close to the speed of light.

With the distribution functions of the form $f_\alpha(p_\phi) = \gamma_\alpha \delta(p_\phi - \gamma_\alpha v_\alpha)$ where the γ factors and velocities of plasma components are given by the $\gamma_o \gg 1$ asymptotics in (5.107), the dielectric

tensor (5.90) in the pulsar frame will have the following form:

$$\begin{aligned}
\epsilon'_{\phi\phi} &= 1 + d\sum_\alpha \gamma_\alpha^2 (1 - n'\,\cos\theta'\,v_\alpha)^2 = \epsilon'_{yy} \\
\epsilon'_{\phi\phi} &= 1 - \sum_\alpha \frac{{\omega_p}^2}{{\omega'}^2\,{\gamma_\alpha}^2\,(1 - n'\,v_\alpha\,\cos\theta')^2} + \sum_\alpha d\,{n'}^2\,\sin^2\theta'\gamma_\alpha^2\,(1 + v_\alpha^2) \\
\epsilon'_{xr} &= -i\,\sqrt{d}\frac{\omega_p}{k'c}\sum_\alpha sign_\alpha\,\gamma_\alpha\,(1 - n'\,\cos\theta'\,v_\alpha) \\
\epsilon'_{x\phi} &= d\sin\theta' n' \sum_\alpha \gamma_\alpha^2 v_\alpha\,(1 - n'\,\cos\theta' v_\alpha) = \epsilon'_{\phi x} \\
\epsilon'_{yz} &= \sum_\alpha \frac{i\,sign_\alpha\,\sqrt{d}\,{n'}^2\,\omega_p\,\sin\theta'\,\gamma_\alpha v_\alpha}{k'c} = -\epsilon'_{zy}
\end{aligned} \tag{5.114}$$

Here γ_α and v_α are given by the $\gamma_o \gg 1$ asymptotics of (5.107) and (5.108). The velocity difference is now $\delta\beta' = 2\,\gamma_o^2/\gamma_p^2$.

Parallel Propagation

In this section we consider the limiting cases of exactly parallel propagation when it is possible to solve the dispersion relation analytically.

Eq. (5.93) for the plasma waves is a fourth order equation in n' corresponding to the waves propagating in each direction in each plasma component. If the relative streaming of electrons and positrons is relativistic, then for sufficiently larger wave vectors $k'c \geq \omega_p/(\delta\beta'\,\gamma_\pm)$ the Langmuir waves in each component have small effect on the waves in the other component and the solution of (5.93) in the laboratory frame may be approximated as:

$$\begin{aligned}
\omega' = &\quad k'v_- \pm \frac{2\gamma_o\omega_p}{\gamma_p} \\
\omega' = &\quad k'v_+ \pm \frac{\omega_p}{2\,\gamma_p\,\gamma_o}
\end{aligned} \tag{5.115}$$

For smaller wave vectors two of the four solutions of (5.93) becomes two-stream unstable.

In the intermediate frequency region (for the wave vectors much larger than those corresponding to the two-stream instability and smaller than $\omega_p/(\delta\beta\,\gamma_\pm)$, we may find a cross-over point for the ordinary wave: $k'c = 2\,\gamma_o\,\gamma_p\,\omega_p$. The ordinary wave is superluminous for smaller wave vectors and subluminous for larger.

Solving (5.94) for the dispersion of the transverse waves under the condition $d \ll 1$, we get

$$\begin{aligned}
n'_{1,2} &= 1 \pm \frac{\sqrt{d}\,\omega_p\,\gamma_o}{2\,k'c\,\gamma_p} + d\frac{\gamma_o^2}{2\,\gamma_p^2} + \frac{d\gamma_o^2\omega_p^2}{2\,{k'}^2c^2} \\
n'_{3,4} &= -1 \pm \frac{2\sqrt{d}\,\omega_p\,\gamma_o\,\gamma_p}{k'c} - 8\,d\,\gamma_o^2\,\gamma_p^2 - \frac{4\,d\,\omega_p^2\,\gamma_o^2\gamma_p^2}{{k'}^2c^2}.
\end{aligned} \tag{5.116}$$

Here $n'_{1,2}$ correspond to the waves propagating in the positive direction (along the direction of the bulk motion) and $n'_{3,4}$ correspond to the waves going in the negative direction. We note that the ordinary mode is two-stream-cyclotron unstable for $k'c < \gamma_o \omega_p^2 / 2\gamma_p \omega_B$.

5.10 Waves in a Relativistic Pair Plasma with Streaming Distributions

In this section we consider waves in a relativistic hot electron-positron plasma.

Expanding the Bessel functions in Eq. (5.90) when $T_\alpha \gg 1$ and keeping only the leading terms, we obtain the dielectric tensor

$$\begin{aligned}
\epsilon_{\phi\phi} &= 1 + d\sum_\alpha (\gamma_\alpha T_\alpha)\left((1 - n\, v_\alpha \cos\theta)^2 + (v_\alpha - n\cos\theta)^2\right) = \epsilon_{yy} \\
\epsilon_{xr} &= -i\sqrt{d}\frac{\omega_p}{kc}\sum_\alpha sign_\alpha\, \gamma_\alpha\, (1 - n\, \cos\theta\, v_\alpha) = -\epsilon_{rx} \\
\epsilon_{x\phi} &= \sum_\alpha d\, n\, \sin\theta\, \gamma_\alpha\, T_\alpha\, (v_\alpha(1 - n\, \cos\theta\, v_\alpha) + (v_\alpha - n\, \cos\theta)) = \epsilon_{\phi x} \\
\epsilon_{r\phi} &= \sum_\alpha \frac{i\, sign_\alpha \sqrt{d}\, n^2\, \omega_p\, \sin\theta}{kc}\, \gamma_\alpha v_\alpha = -\epsilon_{\phi r} \\
\epsilon_{\phi\phi} &= 1 - \sum_\alpha I_\alpha(\theta, \omega, n) + d\, n^2\, \sin^2\theta\, \gamma_\alpha\, T\, (1 + v_\alpha^2)
\end{aligned} \tag{5.117}$$

In what follows we also assume that the temperature of two kinds of particles are the same and equal to T.

5.10.1 Center-of-Momentum Reference Frame

The dielectric tensor in the center-of-momentum frame is then

$$\begin{aligned}
\epsilon_{\phi\phi} &= 1 + 2\, d\, \gamma_o\, T\, (1 + n^2\, \cos\theta^2)\, (1 + \beta_o^2) = \epsilon_{yy} \\
\epsilon_{xr} &= 2\, i\, d\, n^2\, \frac{\omega_B}{kc}\, \beta_o\, \cos\theta \gamma_o = -\epsilon_{rx} \\
\epsilon_{yz} &= 2\, i\, d\, n^2\, \frac{\omega_B}{kc}\, \beta_o\, \sin\theta \gamma_o = -\epsilon_{zy} \\
\epsilon_{x\phi} &= -\,2\, d\, \gamma_o\, T\, n^2 \cos\theta \sin\theta (1 + \beta_o^2) = \epsilon_{\phi x} \\
\epsilon_{\phi\phi} &= 1 - I(\theta, \omega) + +2\, d\, \gamma_o\, T\, n^2\, \sin^2\theta
\end{aligned} \tag{5.118}$$

where now

$$I(\theta,\omega,n)=\begin{cases}\frac{2\,\omega_p^2\,\gamma_o\,T\,(1+\beta_o)^2}{\omega^2} & \text{if } \theta \ll \frac{1}{2\,T\,\gamma_o}\\ \frac{8\,\omega_p^2}{\omega^2\,\theta^4} < \frac{1}{\gamma^3} > & \text{if } \frac{1}{2\,T\,\gamma_o} \ll \theta \ll 1\end{cases} \tag{5.119}$$

If we compare this dielectric tensor with the cold case (5.92) we see that (except in the $\epsilon_{\phi\phi}$ term) in the case of relativistic temperature the particles have equivalent mass $T_p\,(1+\beta_o^2) \approx 2\,T$ higher.

The problem of the propagation and stability of the Langmuir plasma waves in a hot plasma is a very complicated one, and since we are mostly interested in the properties of the quasi-transverse waves propagating almost along the magnetic field we will use approximations (5.119) for the $\epsilon_{\phi\phi}$ and refer the reader to the original works (Silin 1960, Lominadze & Mikhailovskii 1978, Lominadze, Mikhailovskii & Sagdeev 1979, Weatherall 1994) which consider Langmuir waves propagation. Here we just note that the two-stream instability is suppressed by thermal effects if $T \geq \gamma_o\,\beta_o$ and we find the cross-over point, where the ordinary wave becomes subluminous by solving equation $\epsilon_{\phi\phi}=0$ with the index of refraction set to unity:

$$kc > \begin{cases}\sqrt{2}\,\omega_p\gamma_o\,\sqrt{T_p}\,(1+\beta_o) & \text{if } \theta \ll 1/(2\gamma_o T)\\ \frac{2\,\sqrt{2}\,\omega_p\,\sqrt{\gamma_o}}{\theta^2}\,\sqrt{<\frac{1}{\gamma^3}>} & \text{if } \theta \gg 1/(2\gamma_o T)\end{cases} \tag{5.120}$$

For the propagation of the transverse wave along magnetic field, we have the dispersion relations:

$$n^2=\frac{1+2\,d\,\gamma_o\,T\,\left(1+{\beta_o}^2\right)}{1\pm 2\,\sqrt{d}\,\omega_p\,\beta_o/kc-2\,d\,\gamma_o\,T\,\left(1+{\beta_o}^2\right)} \tag{5.121}$$

which gives the hydrodynamic firehose instability for $2\,d\,\gamma_o\,T\,\left(1+{\beta_o}^2\right) > 1$ for both branches and the cyclotron two-stream instability for the slow transverse mode for $kc < 2\,{\omega_p}^2\,\beta_o/\omega_B$.

To find the dispersion relations of the quasi-transverse waves propagating forward with a small angle with respect to magnetic field we follow the same procedure as in Section 5.10 to get for $n^2=1+x$

$$\begin{aligned}(-1+I)\,x^2+\quad & x\left(8\,d\,\gamma_o\,(1-I)\left(\frac{{\omega_p}^2\,{\beta_o}^2}{k^2\,c^2}+T\,\left(1+{\beta_o}^2\right)\right)-I\,\theta^2\right)+\\ & 4\,d^2\,(1-I)\left(4\,d^2\,T^2(1+{\beta_o}^2)-\frac{\omega_p^2\,\beta_o^2}{k^2c^2}\right)+\\ & 4\,d^2\,\theta^2\left(I\,T\,(1+{\beta_o}^2)-(4-I)\frac{\omega_p^2\,\beta_o^2}{k^2c^2}\right)\end{aligned} \tag{5.122}$$

Eq. (5.122) gives the solutions

$$\left.\begin{aligned} n_{st} &= 1 + \frac{\sqrt{d}\,\omega_p\,\beta_o}{kc} + 2\,d\,\gamma_o\left(T_p(1+\beta_o^2) + \frac{3{\omega_p}^2{\beta_o}^2}{k^2c^2}\right) \\ n_{ft} &= 1 - \frac{\sqrt{d}\,\omega_p\,\beta_o}{kc} + 2\,d\,\gamma_o\left(T_p(1+\beta_o^2) + \frac{3{\omega_p}^2{\beta_o}^2}{k^2c^2}\right) - \frac{I\,\theta^2}{4\,(1-I)} \end{aligned}\right\} \quad \text{if } \theta < \theta_{crit}$$

$$\left.\begin{aligned} n_{st} &= 1 + \frac{2\,d\,(1-I)\,{\omega_p}^2\,{\beta_o}^2\,\gamma_o}{I\,k^2c^2\,\theta^2} + 2\,d\,\gamma_o\left(T_p(1+\beta_o^2) + \frac{{\omega_p}^2{\beta_o}^2}{k^2c^2}\right) \\ n_{ft} &= 1 + \frac{I\sin^2\theta}{-1+I} + 2\,d\,\gamma_o\left(T_p(1+\beta_o^2) + \frac{{\omega_p}^2{\beta_o}^2}{k^2c^2}\right) \end{aligned}\right\} \quad \text{if } \theta > \theta_{crit} \qquad (5.123)$$

with

$$\theta_{crit}^2 = \frac{2\sqrt{d}\,|1-I|\,\omega_p\,\beta_o\,\gamma_o}{I\,kc} = \begin{cases} \frac{2\,\omega_p^2\,\beta_o}{\gamma_o\omega_B\,kc} & \text{if } kc \ll \omega_p\,\gamma_o\,\sqrt{T_p}(1+\beta_o) \\ \frac{kc\,\beta_o}{T\,\gamma_o(1+\beta_o^2)\,\omega_B} & \text{if } kc \gg \omega_p\,\gamma_o\,\sqrt{T_p}(1+\beta_o) \end{cases} \qquad (5.124)$$

(we assumed that $\theta_{crit} < 1/(2\,T\,\gamma_o)$ and polarizations given by

$$\left.\begin{aligned} K_{st,ft} &= \pm\frac{I\,\theta}{1-I}, & T_{st,ft} &= \pm 1 + \frac{I\,kc\,\theta^2}{\sqrt{d}\,(-1+I)\,\omega_p\,\beta_o} \\ K_{st} &= \frac{\sqrt{d}\,\omega_p\,\beta_o}{kc\,\theta}, & T_{st} &= \frac{\sqrt{d}\,(1-I)\,\omega_p\,\beta_o}{I\,kc\,\theta^2} \\ K_{ft} &= \frac{\sqrt{d}\,(-1+I)\,\omega_p\,\beta_o}{I\,kc\,\theta^3}, & T_{ft} &= -\frac{\sqrt{d}\,(-1+I)^2\,\omega_p\,\beta_o}{I^2\,kc\,\theta^4} \end{aligned}\right\} \quad \text{if } \theta > \theta_{crit} \qquad (5.125)$$

From (5.123) we find that for the quasi-parallel propagation the extraordinary mode is superluminous for

$$k < \begin{cases} \frac{\omega_B\,\beta_o}{2\,c\,\gamma_o\,T_p} & \text{if } \beta_o \ll 1 \\ \omega_B/(4\,\gamma_o\,T) & \text{if } \beta_o \approx 1 \end{cases} \qquad (5.126)$$

5.10.2 Pulsar Reference Frame

In the pulsar reference frame we will give explicitly the dispersion relations for the quasi-transverse waves for the nonrelativistic streaming only. We also assume that $\gamma_p \ll T_\alpha$.

Following the same procedure we have for exactly parallel propagation:

$$\begin{aligned} n'_{1,2} &= 1 \pm \frac{\sqrt{d}\,\omega_p\,\beta_o}{2\,\gamma_p\,k'c} + \frac{d\,T_p}{2\,\gamma_p^2} \\ n'_{3,4} &= -1 \pm \frac{\sqrt{d}\,\omega_p\,\beta_o\gamma_p}{2\,k'c} - 8d\gamma_p^2\,T_p \end{aligned} \qquad (5.127)$$

where, as before, $n'_{1,2}$ corresponds to the waves propagating forward in the pulsar frame and $n'_{3,4}$ - to the waves propagating backward.

For the forward propagating waves, we find solutions for oblique propagation for $\theta' < 1/(4\,T_p\,\gamma_p)$

$$\left.\begin{aligned} n'_{st,ft} &= 1 + \frac{\sqrt{d}\,\omega_p\,\beta_o}{2\,\gamma_p\,k'c} + \frac{d\,T_p}{2\,\gamma_p^2} \\ n'_{,lt} &= 1 - \frac{\sqrt{d}\,\omega_p\,\beta_o}{2\,\gamma_p\,k'c} + \frac{d\,T_p}{2\,\gamma_p^2} - \frac{I\theta'^2}{4(1-I)} \end{aligned}\right\} \quad \text{if } \theta' < \theta'_{crit}$$

$$\left.\begin{aligned} n'_{st} &= 1 + \tfrac{d\,T}{2\,\gamma_p^2} \\ n'_{ft} &= 1 + \tfrac{I\,\theta'^{\,2}}{2\,(-1+I)} + \tfrac{d\,T_p}{2\,\gamma_p{}^2} \end{aligned}\right\} \qquad \text{if } \theta' > \theta'_{crit} \tag{5.128}$$

where the quantity I is now given by $I = 8\,\omega_p^2\,\gamma_p^2\,T_p/k'^{\,2}c^2$ and polarizations

$$\begin{aligned} K_{st,ft} &= \pm\tfrac{I\,\theta'}{1-I}, & T_{st,ft} &= \pm 1 + \tfrac{\gamma_p\,I\,k'c\,\theta'^{\,2}}{\sqrt{d}\,(1-I)\,\omega_p\,\beta_o} && \text{if } \theta' < \theta'_{crit} \\ K_{st} &= -\tfrac{\sqrt{d}\,\omega_p\,\beta_o}{\gamma_p\,k'c\,\theta'}, & T_{st} &= \tfrac{\sqrt{d}\,(-1+I)\,\omega_p\,\beta_o}{\gamma_p\,I\,k'c\,\theta'^{\,2}} \\ K_{ft} &= \tfrac{8\,\sqrt{d}\,(1-I)\,\omega_p\,\beta_o}{3\,\gamma_p\,I\,k'c\,\theta'^{\,3}}, & T_{ft} &= \tfrac{8\,\sqrt{d}\,(-1+I)^2\,\omega_p\,\beta_o}{3\,\gamma_p\,I^2\,k'c\,\theta'^{\,4}} && \text{if } \theta' > \theta'_{crit} \end{aligned} \tag{5.129}$$

where the critical angle is given by

$$\theta'^{\,2}_{crit} = \frac{2\sqrt{d}\omega_p\,\beta_o|1-I|}{\gamma_p\,k'c\,I} = \begin{cases} \frac{\beta_o\,k'c}{8\,\gamma_p^3\,T\,\omega_B} & \text{if } k'c \gg 2\omega_p\,\gamma_p\,\sqrt{T_p} \\ \frac{\beta_o\,\omega_p^2}{\gamma_p\,k'c\,\omega_B} & \text{if } \frac{\omega_p^2\,\beta_o}{2\,\gamma_p\,\omega_B} \ll k'c \ll 2\omega_p\,\gamma_p\,\sqrt{T_p} \end{cases} \tag{5.130}$$

The cross-over point, where the ordinary wave becomes subluminous, for the parallel propagation is $k'c = 2\sqrt{2}\,\omega_p\,\gamma_p\,\sqrt{T_p}$. For the small wave vectors, the fast transverse mode becomes superluminous for $k'c < \omega_p^2\,\beta_o/2\gamma_p\omega_B$, while for large wave vectors it is superluminous for $\theta' > k'c/2\omega_B$.

5.11 Conclusion

In this chapter we considered the low frequency $\omega \ll \omega_B$ normal modes for a one-dimensional streaming electron-positron plasma in a very strong magnetic field taking into account relative streaming of the plasma species and thermal effects. The dispersion relations for the natural modes are sensitive even to the small streaming motion between the electrons and positrons of the plasma consistent with the global electrodynamic conditions. The difference in the averaged parallel velocity results in the coupling of the two quasi-transverse waves for the angles of propagation with respect to magnetic field less than some critical angle so that the natural modes become *circularly* polarized. For the angles of propagation larger than this angle, the two transverse modes become linearly polarized due to the coupling to the longitudinal plasma modes. In the case of relativistic relative streaming, the plasma modes become quasitransverse for the angles of propagation larger than $1/\gamma_o$.

The distinction between superluminous and subluminous waves is clearly made. In the long wavelength limit the relative velocity of plasma particles results in the two-stream plasma and cyclotron instabilities. The stable transverse wave in this limit becomes superluminous, while both transverse waves were subluminous in the case of zero relative velocity.

The results of this chapter may be relevant to theories of pulsar radio emission generation and wave propagation in pulsar magnetosphere. We have shown that the small relative velocity of plasma components modifies these normal modes considerably changing their polarization and dispersion

properties. Furthermore, as the nature of the outflowing plasma changes, the character of the normal modes will change as well.

Chapter 6 Cyclotron-Cherenkov and Cherenkov-drift Instabilities

In this chapter we consider the physics of the cyclotron-Cherenkov and Cherenkov-drift instabilities (Ginzburg & Eidman 1959, Lyutikov 1997b, Lyutikov, Machabeli & Blandford 1997a, Lyutikov, Machabeli & Blandford 1997b). The terminology used here to describe these instabilities refers to the fact that in the cyclotron-Cherenkov emission, a resonant particle changes its gyrational state (undergoes a transition between two different Landau levels), thereby comes the "cyclotron" part of its name, but the force that induces the emission is due to the presence of a medium (the "Cherenkov" part of the name). The Cherenkov-drift emission is similar to conventional Cherenkov (the gyrational state of the resonant particle remains unchanged) but it involves a nonvanishing curvature drift of the resonant particles.

Both the cyclotron-Cherenkov and Cherenkov-drift instabilities, that we believe can develop in pulsar magnetosphere, operate in the kinetic regime, i.e., they are of a maser type (see Chapter 7). This means that there is some kind of the population inversion in the phase space, which supplies the energy for the development of the instability. In the present case, the source of free energy is the anisotropic distribution function of the fast particles. The condition of a population inversion may be restated that the induced emission dominates over induced absorption for a given transition.

The first two steps in identifying the possible maser-type radio emission generation mechanism are (i) determining which radiative transitions are allowed in a given system and (ii) establishing if the given distribution function allows for the population inversion for the particle in resonance with the emitted waves. In this chapter we will first discuss the microphysics of the two suggested emission mechanisms and then show that the distribution function of the particles present on the open field lines of pulsar magnetosphere does have a population inversion and allows maser action. When discussing the microphysics of the emission process, we will concentrate on the spontaneous emission processes. The induced emission rate, which is important for the development of the instabilities, is derivable from the spontaneous emission in the usual manner. In the process of induced emission, the electron emits a wave in a phase with the incident wave. However, both cyclotron-Cherenkov and Cherenkov-drift masers are broadband and incoherent because a single electron can resonate with several waves simultaneously.

6.1 Physics of Cyclotron-Cherenkov Emission

In this section we discuss the microphysics of electromagnetic wave emission at the anomalous cyclotron resonance

$$\omega(\mathbf{k}) - k_{\|} v_{\|} + \frac{\omega_B}{\gamma} = 0 \tag{6.1}$$

The conventional synchrotron emission and Cherenkov radiation may be regarded as limiting cases of $|n-1| \ll 1$ and $B = 0$ respectively of a synergetic cyclotron-Cherenkov radiation. The interplay between cyclotron (or synchrotron) and Cherenkov radiation has been a long-standing matter of interest. Schwinger et al. 1976 discussed the relation between these two seemingly different emission mechanisms. The important feature of the work of Schwinger et al. 1976 is that the authors neglected a possible motion along the magnetic field thus excluding the anomalous cyclotron-Cherenkov Doppler resonances.

To describe the microphysics of the cyclotron-Cherenkov emission process, we first recall the microphysics of the conventional Cherenkov emission (Ginzburg & Eidman 1959). Consider a charged particle propagating in an unmagnetized dielectric with the dielectric constant $\epsilon > 1$. As the particle propagates, it induces a polarization in a medium. If the velocity of the particle is larger than the velocity of propagation of the polarization disturbances in a medium, which is equal to the phase speed of the waves $v_{ph} = c/\sqrt{\epsilon} < c$, the induced polarization cannot keep up with the particle. This results in a formation of the polarization shock front. At large distances, the electromagnetic fields from this "shock front" have a wavelike form corresponding to Cherenkov emission. Thus the emission is attributed to the polarization shock front and not directly to the particle. This polarization shock front acts on the particle with a drag force, which slows down the particle. This drag force may be considered as a generalization of the radiation reaction force in a medium.

Now let us consider a propagation of a particle in a magnetized dielectric along a spiral trajectory. Similarly, the propagating charged particle induces polarization in a medium. If the velocity of the particle is larger than the phase speed of the waves, a polarization shock front develops, which acts on the particle with a drag force. Now the drag force, averaged over the gyrational period, has two components: along the external magnetic field and perpendicular to it. The parallel part of the drag force always slows the particle down. The surprising result is that the perpendicular component of the drag force acts to *increase* the transverse momentum of the particle. Thus a particle undergoes a transition to the state with *higher* transverse momentum and *emit* a photon. The energy is supplied by the parallel motion. In fact, half of the parallel energy lost by the particle is converted in the radiation and half goes into the transverse motion (Ginzburg & Eidman 1959, Lyutikov 1997b).

The photons emitted by such mechanism correspond to the anomalous Doppler effect $\omega - k_{\|} v_{\|} - \nu \omega_B / \gamma_{res} = 0$, with $\nu < 0$. In a vacuum, only the normal Doppler resonance, with $\nu > 0$, is possible. The necessary condition for the anomalous Doppler effect, $\omega - k_{\|} v_{\|} < 0$, may be

satisfied for fast particles propagating in a medium with the refractive index larger than unity. It is natural to attribute the emission at the normal Doppler resonances to the Lorentz force of the magnetic field acting on the electron, while the emission at the anomalous Doppler resonances to the electromagnetic drag forces from the medium.

The cyclotron-Cherenkov instability may be considered as a maser using the induced cyclotron-Cherenkov emission. The free energy for the growth of the instability comes from the nonequilibrium anisotropic distribution of fast particles. The condition that the emission rate dominates the absorption requires population inversion in the distribution function of fast particle (maser action). Since radiation reaction due to the anomalous Doppler effect induces transition up in quantum levels, for the instability to occur, we need more particles on the *lower* levels. From the kinetic point of view, waves grow if the quantity $\mathbf{k}\frac{\partial f(\mathbf{p})}{\partial \mathbf{p}}$ is positive for some values of $\mathbf{k}$. For an electron in a magnetic field this condition takes the form

$$\frac{\nu\,\omega_b}{v_\perp}\frac{\partial f}{\partial p_\perp} + k_\parallel \frac{\partial f}{\partial p_\parallel} > 0 \tag{6.2}$$

where ν is a harmonic number. Here $\nu > 0$ corresponds to normal Doppler effect (transition down in Landau levels) and $s < 0$ corresponds to anomalous Doppler effect (transition up in Landau levels). If the distribution function is a plateau-like in parallel momentum, then the condition for instability is $\nu\frac{\partial f}{\partial p_\perp} > 0$ which could be satisfied for inverted population for the normal Doppler effect or for the "direct" distribution for anomalous Doppler effect. The latter case takes place for the beam of particles propagating along the magnetic field with no dispersion in transverse moments.

Near the light cylinder the magnetic field strength falls considerably which allows for synchrotron excitation of transverse motion of particle. At the distance 10^9 cm an anomalous Doppler resonance could be fulfilled for the particles of the primary beam and for the fast particle of the tail of plasma distribution.

6.1.1 Quantum Approach to the Anomalous Cyclotron Emission

In discussing the electromagnetic properties in dielectric medium (Sections 6.1.1 - 6.1.2) we will make a simplifying assumption, which is standard in the theory of Cherenkov radiation, that the refractive index of the medium n is independent of the frequency and angle. In reality $n \to 1$ as frequency goes to infinity which provides the upper cutoff for the integration over frequency removing the divergence of some of the integrals involved.

In this section, following the approach of Ginzburg & Eidman 1959, we show the kinematic possibility of spontaneous emission with upward transitions in transverse quantum energy levels for a quantum oscillator propagating with a superluminous velocity in a dielectric medium.

First we note that the energy and momentum of a photon propagating in a medium with the

refractive index n are given by $\hbar\,\omega$ and $\hbar\,\omega\,n/c$ respectively. Now, consider an electron propagating in a magnetic field. The quantum states may be described by the definite values of the momentum along the magnetic field and the projection of the spin of the electron on the magnetic field. The energies of the eigenstates are

$$E_N = \sqrt{(m\,c^2)^2 + 2\,m\,c^2\,w_N + p_\phi^2\,c^2}, \tag{6.3}$$

where E_N is the total energy of the state, $w_N = N\hbar\,\omega_B$ is the energy of the electron in the frame associated with its center of gyration, $N = 1/2 + l + (s+1)/2$ is a principal quantum number, $l = 0\,,1\,,2\,,\ldots$ is a radial quantum number and $s = \pm 1$ is spin quantum number (Sokolov & Ternov 1968). Each state is doubly degenerate except for the ground state $l = 0\,, \nu = -1$.

The conservation of energy and momentum take the form

$$\begin{aligned} E_f - E_i &= \hbar\,\omega, \\ p_{f,z} - p_{i,z} &= \hbar\,k_\phi = \frac{\hbar\,\omega\,n\,\cos\theta}{c}. \end{aligned} \tag{6.4}$$

Indices i and f refer to the initial and final states, θ is the angle between the directions of photon propagation and the magnetic field. Neglecting the terms of the order $\hbar\,\omega\,/(\,m\,c^2) \ll 1$, and requiring that the energy of the emitted quantum be positive, we arrive at the emission condition

$$\omega - k_\parallel v_\parallel - \frac{\nu\omega_B}{\gamma} = 0 \tag{6.5}$$

The change in the transverse energy is

$$\begin{aligned} w_i - w_f = (N_i - N_f)\,\hbar\,\omega_B/\gamma = \nu\,\hbar\,\omega_B/\gamma > 0, \qquad & \text{if } \tfrac{v}{c} n(\omega)\cos\theta < 1 \\ \text{normal Doppler effect,} & \\ w_i - w_f = (N_i - N_f)\,\hbar\,\omega_B/\gamma = \nu\,\hbar\,\omega_B/\gamma < 0, \qquad & \text{if } \tfrac{v}{c} n(\omega)\cos\theta > 1 \\ \text{anomalous Doppler effect,} & \end{aligned} \tag{6.6}$$

where we defined $\nu = N_i - N_f$. In the region of the anomalous Doppler effect the photons are emitted when the electron undergoes a transition *up* in its quantum levels. The energy is supplied by the parallel motion of the particle. The loss in the parallel energy equals the increase of the transverse energy plus the energy of the emitted wave. Alternatively, we may argue that the quantum state of the particle with large parallel energy and small transverse energy has a higher total energy than the state with smaller parallel energy larger and transverse energy which allows for a spontaneous transition from the state with higher total energy to the state with smaller total energy.

It is instructive to consider the emission process in the particle rest frame. In this frame during

the emission process, the emitting particle increases its transverse energy and also acquires some parallel velocity due to the radiation recoil at the anomalous Doppler resonance. A puzzling situation arises: a particle increases its kinetic energy and emits an electromagnetic wave. The resolution of this paradox is that for the superluminous motion when considered in the particle's rest frame the emitted wave has negative energy.

To illustrate this we calculate the energy of the electromagnetic wave traveling in a lossless dielectric medium with permittivity ϵ and permeability $\mu = 1$ along the z axis in the medium rest frame, which will be denoted by primes, and another frame moving also along the z axis with velocity β (see, for example, Dunn 1971, Sturrock 1960). In the primed frame we have

$$\mathbf{D}' = \epsilon \mathbf{E}', \qquad \mathbf{B}' = \mathbf{H}', \tag{6.7}$$

where $\mathbf{E}'$ and $\mathbf{H}'$ are the electric and magnetic fields, $\mathbf{D}'$ and $\mathbf{B}'$ are electric and magnetic induction. The wave fields, viewed in this frame, have the form

$$\begin{aligned} E'_x &= E'_o \exp\left(i(\omega' t' - k' z')\right), \\ H'_y &= \frac{E'_o}{Z'_o} \exp\left(i(\omega' t' - k' z')\right) = B'_y, \\ D'_x &= \epsilon\, E'_o \exp\left(i(\omega' t' - k' z')\right), \end{aligned} \tag{6.8}$$

where the impedance $Z'_o = \omega'/k'c$ and E'_o is an arbitrary constant. The dispersion relation has the form

$$Z'^2_o\, \epsilon = 1, \tag{6.9}$$

which gives two solutions $Z'_o = \pm 1/\sqrt{\epsilon} = \pm 1/n$ for the two waves traveling in the positive $Z'_o > 0$ and negative $Z'_o < 0$ directions.

Making Lorentz transformations of the fields Eq. (6.8) we find in the frame moving in the positive direction z :

$$\begin{aligned} E_x &= E_o \exp\left(i(\omega t - kz)\right), \\ H_y &= \pm\, n\, E_o \exp\left(i(\omega t - kz)\right), \\ D_x &= n\, E_o \frac{(n \pm \beta)}{(1 \pm n\beta)} \exp\left(i(\omega t - kz)\right), \\ B_y &= E_o \frac{(\beta \pm n)}{(1 \pm n\beta)} \exp\left(i(\omega t - kz)\right), \end{aligned} \tag{6.10}$$

where

$$E_o = \frac{\omega' + \beta k' c}{\sqrt{1-\beta^2}\,\omega'} E'_o = \frac{\sqrt{1-\beta^2}\,\omega}{\omega - \beta k c} E'_o. \tag{6.11}$$

We now identify the energy of the wave as

$$W = \frac{1}{2}\left(\mathbf{H}\cdot\mathbf{B} + \mathbf{E}\cdot\mathbf{D}\right), \tag{6.12}$$

whose time-average value is

$$< W >= \frac{1}{4}\,\mathrm{Re}\left(\mathbf{H}\cdot\mathbf{B}^* + \mathbf{E}\cdot\mathbf{D}^*\right). \tag{6.13}$$

Using Eq. (6.10) we can find the time-averaged energy of the forward and backward propagating waves:

$$\begin{aligned} < W >_{forwd} &= \frac{nE_o^2}{2}\,\frac{n-\beta}{1-n\beta}, \\ < W >_{backwd} &= \frac{nE_o^2}{2}\,\frac{n+\beta}{1+n\beta}. \end{aligned} \tag{6.14}$$

The energy of the forward propagating wave thus becomes negative for $n\beta > 1$.

6.1.2 Radiation Reaction due to Emission at Anomalous Doppler Resonance

As mentioned in the introduction, for the different types of Cherenkov emission (conventional Cherenkov and cyclotron-Cherenkov) it is more consistent to consider photons as emitted by the shock front of polarization. The energy for the emitted waves is supplied by the slowing down of the particle by the radiation reaction force. In this approach the emissivity may be calculated as the work done on a particle by the radiation reaction force. The advantage of this method is that it allows us to see explicitly, on a microscopic level, how the recoil of the emitted photons influence the motion of the particle. The very notion of the radiation reaction force assumes that this force acts as a perturbation to the otherwise classical motion of the particle. This will be true for the particles on the high Landau levels. For the particles on the low Landau levels, the radiation reaction force considerably changes the state of the motion and cannot be regarded as a perturbation.

According to Ginzburg & Eidman 1959, the radiation reaction force for a moving charge is given by

$$\begin{aligned} \mathbf{f}_{RR} = \quad & -\frac{e^2}{2\,\pi^2}\sum_j \int_0^t dt' \int d\mathbf{k}\left[\frac{\mathbf{e}_j(\mathbf{v}'\cdot\mathbf{e}_j^*)}{n_j^2}\cos(\omega_j(t-t'))-\right. \\ & \left. i\mathbf{v}\times(\mathbf{k}\times\mathbf{e}_j)\,\frac{(\mathbf{v}'\cdot\mathbf{e}_j^*)}{n_j^2\,\omega_j^2}\sin(\omega_j(t-t'))\right]\exp\left(i\mathbf{k}(\mathbf{R}-\mathbf{R}')\right) + c.c., \end{aligned} \tag{6.15}$$

where the sum is over the emitted eigenmodes ω_j of the medium, n_j is the refractive index corresponding to eigenmodes ω_j, $\mathbf{e}_j$ are the polarization vectors of the modes (unit vectors along

the wave's electric field), $\mathbf{R}$ and $\mathbf{v}$ are the radius vector and the velocity of the particle. The primed functions depend on the t' and the asterisk denotes complex conjugation. The second term in Eq. (6.15) corresponds to the magnetic reaction force which does not do any work.

The energy emitted by the particle equals minus the work of the radiation reaction force on the particle:

$$A = \int_0^T dt\, \mathbf{f}_{RR} \cdot \mathbf{v} = \int_0^T dt\, (v_\phi f_{RR,\phi} + \mathbf{v}_\perp \cdot \mathbf{f}_{RR,\perp}) = A_\parallel + A_\perp, \tag{6.16}$$

where we split this work into parallel and transverse parts. $A_\parallel$ describes the change of the parallel energy of the particle and $A_\perp$ describes the change of the transverse energy of the particle.

The calculations of $A_\parallel$ and $A_\perp$ are given in Appendix L. The resulting expressions for the extraordinary mode, $\mathbf{e}^{(x)} = (0,\, 1,\, 0)$, and ordinary mode, $\mathbf{e}^{(o)} = (\cos\theta,\, 0,\, -\sin\theta)$ are

$$A_\parallel^{(x)} = -\frac{e^2\, v_\perp^2\, v_\phi}{2\,\pi\, c^4} \sum_{\nu=-\infty}^{\nu=\infty} \int d\mathbf{\Omega}\, d\omega\, n^2\, \omega^2\, \cos\theta\, J_\nu'(\lambda)^2 \delta(\omega - s\,\omega_B/\gamma - k_\phi\, v_\phi), \tag{6.17}$$

$$A_\perp^{(x)} = -\frac{e^2\, v_\perp^2\, s\,\omega_B/\gamma}{2\,\pi\, c^3} \sum_{\nu=-\infty}^{\nu=\infty} \int d\mathbf{\Omega}\, d\omega\, n\,\omega J_\nu'(\lambda)^2 \delta(\omega - s\,\omega_B/\gamma - k_\phi\, v_\phi), \tag{6.18}$$

$$A_\parallel^{(o)} = -\frac{e^2\, v_\phi}{2\,\pi\, c^4} \sum_{\nu=-\infty}^{\nu=\infty} \int d\mathbf{\Omega}\, d\omega\, n\,\omega^2 \left(n\, v_\perp \frac{s}{\lambda} - c\,\sin\theta\right) \left(\frac{s}{\lambda} v_\perp\, \cos\theta - v_\phi\, \sin\theta\right) \times J_\nu^2(\lambda) \delta(\omega - s\,\omega_B/\gamma - k_\phi\, v_\phi), \tag{6.19}$$

$$A_\perp^{(o)} = -\frac{e^2\, v_\perp}{2\,\pi\, c^4} \sum_{\nu=-\infty}^{\nu=\infty} \int d\mathbf{\Omega}\, d\omega\, \omega^2\, \frac{s}{\lambda} \frac{(n\, v_\phi - c\cos\theta)^2}{\sin\theta} \times J_\nu(\lambda)^2 \delta(\omega - s\,\omega_B/\gamma - k_\phi\, v_\phi). \tag{6.20}$$

It is straightforward to check that adding transverse and parallel parts, we get the total emissivities for the ordinary and extraordinary modes (Melrose 1978c Eq. 4.33):

$$\eta_x(\omega) = \int d\mathbf{\Omega} \eta_x(\omega,\theta) = \int d\mathbf{\Omega} \sum_{\nu=-\infty}^{\nu=\infty} \frac{e^2\,\omega^2\, v_\perp^2\, n\, J_\nu'(\lambda)^2}{2\,\pi\, c^3} \delta\left(\omega(1 - n\,\beta_z\,\cos\theta) - s\,\tilde{\omega}_H\right),$$

$$\eta_o(\omega) = \int d\mathbf{\Omega} \eta_o(\omega,\theta) = \int d\mathbf{\Omega} \sum_{\nu=-\infty}^{\nu=\infty} \frac{e^2\,\omega^2\, J_\nu(\lambda)^2}{2\,\pi\, c\, n} \frac{(n\,\beta_z - \cos\theta)^2}{\sin^2\theta} \times \delta\left(\omega(1 - n\,\beta_z\,\cos\theta) - \nu\,\tilde{\omega}_H\right). \tag{6.21}$$

From Eq. (6.20) we see that the ϕ components of the work done by the radiation reaction force are always negative; the particle always reduces its parallel momentum. The sign of the transverse component of the work depends on the sign of ν - the type of the resonance: for a normal Doppler resonance ($\nu > 0$) the transverse energy of the particles decreases; however, for an anomalous Doppler resonance ($\nu < 0$), the transverse energy of the particles increases.

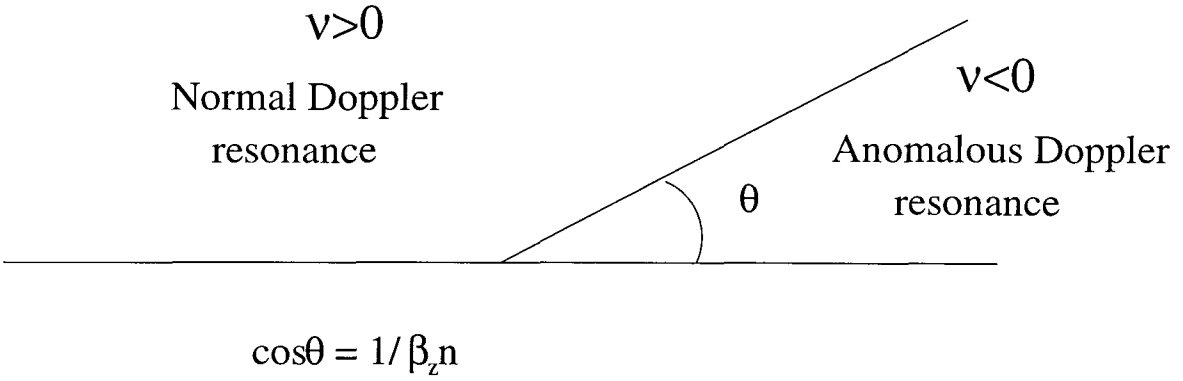

Fig. 2

Figure 6.1: Regions of normal and anomalous Doppler effects.

6.2 Physics of Cherenkov-drift Emission

In this section we discuss this novel emission mechanism of a charged particle streaming with relativistic velocity along curved magnetic field line in a medium. A weak inhomogeneity of the magnetic field results in a curvature drift motion of the particle perpendicular to the local plane of the magnetic field line. A gradient drift (proportional to $\nabla \cdot \mathbf{B}$) is much smaller than the curvature drift and will be neglected. When the motion of the particle parallel to the magnetic field is ultrarelativistic the drift motion even in the weakly inhomogeneous field can become weakly relativistic resulting in a new type of generation of *electromagnetic*, vacuumlike waves. The presence of three ingredients (strong but finite magnetic field, inhomogeneity of the field and a medium with the index of refraction larger than unity) is essential for the emission. We will call this mechanism Cherenkov-drift emission stressing the fact that microphysically it is virtually Cherenkov-type emission process.

Conventional consideration of the curvature emission (Blandford 1975, Zheleznyakov & Shaposhnikov 1979, Luo & Melrose 1992a, Melrose 1978c) emphasize the analogy between curvature emission and conventional cyclotron emission. In our opinion this approach, though formally correct, has limited applicability and misses some important physical properties of the emission mechanism. In a separate approach Kazbegi et al. 1991b considered this process calculating a dielectric tensor of an inhomogeneous magnetized medium, thus treating the emission process as a collective effect. They showed that maser action is possible only if a medium supports subluminous waves. In this work we show how these two approaches can be reconciled and argue that the dielectric tensor approach, which treats the Cherenkov-drift emission as a collective process, has a wider applicability.

The interplay between cyclotron (or synchrotron) and Cherenkov radiation has been a long-

standing matter of interest. Schwinger et al. 1976 discussed the relation between these two seemingly different emission mechanisms. They showed that conventional synchrotron emission and Cherenkov radiation may be regarded as respectively limiting cases of $|n-1| \ll 1$ and $B = 0$ of a synergetic (using the terminology of Schwinger et al. 1976) cyclotron-Cherenkov radiation. In another work Lyutikov 1997b this analogy has been discussed to include cyclotron-Cherenkov emission at the anomalous Doppler resonance. An important new aspect of our work (as compared with Schwinger et al. 1976 and Lyutikov 1997b) is that we take into account inhomogeneity of the medium.

Physical origin of the emission in the case of Cherenkov-type and synchrotron-type processes is quite different. In the case of Cherenkov-type process, the emission may be attributed to the electromagnetic polarization shock front that develops in a dielectric medium due to the passage of a charged particle with speed larger than phase speed of waves in a medium. It is virtually a collective emission process. In the case of synchrotron-type process, the emission may be attributed to the Lorentz force acting on a particle in a magnetic field. Cherenkov-type emission is impossible in vacuum and in a medium with the refractive index smaller than unity.

The very possibility of a coherent curvature emission by the homogeneous distribution has been an appealing and controversial issue in the pulsar physics for almost two decades. Blandford 1975 proved that a coherent curvature emission by the homogeneous distribution is impossible in the limit of infinitely strong magnetic field in vacuum (except near the point of inflection). A later attempt by Beskin, Gurevich & Istomin 1983 and Beskin, Gurevich & Istomin 1986 to create a theory based on the coherent curvature emission by the homogeneous distribution in the infinitely strong magnetic field has been proven to be erroneous (Machabeli 1995, Nambu 1989, Larroche & Pellat 1988).

Two shortcomings of the approach of Blandford 1975 were noted. The first is that in adopting a plane wave formalism, the interaction length for an individual electron, $\approx R_B/\gamma_b$, was essentially coextensive with region over which the waves could interact with any electron. The approach precluded a strong amplification under all circumstances because the wave would have to grow substantially during a single interaction in a manner that could not be easily quantified. The second problem was a neglect of dispersion. We address the first shortcoming by expanding the electromagnetic field in cylindrical waves centered on $r = 0$, and the second explicitly by considering general plasma modes.

When the curvature drift of a particle streaming along magnetic field is included (which requires a finite magnetic field), there is a possibility of a maser action (Zheleznyakov & Shaposhnikov 1979, Chugunov & Shaposhnikov 1981). The curvature maser happens on the Cherenkov-drift resonance (H.1). From the microphysical point of view, Cherenkov-drift emission is quite similar to the conventional Cherenkov emission, except that now one should take into account the drift velocity of the resonant particles.

It is more natural to consider Cherenkov-drift emission in a curved magnetic field as an analog

of the Cherenkov emission with the drift of the resonance particles taken into account, than as the type of a curvature emission. From the microphysical point of view, the emission is again due to the polarization shock front that develops due to the passage of a superluminal particle through a medium, so it is required that the emitting particle propagate with the velocity greater than the phase velocity of the emitted waves. The Cherenkov-drift maser is impossible in vacuum, unlike the curvature emission, which is a close analog of the conventional cyclotron emission and is possible in vacuum. The curvature provides only the drift component of the velocity, which is essential for coupling the resonant particle to the emitted electromagnetic wave.

In a Cherenkov-type emission the resonant particle can interact only with the part of the electric field parallel to the velocity. Thus, if the drift of the resonant particles perpendicular to the plane of the field line is taken into account, it becomes possible to emit a *transverse electromagnetic* wave with the electric field along the drift velocity, i.e., perpendicular to the plane of the curved field line (see Fig. 6.2). The growth occurs on the rising part of the parallel distribution function where $\frac{\partial f_{\parallel}}{\partial p_{\parallel}} > 0$. This is satisfied for the particles of the primary beam.

6.2.1 Airy Function Approximation

Next we consider the Airy function approximation to the curvature emissivities of ultrarelativistic particles *in a medium*. The expression for the emissivity is

$$\eta(\omega) = \frac{\sqrt{\epsilon}\omega^2 q^2 v_\phi^2}{2\pi c}\left(J_\nu'^2(\nu\sqrt{\epsilon}\beta_\phi\cos\theta) + \frac{\tan^2\theta}{\epsilon\beta_\phi^2}J_\nu^2(\nu\sqrt{\epsilon}\beta_\phi\cos\theta)\right)\delta\left(\omega - \nu\beta_\phi c/r\right) \tag{6.22}$$

(emissivity per unit solid angle $d\Omega$).

We assume that a particle is moving through a dielectric with the permittivity $\epsilon > 1$. We show, that for large energies of the particle, when it is moving with the velocity larger than the speed of light in a medium, a qualitatively different expansion of the Airy function should be used.

This is analogous to the cyclotron emission at the anomalous Doppler resonance in the straight magnetic field. Emission at the anomalous Doppler resonance are qualitatively different from the emissivities at the normal Doppler resonance. Emission at the anomalous Doppler resonance is similar to the Cherenkov emission - this is a collective effect in which all the particles of the medium take part.

In the transition region, when the argument of the Bessel functions is large and close to their orders, it is possible to use the Airy function approximation

$$J_\nu\left(\nu + z\nu^{1/3}\right) \approx \left(\frac{2}{\nu}\right)^{1/3} Ai\left(-2^{1/3}z\right) = \begin{cases} \frac{2^{2/3}}{3\nu^{1/3}}\left(J_{1/3}\left(\frac{2^{3/2}}{3}z^{3/2}\right) + J_{-1/3}\left(\frac{2^{3/2}}{3}z^{3/2}\right)\right) & \text{if } z > 0 \\ \frac{2^{2/3}\sqrt{z}}{\sqrt{3}\pi\nu^{1/3}}\ K_{1/3}\left(\frac{2^{3/2}}{3}|z|^{3/2}\right) & \text{if } z < 0 \end{cases} \tag{6.23}$$

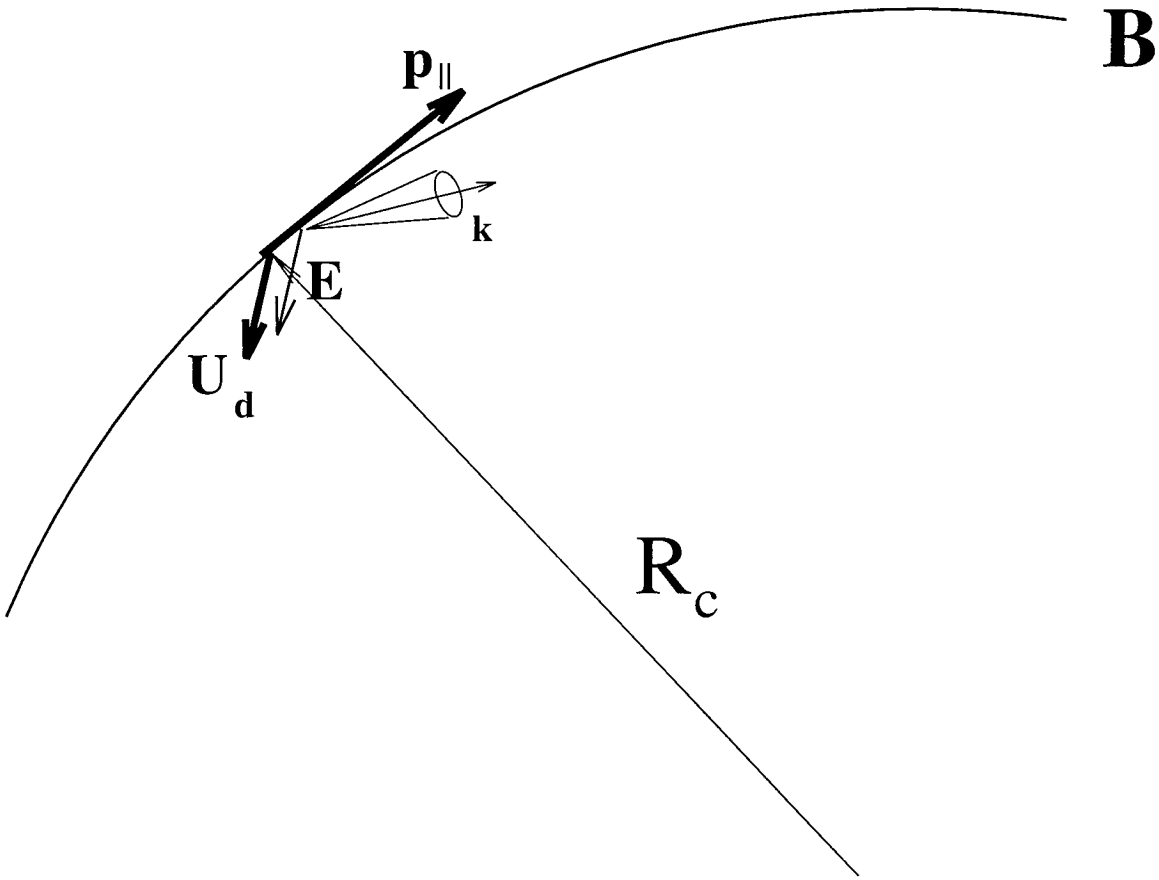

Figure 6.2: Cherenkov-drift emission. Drift velocity $\mathbf{u}_d$ is perpendicular to the plane of the curved field line ($\mathbf{B} - \mathbf{R_c}$ plane, $\mathbf{R_c}$ is a local radius of curvature). The emitted electromagnetic waves are polarized along $\mathbf{u}_d$. The emission is generated in the cone centered at the angle $\theta^{em} = u_d/c$ and with the opening angle $(2\delta)^{1/2} \ll \theta^{em}$.

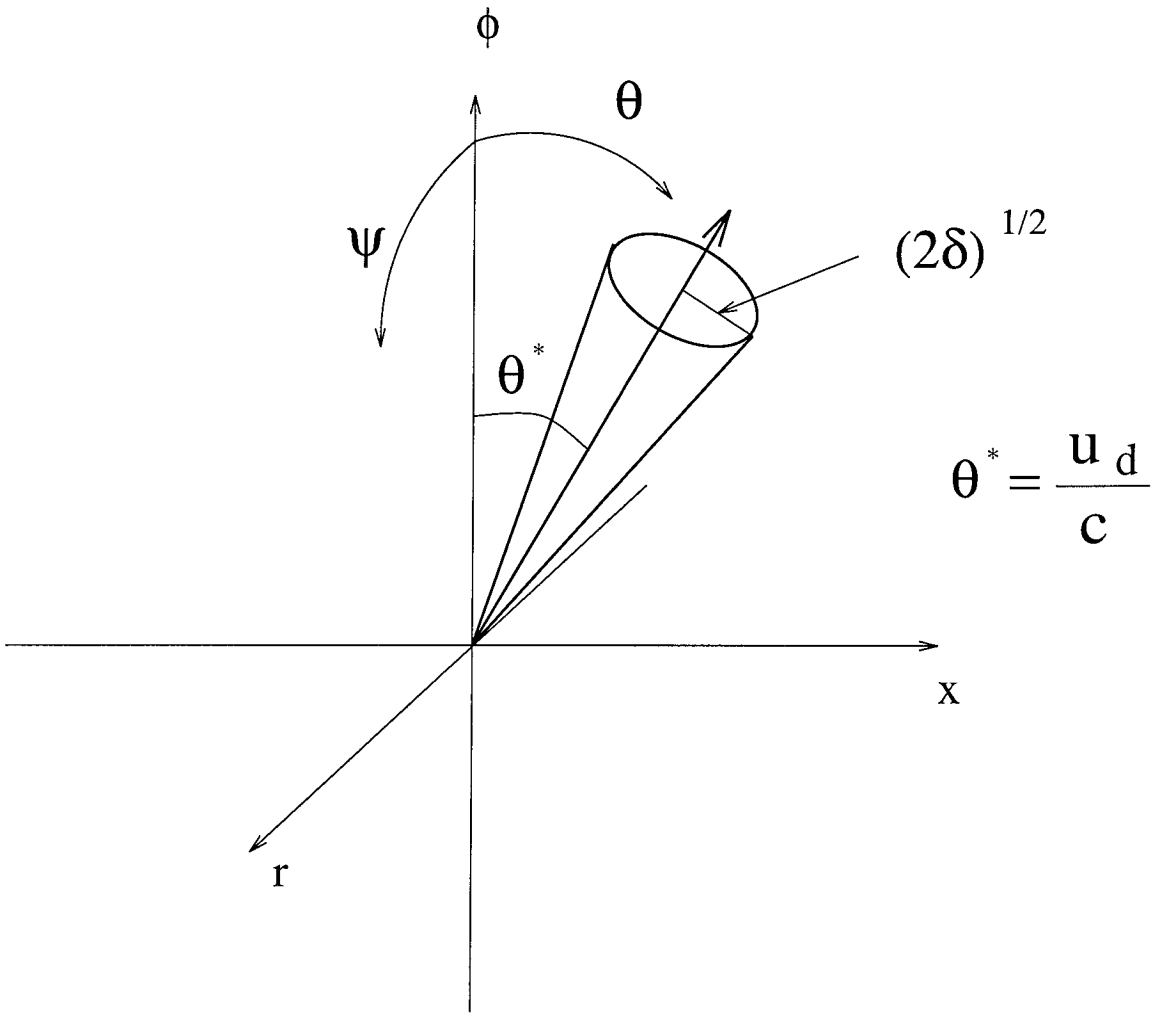

Figure 6.3: Geometry of the Cherenkov-drift resonance. In a given field a particle with a given Lorentz factor resonates with the waves propagating along the cone centered around the instantaneous particle velocity and with the opening angle $(2\delta)^{1/2}$.

where $Ai\,(x)$ is Airy function.

In vacuum the argument of the Bessel functions is always smaller than the order: $\lambda r = \nu\beta_\phi \cos\theta < \nu$. In a medium, the argument of the Bessel functions can become larger than the order. In a dielectric the argument of the Bessel functions is $\hat{\lambda} r = \sqrt{\omega^2\epsilon/c^2 - k_x^2}\, r$. If we introduce a notation $k_x = \omega\sqrt{\epsilon}/c \sin\theta$ (this is a definition of angle θ, the condition of regularity at infinity, $\hat{\lambda}^2 > 0$ insures that $\sin\theta < 1$), then we have $\hat{\lambda} r = \nu\sqrt{\epsilon}\beta_\phi \cos\theta$, which can be larger than ν if $\beta_\phi > 1/\sqrt{\epsilon}$ - for the superluminal motion of a particle. Using these notations we find

$$z = (\sqrt{\epsilon}\beta_\phi \cos\theta - 1)\nu^{2/3} \approx \left(\delta - \frac{1}{2\gamma^2} - \frac{\theta^2}{2}\right)\nu^{2/3} \tag{6.24}$$

for $\epsilon = 1 + 2\delta$, $\delta \ll 1$, $\gamma \gg 1$ and $\theta \ll 1$. It is clear from Eq. (6.24) that in vacuum $z < 0$ and in a medium z becomes positive for superluminal particles.

Following the discussion of Section A.3, we can identify the light cylinder radius for the mode ν as $r_\nu = \nu/\hat{\lambda}$. We can argue that in the case $z > 0$ the resonant interaction of a particle with a wave occurs *outside* the light cylinder

$$r_0 = r_\nu \left(1 + \frac{z}{\nu^{2/3}}\right) \tag{6.25}$$

A transition through point $z = 0$ (light cylinder) is nontrivial. It resembles phase transition (Schwinger et al. 1976) in a sense that correlation length for thermal or quantum fluctuations is very large near the transition. The physical conditions beyond and above the transition point are essentially different.

For superluminal motion, the collective effects of the medium play an important role. In this case the corresponding emission process can be called Cherenkov-curvature emission, stressing the fact that both inhomogeneous magnetic field and a medium are important for the emission. In the vacuum limit, $n \to 1$, Cherenkov-curvature emission reduces to the conventional curvature emission. Conventional Cherenkov radiation may be obtained in the limit $r \to \infty$ after integration over ν (see Schwinger et al. 1976 for the corresponding transition for the cyclotron-Cherenkov radiation).

The emissivity for the Cherenkov-curvature process is

$$\eta(\omega) = \frac{2^{2/3}\sqrt{\epsilon}\omega^2 q^2 v_\phi^2}{2\pi c \nu^{2/3}} \left(\frac{\tan^2\theta}{\epsilon\beta_\phi^2} Ai^2(-2^{1/3}z) + \left(\frac{2}{\nu}\right)^{2/3} Ai'^2(-2^{1/3}z)\right) \delta\left(\omega - \nu\Omega\right) \tag{6.26}$$

For $z < 0$ this reduces to the conventional representation for synchrotron emission in terms of MacDonald functions $K_{1/3}$. For $z > 0$ Eq. (6.26) gives

$$\eta(\omega) = \frac{2^{1/3}\sqrt{\epsilon}\omega^2 q^2 v_\phi^2}{9\pi c \nu^{2/3}} \left(\frac{\tan^2\theta}{\epsilon\beta_\phi^2}\left(J_{1/3}(\xi) + J_{-1/3}(\xi)\right)^2 + \frac{2^{2/3}z^2}{\nu^{2/3}}\left(J_{2/3}(\xi) - J_{-2/3}(\xi)\right)^2\right) \delta\left(\omega - \nu\Omega\right) \tag{6.27}$$

where we used

$$J'_\nu\left(\nu + z\nu^{1/3}\right) \approx \left(\frac{2}{\nu}\right)^{2/3} Ai'\left(-2^{1/3}z\right)$$
$$Ai'(-z) = -\frac{z}{3}\left(J_{-2/3}\left(-2^{1/3}z\right) - J_{2/3}\left(-2^{1/3}z\right)\right) \tag{6.28}$$

The emissivity (6.27) may be simplified in the case $\xi \gg 1$. Then we can use the asymptotic expansion for Airy functions

$$Ai(-z) \approx \frac{1}{\sqrt{\pi}z^{1/4}} \sin\left(\frac{2}{3}z^{3/2} + \frac{\pi}{4}\right)$$
$$Ai'(-z) \approx \frac{z^{1/4}}{\sqrt{\pi}} \cos\left(\frac{2}{3}z^{3/2} + \frac{\pi}{4}\right) \tag{6.29}$$

to find

$$\eta(\omega) = \frac{\sqrt{2}\sqrt{\epsilon}\omega^2 q^2 \beta_\phi^2 \sqrt{z}}{\pi^2 c \nu^{4/3}} \left(\cos^2(\xi + \pi/4) + \frac{\sin^2(\xi + \pi/4)\nu^{2/3}\tan^2\theta}{2z\epsilon\beta_\phi^2}\right) \delta\left(\omega - \nu\Omega\right) \tag{6.30}$$

where $\xi = (2z)^{3/2}/3$.

For $\delta \gg 1/\gamma^2$, and $\delta \gg \theta^2$ the condition $z \gg 1$ implies $\delta\nu^{2/3} \gg 1$. Then (6.30) can be further simplified:

$$\eta(\omega) \approx \frac{\sqrt{2}\sqrt{\epsilon}\sqrt{\delta}\omega^2 q^2 \beta_\phi^2}{\pi^2 c\nu} \cos^2\left(\frac{2^{3/2}\nu}{3}\delta^{3/2} + \frac{\pi}{4}\right) \delta\left(\omega - \nu\Omega\right) \tag{6.31}$$

In this context we note that the total spectral power for the curvature emission in a medium, viz

$$\eta(\omega) = \frac{q^2\omega}{n^2 r}\left(2n^2\beta_\phi^2 J'_{2\nu}(2\nu n\beta_\phi) - (1 - n^2\beta_\phi^2)\int_0^{2\nu n\beta_\phi} dx J_{2\nu}(x)\right) \tag{6.32}$$

for the case of superluminal motion, $n\beta_\phi > 1$, can be reduced to the explicitly Cherenkov-type emission form:

$$\eta(\omega) = \frac{q^2\omega\beta_\phi}{4\pi c}\left(1 - \frac{1}{n^2\beta_\phi^2}\right)\Lambda(z) \tag{6.33}$$

with $\Lambda(z)$ of the order of unity for $z \geq 1$ (Schwinger et al. 1976).

Chapter 7 Instabilities in the Pair Plasma

7.1 Introduction

At the moment the most promising theories of the pulsar radio emission generation are based on the plasma emission model, in which the high brightness radio emission is generated by some kind of instabilities developing in the outflowing plasma (Melrose 1995). In this chapter we consider in generality several possible beam-type instabilities in the strong magnetized electron-positron plasma in a superstrong *rectilinear* magnetic field, i.e., in this chapter we will neglect the curvature of the magnetic field lines. The possible resonances include the Cherenkov and cyclotron resonances of the particles with the Alfven, extraordinary and ordinary modes in two regimes: kinetic and hydrodynamic. The calculations are done for the cases of cold and relativistic hot plasma taking into account angular dependence of the growth rate.

In a pulsar magnetosphere the Cherenkov instabilities occur in the hydrodynamic regimes, while the cyclotron instabilities occur in the kinetic regime. We find that the hydrodynamic-type instabilities are strongly suppressed by the large relativistic γ-factor of the primary beam. In contrast, the cyclotron instabilities are not subject to strong suppression by the large streaming γ-factor. Based on this, we argue that electromagnetic cyclotron-type instabilities on the extraordinary, ordinary and probably Alfvén waves are more likely to develop in the pulsar magnetosphere.

We assume initially that we have a strongly magnetized, one-dimensional, electron-positron plasma with the similar distribution functions for electrons and positrons plus a beam of the high energy, fast particles streaming along the magnetic field. One-dimensional relativistic electron-positron plasmas are very different from their electron-ion counterpart for two separate reasons - their normal modes are quite different and relativistic one-dimensional distribution function considerably modifies the nature of the wave-particle interaction.

In this chapter we consider wave excitation in a strongly magnetized pair plasma in the approximation of straight magnetic field lines, thus omitting an important Cherenkov-drift resonance (Lyutikov, Blandford & Machabeli 1997, Lyutikov, Machabeli & Blandford 1997a). This is an important mechanism that may be responsible for the generation of the cone type emission in pulsars. The electromagnetic Cherenkov-drift instability occurs in the kinetic regime on the high frequency vacuum-like ordinary and extraordinary waves. It has the same advantages as the electromagnetic cyclotron instabilities considered in this paper.

We will give here the simplified calculations: a more detailed consideration can be found in

Lyutikov 1997c. In this chapter we will be working in the plasma frame, which is streaming with the Lorentz factor γ_p with respect to the pulsar frame. We recall that the parameters measured in the pulsar frame are denoted with a prime.

7.2 Hydrodynamic and Kinetic Instabilities

The description of the beam-plasma instabilities is based on the scheme used to solve the general problem of linear oscillations in plasma. The initial equations are the linearized kinetic equations for the particles in a self-consistent electromagnetic field and Maxwell's equations. When the unperturbed state of the beam and plasma is stationary and spatially uniform, we can use Eq. (5.32) to find the normal modes of a medium.

For the beam-plasma system the dielectric tensor $\epsilon_{\alpha\beta}(\omega, \mathbf{k})$ may be represented as a sum of contributions from plasma and beam.

$$\epsilon_{\alpha\beta}(\omega, \mathbf{k}) = \delta_{\alpha\beta} + \frac{4\pi c}{\omega}\sigma_{\alpha\beta}^{plasma} + \frac{4\pi c}{\omega}\sigma_{\alpha\beta}^{beam} \tag{7.1}$$

where $\sigma_{\alpha\beta}^{plasma}$ and $\sigma_{\alpha\beta}^{beam}$ are the conductivity tensors of plasma and beam.

Sometimes it is possible to consider beam as a weak perturbation to the system. Then, in the zeroth approximation, the normal modes of the medium will be determined from (5.32) with $\sigma_{\alpha\beta}^{beam}$ set to zero. This will produce a set of normal modes of the medium $\{\omega(\mathbf{k})^l\}$.

If the plasma alone is stable, then the frequency of the normal modes will have a zero imaginary part. In the first approximation, dispersion relation (5.32) may be expanded taking into account a small contribution to the dielectric tensor from the beam. The frequency shift $\Delta(\mathbf{k})^l$ of the normal mode $\omega(\mathbf{k})^l$ is then determined from

$$\Delta(\mathbf{k})^l \left[\frac{\partial}{\partial\omega}K_p(\omega, \mathbf{k})\right]\Big|_{\omega(\mathbf{k})^l} + K_b(\omega, \mathbf{k}) = 0 \tag{7.2}$$

where $K_p(\omega, \mathbf{k})$ and $K_b(\omega, \mathbf{k})$ are the plasma and beam parts of Eq.(5.32). For stable plasma without a beam, $K_p(\omega, \mathbf{k})$ and $\{\omega(\mathbf{k})^l\}$ are real.

Two separate cases may be distinguished here depending on whether the complex part of the beam contribution to the dispersion relations (7.2) $K_b(\omega, \mathbf{k})$ is zero or nonzero. If $\mathrm{Im}(K_b(\omega, \mathbf{k}) = 0$ then equation (7.2) has real coefficients. The complex solutions of Eq.(7.2) (if any) are complex conjugates. Solutions with the positive complex part correspond to the growing waves. These are hydrodynamic instabilities. In hydrodynamic instabilities, all the particles of the beam resonate with the normal mode of the plasma. This requires that the growth rate of the instability be greater than the intrinsic bandwidth of the growing waves:

$$|\mathbf{k}\cdot\delta\mathbf{v}| \ll \mathrm{Im}(\Delta(\mathbf{k})). \tag{7.3}$$

Here $\mathbf{k}$ is the resonant wave vector, $\delta\mathbf{v}$ is the scatter in the velocity of the beam particles. This is satisfied for a very small scatter in the velocity of the beam particles, so that all the particles from the beam resonate with the beam.

Alternatively, if the complex part of the the beam contribution to the dispersion relations (7.2) $K_b(\omega,\mathbf{k})$ is nonzero, the frequency shift $\Delta(\mathbf{k})$ will always have a complex part. If the complex part of $\Delta(\mathbf{k})^l$ is larger than zero, then the corresponding normal mode $\omega(\mathbf{k})^l$ will be growing at the expense of the beam energy, while for negative $\Delta(\mathbf{k})^l$ the mode will be damped on the resonant particles of the beam. This case corresponds to the kinetic instability. The requirement that the frequency shift $\Delta(\mathbf{k})^l$ due to the complex part of $K_b(\omega,\mathbf{k})$ dominates over the shift due to the large real part of $K_b(\omega,\mathbf{k})$ requires that the growth rate be much less than the the intrinsic bandwidth of the growing waves (reversed inequality (7.3)). This is satisfied for a very large scatter in the velocity of the beam particles, so that at any given moment only a small fraction of the beam particles is in resonance with the wave.

Though the physical interpretations of the kinetic and hydrodynamic instabilities are quite different, they may be considered as two limiting cases of a general beam instability. For a relativistic beam traveling along a magnetic field with average Lorentz factor γ_b, scatter in parallel Lorentz factors $\Delta\gamma$, and average pitch angle ψ the condition of the hydrodynamic approximation (7.3) takes the form

$$k_\parallel c\left(\frac{\psi^2}{2}+\frac{\Delta\gamma}{\gamma^3}\right)+k_\perp c\,\psi+\frac{s\omega_B\Delta\gamma}{\gamma^2} \ll \Gamma \tag{7.4}$$

where s is the harmonic number ($s=0$ for Cherenkov resonance, $s\neq 0$ for cyclotron resonance) and Γ is a growth rate of an instability. For the kinetic instability, this inequality is reversed.

From (7.4) it follows that there exist a critical pitch angle

$$\psi_{crit}=\frac{1}{\gamma}\sqrt{\frac{\Delta\gamma}{\gamma}} \tag{7.5}$$

For $\psi > \psi_{crit}$ the scatter in pitch angles dominates over longitudinal velocity spread. For $\psi > \psi_{crit}$ the average "longitudinal" mass of the beam particles decreases by the factor of $(\psi\gamma_b)^2$ so that the instabilities whose growth rate is inversely proportional to the "longitudinal" mass of the particles (like Cherenkov instability of plasma waves) may be enhanced considerably.

Relativistic particles propagating along the curved magnetic field of a pulsar magnetosphere initially are in the ground quantum state (zero pitch angle). They can develop a finite pitch angle by (i) particle-particle collisions, (ii) interaction with the electromagnetic field (Compton scattering on the diffuse thermal photons or recoil due the emission of electromagnetic waves at anomalous

cyclotron resonance), and (iii) when the adiabatic approximation for the propagation breaks down (when the Larmor radius becomes comparable with the size of the inhomogeneity). The pitch angle of the particles is then determined by the balance of these forces on one hand and radiation damping at the normal synchrotron resonance and the force due to the conservation of adiabatic invariant on the other hand.

In magnetosphere, the particle-particle collision time is very long compared with the dynamical time because of the relatively low density of particles, high speed and the one-dimensional character of the motion. We also assume that the Compton scattering on the diffuse thermal photons is unimportant and that the adiabatic approximation for the propagation of particles is satisfied. The transverse component of the force due to the radiation damping at normal synchrotron resonance dominates the transverse motion of the particles near the neutron star, making the pitch angles equal to zero. Then the pitch angles will remain zero throughout the region where the above conditions are satisfied.

In what follows we assume that plasma is one-dimensional before the development of instabilities. The condition of hydrodynamic approximation (7.4) is then

$$k_{\|} c \frac{\Delta\gamma}{\gamma^3} + \frac{s\omega_B \Delta\gamma}{\gamma^2} \ll \Gamma \tag{7.6}$$

In the kinetic regime this inequality is reversed.

For an instability to be important as a possible source of coherent emission generation, its growth rate, evaluated in the pulsar frame, should be much larger than the pulsar rotation frequency Ω. The growth rates in the pulsar and plasma frames are related by

$$\Gamma' = \frac{\Gamma}{\gamma_p}. \tag{7.7}$$

So the requirement of a fast growth in the plasma frame is

$$\frac{\Gamma}{\gamma_p \Omega} \gg 1. \tag{7.8}$$

Another, more stringent requirement on the growth rate comes from the angular dependence of a growth rate. The emitting plasma propagates in a curved magnetic field. If an instability has a considerable growth inside a characteristic angle $\delta\theta'$, then the growth length should be larger than $\delta\theta R_c$, where R_c is the curvature of the magnetic fields. In the plasma frame this requirement is

$$\Gamma \gg \frac{c\gamma_p^2}{R_c\, \delta\theta}, \tag{7.9}$$

where we used $\delta\theta' \approx \delta\theta/\gamma_p$.

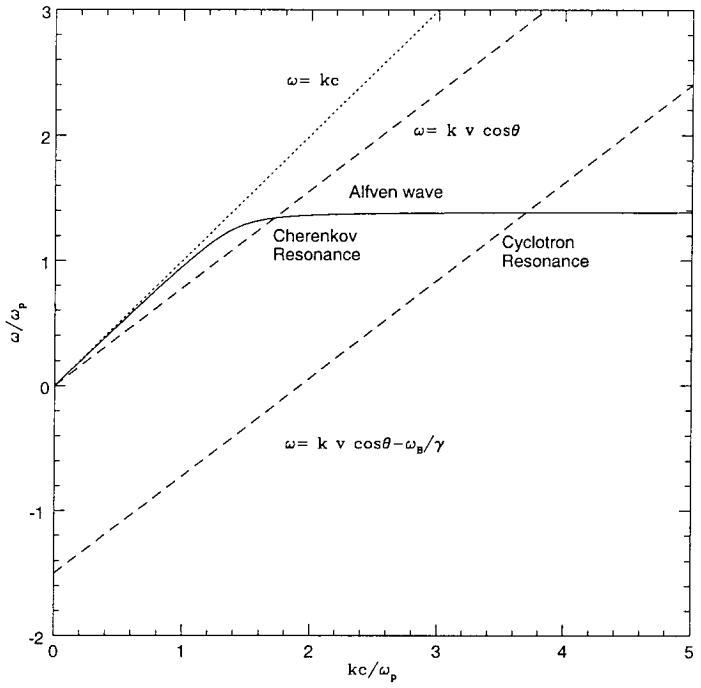

Figure 7.1: Resonances of the Alfvén mode in the cold plasma for $\mu < 1$.

7.3 Resonances in Cold Pair Plasma

In the cold plasma approach the resonant interaction between the fast particles and the plasma may be considered as the interaction of the waves in the plasma with the waves in the beam. The interaction is the strongest when the dispersion relations of the waves intersect. Consequently, we are looking for the possible resonances between the waves in the plasma (5.35) and the waves in the beam (see Fig. 7.1 - 7.3):

$$\omega = v_b \, k_\phi \tag{7.10}$$

$$\omega = v_b \, k \cos\theta \pm \frac{\omega_B}{\gamma_b} \tag{7.11}$$

As we will see in Section 7.5, the resonant interaction of the plasma waves with the Cherenkov waves in the beam (7.10) is described by the cubic equation for the frequency shift, which always has complex conjugate solutions. This implies that the Cherenkov resonant interaction of the waves in the beam and in the plasma is always unstable.

In contrast, the frequency shift due to the cyclotron interaction of the waves in the beam and in the plasma (7.11) is described by a quadratic equation, which has two real solutions for the plus

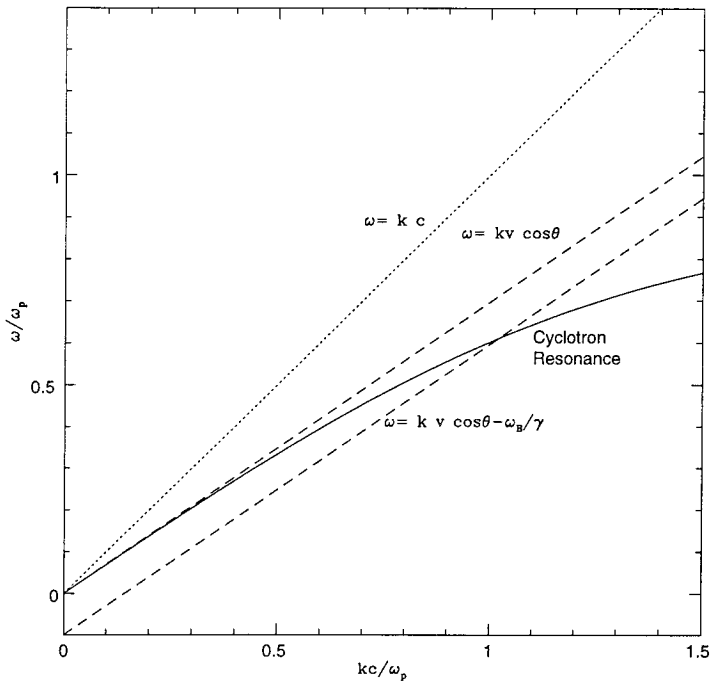

Figure 7.2: Resonances of the Alfvén mode in the cold plasma for $\mu > 1$.

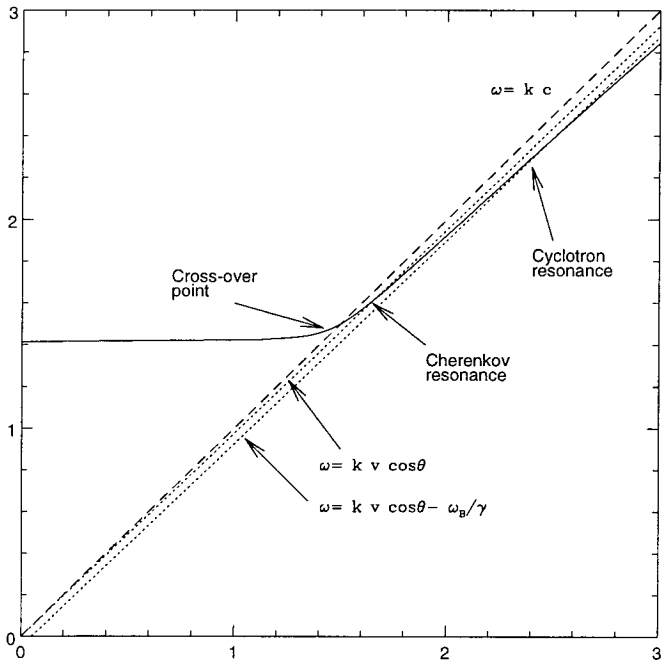

Figure 7.3: Resonances on the ordinary mode in the cold plasma for $\mu > 1$.

sign in (7.11) and two complex solutions for the minus sign in (7.11). Thus, only the minus sign in (7.11) will contribute to the instability growth rate. The resonance (7.11) with the minus sign is called anomalous Doppler resonance. This corresponding instability may be considered as the interaction of the negative energy wave in the beam with the positive energy wave in plasma. Due to the resonant coupling, the amplitudes of both waves grow exponentially.

Now let us consider the condition for the resonances (7.10) and (7.11) to occur. From the low frequency asymptotics of the Alfvén waves (5.46) we infer that the possibility of the Cherenkov excitation of the Alfvén waves depends on the parameter

$$\mu = \frac{2\,\gamma_b\,\omega_p}{\omega_B} \tag{7.12}$$

If $\mu < 1$, then Alfvén waves can be excited by Cherenkov resonance.[1] However, if $\mu > 1$ then Alfvén waves cannot be excited by Cherenkov resonance. Instead, resonance can occur for an O mode subject to the requirement of sufficiently small angles of propagation Fig. 7.3 (see Section 7.3.4 below).

For the cold plasma in the region of open field lines we have

$$\mu = \gamma_b\sqrt{\frac{2\,\lambda\,\Omega}{\gamma_p\omega_B}} = \sqrt{\frac{2\,\lambda\,\Omega}{\omega_B}}\frac{\gamma_b'}{\gamma_p^{3/2}} = 5\times 10^{-3}\left(\frac{r}{R_{NS}}\right)^{3/2} = \begin{cases} <1, & \text{if } \left(\frac{r}{R_{NS}}\right) < 43 \\ >1, & \text{if } \left(\frac{r}{R_{NS}}\right) > 43 \end{cases} \tag{7.13}$$

So, at small radii ($\mu \ll 1$) it is the Alfvén wave that is excited by the Cherenkov resonance, while for larger radii ($\mu \geq 1$) it is the O-mode that can be excited by the Cherenkov resonance. In the outer parts of magnetosphere ($r \geq 100R_{NS}$) the parameter μ becomes much larger than unity: $\mu \gg 1$.

For the parallel propagation (and only in this case) the parts of the ordinary and Alfvén modes that have longitudinal polarization may be considered as forming a single plasma wave with a dispersion $\omega = \sqrt{2}\omega_p$. In this particular case, the excitation of either ordinary or Alfvén part of the longitudinal plasma mode is very similar. But as the waves propagate in the curved magnetic field lines, the parts of the plasma mode corresponding to the ordinary or Alfvén wave will evolve differently resulting in a different observational characteristics of the emergent radiation.

In what follows we consider separately the two possible cases of Cherenkov resonances: $\mu > 1$ and $\mu < 1$.

We also note that the extraordinary wave cannot be excited by the Cherenkov resonance. Though the formal intersection of the Cherenkov wave in the beam (7.10) with the dispersion relation of the extraordinary mode is possible for all frequencies if $\mu = 1$, the transverse polarization of the

[1] In the case of cold plasma this may be considered as a sufficient condition for the Cherenkov excitation of Alfvén waves. In the case of hot plasma this is only a necessary condition (see below).

extraordinary mode excludes a resonant interaction with particles streaming along the magnetic field.

7.3.1 Cherenkov Resonances of the Alfvén Mode ($\mu < 1$)

We can obtain analytical solution for the location of the Cherenkov resonances of the Alfvén mode in the limit $\mu \ll 1$. Then we can take a $\omega_b \to \infty$ approximation in the Alfven wave dispersion. In the limit of infinitely strong magnetic field the dispersion for Alfven waves follows from (5.35):

$$n^2 = \frac{\omega^2 - 2\,\omega_p^2}{\omega^2 - 2\,\omega_p^2\,\cos^2\theta} \tag{7.14}$$

At the Cherenkov resonance we have $n = 1/(\beta_b \cos\theta)$. Solving (7.14) we find the location of the Cherenkov resonance of the Alfvén waves in the cold plasma:

$$\omega_{res} = \left(\frac{2\,\omega_p^2\,\cos^2\theta}{\gamma_b^2\,(1-\beta_b^2\,\cos^2\theta)}\right)^{1/2} = \begin{cases} \sqrt{2}\,\omega_p \cos\theta & \text{if } \theta \ll 1/\gamma_b \\ \frac{\sqrt{2}\,\omega_p\,\cot\theta}{\gamma_b} & \text{if } \theta \gg 1/\gamma_b \end{cases} \tag{7.15}$$

7.3.2 Cyclotron Resonance of an Alfvén Mode

We can similarly distinguish two cases for the cyclotron excitation of the waves. If $\mu < 1$ then only Alfvén waves can possibly be excited by the cyclotron resonance. Alternatively, for $\mu > 1$ all the three waves (Alfvén, ordinary and extraordinary) may be excited by the cyclotron resonance.

For $\mu < 1$ the resonance (7.11) on Alfvén waves always occurs at $kc \gg \omega_p$ (Fig. 7.1). Using the asymptotic expansion for the dispersion of the Alfvén branch in the $kc \gg \omega_p$ limit we find

$$\omega_{res} \approx \sqrt{2}\,\omega_p \cos\theta, \qquad k_{res}c = \frac{\omega_B}{\gamma_b\,\beta_b\cos\theta} \tag{7.16}$$

If $\mu \gg 1$ then the cyclotron resonance of the Alfvén wave occurs for $kc \leq \omega_p$. We may distinguish here two separate cases depending on the angle of propagation. For angles smaller than some critical angle, the resonance occurs near $\omega \approx \sqrt{2}\,\omega_p$ while for larger angles the resonance occurs for $\omega \ll \sqrt{2}\,\omega_p$ (Fig. 7.2).

In the latter case we may use the small k approximation to the dispersion of the Alfvén wave (5.46). The resonance condition (7.11) then reads

$$k_{res}c\,\cos\theta\left(\frac{1}{2\gamma_b^2} - \frac{\omega_p^2}{{\omega_B}^2} - \frac{k^2\,c^2\,\sin^2\theta}{4\omega_p^2}\right) + \omega_B/\gamma_b = 0, \qquad k_{res}c \ll \omega_p \tag{7.17}$$

In the limit $\mu \gg 1$ we can neglect the first term as compared to the second. Then, if the third term is much larger than the second (this occurs for the angles of propagation larger than some critical

angle (7.19)) the resonance occurs at

$$k_{res}c = \left(\frac{4\,\omega_p^2\,\omega_B}{\gamma_b\,\cos\theta\,\sin^2\theta} \right)^{1/3} \tag{7.18}$$

The resonant frequency corresponding to (7.18) is much smaller than the plasma frequency if $\theta \gg 1/\sqrt{\mu}$. From (7.18) we also find a condition that the third term in (7.17) dominates over the second at the resonance point:

$$\theta > \theta_{crit} = \frac{\gamma_b\,\omega_p^4}{{\omega_B}^4} \tag{7.19}$$

This angle is always much smaller than unity throughout the pulsar magnetosphere.

Summarizing the possible cyclotron resonances on Alfvén mode we have

$$k_{res}c = \frac{\omega_B}{\gamma_b\,\beta_b\,\cos\theta}, \qquad \text{if } \mu < 1$$

$$k_{res}c = \begin{cases} \frac{\omega_B}{\gamma_b\,\beta_b} + \frac{\sqrt{2}\,\omega_p}{\beta_b} & \text{if } \mu \gg 1 \text{ and } \theta \ll 1/\sqrt{\mu} \\ \frac{2^{\frac{2}{3}}\,\omega_B^{\frac{1}{3}}\,\omega_p^{\frac{2}{3}}}{\sin^{2/3}\theta\,\cos^{1/3}\theta\,\gamma_b^{1/3}} & \text{if } \mu \gg 1 \text{ and } \theta \gg 1/\sqrt{\mu} \end{cases} . \tag{7.20}$$

7.3.3 Cyclotron Resonance on the Extraordinary Mode

The location of the cyclotron resonance on the extraordinary mode (which is possible only if $\mu > 1$ may be found from (5.39) and (7.11). In the low frequency approximation, $\omega \ll \omega_B$ and for small angles $\theta \ll 1$ we have

$$\omega_{res} = \frac{2\omega_B}{\gamma_b} \left(\frac{2\,\omega_p^2}{{\omega_B}^2} - \gamma_b^{-2} - \theta^2 \right) \tag{7.21}$$

This relation may be simplified in the limit $\mu \gg 1$ when the term γ_b^{-2} can be neglected. The resonance is then possible for $\theta < \omega_p/\omega_B$ with a resonant frequency for the parallel propagation given by

$$\omega_{res} = \frac{{\omega_B}^3}{\gamma_b\,\omega_p^2} \tag{7.22}$$

Since we obtained this resonant frequency in the low frequency approximation, $\omega \ll \omega_B$, it is required that

$$\frac{\omega_p^2 \gamma_b}{{\omega_B}^2} \gg 1 \tag{7.23}$$

Using the fiducial plasma parameters of the cold plasma, we find

$$\frac{\omega_p^2 \gamma_b}{{\omega_B}^2} = \lambda\,\gamma_b \frac{2\Omega}{\gamma_p \omega_B} = \frac{\lambda \gamma_b'}{\gamma_p^2} \frac{\Omega}{\omega_B} = 1.3 \times 10^{-10} \left(\frac{r}{R_{NS}} \right)^3 \tag{7.24}$$

which implies that the extraordinary mode can be excited by the cyclotron resonance only in the

outer parts of magnetosphere for radii satisfying

$$\left(\frac{r_{res}}{R_{NS}}\right) > \left(\frac{\omega_B^* \gamma_p^2}{\lambda \gamma_b' \Omega}\right)^{1/3} \approx 2 \times 10^3 \tag{7.25}$$

The location of the cyclotron resonance is quite sensitive to the choice of the bulk streaming energy. Comparing the resonant frequency (7.22) with the plasma frequency, we find

$$\frac{\omega_{res}}{\omega_p} = \frac{{\omega_B}^3}{\gamma_b \omega_p^3} = \frac{\gamma_p^{3/2}}{\gamma_b \lambda^{3/2}} \left(\frac{\omega_B}{2\Omega}\right)^{3/2} \gg 1 \tag{7.26}$$

which implies that the extraordinary mode is always excited with the frequencies much larger than the plasma frequency.

7.3.4 Cherenkov Resonances of the Ordinary Mode ($\mu > 1$)

$$\omega - k_\phi v_b = 0 \tag{7.27}$$

When $\mu > 1$ there is a possibility of the Cherenkov resonance of the ordinary mode. For $\mu \geq 1$ (in the inner parts of the pulsar magnetosphere, but not very close to the star) the Cherenkov resonances of the ordinary mode occurs at $kc \gg \omega_p$, while for $\mu \gg 1$ the Cherenkov resonances of the ordinary mode occurs at $kc \approx \omega_0$ (near the cross over point). Using the corresponding asymptotics for the ordinary wave (5.45), we find that the ordinary wave is superluminous for the angles of propagation larger than kc/ω_B. Consequently, neither Cherenkov or cyclotron-Cherenkov excitation of the ordinary wave is possible for larger angles. For smaller angles we find

$$k_{res} c = \begin{cases} \frac{\sqrt{2}\,\gamma_b\,\omega_p\,\theta}{\sqrt{-1+\mu^2}} & \theta \ll 1/\gamma_b \\ \theta \omega_B \frac{\mu^2+1}{\mu^2} & \theta \gg 1/\gamma_b \end{cases} \tag{7.28}$$

These relations assume $k_{res} c \gg \omega_p$ and $\mu \geq 1$.

For $\mu \gg 1$ (in the outer parts of the pulsar magnetosphere) the Cherenkov resonance on the ordinary mode occurs at $kc \approx \omega_0$. Using the dispersion relations for the ordinary wave near the cross-over points (5.44) we can find the locations of the Cherenkov resonances on the ordinary mode:

$$\omega_{res}^2 \approx 2\,\omega_p^2 + {\omega_B}^2 \sin^2\theta + \frac{2}{\mu^2}\left(1 + \gamma_b^2 \theta^2\right) \tag{7.29}$$

From which it follows that for $\mu \gg 1$ the Cherenkov resonance on the ordinary modes occurs at $\omega_{res} \approx \omega_0$.

7.3.5 Cyclotron Resonance of the Ordinary Mode

The ordinary mode can also be excited at the cyclotron resonance if $\mu > 1$. The lowest excited resonance frequency of the O-mode is reached for the parallel propagation: $\omega_{res} = {\omega_B}^3/\gamma_b\omega_p^2$. The parameters of pulsar magnetospheric plasma are such that this lowest frequency is much higher than the plasma frequency: $\omega_{res} \gg \omega_p$. So in calculating the resonant frequency of the O-mode we can always use the high frequency approximation for the dispersion relation of the O-mode (5.45).

Assuming that $k_{res} \gg \omega_p$ and $\theta < \omega_p/\omega_B$ the solutions of the Eq.(7.11) are

$$k_{res} = \frac{{\omega_B}^3}{\gamma_b\,\omega_p^2}\left(1 + \frac{{\omega_B}^2(1+\gamma_b^2\,\theta^2)}{2\gamma_b^2\omega_p^2} + \frac{\gamma_b^2\omega_p^4\theta^2}{{\omega_B}^4}\right) = \frac{{\omega_B}^3}{\gamma_b\,\omega_p^2}\left(1 + \frac{{\omega_B}^2}{2\omega_p^2}\left(1+\theta^2\gamma_b^2\right)\right) \tag{7.30}$$

The conditions for the cyclotron excitation of the ordinary mode are also subject to the requirement that the resonant frequency is much less than the cyclotron frequency (7.24). So both ordinary and extraordinary modes can be excited by the cyclotron-Cherenkov resonance in the outer parts of pulsar magnetosphere.

7.3.6 Dielectric Tensor for Cold Beam-Plasma System

The dielectric tensor for beam of the density n_b propagating with the velocity v_b along the magnetic field B through a plasma of the density n can be found from a general expression (Eq 5.28) with zero drift velocity $u_\alpha = 0$ and distribution function $f_\alpha(p_\phi) = n_p\,\delta(p_\phi) + n_b\delta(p_\phi - p_b)$ (n_b is a density of a beam and p_ϕ is a momentum of beam particles):

$$\begin{aligned}
\epsilon_{xx} &= 1 + \frac{2\,{\omega_p}^2}{-\omega^2 + {\omega_B}^2} - \frac{{\omega_b}^2\,\hat{\omega}^2}{\gamma_b\,\omega^2\,\hat{\hat{\omega}}^2} = \epsilon_{rr} \\
\epsilon_{xr} &= \frac{-i\,{\omega_b}^2\,\omega_B\,\hat{\omega}}{{\gamma_b}^2\,\omega^2\,\hat{\hat{\omega}}^2} = -\epsilon_{rx} \\
\epsilon_{x\phi} &= -\frac{k\,{\omega_b}^2\,\hat{\omega}\,v_b\,\sin\theta}{\gamma_b\,\omega^2\,\hat{\hat{\omega}}^2} = \epsilon_{\phi x} \\
\epsilon_{r\phi} &= \frac{i\,k\,{\omega_b}^2\,\omega_B\,v_b\,\sin\theta}{{\gamma_b}^2\,\omega^2\,\hat{\hat{\omega}}^2} = -\epsilon_{\phi r} \\
\epsilon_{\phi\phi} &= 1 - \frac{2\,{\omega_p}^2}{\omega^2} - \frac{{\omega_b}^2}{{\gamma_b}^3\,\hat{\omega}^2} - \frac{k^2\,{\omega_b}^2\,{v_b}^2\sin^2\theta}{\gamma_b\,\omega^2\,\hat{\hat{\omega}}^2}
\end{aligned} \tag{7.31}$$

where $\hat{\omega} = \omega - k\,v_b\,\cos\theta$, $\hat{\hat{\omega}} = (\omega - k\,v_b\,\cos\theta)^2 - {\omega_B}^2/\gamma_b^2$ and $\gamma_b = 1/\sqrt{1 - \frac{v_b^2}{c^2}}$.

We will always assume that beam can be considered as a weak perturbation, so that we can employ the expansion procedure described in Section 7.2.

7.4 Hydrodynamic Instabilities for Parallel and Perpendicular Propagation

7.4.1 Parallel Propagation

In this section we calculate the growth rates for the beam instabilities for the waves propagating along the magnetic field, that we will use later as guide lines for the general case of oblique propagation.

For the propagation along the magnetic field the dispersion relation (5.32) with a dielectric tensor 7.31 factorizes:

$$-1 + \frac{2\,\omega_p^2}{\omega^2} + \frac{\omega_b^2}{\gamma_b^3\,\hat{\omega}^2} = 0 \tag{7.32}$$

$$-1 + n^2 + \frac{2\,{\omega_p}^2}{\omega^2 - {\omega_B}^2} + \frac{{\omega_b}^2\,\hat{\omega}}{\gamma_b\,\omega^2\,(\pm\,\omega_B/\gamma_b + \hat{\omega})} = 0 \tag{7.33}$$

Equation (7.32) describes hydrodynamic excitation of longitudinal plasma waves. As discussed above, this may be a longitudinal part of Alfvén or ordinary mode depending on the parameters of plasma.

Equation (7.33) describes the cyclotron excitation of the ordinary and extraordinary modes. For the parallel propagation the cyclotron excitation of the Alfvén wave does not occur.

7.4.2 Cherenkov Excitation of Plasma Waves for $\theta = 0$

We now look for the correction to the relations (5.36) and (7.10) when the two intersect.

$$\begin{aligned} \omega &= \sqrt{2}\omega_p + \Delta \\ \omega &= v_b\,k\cos\theta + \Delta \end{aligned} \tag{7.34}$$

Expanding in small Δ, we find that the frequency shift satisfies a third order equation:

$$-\frac{\sqrt{2}\,\Delta^3}{\omega_p} + \frac{{\omega_b}^2}{{\gamma_b}^3} = 0 \tag{7.35}$$

Equation (7.35) always has one real and two complex conjugated roots. The complex root with the positive complex part corresponds to the instability.

Solving Eq. (7.35), we find the complex part of the frequency shift:

$$Im(\,\Delta) = \frac{\sqrt{3}\,{\omega_p}^{\frac{1}{3}}\,{\omega_b}^{\frac{2}{3}}}{2^{\frac{7}{6}}\,\gamma_b} = \frac{\sqrt{3}\lambda^{1/6}\sqrt{\Omega\omega_B}}{2^{2/3}\gamma_b\sqrt{\gamma_p}} \tag{7.36}$$

This is a growth rate for the Cherenkov excitation of plasma waves (c.f. Godfrey et al. 1975,

Egorenkov et al. 1983).

We can compare the importance of the Cherenkov excitation of plasma waves by evaluating growth rate (7.36) for the set of fiducial parameters of a cold plasma and comparing it with the dynamical time (7.7):

$$\frac{Im(\ \Delta)}{\gamma_p \Omega} \approx \frac{\lambda^{1/6}}{\gamma_b \gamma_p^{3/2}} \sqrt{\frac{\omega_B}{\Omega}} = 86 \left(\frac{r}{R_{NS}} \right)^{-3/2} \tag{7.37}$$

From which it follows that this instability may be important for $r \leq 20$. We will see in Section 7.5 that the second criterion (7.9) is not satisfied for the Cherenkov excitation of Alfvén or ordinary waves, so that the Cherenkov instability does not develop.

7.4.3 Cyclotron Excitation of Transverse Waves for $\theta = 0$

We expect that the hydrodynamic instability will be strongest at small wave vectors. We can then use the low frequency approximation (5.39) to the dispersion of the transverse waves. We seek the correction to the relations (5.39) and (7.11) when the two intersect.

$$\begin{aligned} \omega &= kc \left(1 - \frac{\omega_p^2}{{\omega_B}^2} \right) + \Delta \\ \omega &= k v_b \cos\theta - \frac{\omega_B}{\gamma_b} + \Delta \end{aligned} \tag{7.38}$$

Expanding in small Δ, we find that the frequency shift satisfies the quadratic equation:

$$-\frac{\Delta\, k^2 c^2}{\omega^3} \pm \frac{\omega_B\, {\omega_b}^2}{\Delta\, \gamma_b\, \omega^2} = 0 \tag{7.39}$$

The $\pm$ sign in (7.39) corresponds to the two signs in (7.33). For the normal Doppler resonance (plus sign in (7.33) and (7.39)) the resulting frequency shift is real. For the anomalous Doppler resonance, the frequency shift is complex:

$$\Delta = \pm \frac{i \sqrt{\omega}\, \sqrt{\omega_B}\, \omega_b}{2 \gamma_b\, kc} \tag{7.40}$$

which gives near the resonant frequency (7.21)

$$Im(\Delta) = \frac{i\, \omega_p\, \omega_b}{2 \sqrt{\gamma_b}\, \omega_B} = \frac{\sqrt{\lambda}\Omega}{\gamma_p \sqrt{\gamma_b}} \tag{7.41}$$

For the parameters of a cold plasma the growth rate (7.41) is much longer than the dynamical time everywhere inside the light cylinder.

$$\frac{\mathrm{Im}(\ \Delta)}{\gamma_p \Omega} \approx \frac{\sqrt{\lambda}}{\gamma_p^2 \sqrt{\gamma_b}} = 10^{-4} \ll 1 \tag{7.42}$$

Which implies that hydrodynamic regime of the cyclotron instability is probably unimportant.

7.4.4 Perpendicular Propagation

Next, we consider the hydrodynamic instabilities for the waves propagating perpendicular to the magnetic field (magnetized Wiebel instability (Weibel 1959)). The normal modes of plasma without a beam for $\theta = \pi/2$ follow from Eq. (5.32):

$$\omega^2 = k^2 + 2\,{\omega_p}^2 \tag{7.43}$$

$$\omega^2 = {\omega_B}^2 + 2\,{\omega_p}^2 \tag{7.44}$$

$$n^2 = 1 + \frac{2\,{\omega_p}^2}{-\omega^2 + {\omega_B}^2} \tag{7.45}$$

In the limit $\omega_B \to \infty$ the two solution of the biquadratic Eq. (7.45) may be expanded in large ω_B:

$$\omega^2 = {\omega_B}^2 + 2\,{\omega_p}^2 + \frac{2\,c^2\,k^2\,{\omega_p}^2}{{\omega_B}^2} \tag{7.46}$$

$$\omega^2 = c^2\,k^2 \left(1 - \frac{2\,{\omega_p}^2}{{\omega_B}^2}\right) \tag{7.47}$$

In the limit $kc \ll \omega_B$ the dispersion curves (7.46) and (7.44) approach each other near the upper hybrid frequency: $\omega^2 = {\omega_B}^2 + 2\,{\omega_p}^2$. We then expand determinant (7.31) for $\theta = \pi/2$ near the upper hybrid frequency $\omega = \sqrt{{\omega_B}^2 + 2\,\omega_p^2} + \Delta$ keeping the terms up to the second order in Δ.

$$-\frac{\Delta^2\,{\omega_B}^2}{\omega_p^4} + \frac{c^2\,\Delta\,k^2}{\omega_B\,\omega_p^2} - \frac{c^2\,k^2\,{\omega_b}^2}{\gamma_b\,{\omega_B}^4} = 0 \tag{7.48}$$

Solving Eq. (7.48), we find the frequency shift

$$\Delta = \frac{k\,{\omega_p}^2 \left(\sqrt{\gamma_b}\,k - \sqrt{\gamma_b\,k^2 - 4\,{\omega_b}^2}\right)}{2\,\sqrt{\gamma_b}\,{\omega_B}^3} \tag{7.49}$$

which shows an instability for $kc < 2\omega_b/\gamma_b$ with a maximum growth rate

$$Im(\ \Delta)_{max} \approx \frac{{\omega_p}^2\,{\omega_b}^2}{{\gamma_b}^{\frac{3}{2}}\,{\omega_B}^3} \tag{7.50}$$

which is negligible for all reasonable pulsar plasma parameters.

7.5 Hydrodynamic Regimes of Oblique Wave Excitation in Cold Plasma

In this section we develop a general theory of the hydrodynamic weak beam instabilities in the cold magnetized electron-positron plasma. We expand (7.31) in small ω_b keeping only first terms. After considerable algebra we obtain

$$\left(1-n^2+\frac{2\,{\omega_p}^2}{-\omega^2+{\omega_B}^2}\right)\left(\left(-1+n^2+\frac{2\,{\omega_p}^2}{\omega^2}\right)\left(1-\frac{2\,{\omega_p}^2}{\omega^2-{\omega_B}^2}\right)+\frac{2\,n^2\,{\omega_B}^2\,{\omega_p}^2\cos^2\theta}{\omega^2\,(\omega^2-{\omega_B}^2)}\right)+$$
$$\frac{{\omega_b}^2}{\gamma_b^3\,\hat{\omega^2}}\left(-1+n^2\cos^2\theta+\frac{2\,\omega_p^2}{\omega^2-{\omega_B}^2}\right)\left(-1+n^2+\frac{2\,\omega_p^2}{\omega^2-{\omega_B}^2}\right)+$$
$$\frac{{\omega_b}^2}{\gamma_b\hat{\omega}^2}\left(\frac{2\,kc\,n^2\left(-1+n^2+\frac{2\,{\omega_p}^2}{\omega^2-{\omega_B}^2}\right)\omega'\,\beta_b\,\cos\theta\sin^2\theta}{\omega^2}+\right.$$
$$\frac{k^2c^2\left(-1+n^2\right)\,{\beta_b}^2\,\left(-1+n^2\cos^2\theta\right)\,\sin^2\theta}{\omega^2}+$$
$$2\,k^2c^2\,{\omega_p}^2\,{\beta_b}^2\left(\frac{2\,\left(-\omega^2+{\omega_B}^2+{\omega_p}^2\right)}{\omega^2\,\left(-\omega^2+{\omega_B}^2\right)^2}+\frac{n^2\,\left(1+\cos^2\theta\right)}{\omega^2\,\left(\omega^2-{\omega_B}^2\right)}\right)\sin^2\theta+$$
$$\left.\frac{\hat{\omega^2}\left(\left(-1+\frac{2\,{\omega_p}^2}{\omega^2}\right)\left(-2+n^2+\frac{4\,{\omega_p}^2}{\omega^2-{\omega_B}^2}+n^2\cos^2\theta\right)+n^2\left(-2+n^2+\frac{4\,{\omega_p}^2}{\omega^2-{\omega_B}^2}\right)\sin^2\theta\right)}{\omega^2}\right)\quad(7.51)$$

The term containing $1/\hat{\omega^2}$ contribute to Cherenkov excitation and the term containing $1/\hat{\hat{\omega}}^2$ contribute to the cyclotron excitation.

To find the growth rates we expand the plasma part of (7.51) near the plasma modes (Eqs. (5.34) and (5.35)) and the beam part near the resonances $\omega' = 0$ (for Cherenkov excitation) or $\omega'' = 0$ (for cyclotron instability). The expansion of the plasma part of (7.51) near the plasma modes is done according to the relation

$$\omega = \omega^{(0)} + \Delta\left(\frac{\partial K_p}{\partial\omega}\right)\Big|_{\omega^{(0)}} \qquad (7.52)$$

where K_p is the plasma part of the determinant (7.31)

$$K_p = \left(1-n^2+\frac{2\,{\omega_p}^2}{-\omega^2+{\omega_B}^2}\right)\left(\left(-1+n^2+\frac{2\,{\omega_p}^2}{\omega^2}\right)\left(1-\frac{2\,{\omega_p}^2}{\omega^2-{\omega_B}^2}\right)+\frac{2\,n^2\,{\omega_B}^2\,{\omega_p}^2\cos^2\theta}{\omega^2\,(\omega^2-{\omega_B}^2)}\right) \qquad (7.53)$$

and $\omega^{(0)}$ are the solutions of the equation $K_p = 0$.

Simultaneously, in the beam part of the Eq. (7.51) we should use the normal modes of the medium for the estimates of ω and the refractive index n.

We skip the details of calculations of the growth rate and conclude this section by the table of the hydrodynamic growth rate in a cold plasma (Table 7.1). For the details of calculations, see Lyutikov 1997c.

Resonances	Extraordinary wave	Ordinary wave		Alfven wave	
Cherenkov	$\mathrm{Im}(\Delta) = 0$	$\mathrm{Im}(\Delta) = \frac{\sqrt{6}\,\omega_B{}^{\frac{2}{3}}\,\omega_p\,\omega_b{}^{\frac{2}{3}}\,\sin\theta}{2\,\gamma_b{}^{\frac{2}{3}}\,(-1+\mu^2)^{\frac{1}{6}}\,(8\,\omega_p{}^4+2\,\omega_B{}^2\sin^2\theta)^{\frac{1}{3}}}$	$\mu \geq 1$	$\mathrm{Im}(\Delta) = \frac{\sqrt{3}\,\omega_p^{\frac{1}{3}}\,\omega_b{}^{\frac{2}{3}}\,\cos\theta^{\frac{1}{3}}}{2^{\frac{7}{6}}\,\gamma_b}$	if $\theta \ll 1/\gamma_b$
		$\mathrm{Im}(\Delta) = \frac{\sqrt{3}\,\omega_p^{\frac{2}{3}}\,\omega_b{}^{\frac{2}{3}}\,\sqrt{2\,\omega_p^2+\omega_B{}^2\sin^2\theta}}{2\,\gamma_b\left(4\,\omega_p^4+\omega_B{}^4\sin^2\theta\right)^{\frac{1}{3}}}$	$\mu \gg 1$	$\mathrm{Im}(\Delta) = \frac{\sqrt{3}\,\omega_p^{\frac{1}{3}}\,\omega_b{}^{\frac{2}{3}}\,\cot\theta}{2^{\frac{7}{6}}\,\gamma_b^{\frac{8}{3}}}$	if $\theta \gg 1/\gamma_b$
		0	$\mu > 1$		
Cyclotron	$\mathrm{Im}(\Delta) = \frac{\omega_p\,\omega_b}{2\sqrt{\gamma_b}\,\omega_B}$	$\mathrm{Im}(\Delta) = \frac{\sqrt{\omega_B}\omega_b}{2\gamma_b\sqrt{\omega}}$	$\theta < \frac{\omega_p}{\omega_B}\,, \mu > 1$	$\mathrm{Im}(\Delta) = \frac{\sqrt{\omega}_p\,\omega_b\,\sqrt{\cos\theta}\,\sin\theta}{2^{\frac{5}{4}}\,\sqrt{\omega_B}}$	if $\mu \leq 1$
		$\omega = \frac{\omega_B^3}{\gamma_b\omega_p^2}\left(1+\frac{\omega_B^2}{2\omega_p^2}\left(1+\theta^2\gamma_b^2\right)\right)$		$\mathrm{Im}(\Delta) = \frac{\omega_B{}^{\frac{1}{3}}\,\omega_b\tan\theta^{\frac{1}{3}}}{2^{\frac{5}{6}}\,\gamma_b^{\frac{5}{6}}\,\omega_p^{\frac{1}{3}}}$	if $\mu \gg 1$

Table 7.1: Hydrodynamic growth rates in cold plasma

7.6 Resonances in the Relativistic Hot Pair Plasma

From the low frequency approximation to the Alfvén waves dispersion we find that the possibility of Cherenkov excitation of Alfvén wave in a relativistic hot plasma depends on the parameter

$$\mu_h = \sqrt{\frac{2\gamma_b^2\, T_p \omega_p^2 (1+\beta_T^2)}{{\omega_B}^2}} \approx \frac{2\gamma_b \sqrt{T_p}\omega_p}{\omega_B} \tag{7.54}$$

(compare with (7.12)).

Using our fiducial numbers parameter μ may be estimated

$$\mu_h = 2\gamma_b \sqrt{\frac{T_p \lambda \Omega}{\omega_B \gamma_p}} = \gamma_b' \sqrt{\frac{T_p \lambda \Omega}{\gamma_p^3 \omega_B}} = 5\times 10^{-3} \left(\frac{r}{R_{NS}}\right)^{3/2} = \begin{cases} <1, & \text{if } \left(\frac{r}{R_{NS}}\right) < 43 \\ >1, & \text{if } \left(\frac{r}{R_{NS}}\right) > 43 \end{cases} \tag{7.55}$$

Numerically μ_h and μ are equal for the chosen set of the fiducial numbers for the cold and hot cases.

Similarly to the cold case, the parameter μ_h determines the possibility of the excitation of the Alfvén and ordinary waves. If $\mu_h < 1$ then the ordinary wave cannot be excited by Cherenkov resonance. In this case the Alfvén wave may be excited by the Cherenkov interaction subject to the condition that the resonance occurs on the parts of the dispersion curve that are not strongly damped (see below). If $\mu_h > 1$ then the ordinary wave may excited by Cherenkov resonance for the angles of propagation $\theta < \frac{\sqrt{T_p}\omega_p}{\omega_B}$.

Another limitation on the possible resonance comes from the requirement that the waves in the plasma are not strongly damped at the location of the resonance. This is an important constraint on the resonance of the Alfvén wave, which is strongly damped at large wave vectors.

7.6.1 Cherenkov Resonance of an Alfvén Mode ($\mu_h < 1$)

Solving (5.72) with $n = 1/(\beta_b \cos\theta)$, we find the location of the Cherenkov resonance of the Alfvén wave:

$$\omega_{res}^2 = \frac{2\,\omega_p^2\,\beta_b^2\,\cos^2\theta}{\gamma_b^2\; T_p\; \left(-\beta_b^2+{\beta_T}^2\right)\; \left(-1+\beta_b^2\,\cos^2\theta\right)} \approx \begin{cases} 2\,T_p\omega_p^2\beta_b^2\,\cos^2\theta & \text{if } \theta \ll 1/\gamma_b \\ \frac{2\,T_p\omega_p^2\beta_b^2\,\cot^2\theta}{\gamma_b^2} & \text{if } \theta \gg 1/\gamma_b \end{cases} \tag{7.56}$$

(see Fig. 7.4).

7.6.2 Cyclotron Resonance of an Alfvén Wave

The dispersion relation for the Alfvén waves in a relativistic hot pair plasma is complicated even in the limit of infinitely strong magnetic field (5.72). To find the location of the cyclotron resonances

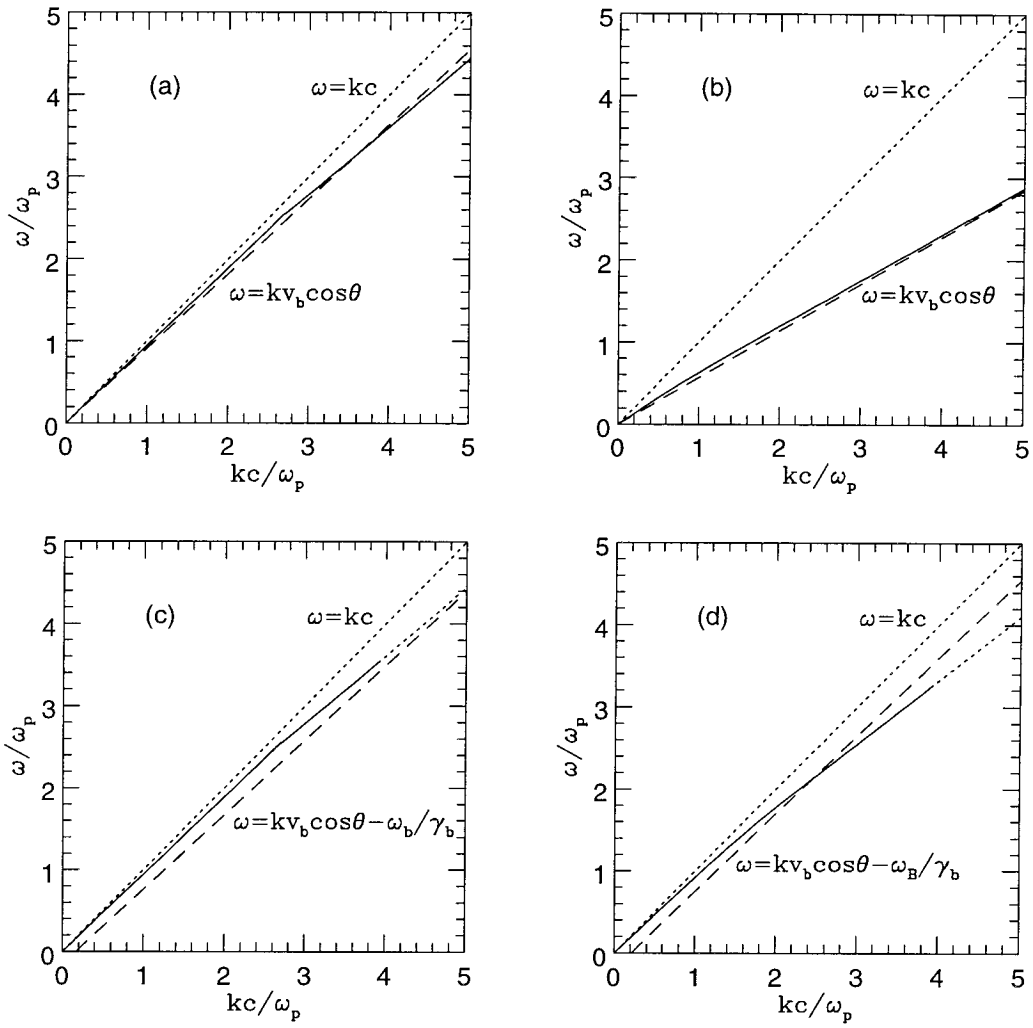

Figure 7.4: Alfvén wave resonances in hot pair plasma. (a) Cherenkov resonance for $\theta \ll 1\gamma_b$ ($\mu_h < 1$); (b) Cherenkov resonance for $\theta \gg 1\gamma_b$ ($\mu_h < 1$); (c) Cyclotron resonance for very hot plasma ($\eta \ll 1$); (d) Cyclotron resonance for warm plasma ($\eta \geq 1$). On the plots (c) and (d) the dashed parts of the Alfvén wave dispersion curve indicate a strong damping on the plasma particles.

we will use the asymptotic expansion for the dispersion relations of the Alfvén waves far from the cross-over points (5.46).

First we assume that cyclotron resonance occurs at the frequencies much larger than the cross-over frequency $\omega \gg \omega_o$ and find the condition for this. Alfvén waves are strongly damped in this limit and there will be no excitation. Using the asymptotic expansion (5.46) to solve (7.11) we find the cyclotron resonant frequency of the Alfvén wave.

$$\omega_{res,A} = \frac{T_p^2 \omega_B}{\gamma_b}\left(1+\sqrt{1+a}\right) = \begin{cases} \frac{2\,T_p^2 \omega_B}{\gamma_b} & \text{if } a \ll 1 \\ \\ \frac{\omega_p}{\sqrt{2\,T_p}\beta_T^{3/2}\sqrt{1-\beta_T^2\cos^2\theta}} & \text{if } a \gg 1 \end{cases} \tag{7.57}$$

where

$$a = \frac{2\gamma_b^2\omega_p^2\cos^2\theta}{T_p^5{\omega_B}^2\beta_T\left(1-\beta_T^2\cos^2\theta\right)} = \begin{cases} \frac{2\,\gamma_b^2\,\omega_p^2}{T_p^5\,{\omega_B}^2\,\beta_T} & \text{if } \theta \ll \frac{1}{T_p} \\ \\ \frac{2\,\gamma_b^2\,\omega_p^2\cot\theta^2}{T_p^5\,{\omega_B}^2\,\beta_T} & \text{if } \theta \gg \frac{1}{T_p} \end{cases} \tag{7.58}$$

The condition that the resonant frequency (7.57) be much larger than the cross-over frequency (evaluated for the parallel propagation) gives

$$\frac{\omega_{res}}{\omega_o} = \begin{cases} \frac{\sqrt{2}\,T_p^{\frac{3}{2}}\,\omega_B}{\gamma_b\,\omega_p} & \text{if } a \ll 1 \\ \\ \frac{\sqrt{2}}{\sqrt{\beta_T}} \approx 1 & \text{if } a \gg 1 \text{ and } \theta \ll \frac{1}{T_p} \\ \\ \frac{\cot\theta}{T_p\sqrt{\beta_T}} & \text{if } a \gg 1 \text{ and } \theta \gg \frac{1}{T_p} \end{cases} \tag{7.59}$$

Which implies that our assumption $\omega_{res} \gg \omega_o$ may be satisfied only if

$$\eta = \frac{\gamma_b\,\omega_p}{T_p^{\frac{3}{2}}\,\omega_B} \ll 1 \tag{7.60}$$

which may be true for a very hot plasma. If the condition (7.60) is satisfied then the cyclotron resonance of the Alfvén wave occurs for $\omega \gg \omega_o$ (Fig. 7.5).

If we used a more realistic distribution function, then in this limit there will be many particles satisfying the Cherenkov resonance and the wave will be strongly damped, so we can make a conclusion that if the condition (7.60) is satisfied then the cyclotron excitation of the Alfvén wave is unimportant. If condition (7.60) is not satisfied (warm plasma), then the cyclotron resonance for Alfvén waves occur at a frequency $\omega_{res} \approx \omega_o$ which is not strongly damped.

Another analytical approximation to the location of the cyclotron resonance for Alfvén waves

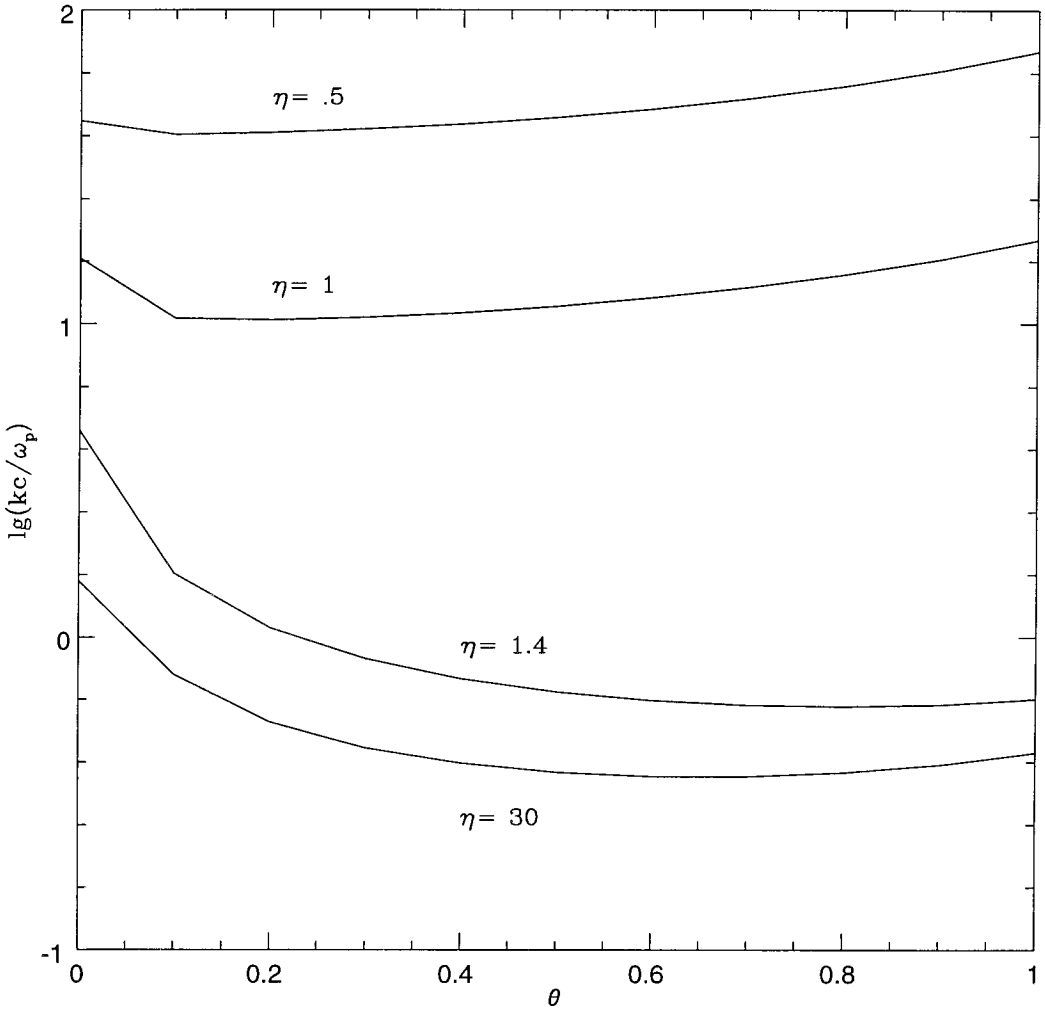

Figure 7.5: Location of a cyclotron resonance of the Alfvén wave. For $\eta \leq 1$ (very hot plasma) cyclotron resonance on Alfvén waves occurs at $kc \gg T_p^{1/2}\omega_p$, where the waves are strongly damped.

may be obtained for large angles of propagation $\theta^2 > \frac{\omega_B}{\gamma_b \sqrt{T_p}\,\omega_p}$ when the resonance occurs at $\omega \ll \omega_o$:

$$\omega_{res} = \frac{2^{\frac{2}{3}}\, T_p^{\frac{1}{3}}\, {\omega_B}^{\frac{1}{3}}\, \omega_p^{\frac{2}{3}}\, \cot\theta^{\frac{2}{3}}}{\gamma_b^{\frac{1}{3}}}, \qquad \text{if } \theta > \frac{\omega_B}{\gamma_b \sqrt{T_p}\,\omega_p} \tag{7.61}$$

Cherenkov Resonance of an Ordinary Mode ($\mu_h > 1$)

By analogy with the cold case (Section 7.5) we find that the Cherenkov resonance on the ordinary mode with for $\mu_h \gg 1$ occurs approximately at the cross-over point $\omega_0^{(h)\,2} = 2\,T_p\omega_p^2 + \omega_B^2 \sin^2\theta$, while for $\mu_h \geq 1$ the Cherenkov resonance on the ordinary mode occurs at $\omega \gg \sqrt{T_p}\omega_p$:

$$\omega_{res} = \begin{cases} \frac{\sqrt{2\,T_p}\gamma_b\omega_p\theta}{\sqrt{\mu_h^2-1}} & \theta \ll 1/\gamma_b \\ \omega_{res} = \omega_B\theta\frac{\mu_h^2+2}{\mu_h^2} & \theta \gg 1/\gamma_b \end{cases} \tag{7.62}$$

7.6.3 Cyclotron Resonance of Ordinary and Extraordinary Modes

To find the location of the cyclotron resonance on the ordinary and extraordinary modes, we first assume that a cyclotron resonance occurs at frequencies much larger than the cross-over frequency $\omega \gg \omega_o$. Using the high frequency approximation (5.46), we find

$$\begin{aligned} k_{res,X}c &= \frac{2\,\omega_B}{\gamma_b\left(d\,T_p(1+\beta_T^2) - \theta^2 - \gamma_b^{-2}\right)} \approx \frac{{\omega_B}^3}{\gamma_b\, T_p\omega_p^2}\left(1 + \frac{{\omega_B}^2\,\theta^2}{T_p\omega_p^2}\right) \\ k_{res,O}c &= \frac{2\,\omega_B}{\gamma_b\left(d\,T_p(1+\beta_T^2) - \theta^2 - \gamma_b^{-2}\right)} + \frac{\gamma_b\omega_p^2\sin^2\theta}{T_p\omega_B(1-\beta_T^2\cos^2\theta)} \\ &\approx \frac{{\omega_B}^3}{\gamma_b\, T_p\omega_p^2}\left(1 + \frac{{\omega_B}^2\,\theta^2}{T_p\omega_p^2}\right) + \frac{\gamma_b\, T_p\omega_p^2\,\theta}{\omega_B\left(1+\theta^2\,T_p^2\right)} \end{aligned} \tag{7.63}$$

The relations (7.63) are valid for the small angles of propagation: $\theta \ll \frac{\sqrt{T_p}\omega_p}{\omega_B}$.

7.6.4 Summary of the Conditions for Wave Excitation in Hot Plasma

Summarizing the results of this Section we note that the possibility of the Cherenkov excitation of Alfvén or ordinary mode depends on the parameter μ_h (Eq. (7.54) for $\mu_h > 1$ it is the ordinary mode that is excited by the Cherenkov instability, for $\mu_h < 1$ Alfvén wave can be excited by the Cherenkov instability). All the branches (extraordinary, ordinary and Alfvén) can be excited by the cyclotron instability. If $\mu_h < 1$, then the condition that Alfvén waves are not strongly damped in the resonance region require plasma to be mildly hot: $\eta < 1$ (for $\eta \geq 1$ Alfvén waves in the resonance region are strongly damped).

7.7 Hydrodynamic Wave Excitation in Relativistic Pair Plasma

7.7.1 Dielectric Tensor for the Beam-Hot Plasma System

To simplify the analysis we will use the low frequency approximation $\omega \ll \omega_B$ and the assumption of a very strong magnetic field $\frac{T_p \omega_p^2}{{\omega_B}^2} \ll 1$ from the very beginning. The dielectric tensor is then given by

$$\begin{aligned}
\epsilon_{xx} &= 1 + d\, T_p \left(1 + n^2 \beta_T^2 \cos^2\theta\right) - \frac{{\omega_b}^2 \hat{\omega}^2}{\gamma_b \omega^2 \hat{\hat{\omega}}^2} = \epsilon_{rr} \\
\epsilon_{xr} &= \frac{-i\, {\omega_b}^2 \omega_B \hat{\omega}}{{\gamma_b}^2 \omega^2 \hat{\hat{\omega}}^2} = -\epsilon_{rx} \\
\epsilon_{x\phi} &= d\, T_p\, n^2 \beta_T^2 \cos\theta \sin\theta - \frac{k\, {\omega_b}^2 \hat{\omega} \beta_b \sin\theta}{\gamma_b \omega^2 \hat{\hat{\omega}}^2} = \epsilon_{\phi x} \\
\epsilon_{r\phi} &= \frac{i\, k\, {\omega_b}^2 \omega_B \beta_b \sin\theta}{{\gamma_b}^2 \omega^2 \hat{\hat{\omega}}^2} = -\epsilon_{\phi r} \\
\epsilon_{\phi\phi} &= 1 - \frac{2\, n^2 \omega_p^2}{T_p \left(1 - n^2 \beta_T^2 \cos^2\theta\right)} + d\, T_p\, n^2 \sin^2\theta - \frac{\omega_b^2}{\gamma_b^3 \omega'^2} - \frac{k^2 {\omega_b}^2 {\beta_b}^2 \sin^2\theta}{\gamma_b \omega^2 \omega''^2}
\end{aligned} \tag{7.64}$$

7.7.2 Parallel Propagation

For parallel propagation Eq. (5.32) with the dielectric tensor (7.64) factorizes:

$$1 - \frac{2\, n^2 \omega_p^2}{T_p \left(1 - n^2 \beta_T^2\right)} - \frac{\omega_b^2}{\gamma_b^3 \hat{\omega}^2} = 0 \tag{7.65}$$

$$1 - n^2 + \frac{{\omega_b}^2 \hat{\omega}}{\gamma_b \omega^2 \left(\omega_B/\gamma_b - \hat{\omega}\right)} + d\, T_p \left(1 + n^2 \beta_T^2\right) = 0 \tag{7.66}$$

$$1 - n^2 - \frac{{\omega_b}^2 \hat{\omega}}{\gamma_b \omega^2 \left(\omega_B/\gamma_b + \hat{\omega}\right)} + d\, T_p \left(1 + n^2 \beta_T^2\right) = 0 \tag{7.67}$$

Following the same procedure of expanding the dispersion relations in small frequency shifts Δ near the intersection of the two resonant curves, we find from (7.65) the growth rate for the Cherenkov excitation of plasma waves:

$$\mathrm{Im}(\Delta) = \frac{\sqrt{3}\, \omega_p^{\frac{1}{3}}\, {\omega_b}^{\frac{2}{3}}}{2^{\frac{7}{6}}\, \gamma_b \sqrt{T_p}} = \frac{\sqrt{3}\sqrt{\Omega \omega_B}\, \lambda^{1/6}}{2^{2/3} \gamma_b \sqrt{\gamma_p\, T_p}} \tag{7.68}$$

(cf. with Egorenkov et al.).

Using the relations between parameters of the hot plasma (Eq. 4.5 with $< \gamma >= 2 T_p \gamma_p$), the condition of a fast growth (7.8) for the growth rate (7.68) takes the form

$$\frac{\mathrm{Im}(\Delta)}{\gamma_p \Omega} \approx \frac{\lambda^{1/6}}{\gamma_b \gamma_p^{3/2} T_p^{1/2}} \sqrt{\frac{\omega_B}{\Omega}} = 20 \left(\frac{r}{R_{NS}}\right)^{-3/2} \tag{7.69}$$

For the fixed values of γ_b and γ_p the growth rate for the Cherenkov excitation of plasma waves in a hot plasma is smaller by the factor $T_p^{2/3}$ as compared with the cold plasma.

Solving Eq. (7.67), we find the growth rate for the cyclotron excitation of transverse waves

$$\Delta = i\frac{\sqrt{T_p}\,\omega_p\,\omega_b}{2\sqrt{\gamma}_b\,\omega_B} = \sqrt{\frac{\lambda T_p}{\gamma_b}}\frac{\Omega}{\gamma_p} \tag{7.70}$$

Comparison of this growth rate with the dynamical time gives

$$\frac{\mathrm{Im}(\Delta)}{\Omega\gamma_p} = \frac{1}{\gamma_p^2}\sqrt{\frac{\lambda T_p}{\gamma_b}} \approx \frac{1}{\gamma_p^2}\left(\frac{r}{R_{NS}}\right)^{3/2} = 10^{-4}\left(\frac{r}{R_{NS}}\right)^{3/2} < 1 \tag{7.71}$$

From (7.71) and (7.42) if follows that the cyclotron excitation of the transverse waves in the hydrodynamic regime is not affected by the relativistic temperature of the plasma particles and is not important in the pulsar magnetosphere.

Similarly to the cold case we omit the details of the calculations of the growth rates and conclude this section by the table of the hydrodynamic growth rates in the relativistic hot pair plasma (Table 7.2).

7.8 Kinetic Instabilities

As we have discussed in Section 7.2, a general beam instability may be treated analytically in the hydrodynamic and kinetic limiting cases. We have considered hydrodynamic beam instabilities in pair plasma in Sections 7.5 and 7.7. Now we turn to the kinetic regime of instabilities. The condition for the kinetic consideration to apply is the opposite of the condition (7.3). It requires a substantial scatter in the velocities of the resonant particles. In what follows we assume that distribution of the beam particles is described by the relativistic, one-dimensional Maxwellian distribution:

$$f(p_\phi) = n_b\,\frac{1}{2\,K_1(\frac{1}{T_b})\gamma_b}\exp\left(-\frac{p_\mu U^\mu}{T_b}\right) \tag{7.72}$$

where n_b is the density of the beam measured in the laboratory frame (the Lorentz invariant proper density is $n_b\gamma_b$), $U^\mu = (\gamma_b, \beta_b\gamma_b)$ is the four velocity of the rest frame of the beam, T_b is the beam temperature in units mc^2, K_1 is a modified Bessel function.

This function may be simplified in the limit of cold beam (in its frame) $T_b \ll 1$ and large streaming velocity $\gamma_b \gg 1$. We find then

$$f(p_\phi) = \frac{n_b}{\sqrt{2\pi}p_t}\exp\left(-\frac{(p_\phi - p_b)^2}{2p_t^2}\right) \tag{7.73}$$

where $p_t^2 = \gamma_b^2 T_b mc$ is the scatter in parallel moments.

Resonances	Extraordinary wave	Ordinary wave	Alfven wave
Cherenkov	$\mathrm{Im}(\Delta) = 0$	$\mathrm{Im}(\Delta) =$ $\mu \geq 1$ $\mathrm{Im}(\Delta) = \frac{\gamma_o{}^{\frac{1}{3}}\,\omega_p{}^{\frac{2}{3}}\,\omega_b{}^{\frac{2}{3}}\sqrt{6\,\gamma_o\,\omega_p^2+3\,\omega_B{}^2\sin^2\theta}}{2\,\gamma_b\left(4\,\gamma_o{}^4\,\omega_p^4+\omega_B{}^4\sin^2\theta\right)^{\frac{1}{3}}}$ $\mu \gg 1$ 0 $\mu > 1$	$\mathrm{Im}(\Delta) = \frac{\sqrt{3}\,\omega_p{}^{\frac{1}{3}}\,\omega_b{}^{\frac{2}{3}}\cos^{1/3}\theta}{2^{\frac{1}{6}}\,\gamma_b\sqrt{\gamma_o}}$ if $\theta \ll 1/\gamma_b$ $\mathrm{Im}(\Delta) = \frac{\gamma_o^{\frac{1}{6}}\,\omega_p{}^{\frac{1}{3}}\,\omega_b{}^{\frac{2}{3}}\cot\theta}{2^{\frac{1}{6}}\sqrt{3}\,\gamma_b{}^{\frac{8}{3}}\,\beta_b{}^{\frac{1}{3}}}$ if $\theta \gg 1/\gamma_b$
Cyclotron	$\mathrm{Im}(\Delta) = \frac{\sqrt{\gamma_o}\,\omega_p\,\omega_b}{2\sqrt{\gamma}_b\,\omega_B}$	$\frac{\omega_b\sqrt{\omega_B}}{\sqrt{2\omega}\gamma_b^{3/2}}$ $\theta < \frac{\gamma_o\omega_p}{\omega_B}$ $\mu_h > 1$ $\omega Eq.129$	$\mathrm{Im}(\Delta) = 0$ if $\mu \leq 1$ $\mathrm{Im}(\Delta) = \frac{\omega_B{}^{\frac{1}{3}}\,\omega_b\,\tan^{\frac{1}{3}}\theta}{2^{\frac{5}{6}}\,\gamma_b^{\frac{5}{6}}\,\gamma_o^{\frac{1}{6}}\,\omega_p^{1/3}}$ if $\mu \gg 1$ and $\eta > 1$

Table 7.2: Hydrodynamic growth rates in hot plasma

In case of kinetic instabilities the growth rate is given by (e.g., Melrose 1978c)

$$\Gamma = -\frac{(e^*_\alpha \epsilon''_{\alpha\beta} e_\beta)}{\frac{1}{\omega^2}\frac{\partial}{\partial\omega}\omega^2 (e^*_\alpha \epsilon'_{\alpha\beta} e_\beta)}\Bigg|_{\omega=\omega(\mathbf{k})} \tag{7.74}$$

where $\epsilon'_{\alpha\beta}$ and $\epsilon''_{\alpha\beta}$ are hermitian and antihermitian parts of the dielectric tensor, $\omega(\mathbf{k})$ is the frequency of the excited normal modes of the medium, and e_α is its polarization vector. The antihermitian parts of the dielectric tensor are due to the resonant interaction of the particles from the beam at Cherenkov (7.10) and cyclotron resonances (7.11). Using the Plemeij formula we find

$$\begin{aligned}
\epsilon''_{xx} &= -i\frac{2\pi^2 q^2}{\omega^2 m}\int \frac{dp_\phi}{\gamma}\omega' f(p_\phi)\delta\left(\omega' - \frac{\omega_B}{\gamma}\right) = \epsilon''_{yy} \\
\epsilon''_{\phi\phi} &= i\frac{4\pi^2 q^2}{\omega}\int dp_\phi v_\phi \frac{\partial f(p_\phi)}{\partial p_\phi}\delta(\omega') - i\frac{2\pi^2 q^2 \sin^2\theta k^2 c^2}{\omega^2\omega_B}\int dp_\phi \gamma v_\phi^2 f(p_\phi)\delta\left(\omega' - \frac{\omega_B}{\gamma}\right) \\
\epsilon''_{x\phi} &= -i\frac{2\pi^2 q^2 k\sin\theta}{m\omega^2\omega_B}\int dp_\phi \omega' v_\phi f(p_\phi)\delta\left(\omega' - \frac{\omega_B}{\gamma}\right) = \epsilon''_{\phi x} \\
\epsilon''_{xr} &\approx 0 = \epsilon''_{rx} = \epsilon''_{r\phi} = \epsilon''_{\phi r}
\end{aligned} \tag{7.75}$$

Using the polarization vectors (5.84),(5.85) we find that for the quasitransverse waves (ordinary mode $\omega \gg \omega_0^{(h)}$, Alfvén mode $\omega \ll \omega_0^{(h)}$ and ordinary mode $\omega \approx \omega_0^{(h)}$, $\theta \gg \omega_B^2/(T_p\omega_p^2)$), while for the ordinary mode at the cross-over point and $\theta \ll \omega_B^2/(T_p\omega_p^2)$

$$\frac{1}{\omega^2}\frac{\partial}{\partial\omega}\omega^2(\mathbf{e}\cdot\epsilon'\cdot\mathbf{e}) = \begin{cases} \frac{2}{\omega} & \text{cold plasma} \\ \frac{T_p\omega}{\omega_p^2} & \text{hot plasma} \end{cases} \tag{7.76}$$

With polarization vectors (5.60) and (5.62) we find from (7.75), that for quasitransverse parts of the waves

$$(\mathbf{e_X}\cdot\epsilon''\cdot\mathbf{e_X}) = -i\frac{2\pi^2 q^2}{\omega^2 m}\int \frac{dp_\phi}{\gamma}\omega' f(p_\phi)\delta\left(\omega' - \frac{\omega_B}{\gamma}\right) \tag{7.77}$$

$$\begin{aligned}
(\mathbf{e_O}\cdot\epsilon''\cdot\mathbf{e_O}) &= \frac{4\pi^2 q^2}{m\omega}\int dp_\phi v_\phi \frac{\partial f(p_\phi)}{\partial p_\phi}\delta(\omega')\sin^2\theta \\
&+\frac{2\pi^2 q^2}{\omega^2\omega_B m}\int dp_\phi \left(kv_\phi - \omega\cos\theta\right)^2 f(p_\phi)\delta\left(\omega' - \frac{\omega_B}{\gamma}\right) = \epsilon''^{Ch}_O + \epsilon''^{C}_O
\end{aligned} \tag{7.78}$$

$$\begin{aligned}
(\mathbf{e_A}\cdot\epsilon''\cdot\mathbf{e_A}) &= \frac{\pi^2 q^2}{m\omega}\frac{\omega^4}{\omega_p^4}\int dp_\phi v_\phi \frac{\partial f(p_\phi)}{\partial p_\phi}\delta(\omega')\tan^2\theta \\
&+\frac{2\pi^2 q^2}{\omega^2\omega_B m}\int dp_\phi \left(\omega - kv_\phi\cos\theta\right)^2 f(p_\phi)\delta\left(\omega' - \frac{\omega_B}{\gamma}\right) = \epsilon''^{Ch}_A + \epsilon''^{C}_A
\end{aligned} \tag{7.79}$$

where we split the antihermitian part for the ordinary and Alfvén modes in two parts: ϵ''^{Ch} is due to the Cherenkov resonance and ϵ''^{C} is due to the cyclotron resonance.

Most of the relations (7.79), excepting ϵ''^{Ch}_A, are valid for both cold and hot plasma. For hot

plasma we have

$$\epsilon_A^{\prime\prime\, Ch\,(h)} \equiv (\mathbf{e_A}\cdot\epsilon^{\prime\prime}\cdot\mathbf{e_A})^{(h)} = \frac{\pi^2 q^2}{m\omega}\,\frac{\omega^4}{T_p^2\omega_p^4}\int dp_\phi v_\phi \frac{\partial f(p_\phi)}{\partial p_\phi}\delta(\omega')\tan^2\theta \tag{7.80}$$

For the Cherenkov excitation of the ordinary mode in the limit $\mu_h \gg 1$ (when the resonance occurs at the cross-over point) we find

$$(\mathbf{e_O}\cdot\epsilon^{\prime\prime}\cdot\mathbf{e_O})_{Ch} = \begin{cases} \frac{4\pi^2 q^2}{m\omega}\int dp_\phi v_\phi \frac{\partial f(p_\phi)}{\partial p_\phi}\delta(\omega') & \theta \ll \frac{2\omega_p^2}{\omega_B^2} \\ \frac{4\pi^2 q^2}{m\omega}\,\frac{\omega_0^4}{\omega_B^4\cos^2\theta\sin^2\theta}\int dp_\phi v_\phi \frac{\partial f(p_\phi)}{\partial p_\phi}\delta(\omega') & \theta \gg \frac{2\omega_p^2}{\omega_B^2} \end{cases} \tag{7.81}$$

The calculations of the integrals in (7.77 - 7.81) are given in Appendix M

7.8.1 Parallel Propagation

We first consider an important, separate case of parallel propagation.

Using the polarization vectors $\mathbf{e_l} = (0,0,1)$ for longitudinal waves and $\mathbf{e_t} = (1,0,0)$ for transverse waves we find

$$(\mathbf{e_t}\cdot\epsilon^{\prime\prime}\cdot\mathbf{e_t}) = -i\frac{2\pi^2 q^2}{\omega^2 m}\int \frac{dp_\phi}{\gamma}\omega' f(p_\phi)\delta\left(\omega' - \frac{\omega_B}{\gamma_b}\right) \tag{7.82}$$

$$\frac{\partial}{\partial\omega}\omega^2(\mathbf{e_t}\cdot\epsilon'\cdot\mathbf{e_t}) \approx 2\omega \tag{7.83}$$

$$(\mathbf{e_l}\cdot\epsilon^{\prime\prime}\cdot\mathbf{e_l}) = i\frac{4\pi^2 q^2}{\omega}\int dp_\phi v_\phi \frac{\partial f(p_\phi)}{\partial p_\phi}\delta(\omega') \tag{7.84}$$

$$\frac{1}{\omega^2}\frac{\partial}{\partial\omega}\omega^2(\mathbf{e_l}\cdot\epsilon'\cdot\mathbf{e_l}) = \begin{cases} \frac{1}{\sqrt{2}\omega_p}, & \text{cold plasma} \\ \frac{T_p\omega}{\omega_p^2}, & \text{hot plasma} \end{cases} \tag{7.85}$$

The corresponding growth rates are

$$\Gamma_t = \frac{\pi\omega_{p,res}^2}{4\omega}(f)_{res} \tag{7.86}$$

$$\Gamma_l = \frac{\pi\omega_p^2\omega_{p,res}^2}{T_p k c\omega^2}\left(\gamma^3\frac{\partial f}{\partial\gamma}\right)_{res} \tag{7.87}$$

With the distribution function of the form (7.73) we find

$$\Gamma_t \approx \frac{\pi\omega_{p,res}^2}{\omega\Delta\gamma}, \qquad \omega = \frac{\omega_B^3}{\gamma_b T_p\omega_p^2} \tag{7.88}$$

$$\Gamma_l \approx \frac{n_b}{n_p}\,\frac{\pi\omega_p\gamma_b^3}{T_p^{5/2}\Delta\gamma^2}, \qquad \omega = \omega_0 = \sqrt{2\,T_p}\omega_p \tag{7.89}$$

The kinetic growth rates (7.88) and (7.89) can be compared with growth rates in hydrodynamic

regime (Eqns (7.36) and (7.40)). In a hydrodynamic regime both cyclotron and Cherenkov growth rates are proportional to the negative powers of the particle's Lorentz factor. This is a significant factor for the primary beam and for the particles from the tail of plasma distributions. In contrast, kinetic growth rates (7.88) and (7.89) are not suppressed by the relativistic streaming of resonant particles. On the other hand, kinetic growth rates (7.88) and (7.89) scale linearly with a small ratio of the beam density to plasma density while hydrodynamic growth rates (7.36) and (7.40) are proportional to 1/3 and 1/2 power of this ratio.

7.8.2 Excitation of Oblique Alfvén Waves in a Kinetic Regime

Cherenkov Resonance

Using (7.74), (7.79), (5.80), (7.80) and (7.74), we find a growth rate for the Cherenkov excitation of Alfvén wave in a cold plasma:

$$\Gamma = \frac{\pi}{8}\frac{\omega_b^2}{kc\cos\theta}\frac{\omega^4}{\omega_p^4}\tan^2\theta\frac{\gamma^3}{\Delta\gamma^2} \tag{7.90}$$

with the resonant ω and k given by (7.15) for cold plasma and (7.56) for the hot plasma. In a hot plasma the growth rate is decreased by a factor T_p^2.

This growth rate is very small. Alfvén waves in the limit $\omega \ll \omega_p$ are almost transverse and are not excited effectively by the Cherenkov resonance. A strong dependence on ω and θ corresponds to the increasing potential part of Alfvén waves for larger ω and θ.

Cyclotron Resonance

Using (7.74), (7.79), (5.80) and (7.74), the growth rate for the cyclotron excitation of Alfvén waves is

$$\Gamma = \frac{\pi}{4}\frac{\omega_b^2}{\omega_{res}\Delta\gamma} \tag{7.91}$$

with the resonant frequency given by (7.20) in the cold case or (7.61) in the warm case.

7.8.3 Excitation of the Oblique Ordinary Waves in a Kinetic Regime

Cherenkov Excitation

The Cherenkov excitation of the ordinary mode strongly depends on the parameter μ_h and the angle of propagation. Excitation is possible only for $\mu_h > 1$. For $\mu_h \geq 1$ the resonance occurs at $\omega \gg \omega_0^{(h)}$. Then, using the polarization vector Eq. (5.60), the resonance frequency (7.28) and Eq. (7.75) we find from (7.74)

$$\Gamma = \frac{\pi}{2}\frac{\omega_b^2}{k_{res}c}\frac{\gamma_b^3\sin^2\theta}{\Delta\gamma^2} \tag{7.92}$$

For $\mu_h \gg 1$ the Cherenkov resonance occurs approximately at the cross-over point $\omega_0^{(h)}$. Using the polarization vector (5.61), the resonance frequency (5.40) and Eq. (7.75) we find from Eq. (7.74)

$$\Gamma = \begin{cases} \frac{\pi}{\sqrt{22}} \frac{\omega_b^2}{\omega_p} \frac{\gamma_b^3}{\Delta\gamma^2} & \theta \ll \frac{2\omega_p^2}{\omega_B^2} \\ \frac{\pi}{2} \frac{\omega_b^2 \omega_0^{(h)\,3}}{\omega_B^4 \sin^2\theta \cos^2\theta} \frac{\gamma_b^3}{\Delta\gamma^2} & \theta \gg \frac{2\omega_p^2}{\omega_B^2} \end{cases} \tag{7.93}$$

Equations (7.92) and (7.93) imply that the Cherenkov excitation of the ordinary mode is effective only if $\mu_h \gg 1$ and in the narrow angle $\theta \ll \frac{2\omega_p^2}{\omega_B^2}$. This condition may be satisfied only in the outer regions of the pulsar magnetosphere. The growth rate of the Cherenkov excitation of the ordinary mode in the kinetic regime is proportional to the density of the resonant particles. In the outer parts of pulsar magnetosphere, the density has decreased considerably which prevents the development of the Cherenkov instability. Numerically, it turns out that in the pulsar magnetosphere the kinetic instabilities may be stronger than hydrodynamic.

Cyclotron Excitation of the Ordinary Mode

Using (7.78), (5.80) and (7.74) the growth rate for the cyclotron excitation of the ordinary wave is

$$\Gamma = \frac{\pi}{4} \frac{\omega_{p,res}^2}{\omega_{res} \cos^2\theta \Delta\gamma} \tag{7.94}$$

with the resonant frequency given by (7.30) in the cold case or (7.63) in the hot case. Here $\omega_{p,res}$ is the plasma frequency of the resonant particles. The angle of emission is limited by $\theta \leq \omega_p/\omega_B$. The maximum growth rate, which is attained with parallel propagation, is estimated below.

7.8.4 Excitation of the Extraordinary Mode

Using (7.77), (5.80) and (7.74) the growth rate for the cyclotron excitation of the extraordinary wave is

$$\Gamma = \frac{\pi}{4} \frac{\omega_{p,res}^2}{\omega_{res} \Delta\gamma} \tag{7.95}$$

Using the resonant frequency (7.63) we find

$$\Gamma = \frac{\pi}{4} \frac{\omega_{p,res}^2 \omega_p^2 \gamma_b T_p}{\omega_B^3 \Delta\gamma} = \frac{\pi \lambda_{res} \lambda \gamma_b T_p}{\Delta\gamma \gamma_p} \frac{\Omega^2}{\omega_B} \tag{7.96}$$

The conditions of the fast growth are

$$\frac{\Gamma}{\Omega} > 1, \qquad \text{if } \left(\frac{R}{R_{NS}}\right) > 300 \tag{7.97}$$

$$\frac{R_c \delta\theta \Gamma}{c\gamma_p^2} = \frac{\pi \lambda_{res} \lambda^{3/2}}{\Delta\gamma} \frac{R_c \Omega}{c} \left(\frac{\Omega}{\omega_B}\right)^{3/2} \tag{7.98}$$

Since cyclotron instability develops in the outer regions of pulsar magnetosphere, condition (7.98) can be satisfied for the regions close to the the magnetic axis with $R_c \approx 10^{10}$ cm. The lower streaming Lorentz factors increase the cyclotron instability growth rate.

We conclude this section by the table of kinetic growth rates (Table 7.3).

7.9 Hydrodynamic and Kinetic Regimes of the Beam Instability

Having calculated the growth rates for the hydrodynamic and kinetic regimes of the Cherenkov and cyclotron instabilities, we can check whether the conditions of the corresponding regimes are satisfied.

7.9.1 Cherenkov Resonance

The condition of the hydrodynamic regime for the Cherenkov excitation is given by (7.4) with $\nu = 0$ (the condition for the kinetic regime is reversed). We can distinguish two separate cases: when the scatter in velocity of the resonant particles is due to the the scatter in parallel velocity or to the scatter in pitch angles. In the former case condition (7.4) with the parallel growth rate (7.68) gives the following requirement for the hydrodynamic-type Cherenkov instability:

$$\frac{\gamma_b^2}{\sqrt{T_p}\Delta\gamma\lambda^{1/3}} \gg 1 \tag{7.99}$$

which is well satisfied for the chosen plasma parameters.

In the case when the scatter in pitch angles dominates over the scatter in parallel velocity the condition for the hydrodynamic type Cherenkov instability reads

$$\psi^2 \ll \frac{1}{\gamma_b\sqrt{T_p\lambda}} \tag{7.100}$$

This is not satisfied. This implies that if the primary beam does not acquire any significant transverse gyrational energy as it propagates out in the pulsar magnetosphere, then the Cherenkov-type instabilities occur in the hydrodynamic regime.

We can also verify that the condition for the kinetic growth of the beam without any scatter in pitch angles is not satisfied. The inverse of the condition (7.4) with the parallel growth rate in the kinetic regime (7.93) give the following condition for the validity of the kinetic approximation

$$\frac{\gamma_b^5}{\lambda T_p^3\Delta\gamma^3} \ll 1 \tag{7.101}$$

Resonances	Extraordinary wave	Ordinary wave	Alfven wave
Cherenkov	0	$\Gamma = \frac{\pi}{2}\frac{\omega_b^2}{k_{res}c}\frac{\gamma_b^3 \sin^2\theta}{\Delta\gamma^2}$, $\omega - Eq.(55)$ $\quad \mu_h \geq 1$ $\Gamma = \begin{cases} \frac{\pi}{\sqrt{22}}\frac{\omega_b^2}{\omega_p}\frac{\gamma_b^3}{\Delta\gamma^2} & \theta \ll \frac{2\omega_p^2}{\omega_B^2} \\ \frac{\pi}{2}\frac{\omega_b^2\omega_0^{(h)3}}{\omega_B^4 \sin^2\theta\cos^2\theta}\frac{\gamma_b^3}{\Delta\gamma^2} & \theta \gg \frac{2\omega_p^2}{\omega_B^2} \end{cases}$ $\quad \mu_h \gg 1$	$\Gamma = \frac{\pi}{8}\frac{\omega_b^2}{kc\cos\theta}\frac{\omega^4}{\omega_p^4}\tan^2\theta\frac{\gamma^3}{\Delta\gamma^2}$ ω *Eq. (42) or Eq. (122)*
Cyclotron	$\Gamma = \frac{\pi}{4}\frac{\omega_{p,res}^2\omega_p^2\gamma_b T_p}{\omega_B^3\Delta\gamma}$	$\Gamma = \frac{\pi}{4}\frac{\omega_{p,res}^2}{\omega_{res}\cos^2\theta\Delta\gamma}$ ω *Eq. (7.30) or Eq. (7.63)*	$\Gamma = \frac{\pi}{4}\frac{\omega_b^2}{\omega_{res}\Delta\gamma}$ ω *Eq. (7.20) or Eq. (7.60)*

Table 7.3: Kinetic growth rate in a pair plasma

which is not satisfied for the chosen plasma parameters.

We deduce that the Cherenkov instability for the parallel propagation is in the hydrodynamic regime.

7.9.2 Cyclotron Resonance

For the cyclotron resonances the left-hand side of (7.4) is dominated by the last term. For the cyclotron excitation of the extraordinary mode condition (7.4) with the growth rate (7.41) give for the hydrodynamic type instability to apply

$$\Delta\gamma \ll \sqrt{T_p\lambda}\frac{\gamma_b^{3/2}\Omega}{\gamma_p\omega_B} = 10^{-7}\left(\frac{R}{R_{NS}}\right)^3 \tag{7.102}$$

which is most probably not satisfied even in the outer regions of the pulsar magnetosphere.

The condition for the kinetic approximation for the cyclotron excitation of the extraordinary mode follows from (7.4) and (7.96):

$$\Delta\gamma \gg \left(\frac{\gamma_{res}^3\lambda\lambda_{res}T_p}{\gamma_p}\right)^{1/2}\frac{\Omega}{\omega_B} \tag{7.103}$$

which is well satisfied inside the pulsar magnetosphere.

From these estimates we conclude that the cyclotron instability in the pulsar magnetosphere occurs in the kinetic regime. This is different from the electrostatic Cherenkov instabilities on the primary beam, that occur in a hydrodynamic regime (see also Section 7.10).

This difference is very important for the theories of the pulsar radio emission. The kinetic instabilities, in contrast to the hydrodynamic, are not suppressed by the large relativistic factor of the resonant particles. Thus, the kinetic instabilities are more favorable as a possible source of the pulsar radio emission.

It is possible to illustrate graphically the difference between the hydrodynamic regime of the Cherenkov instability and the kinetic regime of the cyclotron instability. On the frequency-wave vector diagram (Fig. 7.2 and 7.4), the dispersion curves of the cyclotron wave in the beam $\omega = kv_b\cos\theta - \omega_B/\gamma_b$ is almost parallel to the dispersion curves of the excited waves in plasma at the location of the resonance. Thus, a small change in the velocity of the resonant particles results in a considerable change of the resonant frequency. This vindicates the kinetic approximation that requires a large bandwidth of the growing waves. In contrast, for the very large streaming γ-factor of the primary beam (so that $\mu,\ \mu_h \gg 1$), the Cherenkov resonances on the ordinary and extraordinary modes occur approximately at the cross-over frequency in a narrow frequency band.

7.10 Streaming Instability Due the Relative Drift of Plasma Components

As we have shown in the previous sections, the Cherenkov-type instability on the primary beam does not develop in the pulsar magnetosphere. This is due to the very large "parallel" mass of the primary particles, i.e., to their large γ-factor. It has been suggested by that the analogous two-stream instability due to the relative drift of plasma components may develop in a pulsar magnetosphere. The difference in velocities between electrons and positrons of the secondary plasma is due to the requirement that the total charge density of all three components (electrons and positrons of the plasma and the primary beam) is equal to the local Goldreich-Julian density with a total current required by the global electromagnetic conditions in the magnetosphere $j \approx |en_{GJ}c|$.

We expect that the plasma components are relativistically hot, so that in the center of momentum frame, the average energies of the particles are comparable relative streaming energies. For the two-stream instability to develop, the relative streaming of the plasma component should be relativistic. The relative velocity between the components depends on the density of the secondary plasma. The critical value for the parameter λ at which the relative velocity of the particles become relativistic may be estimated as $\lambda^* = (\gamma_b'/T_p)^{2/3}$ (γ_b' is the energy of the primary beam in the pulsar frame, T_p is the energy spread in each component). For the characteristic beam energy $\gamma_b \approx 10^7$ this gives for the relativistically hot components $\lambda^* \approx 10^4$. This estimate assumes that the relative streaming between the plasma components reaches its maximal possible value. This is not true for the region near the pulsar surface where the two-stream instability is supposed to operate.

Next, let us estimate the conditions for the development of the two-stream instability due to the relative streaming of plasma particles. If the center-of-momentum frame moves with the γ-factor γ_p with respect to pulsar frame and in the center-of-momentum frame γ-factors of each components' rest frame is γ_r, then in the limit $\gamma_p \gg \gamma_s \gg 1$ the rest frame of the slow and fast components move in the pulsar frame with a γ-factor $\gamma_s = \gamma_p/(2\gamma_r)$ and $\gamma_c = 2\gamma_r\gamma_p$. In the rest frame of the slow component, the γ-factor of the fast component is $\gamma_c = 2\gamma_r^2$. The γ-factor of the relative streaming γ_r in the case of the relativistic relative streaming is $\gamma_r \approx \gamma_p/\sqrt{2\lambda}$. Then, it is required for the development of the instability that $\gamma_c \gg T_p$, which can be expressed as

$$\gamma_p^2 \gg \lambda T_p \tag{7.104}$$

This condition is quite hard to satisfy. It requires cold and not very dense plasma. Using the equipartition condition (4.5), inequality (7.104) may be written as $\gamma_p \gg \gamma_b^{1/3} \approx 3 \times 10^2$.

An important factor in the development of the two-stream instability on the relative drift of plasma particles is that the excited waves belong to the Alfvén branch. This can be seen from the

fact that the maximum phase velocity of the Alfven waves in the slow component $v_A = c(1 - \frac{\omega_p^2 T_p}{2\omega_B^2})$ (minimal phase velocity of the ordinary wave) is much larger than the relative streaming velocity $v_r = c(1 - 1/(2\gamma_c^2))$ of the secondary plasma component. This corresponds to the case of Fig. 7.4.a. Alfvén waves cannot be adiabatically transformed into vacuum waves. Therefore, they have to be converted into escaping radiation through some nonlinear process.

7.11 Conclusion

In this chapter we considered wave excitation in the strongly magnetized electron-positron plasma. We found the location of resonances and calculated the growth rates for the Cherenkov and cyclotron excitation of the ordinary, extraordinary and Alfvén waves. We have considered wave excitation in cold and relativistically hot plasma in two possible different regimes of hydrodynamic and kinetic instabilities taking into account angular dependence of the growth rates. The main results of the chapter are

(i) Cherenkov instabilities develop in the hydrodynamic regime while cyclotron instabilities develop in the kinetic regime.

(ii) Cherenkov instability on the primary beam develops on the Alfvén waves in the regions close to the stellar surface and on the ordinary mode in the outer regions of the pulsar magnetosphere (7.13), (7.55).

(iii) Cyclotron instability can develop on all three wave branches. On the Alfvén branch, the cyclotron instability does not develop in a very hot plasma (7.60).

(iv) The typical range of angles (in the plasma frame) with the highest growth rates are

$\delta\theta \approx \omega_p^2/\omega_B^2$ for Cherenkov excitation of the ordinary mode

$\delta\theta \approx 1/\gamma_b$ for Cherenkov excitation of the Alfvén mode

$\delta\theta \approx \omega_p/\omega_B$ for cyclotron excitation of the ordinary and extraordinary modes

$\delta\theta \approx 1$ for cyclotron excitation of the Alfvén mode

(v) Cherenkov instability due to the relative drift of the plasma particles can develop only on the Alfvén mode.

Cherenkov instabilities have largest growth rate near the stellar surface, where the Cherenkov resonance occurs on the Alfvén mode. However, this mode cannot escape to infinity. In addition, Cherenkov instabilities grow within a much narrower angle than cyclotron instabilities. Cherenkov instabilities, developing in the hydrodynamic regime, are also strongly suppressed by the large relativistic Lorentz factor of the primary beam. These arguments suggest that electromagnetic cyclotron instabilities are more likely to develop in the pulsar magnetosphere than electrostatic.

Chapter 8 A Model of Pulsar Radio Emission

In this chapter it is shown that the pulsar radiation may be generated by two kinds of *electromagnetic* plasma instabilities – cyclotron-Cherenkov and Cherenkov-drift instabilities. The cyclotron-Cherenkov instability is responsible for the generation of the core-type emission and the Cherenkov-drift instability is responsible for the generation of the cone-type emission (Rankin 1992). The waves generated by these instabilities are vacuum-like electromagnetic waves: they may leave the magnetosphere directly.

We assume that the distribution function, displayed in Fig. 1.1, remains unchanged throughout the inner magnetosphere. This requires that no Cherenkov-type two-stream instabilities develop and that the high energy particles are not excited to the high gyrational states by the mutual collisions or by the inverse Compton effect. Then in the outer regions of the pulsar magnetosphere two instabilities can develop: (i) cyclotron-Cherenkov instability and (ii) Cherenkov-drift instability.

A detailed consideration of the conditions necessary for the development of the cyclotron-Cherenkov and Cherenkov-drift instabilities are given in Appendix F and H. Both cyclotron-Cherenkov and Cherenkov-drift instabilities develop in the outer regions of the pulsar magnetosphere at radii $R \approx 10^9$ cm.

The frequencies of the waves generated by the cyclotron-Cherenkov instability are given by (F.3)

$$\omega = \frac{4\,\gamma_p^3 \omega_B^3}{\gamma_{res} T_p \omega_p^2} \tag{8.1}$$

which may be solved for the radius at which the waves with frequency ω are emitted:

$$R = R_{NS} \left(\frac{2\gamma_p^3}{\lambda \gamma_{res} T_p} \right)^{1/6} \left(\frac{\omega_B^{*2}}{\omega \Omega} \right)^{1/6} = 1.8 \times 10^9 \,\mathrm{cm}\, B_{12}^{1/3}\, \nu_9^{-1/6}\, P_{0.5}^{1/6} \gamma_{res,5}^{-1/6} \tag{8.2}$$

The relationship (8.2) may be regarded as a "radius-to-frequency" mapping. For a given γ_{res} the radial dependence of the right-hand side of Eq.(8.1) will result in a radial dependence of the emitted frequency. The radial dependence of the parameters in (F.3) will result in emission of higher frequencies deeper in the pulsar magnetosphere, exactly what is observed. The simple "radius-to-frequency" mapping will be "blurred" by the scatter in energies of the resonant particles, but the general trend that lower frequencies are emitted higher in the magnetosphere will remain.

The frequencies emitted at the Cherenkov-drift resonance do not have a simple dependence on radius from the neutron star. They are determined by several emission conditions which limit the development of the instabilities to the particular location in the magnetosphere and particular

frequencies.

The conditions that the instabilities should satisfy are:

(i) small growth length in a curved field lines $\frac{c}{\Gamma} < \Delta\theta R_B$, where $\Delta\theta$ is the range of the emitted resonant angles

(ii) condition of kinetic instability $|\mathbf{k}\delta\mathbf{v}_{res}| \gg \Gamma$

In addition to these, the Cherenkov-drift instability should also satisfy another condition:

(iii) the condition of a large drift $u_d/c > \sqrt{2\delta}$.

The condition (i) states that an emitting particle can stay in a resonances with the wave for many growth lengths. The condition (ii) is a requirement that the growth rate of instability is much smaller than the bandwidth of the growing waves. This condition is necessary for the random phase approximation to the wave-particle interaction to apply.

In Appendices F, H and I we show that the above conditions can be satisfied for the chosen set of parameters both in normal pulsar and millisecond pulsars. The conditions for the development of the cyclotron-Cherenkov and Cherenkov-drift instabilities depend in a different way on the parameters of the plasma. They may develop in the different regions of the pulsar magnetosphere.

8.1 Pulsar Phenomenology

8.1.1 Energetics

In both cyclotron-Cherenkov and Cherenkov-drift mechanism, the emission is generated by the fast particles which supply the energy for the growth of the waves. The total energy available for the conversion into radio emission is of the order of the energy of the particle flow along the open field lines of pulsar magnetosphere:

$$E \approx n_{GJ}\,\pi R_{pc}^2\,\gamma_b mc^3 \approx 10^{33}\mathrm{erg\,s^{-1}} \tag{8.3}$$

where $R_{pc} = R_{NS}\sqrt{\frac{R_{NS}\Omega}{c}}$ is the radius of a polar cap. This is enough to explain the radio luminosities of the typical pulsar if the effective emitting area is about one hundredth of the total open field line cross section.

8.1.2 Emission Pattern

The emission pattern for the "core"-type pulsars (according to the classification of (Rankin 1992)) is a circle with the angular extent of several degrees. In our model the region of the cyclotron-Cherenkov instability is limited to the almost straight field lines (see Fig. 8.1). The curvature of the magnetic field destroys the coherence between the waves and the resonant particles. To produce an observable emission, the waves need to travel in resonance with the particle at least several

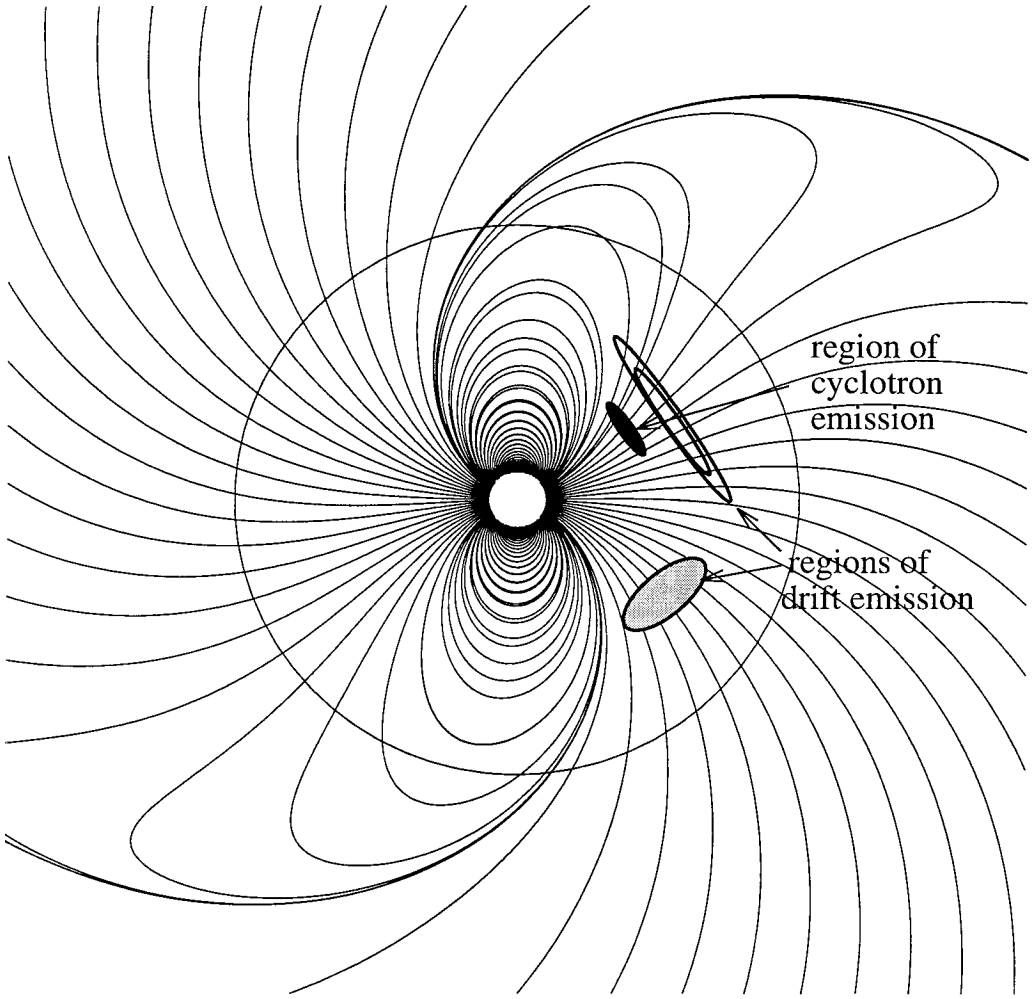

Figure 8.1: Top view of the field lines in the equatorial plane of a rotating point dipole in vacuum (Yadigaroglu 1997). Circle indicates light cylinder. The locations of cyclotron-Cherenkov and drift instabilities are shown (similar regions will be on the other side of the pulsar). The cyclotron-Cherenkov instability develops in the region of almost straight field lines. The location of the Cherenkov-drift emission depends sensitively on the curvature of magnetic field line. Two possible locations of the Cherenkov-drift emission are shown: ringlike near the magnetic axis and in the region of swept field lines (shaded ellipse). When the effects of plasma loading are taken into account, the field lines will become more curved. The current flowing along the open field lines will also produce a torsion in the field lines, so that at the light cylinder the structure of the field will be changed considerably.

instability folding lengths. Far from the magnetic axis, where the field lines are almost straight, the waves leave the resonance cone before they travel a growth length and no substantial amplification occurs. Near the magnetic field axis the radius of curvature is very large and waves can stay in a resonance with a particle for a long time and grow to large amplitudes.

The Cherenkov-drift instability requires a considerable curvature of the field lines on one hand but its growth rate may be limited by the coherence condition. In a dipole geometry this will limit the location of the Cherenkov-drift emission region to a ringlike region around the central field line.

The core emission is always generated on the almost straight central field lines. In contrast, the conditions for the development of the Cherenkov-drift instability depend on the plasma parameters and the radius of curvature of the magnetic field in a complicated way. This results in a broader range of phenomena observed in the cone emission. If the parameters of the plasma change due to the changing conditions at the pair production front, the location of the Cherenkov-drift instability may change considerably. This may account for the mode switching observed in the cone emission of some pulsars. The changing plasma parameters, which change the conditions for the development of the Cherenkov-drift instability, may also be responsible for nulling and the ultimate death of pulsars.

8.1.3 Polarization

If the average energy of the electrons and positrons of the secondary plasma is the same, the fundamental modes of such strongly magnetized plasma are linearlly polarized. Both of the two quasi–transverse modes (one with electric field lying in the $\mathbf{k} - \mathbf{B_o}$ plane, another with $\mathbf{E}$ perpendicular to this plan) may be emitted by the cyclotron-Cherenkov mechanism. This may naturally explain the two orthogonal modes observed in pulsars (Kazbegi et al. 1991b, Kazbegi et al. 1991c, Lominadze, Machabeli & Usov 1983). The small difference in the dispersion relations and in the emission conditions between ordinary and extraordinary modes may explain the difference in the observed intensities of these modes.

The rotation of the magnetized neutron star produces a difference in the average streaming velocities of the plasma components. This results in the circular polarization of the quasi–transverse modes for the angles of propagation with respect to the local magnetic field less than some critical angle. This may explain in a natural way the occurrence of the circular polarization in the "core" emission.

If the cyclotron-Cherenkov instability occurs on the tail of the plasma distribution function, then the particles of both signs of charge can resonate with the wave. In a curved magnetic field, electrons and positrons will drift in opposite directions (Fig. 8.2). As the line of sight crosses the emission region, the observer will first see the left circularly polarized wave emitted by the electrons in the direction of their drift. When the line of sight becomes parallel to the local magnetic field, the wave will resonate with both electrons and positrons in the plasma tail, so that the resulting

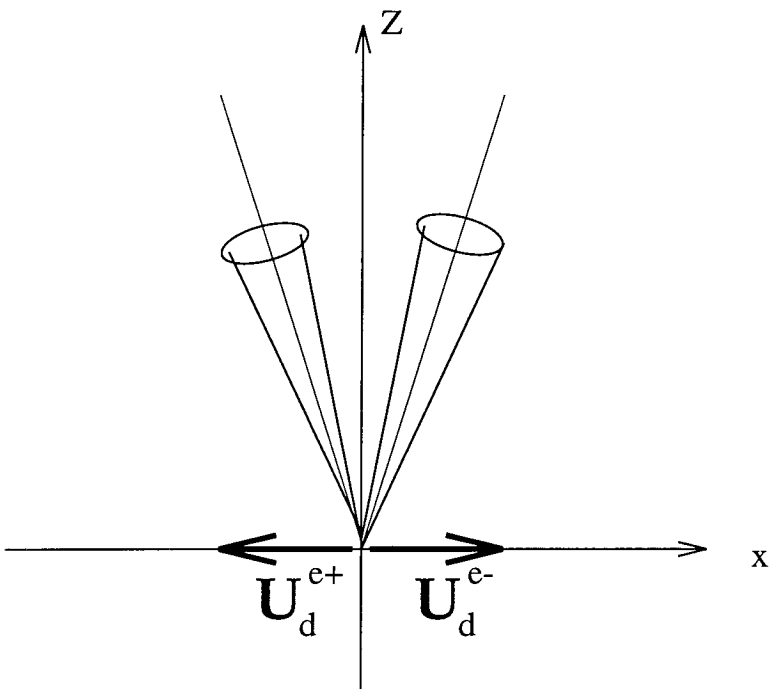

Figure 8.2: Switch of the sense of the circular polarization due to the cyclotron-Cherenkov resonance on the tail of the plasma distribution. The drift velocity of the electron and positron is in the opposite direction. As the line of sight crosses the emission region, the observer first will see the waves emitted by the particles of one sign of charge and then the other. The waves emitted by electron and positron have different circular polarization.

circular polarization will be zero. Finally, the observer will see the wave emitted by positrons in the direction of their drift. This can explain the switch of the circular polarization observed in some pulsars.

The cone emission, which is due to the Cherenkov-drift instability naturally has one linear polarization. An important difference from the bunching theory is that the waves emitted at the Cherenkov-drift resonance are polarized perpendicular to the plane of the curved magnetic field line. This may be used as a test to distinguish between the two theories. To do so, one needs to determine the absolute position of the rotation axis of a pulsar - a possible but a difficult task. One possible experiment would involve Harrison-Tademaru effect (Harrison & Tademaru 1975), which predicts that the spins of neutron stars may be aligned with their proper motion due to the quadrupole magnetic radiation if the magnetic moment is displaced from the center of the star. Unfortunately, the current data does not support this theory (in Crab the spin of the neutron star is within 10^o of from the direction of the proper motion, while for Vela it is approximately perpendicular). Symmetry of plerions and direct observation of jets from pulsars (like the one observed in Vela pulsar (Markwardt & Ogelman 1995)) may provide an additional information on the location of the neutron star rotation axis.

It may be also possible to explain in the framework of our model the phenomenon of "wide beam geometry" observed in some pulsars (Manchester 1996). The Cherenkov-drift instability may occur in the region, where the field lines are swept back considerably. Then the emission will be generated in what could be called a "wide beam geometry." Since the waves emitted by the Cherenkov-drift instability are expected to be highly polarized, we may expect that the linear polarization will be higher if the Cherenkov-drift instability occurs in the region with a more regular pattern of the field lines than in the dipole geometry. This may explain the unusually high linear polarization of the wide beams (Manchester 1996).

8.1.4 Radius-to-frequency Mapping

The condition for the cyclotron-Cherenkov resonance (Eq. F.3) gives a radial dependence of the emitted frequencies. Higher frequencies are emitted lower in the magnetosphere with the resonant frequency increasing $\propto R^6$. If the conditions for the development of the cyclotron-Cherenkov instability are satisfied for both primary beam and for the particles from the tail of plasma distribution, then a given frequency may resonate with beam and tail particles at different radii.

8.1.5 Coherent Size

It is possible in the framework of our theory to explain the observations of Gwinn et al. 1997 who observed a coherent size of 500 km for the emission region in Vela pulsar. The Cherenkov-drift instability occurs at a distance of approximately 10^9 cm from the star surface. At that distance, the coherent size of 500 km subtends an angle $\alpha \approx 5 \times 10^{-2}$. We recall that in the Cherenkov-drift instability, the waves are emitted at an angle $\theta^{em} \approx u_d/c$ to the magnetic field in the direction perpendicular to the plane of the field lines and in the cone with the width $\Delta\theta \approx \sqrt{\delta}$. We find then, that the angle that the emitting region subtends is approximately the angle of the wave emission with respect to the magnetic field: $\alpha \approx \theta^{em} = u_d/c \approx 10^{-2}$ (see Fig. 8.3). In a dipole geometry for the point 1 on Fig. 8.3 to emit in a direction of the observer B, the field lines must have a nonzero torsion. Then the emission will be generated in a cone with the angle $\theta^{em} \approx u_d/c$ with respect to the magnetic field line. Taking into account that for a point on a field line near the magnetic axis, the angle between the local magnetic field and the direction of the magnetic axis is approximately equal to the angle between the radius vector of the point and the direction of the magnetic axis ($\alpha = 2\theta/3$, to be more precise); we see that the observer at two points A and B on Fig. 8.3 will detect a coherently emitting size of 500 km.

We would like to stress that it is impossible to explain the observations of Gwinn et al. 1997 in the frame work of bunching theory without invoking unrealistic assumptions. In the bunching theory the emission is generated only along the local magnetic field lines. In our theory the emission

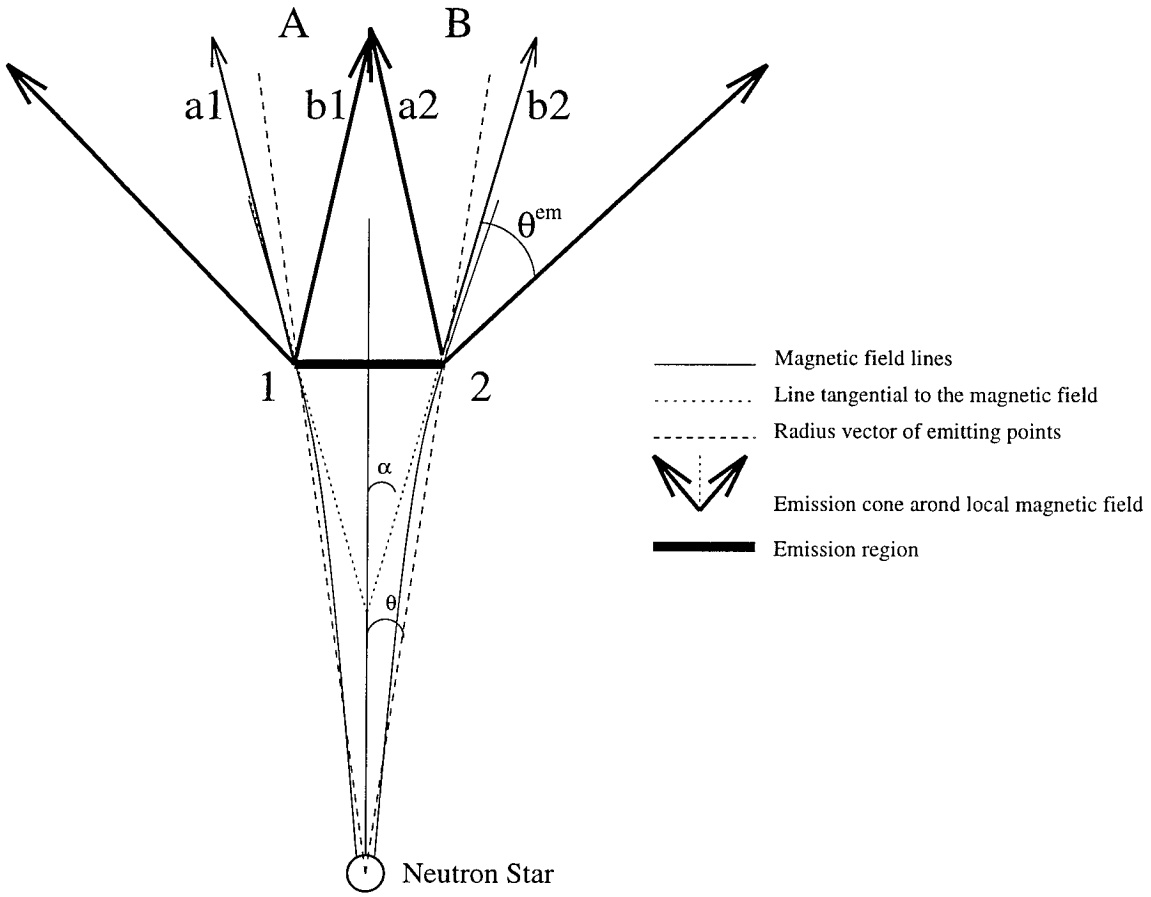

Figure 8.3: Coherent size of the emitting region. The angular size of the emission region is approximately equal to the emission cone θ^{em} around a local magnetic filed: $\theta = 2/3\alpha \approx \theta^{em}$. Two observers **A** and **B** see the rays **a1**, **a2** and **b1**, **b2** emitted by the two emission points separated by the distance of 500 km. We stress that the emission angle θ^{em} is determined by the instability emission condition.

is naturally generated at angles to the magnetic field.

8.1.6 Formation of Spectra

Cyclotron-Cherenkov and Cherenkov-drift instabilities produce emission in a limited frequency window determined by the resonant conditions. The original exponential growth is limited by the nonlinear processes: quasi-linear diffusion, induced scattering and wave decay. Also, as the waves propagate in a magnetosphere, they may be absorbed by the particles of the bulk plasma (Lyutikov & Machabeli 1997). The emergent spectra are the combined results of these processes: emission, nonlinear saturation and absorption.

In this work we considered two most like nonlinear saturation effects: quasilinear diffusion (see Section 9.1) and induced Raman scattering (Section 9.2). Both these processes are likely candidates for the saturation mechanism. They produce fluxes of the order of observed ones. The quasilinear diffusion produces an average spectral index -2, which is close to the observed mean value of -1.6 (Lorimer et al. 1995). The spectrum flattens at high frequencies - this may be related to the possible turn-up in the flux densities at mm-wavelegnths (Kramer et al. 1996). The The induced Raman scattering may also play an important role for the scattering of the radiation that has been generated lower in the magnetosphere. The threshold intensities for the strong Raman scattering are comparable to the observed.

The absorption process are considered in Chapter 9.3. The waves may be strongly damped on the three possible resonances: Cherenkov, Cherenkov-drift and cyclotron. Alfvén wave is always strongly damped on the Cherenkov resonances and possibly on the Cherenkov-drift resonance and cannot leave magnetosphere. Both ordinary and extraordinary waves may be damped on the Cherenkov-drift resonance. In this case Cherenkov-drift resonance affects only the ordinary and extraordinary waves with the electric field perpendicular to the plane of the curved magnetic field line. The high frequency parts of the extraordinary and ordinary wave may also be damped on the cyclotron resonances, but the observed circular polarization in the pulsar radio emission implies that the extraordinary and ordinary waves get detached from plasma escaping absorption. In this case two orthogonal linear polarizations will be observed.

8.1.7 High Energy Emission

It may be possible also to relate the pulsed high energy emission to the radio mechanisms. The development of the cyclotron-Cherenkov instability at the anomalous Doppler effect leads to the finite pitch angles of the resonant particles. The particles will undergo a cyclotron transition at the normal Doppler effect decreasing their pitch angle. The frequency of the wave emitted in such a

transition will fall in the soft X-ray range with the frequencies

$$\omega \approx \gamma_b \omega_B = 10^{18} \mathrm{rad\,sec}^{-1} \quad (E \approx 1\mathrm{keV}) \tag{8.4}$$

In such a model the high energy emission will coincide with the core component of the radio emission, which is what is observed in Crab pulsar and some other pulsars. We also note, that this may be a feasible theory for the pulsed soft X-ray emission. The hard X-ray and γ-emission cannot be explained by this mechanism since the total energy flux in the primary beam is not enough to account for the very high energy emission (see, for example, Usov 1996).

8.2 Observational Predictions

8.2.1 General Predictions of the Maser-type Instability

The formalism of the maser-type emission assumes a random phase approximation for the wave-particle interaction. Any given particle can simultaneously resonate with several waves whose phases are not correlated. This is different from the reactive-type emission (like coherent emission by bunches) when the phases of the waves with different frequencies are strongly correlated. Thus any observation of the fine frequency structure in the pulsar radio emission may be considered as a strong argument against the reactive-type emission and in favor of the maser-type emission.

8.2.2 Cyclotron-Cherenkov Instability

Frequency Dependence of the Circular Polarization

The cyclotron-Cherenkov instability can develop both on the primary beam particles and the particles from the tail of the plasma distribution. The cyclotron-Cherenkov instability on the primary beam produces a pulse which has a maximum circular polarization in its center. The cyclotron-Cherenkov instability on the tail particles produces a pulse with the switching of the sense of the circular polarization in its center. Since the resonance on the tail particles occurs on larger frequencies (Eq. F.3), the effects of the switching sense of the circular polarization should be more prominent on the higher frequencies.

8.2.3 Cherenkov-drift Instability

Linear Polarization of the Cone Radiation

Cherenkov-drift instability produces waves with the linear polarization perpendicular to the plane of the curved field line. This is in a sharp contrast to many other theories of the radio emission that tend to generate waves with the electric field in the plane of the curved field line. If one can determine

the absolute position of the rotational axis, magnetic moment and the electric vector of the linear polarization, then, assuming a dipole geometry, it will be possible to determine unambiguously the position of the electric vector of the emitted wave with respect to the plane of the magnetic field line. Unfortunately, the results are sensitive to the assumed magnetic field geometry. The distortion of the magnetic field lines in the outer regions of pulsar magnetosphere (sweep back) can smear out the simple picture that a pure dipolar field would have produced.

8.2.4 No Cyclotron-Cherenkov Instability in Millisecond Pulsars

In Appendix I we show that the cyclotron-Cherenkov instability does not develop in the magnetospheres of the millisecond pulsars. Since in our model the cyclotron-Cherenkov instability produces core-type emission we predict that millisecond pulsars will not show core-type emission. At present, the existing observations do not allow a separation into the core and cone type emission in the millisecond pulsars.

Chapter 9 Nonlinear Effects and Formation of the Pulsar Radio Spectrum

9.1 Quasilinear Diffusion

9.1.1 Introduction

In this Chapter we consider pulsar spectrum formation due to the quasilinear saturation of the cyclotron-Cherenkov instability. The cyclotron-Cherenkov instability develops at the anomalous Doppler resonance

$$\omega(\mathbf{k}) - k_{\|} v_{\|} - s\frac{\omega_B}{\gamma} = 0 \quad \text{for } s < 0 \tag{9.1}$$

The nonlinear saturation of the cyclotron-Cherenkov instability due to the diffusion of the resonant particles has been previously considered by several authors. Kawamura & Suzuki 1977 neglected the possible stabilizing effects of the radiation reaction force due to the cyclotron emission at the normal Doppler resonance and the force arising in the inhomogeneous magnetic field due to the conservation of the adiabatic invariant. These forces result in a saturation of the quasilinear diffusion.

Lominadze, Machabeli & Mikhailovskii 1979 were the first to notice the importance of the radiation reaction force due to the emission at the normal Doppler resonance on the saturation of the quasilinear diffusion. Unfortunately, Lominadze, Machabeli & Mikhailovskii 1979 used an expression for the cyclotron damping rates which is applicable only for the nonrelativistic transverse motions, when $\gamma\psi$ (ψ is the pitch angle) is much less than unity. In the pulsar magnetospheres the development of the cyclotron-Cherenkov instability results in a diffusion of particles in transverse moments, quickly increasing their transverse energy to relativistic values.

In a review paper Lominadze, Machabeli & Usov 1983 took correct account of the radiation reaction force due to the emission at the normal Doppler resonance and pointed out the importance of the force arising in the inhomogeneous magnetic field due to the conservation of the adiabatic invariant (**G** force Eq. (9.10)). When considering the deceleration of the beam Lominadze, Machabeli & Usov 1983 incorrectly neglected the radiation reaction force due to the emission at the anomalous Doppler resonance in comparison with the radiation reaction force due to the emission at the normal Doppler resonance.

In this work we reconsider and extend the treatment of the quasilinear stage of the cyclotron-

Cherenkov instability. We have found a state, in which the particles are constantly slowing down their parallel motion, mainly due to the component along magnetic field of the radiation reaction force of emission at the anomalous Doppler resonance. At the same time they keep the pitch angle almost constant due to the balance of the force **G** and the component perpendicular to the magnetic field of the radiation reaction force of emission at the anomalous Doppler resonance. We calculate the distribution function and the wave intensities for such quasilinear state.

In the process of the quasilinear diffusion the initial beam looses a large fraction of its initial energy $\approx 10\%$, which is enough to explain the typical luminosities of pulsars. The theory predicts a spectral index $F(\nu) \propto \nu^{-2}$ ($F(\nu)$ is the spectral flux density) which is very close to the observed mean spectral index of -1.6 (Lorimer et al. 1995). The predicted spectra also show a turn off at the low frequencies $\nu \leq 300MHz$ and a flattering of spectrum at large frequencies $\nu \geq 1GHz$.

9.1.2 Quasilinear Diffusion

A particle moving in a dielectric medium in magnetic field with the velocity larger than the velocity of light in a medium is emitting electromagnetic waves at the anomalous Doppler resonance ($s < 0$ in Eq. (9.1)) and at the normal Doppler resonance ($s > 0$ in Eq. (9.1)). The radiation reaction due to the emission at the normal Doppler resonance slows the particle's motion along magnetic field and decreases its transverse momentum. The radiation reaction due to the emission at the anomalous Doppler resonance increases its transverse momentum and also slows the particle's motion along magnetic field (Ginzburg & Eidman 1959). As the particle propagates into the region of lower magnetic field, the force **G** decreases the its transverse momentum and increases the parallel momentum. The stationary state in transverse moments may be reached when the actions of the **G** force and radiation reaction due to the emission at the normal Doppler resonance is balanced by the radiation reaction due to the emission at the anomalous Doppler resonance.

The quasisteady stage may also be considered in terms of a detailed balance of the particle transitions between the Landau levels. The quasisteady stage is reached when the number of induced transitions *up* in Landau level due to the emission at the anomalous Doppler resonance is balanced by the number of the spontaneous transitions *down* in Landau levels due to the emission at the anomalous Doppler resonance.

The equations describing the quasilinear diffusion in the magnetic field due to the effects of induced emission at the anomalous Doppler resonance are

$$\frac{df(\mathbf{p})}{dt} = \frac{1}{\sin\psi}\frac{\partial}{\partial\psi}\left[\sin\psi\left(D_{\psi\psi}\frac{\partial}{\partial\psi} + D_{\psi p}\frac{\partial}{\partial p}\right)f(\mathbf{p})\right] \\ \frac{1}{p^2}\frac{\partial}{\partial p}\left[p^2\left(D_{p\psi}\frac{\partial}{\partial\psi} + D_{pp}\frac{\partial}{\partial p}\right)f(\mathbf{p})\right] \tag{9.2}$$

$$\begin{pmatrix} D_{\psi\psi} \\ D_{\psi p} = D_{p\psi} \\ D_{pp} \end{pmatrix} = \sum_{s<0} \int \frac{d\mathbf{k}}{(2\pi)^3} w(s,\mathbf{p},\mathbf{k}) n(\mathbf{k}) \begin{pmatrix} (\Delta\psi)^2 \\ (\Delta\psi)(\Delta p) \\ (\Delta p)^2 \end{pmatrix} \tag{9.3}$$

$$\frac{dn(\mathbf{k})}{dt} = \sum_{s<0} \int d\mathbf{p} w(s,\mathbf{p},\mathbf{k}) \left(n(\mathbf{k})\hbar \left(\frac{\partial}{\partial p} + \frac{\cos\psi - (kv/\omega)\cos\theta}{p\sin\psi} \frac{\partial}{\partial\psi} \right) f(\mathbf{p}) \right) \tag{9.4}$$

Where

$$\Delta p = \frac{\hbar\omega}{v} \qquad \Delta\psi = \frac{\hbar(\omega\cos\psi - k_\parallel v)}{pv\sin\psi} \tag{9.5}$$

$$n(\mathbf{k}) = \frac{E^2(\mathbf{k})}{\hbar\omega(\mathbf{k})} \tag{9.6}$$

$$w(s,\mathbf{p},\mathbf{k}) = \frac{8\pi^2 q^2 R_E(\mathbf{k})}{\hbar\omega(\mathbf{k})} \left| \mathbf{e}(\mathbf{k}) \cdot \mathbf{V}(s,\mathbf{p},\mathbf{k}) \right|^2 \delta(\omega(\mathbf{k}) - s\omega_B/\gamma - k_\parallel v_\parallel) \tag{9.7}$$

$$\mathbf{V}(s,\mathbf{p},\mathbf{k}) = \left(v_\perp \frac{s}{z} J_s(z),\ -i\sigma s v_\perp J_s(z)',\ v_\parallel J_s(z) \right) \tag{9.8}$$

$E^2(\mathbf{k})d\mathbf{k}/(2\pi)^3$ is the energy density of the waves in the unit element range of $\mathbf{k}$-space. $E^2(\mathbf{k})$ has a dimension of energy.

In Eq. (9.21) we neglected spontaneous emission at the anomalous Doppler resonance and the induced emission at the normal Doppler resonance. The net effect of the spontaneous emission at the normal Doppler resonance is treated as a damping force acting on each particle in the Boltzman-type left-hand side of equation (9.9). To be exact, we should have treated the effects of spontaneous emission at the normal Doppler resonance as stochastic terms in the Fokker-Plank-type terms on the right-hand side of equation (9.9). But the emission at the normal Doppler resonance occurs at very high frequencies where the presence of a medium is unimportant and can be neglected. This allows one to integrate the corresponding terms over angles and sum over harmonics to obtain a classical synchrotron radiation damping force, that can be treated using the Boltzman approach. Thus, the total time derivative of the distribution function is

$$\frac{df(\mathbf{p})}{dt} = \frac{\partial f(\mathbf{p})}{\partial t} + \mathbf{v}\frac{\partial f(\mathbf{p})}{\partial \mathbf{r}} + \frac{\partial}{\partial \mathbf{p}} \left[\left(\mathbf{G} + \mathbf{F} + \frac{q}{c}(\mathbf{v} \times \mathbf{B_0}) \right) f(\mathbf{p}) \right] \tag{9.9}$$

where $\mathbf{G}$ is the force due to the conservation of the adiabatic invariant

$$G_\parallel = \beta_R \gamma \psi^2, \qquad G_\perp = -\beta_R \gamma \psi, \qquad \beta_R = \frac{mc^2}{R_B} \tag{9.10}$$

Here $R_B \approx 10^9$ cm is the radius of curvature and $\mathbf{F}$ is the radiation damping force due to the spontaneous synchrotron emission at the normal Doppler resonance:

$$F_\parallel = -\alpha\gamma^2\psi^2, \qquad F_\perp = -\alpha\psi\left(1 + \gamma^2\psi^2\right), \qquad \alpha = \frac{2q^2\omega_B^2}{3c^2} \tag{9.11}$$

From (9.10) and (9.12) we find that

$$\frac{F_\parallel}{G_\parallel} = \frac{\alpha}{\beta_R}\gamma, \qquad \frac{F_\perp}{G_\perp} = \frac{\alpha}{\beta_R}\gamma\psi^2, \quad \text{for } \gamma\psi \gg 1 \tag{9.12}$$

where $r_L = c/\omega_B$ is a Larmor radius and $r_e = q^2/(mc^2) = 2.8 \times 10^{-13}$cm is the classical radius of an electron.

The dimensionless ratio in (9.12) is

$$\frac{\alpha}{\beta_R} = \frac{2R_B r_e}{r_L^2} = 5 \times 10^{-4} R_{B,9} R_9^{-6} \tag{9.13}$$

$R_{B,9} = R_B/10^9$cm is the radius of curvature in units of 10^9 cm, $R_9 = R/10^9$cm is the distance from the neutron star surface in units of 10^9 cm.

Using (9.13) we find that, for the primary particles with $\gamma \approx 10^7$

$$\begin{aligned} &\frac{F_\parallel}{G_\parallel} \gg 1 \\ &\frac{F_\perp}{G_\perp} \ll 1, \qquad \text{for } \psi \ll \sqrt{\frac{r_L^2}{2R_B r_e \gamma}} \approx 10^{-2} \end{aligned} \tag{9.14}$$

The total derivative (9.9) then may be written as

$$\frac{df(\mathbf{p})}{dt} = \frac{\partial f(\mathbf{p})}{\partial t} + \mathbf{v}\frac{\partial f(\mathbf{p})}{\partial \mathbf{r}} + \frac{1}{p\sin\psi}\frac{\partial}{\partial \psi}\left(\sin\psi G_\perp f(\mathbf{p})\right) + \frac{1}{p^2}\frac{\partial}{\partial p}\left(p^2 F_\parallel f(\mathbf{p})\right) \tag{9.15}$$

We are interested in the quasilinear diffusion of the particles due to the resonant interaction with the waves at the anomalous Doppler effect. We expand the transition currents (9.8) in small $v_\perp$ keeping only $s = -1$ terms: $\mathbf{V}(-1, \mathbf{p}, \mathbf{k}) = v_\perp/2\,(1, i\sigma, 0)$. Then, for the waves propagating along magnetic field $\mathbf{e}(\mathbf{k}) = (1, 0, 0)$ we find

$$w(\pm 1, \mathbf{p}, \mathbf{k}) = \frac{\pi^2 q^2 v_\perp^2}{\hbar\omega(\mathbf{k})}\delta(\omega(\mathbf{k}) - s\omega_B/\gamma - k_\parallel v_\parallel) \tag{9.16}$$

where we take into account that $R_E(\mathbf{k}) \approx 1/2$.

We now can find the diffusion coefficients in the approximation of a one-dimensional spectrum of the waves.

$$n(\mathbf{k}) = \frac{2\pi\delta(\theta)}{k^2\sin\theta}n(k), \qquad n(k) = \int d\mathbf{\Omega}_\mathbf{k}\frac{k^2}{(2\pi)^2 n(\mathbf{k})} \tag{9.17}$$

We first note that we can simplify the change in the pitch angle (9.5) in the limit $\psi^2 \ll \delta$ and $1/\gamma^2 \ll \delta$

$$\Delta\psi \approx -\frac{\hbar\omega\delta}{pv\sin\psi} \tag{9.18}$$

We then find

$$\begin{pmatrix} D_{\psi\psi} \\ D_{\psi p} = D_{p\psi} \\ D_{pp} \end{pmatrix} = \begin{pmatrix} D\frac{\delta}{\gamma^2}E_k^2 \mid_{k=k_{res}} \\ -D\frac{\psi mc}{\gamma}E_k^2 \mid_{k=k_{res}} \\ D\frac{\psi^2 m^2 c^2}{\delta}E_k^2 \mid_{k=k_{res}} \end{pmatrix}, \quad D = \frac{\pi^2 q^2}{m^2 c^3} = \frac{\pi^2 r_e}{mc} \tag{9.19}$$

where

$$E_k^2 = \hbar\omega(k)n(k) = \int \frac{k^2 d\mathbf{\Omega}}{(2\pi)^2}\hbar\omega(\mathbf{k})n(\mathbf{k}) \tag{9.20}$$

is energy density per unit of one-dimensional wave vector and we assumed that $\omega(\mathbf{k})$ is an isotropic function of $\mathbf{k}$.

We next solve the partial differential equation describing the evolution of the distribution function by successive approximations. We first expand equation (9.21) in small ψ assuming that $\partial/\partial\psi \simeq 1/\psi$. We also neglect the convection term assuming that the characteristic time for the development of the quasilinear diffusion is much smaller that the dynamic time of the plasma flow. Then we assume that it is possible to separate the distribution function into the parts depending on the ψ and p:

$$f(\mathbf{p}) = Y(\psi)f(p) \tag{9.21}$$

with

$$f(p) = 2\pi \int \sin\psi d\psi f(\mathbf{p}), \qquad \int dp p^2 f(p) = 1 \tag{9.22}$$

In the lowest order in ψ we obtain an equation:

$$-\frac{1}{p\sin\psi}\frac{\partial}{\partial\psi}\left(\sin\psi G_\perp Y(\psi)\right) = \frac{1}{\sin\psi}\frac{\partial}{\partial\psi}\left[\sin\psi D_{\psi\psi}\frac{\partial Y(\psi)}{\partial\psi}\right] \tag{9.23}$$

which has a solution

$$Y(\psi) = \frac{1}{\pi\psi_0^2}\exp\left(-\frac{\psi^2}{\psi_0^2}\right), \qquad \psi_0^2 = \frac{Dmc\delta E_k^2}{\beta_R\gamma^2} = \frac{DR_B\delta E_k^2}{c\gamma^2} = \frac{\pi^2\delta R_B r_e E_k^2}{\gamma^2 mc^2} \tag{9.24}$$

The next order in ψ gives

$$\frac{\partial f(\mathbf{p})}{\partial t} + \frac{\partial}{\partial p}\left(F_\parallel f(\mathbf{p})\right) = \frac{1}{\sin\psi}\frac{\partial}{\partial\psi}\left[\sin\psi D_{\psi p}\frac{\partial f(\mathbf{p})}{\partial p}\right] + \frac{1}{p^2}\frac{\partial}{\partial p}\left[p^2 D_{p\psi}\frac{\partial f(\mathbf{p})}{\partial\psi}\right] \tag{9.25}$$

By integrating (9.25) over ψ with a weight ψ we find the equation for the parallel distribution function:

$$\frac{\partial f(p)}{\partial t} - \frac{\partial}{\partial p}\left(AE_k^2\gamma^2 f(p)\right) = \frac{2}{p^2}\frac{\partial}{\partial p}\left(pDm^2c^2E_k^2 f(p)\right) \tag{9.26}$$

where

$$A = \frac{\alpha\psi_0^2}{E_k^2} = \frac{2q^2\omega_B^2\psi_0^2}{3c^2E_k^2} = \frac{2\pi^2\omega_B^2q^4R_B\delta}{3\gamma^2m^2c^6} = \frac{2\pi^2R_Br_e^2\delta}{3\gamma^2r_L^2} \tag{9.27}$$

The term containing A describes the slowing of the particles due to the radiation reaction force and the term containing D describes the slowing of the particles due to the quasilinear diffusion, or, equivalently, due to the radiation reaction force of the anomalous Doppler resonance. To estimate the relative importance of these terms, we consider a ratio

$$\frac{A\gamma^3}{Dmc} = \frac{\alpha\delta\gamma}{\beta_R} = \frac{2\delta\gamma}{3}\frac{R_Br_e}{r_L^2} \ll 1 \tag{9.28}$$

Neglecting the second term on the left-hand side of (9.28) we find

$$\frac{\partial f(p)}{\partial t} - \frac{2}{p^2}\frac{\partial}{\partial p}\left(pDm^2c^2E_k^2f(p)\right) == 0 \tag{9.29}$$

If the cyclotron quasilinear diffusion has time to fully develop and reach a steady state, then the distribution function of the resonant particles is

$$f(p) \propto \frac{1}{p\,E_k^2} \tag{9.30}$$

Next we turn to the equation describing the temporal evolution of the wave intensity (9.4). Neglecting the spontaneous emission term and the wave convection, we find

$$\frac{\partial E_k^2}{\partial t} = -\Gamma E_k^2 f(\gamma)_{res} \tag{9.31}$$

where

$$\Gamma = \frac{1}{f(\gamma)_{res}}\sum_s \int d\mathbf{p}w(s,\mathbf{p},\mathbf{k})\left(\hbar\left(\frac{\partial}{\partial p} + \frac{\cos\psi - (kv/\omega)\cos\theta}{p\sin\psi}\frac{\partial}{\partial\psi}\right)f(\mathbf{p})\right) \tag{9.32}$$

and we introduced

$$f(\gamma)\gamma^2d\gamma = f(p)p^2dp \tag{9.33}$$

We will estimate this growth rate for the emission along the external magnetic field for distribution (9.22), (9.24). Neglecting $\partial/\partial p$ and assuming that $\psi^2 \ll 2\delta$ (so that most of the particles are moving with the superluminal velocity), we find, that for $s = -1$,

$$\Gamma = \frac{\pi\omega_{p,res}^2}{2\omega}\gamma_{res}^2 \tag{9.34}$$

(It is important to note that in the limit $\psi^2 \ll 2\delta$ the growth rate does not depend on the scatter in pitch angles.)

Equations (9.29) and (9.34) may be combined to a quasilinear expression

$$\frac{\partial}{\partial t}\left(f(\gamma)+\frac{2}{p^2}\frac{\partial}{\partial p}\left(\frac{pDm^2c^2E_k^2}{\Gamma}\right)\right)=0 \tag{9.35}$$

which after integration gives

$$f(\gamma)-\frac{2}{\gamma^2}\frac{\partial}{\partial \gamma}\left(\frac{\gamma D E_k^2}{\Gamma}\right)=f^0(\gamma) \tag{9.36}$$

Neglecting the initial density of particles in the region of quasilinear relaxation and using Eqs. (9.30) and (9.36), we can find a distribution function and the asymptotic spectral shape:

$$f(\gamma)=\frac{1}{2\gamma^3}\left(\frac{1}{\log(\gamma_{max}/\gamma)\log(\gamma_{max}/\gamma_{min})}\right)^{1/2} \tag{9.37}$$

$$E_k^2=\frac{mc^2\delta r_L\gamma^2}{2\pi r_e r_S^2}\left(\frac{\log(\gamma_{max}/\gamma)}{\log(\gamma_{max}/\gamma_{min})}\right)^{1/2}=\frac{mc^4\delta^3}{2\pi\omega^2 r_e r_L r_S^2}\left(\frac{\log(\omega/\omega min)}{\log(\gamma_{max}/\gamma_{min})}\right)^{1/2} \tag{9.38}$$

where $\omega_{min}=\omega_B/(\delta\gamma_{max})$.

It is noteworthy that a simple power law distribution for the spectral intensity and distribution function cannot satisfy both Eqs. (9.30) and (9.36). The particle distributions function and the energy spectrum of the waves are displayed in Figs. 9.1 and 9.2.

We can now estimate the flux per unit frequency:

$$F(\nu)=2\pi E_k^2=\frac{mc^4\delta^3}{\omega^2 r_e r_L r_S^2}\left(\frac{\log(\omega/\omega_{min})}{\log(\gamma_{max}/\gamma_{min})}\right)^{1/2}, \tag{9.39}$$

characteristic pitch angle

$$\psi_0=\delta\left(\frac{\pi R_B r_L}{r_S^2}\right)^{1/2}\left(\frac{\log(\gamma_{max}/\gamma)}{\log(\gamma_{max}/\gamma_{min})}\right)^{1/4}\approx 10^{-6}, \tag{9.40}$$

which remarkably stays almost constant for a broad range of particles' energies and also for different values of γ_{min}, and the total energy density in the waves

$$E_{tot}=\int_{\nu_{\min}}^{\nu_{\max}}F(\nu)d\nu\approx\frac{mc^2\gamma_{max}}{4\sqrt{\pi}r_e r_S^2\log^{1/2}(\gamma_{max}/\gamma_{min})} \tag{9.41}$$

This total energy can be compared with the kinetic energy density of the beam:

$$\frac{E_{tot}}{\gamma_b mc^2 n_{GJ}}\approx\sqrt{\frac{\pi}{\log(\gamma_{max}/\gamma_{min})}} \tag{9.42}$$

It means that some considerable fraction of the beam energy can be transformed into waves.

In Appendix N we show that a particle emitting radiation at anomalous Doppler resonance along magnetic field can lose approximately half of its energy into radiation. This is due to the fact that a

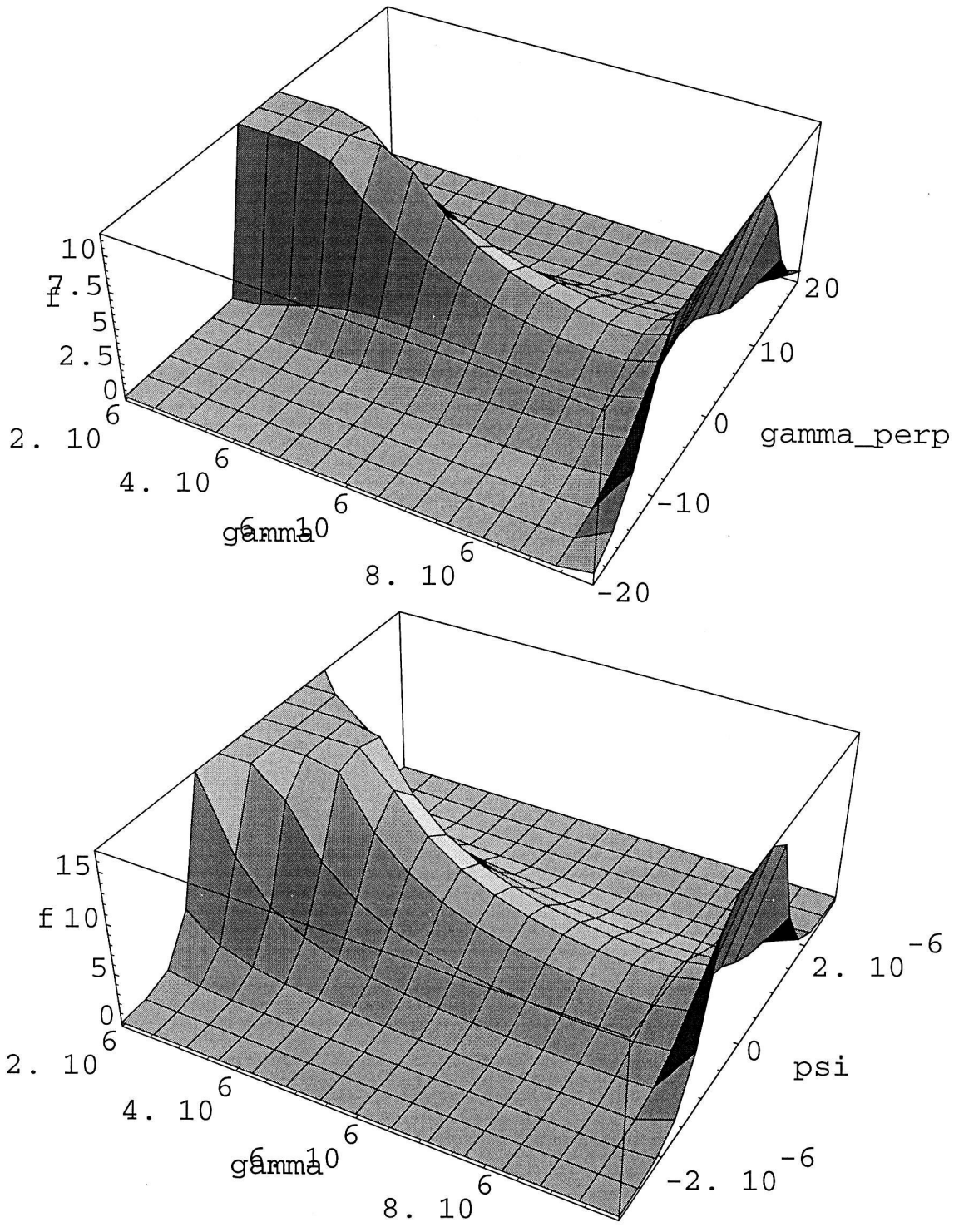

Figure 9.1: Asymptotic distribution functions in $\gamma - p_\perp$ and $\gamma - \psi$ spaces in arbitrary units for $\gamma_{max} = 10^7$. The spike at the $\gamma = \gamma_{max}$ is an artifact of the initial distribution function $f(\gamma)^0 = \delta(\gamma - \gamma_{max})$. The divergence at $\gamma = \gamma_{max}$ is weak (logarithmic) and would be removed if the more realistic initial distribution function were used.

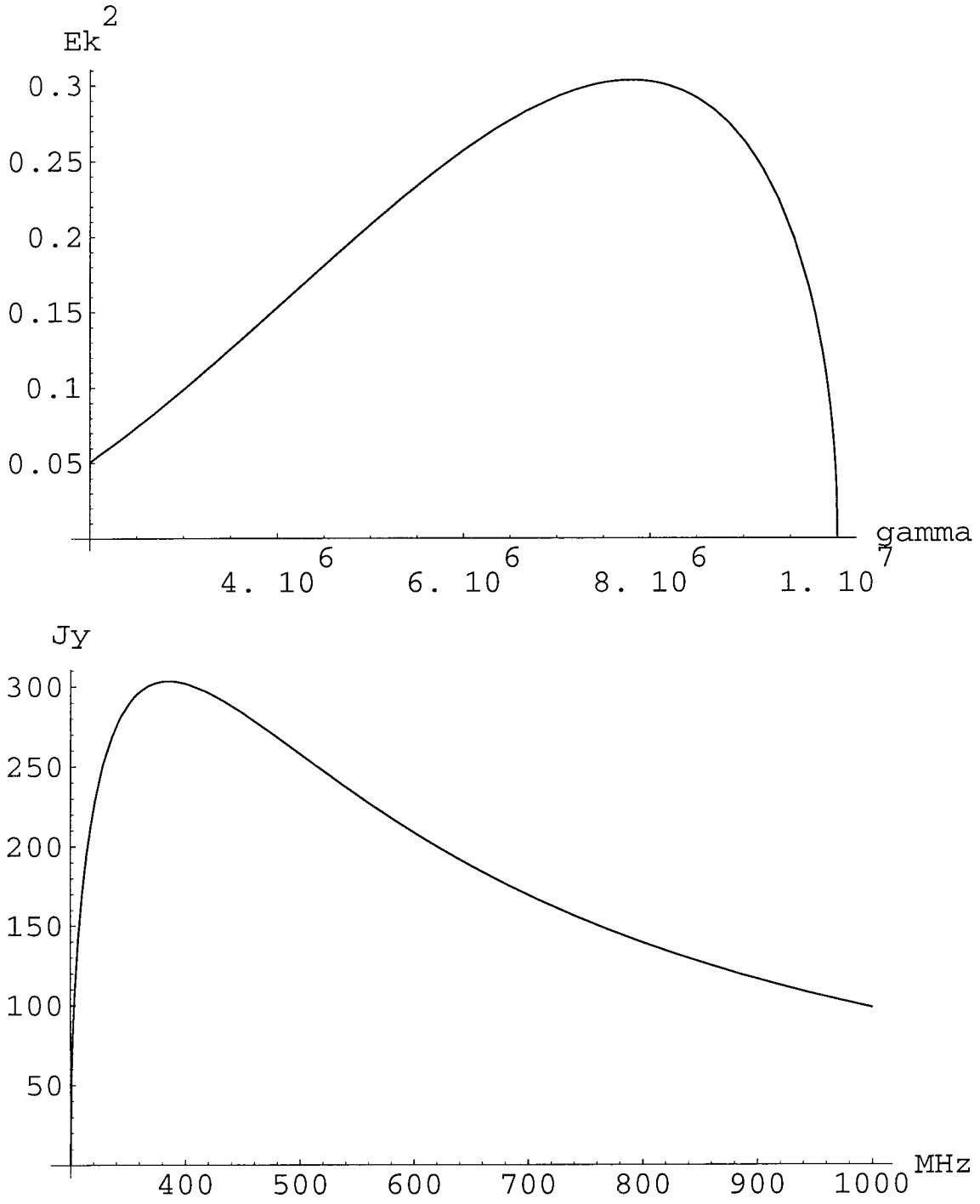

Figure 9.2: Asymptotic one-dimensional energy density in the waves in the γ-space (arbitrary units), and the predicted observed flux.

$E^2(\mathbf{k})$	E_k^2	$n(\mathbf{k})$	$n(k)$	$\alpha,\ \beta$	$D_{\psi\psi}$	$D_{\psi p}$	D_{pp}	D	A	$f(p)p^2dp,\ f(\gamma)d\gamma$
erg	$\frac{\text{erg}}{\text{cm}^2}$	1	$\frac{1}{cm^2}$	$\frac{\text{erg}}{\text{cm}}$	$\frac{1}{\text{sec}}$	$\frac{\text{erg}}{\text{cm}}$	$\frac{\text{erg}^2\,\text{sec}}{\text{cm}^2}$	$\frac{\text{cm}^2}{\text{erg sec}}$	cm	1

Table 9.1: Dimension of the main used quantities

particle is decelerated by the radiation reaction force, which eventually reduces the parallel velocity to subliminous values.

We can also estimate the energy flux (9.39) at the Earth. Assuming that distance to the pulsar is $d \approx 1\text{kpc}$, we find

$$F^{obs}(\nu) \approx 300\, Jy \left(\frac{\nu}{400\text{MHz}}\right)^{-2} \tag{9.43}$$

With time, the value of γ_{min} decreases as the particles are slowed down by the radiation reactions force. Since at the given radius, the particles with lower energies resonate with waves having larger frequencies, more energy will be transported to higher frequencies hardening the spectrum. The lower frequency cutoff is determined by the initial energy of the beam. No energy is transported to frequencies lower than

$$\omega_{min} = \frac{\omega_B}{\gamma_b \delta} \tag{9.44}$$

This simple picture, of course, will be modified due the propagation of the flow in the inhomogeneous magnetic field of pulsar magnetosphere.

9.2 Induced Raman Scattering in Pulsar Magnetospheres

In this section it is shown that induced Raman scattering of electromagnetic waves in the strongly magnetized electron-positron plasma of pulsar magnetosphere may be important for wave propagation and as an effective saturation mechanism for instabilities of electromagnetic waves. The frequencies, at which strong Raman scattering occur in the outer parts of magnetosphere, fall into the observed radio band. The typical threshold intensities for the strong Raman scattering are of the order of the observed intensities, implying that pulsar magnetosphere may be optically thick to Raman scattering of electromagnetic waves.

9.2.1 Introduction

We aim to estimate the effects of the induced Raman scattering of the strong electromagnetic wave propagating in pulsar magnetosphere. Effects of the induced Raman scattering in astrophysical setting (in active galactic nuclei) were also investigated by Levinson & Blandford 1995 and Krishan 1997. Induced Raman scattering may be considered as a parametric decay of the initial transverse electromagnetic wave in the another electromagnetic wave and plasma wave. Another type of induced scattering - induced Brillouin scattering, i.e., the decay of the initial transverse electromagnetic wave in the another electromagnetic wave and ion sound is prohibited in electron-positron plasma, since pair plasma does not support low frequency, density perturbing waves (like ion sound wave in electron-ion plasma).

Strong nonlinear coupling occurs when two waves beat together and the sum or difference frequency and wavelength match the frequency and wavelength of the third wave:

$$\omega_3 = \omega_1 + \omega_2$$
$$\mathbf{k}_3 = \mathbf{k}_1 + \mathbf{k}_2 \tag{9.45}$$

In quantum language, these relations may be interpreted as conservation of energy and momentum, respectively. The energy transfer between the modes will be efficient if the energy of the pump wave is strong enough to overcome the damping losses or escape of the generated waves. Thus, the induced Raman scattering is a threshold process: if the intensity of the pump wave exceeds the threshold value, the initial electromagnetic wave starts converting energy into the decay waves decreasing its amplitude exponentially.

Induced Raman scattering may be important in the pulsar environment in two ways. First, it may provide en effective damping of the existing electromagnetic wave, that has been generated by some emission mechanism at the lower altitude in the pulsar magnetosphere, where the resonant conditions for the induced Raman scattering were not satisfied. This may result in a short time

scale variability which is generally observed in pulsar radio emission. Secondly, it may provide an effective saturation mechanism for the growth of the electromagnetic wave provided that the conditions for the wave excitation by some mechanism are satisfied in the region where an effective Raman scattering takes place.

The first possibility, i.e., the scattering of the existent pump wave, is simpler to consider. As a first approximation, we can treat the intensity of the pump wave as a constant. Then the nonlinear equations describing the wave coupling become linear in amplitudes of the decayed waves. The exponentially growing solutions will imply an effective energy transfer out of the pump wave. As the intensities of the decay waves grow, this approximation breaks down in two cases: when the amplitudes of the decay waves become comparable to the pump wave or when the amplitude of the decay waves enter the nonlinear stage and the waves start loosing energy due to some nonlinear process (like particle trapping and acceleration). The net effect of any energy loss by the decay wave is depletion of the original pump wave. For practical estimates, we can neglect the nonlinear stages of evolution (like cyclic energy transfer between the pump and the daughter waves) and assume that if the intensity of the pump wave begins to decrease exponentially in the linear stage, then the wave decays completely.

The second possibility, when the induced Raman scattering provides a nonlinear saturation mechanism, is more complicated, since the intensities of all waves may be of the same order. A considerable simplification in this case may be obtained if the damping of one of the decay modes is very strong or if it leaves the region of the resonant interaction fast enough. Then, after a short period of time (when the intensities of the other weakly damped waves grow considerably) the intensity of this damped mode is much smaller than the intensities of the two other modes and can be neglected.

In what follows we neglect the possible nonlinear stages of the development of Langmuir turbulence (particle trapping or quasilinear diffusion). We also assume that the pump wave is broadband. This is quite different from the conventional laboratory case of a monochromatic laser-plasma interaction. The condition of a broadband pump wave implies that its band width $\Delta\omega$ is much larger than the typical growth rate of the decay instability Γ:

$$\Delta\omega \gg \Gamma \tag{9.46}$$

If this condition is satisfied, then we can use a random phase approximation for the statistical description of the interacting waves. On the other hand, the condition of weak turbulence allows one to calculate the matrix elements of the interaction in the approximation of stationary phases.

The general expression for the third order nonlinear current in plasma in a magnetic field has been written down by Tsytovich & Shvartsburg 1965. An extremely complicated form of the corresponding

expressions makes the general case of Raman scattering very difficult to consider. Several important simplifications can be done when considering induced Raman scattering in the pulsar magnetosphere. First, the superstrong magnetic field allows an expansion of the currents in $1/\omega_B$. Second, in the pair plasma with the same distributions of electrons and positrons, some of the nonlinear currents cancel out since they are proportional to the third power of the electric charge (this cancellation is exact in the unmagnetized electron-positron plasma). The third, less justified approximation that we will make is that all the three interacting waves propagate along magnetic field. This is an important assumption. It allows us to simplify the consideration considerably and to obtain some analytical estimates of the effects of induced Raman scattering.

A short overview of the work on the nonlinear process in the pulsar magnetosphere will be appropriate here. The possible decay processes for the transverse waves and the corresponding references are (t denotes transverse wave, l denotes longitudinal wave and e denotes a charged particle) (i) a decay of a transverse wave into two transverse wave $t \to t' + t''$ (Gedalin & Machabeli 1982), (ii) a decay of a transverse wave into two Langmuir waves $t \to l + l'$ (Gedalin & Machabeli 1983), (iii) a decay of a transverse wave into another transverse and Langmuir wave $t \to t' + l$ (Gedalin & Machabeli 1983) [1], (iv) induced scattering of transverse waves $t + e \to t' + e$ (Blandford & Scharlemann 1976, Sincell & Krolik 1992, Ochelkov & Usov 1983, Wilson 1982). The possible processes for Langmuir waves are (i) a decay of a Langmuir wave into another Langmuir and transverse wave $l \to t + l'$ (Gedalin & Machabeli 1983), (ii) a decay of a Langmuir wave into two transverse waves $l \to t + t'$ (Mikhailovski 1980), (iii) Langmuir wave merger $l + l' \to t$ (Mamradze, Machabeli & Melikidze 1980), (iii) induced scattering of Langmuir waves (Lyubarskii 1993). When treating the nonlinear process involving transverse waves, the matrix elements in above works have been calculated in the drift approximation, when the expansion in parameter $1/\omega_B$ was done in the very beginning ($\omega_B = |q|B/mc$ is the positive nonrelativistic cyclotron frequency, B is magnetic field, m is mass of an electron and c is the speed of light).

9.2.2 Kinematics of Raman Scattering in Pair Plasma

Wave dispersion

We recall that the normal modes of relativistic pair plasma for the case of parallel propagation consist of two transverse waves with the dispersion relation

$$\omega = kc(1 - \delta), \quad \delta = \frac{\omega_p^2 T_p}{\omega_B^2} \tag{9.47}$$

[1] The final answer for the matrix element contains probably an insignificant typographical error.

and a plasma Langmuir wave with a dispersion relation

$$\omega^2 = \frac{2\,\omega_p^2}{T_p} + k^2 c^2 \beta_T^2 \tag{9.48}$$

where in Eq. (9.48) the wave vectors should not be much larger than cross-over point:

$$\omega_o^2 = k_o^2 c^2 = 2\omega_p^2 < \gamma(1+\beta)^2 > \tag{9.49}$$

We have introduced here a plasma frequency in the plasma frame $\omega_p^2 = 2\omega_B \Omega \lambda/\gamma_p$, where Ω is the pulsar rotation angular velocity, λ is the multiplicity factor, γ_p is the Lorentz factor of the plasma frame, $T_p \approx< \gamma >$ is Lorentz invariant temperature of plasma, γ is Lorentz factor of a particle and $\beta_T = \sqrt{T_p^2 - 1}/T_p$ is a characteristic (dimensionless) thermal velocity of particles, β is (dimensionless) velocity. The brackets denote averaging over the distribution function.

At the point $\{\omega_o, k_o\}$ the dispersion curve of plasma waves intersect that of waves in vacuum, so that for $k > k_o$ the plasma waves become subluminous. The necessary requirement for that is that the distribution function falls fast enough at large values of momentum (faster than $1/p^4$) (Lominadze & Mikhailovskii 1978).

In the subluminous region, the plasma wave dispersion relation may be written as

$$\begin{aligned} &\omega = kc - \eta(k - k_o)c, \qquad \text{where} \\ &\eta = 1 - \left(\frac{\partial \epsilon_{zz}}{\partial k}\right) \Big/ \left(\frac{\partial \epsilon_{zz}}{\partial \omega}\right)\Big|_{\omega_o, k_o} = \frac{< \gamma(1+\beta)^2 >}{< \gamma^3(1+\beta)^3 >} \approx \frac{1}{T_p^2} \end{aligned} \tag{9.50}$$

Scattered frequencies

From the resonant conditions

$$\begin{aligned} \omega_3 &= \omega_1 + \omega_2 \\ k_3 &= k_1 + k_2 \end{aligned} \tag{9.51}$$

it follows that the only kinematically allowed Raman scattering process is a back scattering ($k_1 < 0$) of the initial electromagnetic wave (see Fig. 9.3). We find then

$$\begin{aligned} k_3 &= \frac{1}{2c}\left(\frac{\omega_2}{1-\delta} + k_2\, c\right) \\ |k_1| &= \frac{1}{2c}\left(-\frac{\omega_2}{1-\delta} + k_2\, c\right) \end{aligned} \tag{9.52}$$

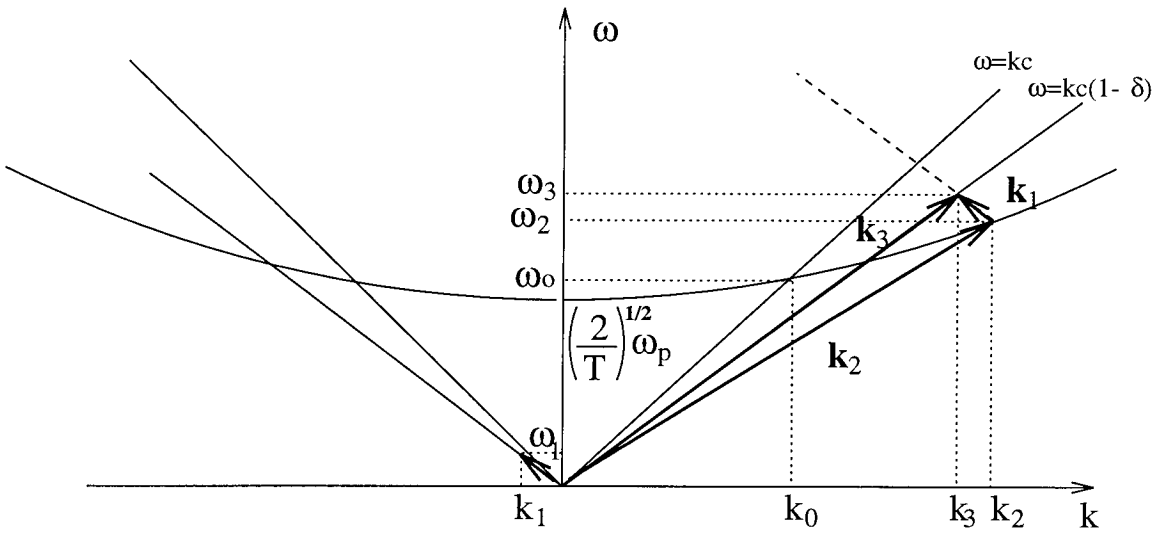

Figure 9.3: Kinematics of backwards Raman scattering in the plasma frame. The vacuum dispersion relation $\omega = kc$, the transverse wave dispersion relations $\omega = kc(1-\delta)$ and the plasma wave dispersion relations (which starts from $\left(\frac{2}{T}\right)^{1/2}\omega_p$) for the parallel propagation are shown. The bold faced vectors represent $\mathbf{k} \equiv \{\omega, k\}$. Cross-over point is given by k_o and ω_o. Only waves with $k > k_t$ can be scattered.

In the region just above the cross-over point $\{\omega_o, k_o\}$, it is possible to use the expansion (9.50) for the dispersion of the plasma waves. The resonant wave vectors are then given by

$$k_3 = \frac{k_2 + k_o}{2}\left(1 - \frac{k_2 - k_o}{4T^2 k_o}\right), \qquad |k_1| = \frac{k_2 - k_o}{2} \tag{9.53}$$

The wave vectors in Eq. (9.53) are limited by $k_2 - k_o \leq k_o$, $|k_1| \leq k_o$.

Induced Raman versus Induced Compton Scattering

Induced Raman scattering is closely related to the induced Compton scattering of waves by the plasma particles. In the conventional treatment of induced Compton scattering in pulsar setting (e.g. Blandford & Scharlemann 1976, Sincell & Krolik 1992), the collective effects of the plasma are ignored. In the case of induced Raman scattering, collective effects play a major role. Raman scattering is a limit of the induced Compton scattering of waves by particles in a medium when the beat wave of the incoming and scattered wave becomes a normal mode of the medium (equivalently, it falls on the "mass surface" of the medium dispersion equation).

In the nonrelativistic plasma the collective treatment of the wave scattering by plasma particles is justified if the following condition is true:

$$\Delta k \lambda_D \ll 1 \tag{9.54}$$

where Δk is the change in the wave number of the scattered wave and λ_D is the Debye length. Condition (9.54) states that the wave number of the oscillations of the electron on the beat of the two scattered waves be much less than the inverse of the Debye length. If condition (9.54) is not satisfied, then the beat wave will either experience a strong Cherenkov damping (if $\Delta k \lambda_D \approx 1$) or the beat wave will not feel the presence of a medium (if $\Delta k \lambda_D \gg 1$), so that the scattering process will be described as induced Compton scattering.

In the relativistic plasma with the characteristic Lorentz factor of the particles $< \gamma > \gg 1$, the condition (9.54) is modified. To find the generalization of condition (9.54) to the case of relativistic plasma, we note that condition (9.54) may be rewritten in terms of the phase velocities of the beat wave $v_{ph} = \omega/k$ (which is a plasma wave in case of Raman scattering) and the thermal velocities of the plasma particles $v_T =< v^2 >^{1/2}$. Condition (9.54) can then be rewritten

$$v_{ph} \gg v_T \tag{9.55}$$

Using (9.50) we find that the phase velocity of the subluminous plasma waves becomes equal to the thermal velocity of plasma particles approximately at $k \approx 2k_o$. Thus, the following condition should hold for the wave-particles scattering in relativistic pair plasma to be considered as a Raman scattering:

$$\Delta k < 2k_o \approx 4\sqrt{2 < \gamma >}\omega_p \tag{9.56}$$

When $\Delta k \approx 2k_o$ the plasma waves are strongly damped and when $\Delta k \gg 2k_o$ the wave-particles scattering is described as single particle Compton scattering. As we will see later (Eq. (9.85)), the condition (9.56) is satisfied in our problem.

9.2.3 Transition Probabilities

First we calculate the matrix elements for the nonlinear three wave interaction in the strongly magnetized electron-positron plasma when all three waves have their wave vectors along the magnetic field. We represent the electric fields of the three interacting waves in the form

$$\mathbf{E}(\mathbf{r},t) = \Re\left[\mathbf{E}_1 \exp\{i(\mathbf{k_1 r} - \omega_1 t)\} + \mathbf{E}_2 \exp\{i(\mathbf{k_2 r} - \omega_2 t)\} + \mathbf{E}_3 \exp\{i(\mathbf{k_3 r} - \omega_3 t)\}\right] \tag{9.57}$$

The indices $1, 2, 3$ refer to the scattered electromagnetic wave, plasma wave and the initial electromagnetic wave respectively. We consider linearly polarized waves. For the parallel propagation the case of circularly polarized waves may be trivially reduced to the scattering of two linearly polarized waves. Implicit assumption here is that the coupling between the waves is weak, so that the waves retain their identity as eigenmodes of the medium during the times much longer than inverse of their frequencies.

We calculate transition probabilities by finding the coupling coefficients for the resonant three-wave interaction. The interaction of two transverse and one longitudinal wave propagating along magnetic field in a relativistic plasma has been considered by Brodin & Stenflo 1989. For the decay process $\omega_3 = \omega_1 + \omega_2$ and $k_3 = k_1 + k_2$, the coupling of the waves is described by the system of equations

$$\begin{aligned}
\frac{dE_1}{dt} &= c_1 E_2^* E_3 \\
\frac{dE_2}{dt} &= c_2 E_1^* E_3 \\
\frac{dE_3}{dt} &= c_3 E_1^* E_3
\end{aligned} \tag{9.58}$$

where

$$\begin{aligned}
c_1 &= -\frac{\omega_1^2}{\left(\frac{\partial \omega^2 \epsilon_\pm^\perp}{\partial \omega}\right)_1} C_\pm \\
c_2 &= -\frac{1}{\left(\frac{\partial \epsilon_{zz}}{\partial \omega}\right)_2} C_\pm \\
c_3 &= \frac{\omega_3^2}{\left(\frac{\partial \omega^2 \epsilon_\pm^\perp}{\partial \omega}\right)_3} C_\pm
\end{aligned} \tag{9.59}$$

and

$$\begin{aligned}
&\epsilon_{zz} = 1 + \sum \frac{\omega_p^2 m}{k} \int \frac{d\mathbf{p}}{\omega - k v_z} \frac{\partial F(\mathbf{p})}{\partial p_z} \\
&\epsilon_\pm^\perp = 1 + \frac{1}{2} \sum \frac{\omega_p^2}{\omega^2} \int \frac{d\mathbf{p}}{\gamma} \left[\frac{(\omega - k v_z) p_\perp}{\omega - k v_z \mp \omega_c} \frac{\partial F(\mathbf{p})}{\partial p_\perp} + \frac{k\, p_\perp^2}{m\gamma(\omega - k v_z \mp \omega_c)} \frac{\partial F(\mathbf{p})}{\partial p_z} \right] \\
&C_\pm = -\sum \frac{\omega_p^2 q}{\omega_1 \omega_2 m} \int d\mathbf{p} \left\{ \frac{m}{\gamma \hat{\omega}_2} \frac{\partial F(\mathbf{p})}{\partial p_z} \right. \\
&\mp \frac{\partial}{\partial p_\perp^2} \left[\frac{\omega_c p_\perp^2}{\gamma^4 \hat{\omega}_2} \left(\frac{k_3}{(\hat{\omega}_1 \mp \omega_c)(\hat{\omega}_3 \mp \omega_c)} - \frac{k_1}{(\hat{\omega}_1 \mp \omega_c)(\hat{\omega}_3 \mp \omega_c)} - \frac{\gamma^2 v_z}{c^2} \frac{\hat{\omega}_1 + \hat{\omega}_3 \mp \omega_c}{\omega_1 \omega_3} \right) \right] F(\mathbf{p}) \\
&- \frac{p_\perp^2}{2\gamma^3 m c^2 \hat{\omega}_2} \left[1 - \frac{k_1 k_3 c^2}{\gamma^2 (\hat{\omega}_1 \mp \omega_c)(\hat{\omega}_3 \mp \omega_c)} - \right. \\
&\left. \left. v_z \left(\frac{k_3}{(\hat{\omega}_3 \mp \omega_c)} + \frac{k_1}{(\hat{\omega}_1 \mp \omega_c)} \mp \frac{\omega_c k_1}{(\hat{\omega}_1 \mp \omega_c)\hat{\omega}_2} \pm \frac{\omega_c k_3}{(\hat{\omega}_3 \mp \omega_c)\hat{\omega}_2} \right) \right] \times \frac{\partial F(\mathbf{p})}{\partial p_z} \right\}
\end{aligned} \tag{9.60}$$

where $\hat{\omega}_{1,2,3} = \omega_{1,2,3} - k_{1,2,3} v_z$ and $\omega_c = qB_0/\gamma mc$ is the relativistic cyclotron frequency.

To facilitate the relation between the notations used in the paper and the physical quantities, in Table 9.2.3 we give the dimensions of some of the quantities used.

We now simplify these relations for the case of one-dimensional pair plasma with the same distribution functions. Setting $F(\mathbf{p}) = \frac{1}{\pi}\delta(p_\perp^2) f(p_z)$ and introducing a positive nonrelativistic gy-

E	c_i	C	$Fd\mathbf{p}$	$u(\mathbf{k}_i)$	$u(k_i)$	$n(\mathbf{k})$	$n(k)$
$\frac{\sqrt{g}}{\sqrt{\text{cm}}\,\text{sec}}$	$\frac{\sqrt{\text{cm}}}{\sqrt{g}}$	$\frac{\sqrt{\text{cm}}\,\text{sec}}{\sqrt{g}}$	1	cm^6/sec	$\frac{\text{cm}^4}{\text{sec}}$	1	$\frac{1}{\text{cm}^2}$

Table 9.2: Dimension of the main used quantities

rofrequency $\omega_B = \sigma_q q B_0/mc$ (σ_q is the sign of the charge), we find

$$\epsilon_{zz} = 1 + \frac{2\omega_p^2}{k}\int \frac{dp_z}{\omega - kv_z}\frac{\partial f(p_z)}{\partial p_z} \tag{9.61}$$

$$\epsilon^{\perp} = 1 - 2\omega_p^2 \int \frac{dp_z}{\gamma}\frac{(\omega - kv_z)^2}{(\omega - kv_z)^2 - \omega_B^2/\gamma^2} f(p_z) \tag{9.62}$$

$$C = -\frac{2\omega_p^2|q|}{\omega_1\omega_3 m}\int \frac{dp_z}{\gamma^5}\frac{\omega_B}{\hat{\omega}_2^2}\left(\frac{k_3\hat{\omega}_1}{\hat{\omega_1}^2 - \omega_B^2/\gamma^2} - \frac{k_1\hat{\omega}_3}{\hat{\omega_3}^2 - \omega_B^2/\gamma^2}\right) f(p_z) \tag{9.63}$$

The probability of the decay is (Melrose 1978c, Eq. 10.124)

$$u(\mathbf{k_3}, \mathbf{k_2}, \mathbf{k_1}) = (2\pi)^5\hbar\frac{R_E^1 R_E^2 R_E^3}{\omega_3\omega_1\omega_2}\left|\omega_1\omega_2\omega_3 C\right|^2 \delta(\mathbf{k_3} - \mathbf{k_2} - \mathbf{k_1})\,\delta(\omega_3 - \omega_2 - \omega_1) =$$
$$\frac{(2\pi)^5\hbar q^2\omega_p^4\omega_B^2\omega_2}{2m^2\omega_1\omega_3}\left|\int \frac{dp_z}{\gamma^5\hat{\omega}_2^2}\left(\frac{k_3\hat{\omega}_1}{\hat{\omega_1}^2 - \omega_B^2/\gamma^2} - \frac{k_1\hat{\omega}_3}{\hat{\omega_3}^2 - \omega_B^2/\gamma^2}\right) f(p_z)\right|^2$$
$$\delta(\mathbf{k_3} - \mathbf{k_2} - \mathbf{k_1})\,\delta(\omega_3 - \omega_2 - \omega_1) \tag{9.64}$$

with $R_E^1 = R_E^2 = R_E^3 = 1/2$

In the cold case we have

$$u(\mathbf{k_3}, \mathbf{k_2}, \mathbf{k_1}) = \frac{(2\pi)^5\hbar q^2\omega_p^4\omega_B^2}{2m^2\omega_1\omega_3\omega_2^3}\left|\frac{k_3\omega_1}{\omega_1^2 - \omega_B^2} - \frac{k_1\omega_3}{\omega_3^2 - \omega_B^2}\right|^2 \delta(\mathbf{k_3} - \mathbf{k_2} - \mathbf{k_1})\,\delta(\omega_3 - \omega_2 - \omega_1) \tag{9.65}$$

which may be obtained from Melrose 1978c, Eq. 10.105.

Equations (9.61) and (9.63) can be simplified in the limit of a very strong magnetic field

$$\epsilon^{\perp} = 1 + \frac{2\omega_p^2}{\omega_B^2}\int dp_z\gamma(\omega - kv_z)^2 f(p_z) \tag{9.66}$$

$$C = \pm\frac{2\omega_p^2|q|}{m}\int \frac{dp_z}{\gamma^3}\frac{1}{\hat{\omega}_2^2\omega_B}\left(\frac{k_3}{\omega_3} - \frac{k_1}{\omega_1}\right) f(p_z) \tag{9.67}$$

Using Eq. (9.61) the Eq. (9.67) may be rewritten in the form

$$C = \pm\frac{2|q|}{m\omega_B}\left(\frac{k_3}{\omega_3} - \frac{k_1}{\omega_1}\right)(\epsilon_{zz} - 1) \tag{9.68}$$

For the back scattering Eq. (9.67) gives

$$C \approx \pm \frac{2|q|k_2}{\omega_{1,3}\omega_B m} (\epsilon_{zz} - 1) \tag{9.69}$$

For the plasma waves on the mass surface $\epsilon_{zz} = 0$ and

$$C = \pm \frac{2|q|k_2}{\omega_{1,3}\omega_B m}$$
$$u(\mathbf{k}_3, \mathbf{k_2}, \mathbf{k}_1) = \frac{2^2 q^2 k_2^2 (2\pi)^5 \hbar}{m^2 \omega_B^2} \omega_2 \delta(\mathbf{k}_3 - \mathbf{k_2} - \mathbf{k}_1)\, \delta(\omega_3 - \omega_2 - \omega_1) \tag{9.70}$$

We can compare this probability with the unmagnetized case (Tsytovich 1970). In the strongly magnetized plasma, the probability of Raman scattering is decreased by a ratio $\omega_{1,3}^2/\omega_B^2$. This is similar to the suppression of the Thompson scattering, whose probability is decreased by the same ratio.

It is convenient to describe the wave distribution in terms of photon occupation numbers

$$n_{\mathbf{k}} = \frac{E_{\mathbf{k}}^2}{\hbar\omega(\mathbf{k})} \tag{9.71}$$

where $E_{\mathbf{k}}^2$ is the spectral energy density, which is related to the total energy density

$$W = \int \frac{d\mathbf{k}}{(2\pi)^3} E_{\mathbf{k}}^2 \tag{9.72}$$

The kinetic equation for the Raman scattering are (Melrose 1978c, Eq. (5.93))

$$\frac{dn_1(\mathbf{k}_1)}{dt} = -\int \frac{d\mathbf{k}_3}{(2\pi)^3} \int \frac{d\mathbf{k}_2}{(2\pi)^3} u(\mathbf{k}_3, \mathbf{k}_1, \mathbf{k}_2) \left(n_1(\mathbf{k}_1) n_2(\mathbf{k}_2) - n_3(\mathbf{k}) \left(n_1(\mathbf{k}_1) + n_2(\mathbf{k}_2)\right)\right)$$
$$+\Gamma_3 n_3(\mathbf{k}_3), \tag{9.73}$$
$$\frac{dn_2(\mathbf{k}_2)}{dt} = -\int \frac{d(\mathbf{k}_1)}{(2\pi)^3} \int \frac{d\mathbf{k}_3}{(2\pi)^3} u(\mathbf{k}_3, \mathbf{k}_1, \mathbf{k}_2) \left(n_1(\mathbf{k}_1) n_2(\mathbf{k}_2) - n_3(\mathbf{k}_3) \left(n_1(\mathbf{k}_1) + n_2(\mathbf{k}_2)\right)\right) +$$
$$\Gamma_2 n_2(\mathbf{k}_2), \tag{9.74}$$
$$\frac{dn_3(\mathbf{k}_3)}{dt} = \int \frac{d(\mathbf{k}_1)}{(2\pi)^3} \int \frac{d\mathbf{k}_2}{(2\pi)^3} u(\mathbf{k}_3, \mathbf{k}_1, \mathbf{k}_2) \left(n_1(\mathbf{k}_1) n_2(\mathbf{k}_2) - n_3(\mathbf{k}_3) \left(n_1(\mathbf{k}_1) + n_2(\mathbf{k}_2)\right)\right) +$$
$$\Gamma_3 n_3(\mathbf{k}_3) \tag{9.75}$$

Where $\Gamma_{1,2,3}$ are the corresponding damping or growth rates. The most unimportant damping is the Landau damping of the plasma waves $n_2(\mathbf{k}_2)$ on the particles of plasma. In (9.75) the total derivative on the left-hand side is

$$\frac{d}{dt} = \frac{\partial}{\partial t} + \frac{\partial \omega}{\partial \mathbf{k}} \frac{\partial}{\partial \mathbf{r}} - \frac{\partial \omega}{\partial \mathbf{r}} \frac{\partial}{\partial \mathbf{k}} \tag{9.76}$$

with the second term describing the convective transport of the waves.

Next we integrate over transverse wave vectors to find the system of equations describing the scattering of the waves propagating along magnetic field

$$\frac{dn_1(k_1)}{dt} = -\int \frac{dk_2}{(2\pi)} \int \frac{dk_3}{(2\pi)} u(k_2,k_1,k_2)\left(n_1(k_1)n_2(k_2) - n_3(k_3)\left(n_1(k_1)+n_2(k_2)\right)\right) + \Gamma_1 n_1(k_1), \tag{9.77}$$

$$\frac{dn_2(k_2)}{dt} = -\int \frac{dk_1}{(2\pi)} \int \frac{dk_3}{(2\pi)} u(k_2,k_1,k_2)\left(n_1(k_1)n_2(k_2) - n_3(k_3)\left(n_1(k_1)+n_2(k_2)\right)\right) + \Gamma_2 n_2(k_2), \tag{9.78}$$

$$\frac{dn_3(k_3)}{dt} = \int \frac{dk_1}{(2\pi)} \int \frac{dk_2}{(2\pi)} u(k_2,k_1,k_2)\left(n_1(k_1)n_2(k_2) - n_3(k_3)\left(n_1(k_1)+n_2(k_2)\right)\right) + \Gamma_3 n_3(k_3) \tag{9.79}$$

where

$$n_i(k_i) = \int \frac{d^2k_{i,\perp}}{(2\pi)^2} n_i(\mathbf{k}_i), \qquad i = 1,2,3 \tag{9.80}$$

and

$$u(k_2,k_1,k_2) = \frac{2^2q^2k_2^2(2\pi)^5\hbar\omega_2}{m^2\omega_B^2}\delta(k_3-k_2-k_1)\,\delta(\omega_3-\omega_2-\omega_1) \tag{9.81}$$

The two δ-functions in $u(k_2,k_1,k_2)$ allow us to perform integrations in (9.79).

$$\frac{dn_1(k_1)}{dt} = -\frac{2^2q^2k_2^2(2\pi)^3\hbar\omega_2}{m^2\omega_B^2\left(\frac{\partial\omega_3}{\partial k_3}\right)}\left(n_1(k_1)n_2(k_2) - n_3(k_3)\left(n_1(k_1)+n_2(k_2)\right)\right) + \Gamma_1 n_1(k_1), \tag{9.82}$$

$$\frac{dn_2(k_2)}{dt} = -\frac{2^2q^2k_2^2(2\pi)^3\hbar\omega_2}{m^2\omega_B^2\left(\frac{\partial\omega_1}{\partial k_1}\right)}\left(n_1(k_1)n_2(k_2) - n_3(k_3)\left(n_1(k_1)+n_2(k_2)\right)\right) + \Gamma_2 n_2(k_2), \tag{9.83}$$

$$\frac{dn_3(k_3)}{dt} = \frac{2^2q^2k_2^2(2\pi)^3\hbar\omega_2}{m^2\omega_B^2\left(\frac{\partial\omega_2}{\partial k_2}\right)}\left(n_1(k_1)n_2(k_2) - n_3(k_3)\left(n_1(k_1)+n_2(k_2)\right)\right) + \Gamma_3 n_3(k_3) \tag{9.84}$$

Implicit assumption in Eqs. (9.82) - (9.84) is the assumption that the wave vectors on the right-hand side of Eqs. (9.82), (9.83) and (9.84) satisfy the resonance conditions. Thus in Eq. (9.82), for example, the two independent variables are time t and wave vector k_1. The explicit relations between wave vectors, corresponding to Eqs. (9.82), (9.83) and (9.84), are

$$\begin{aligned}
&k_3 \approx k_2 = 2T^2|k_1| + k_o, \qquad \omega_2 = (2T^2|k_1| + k_o - 2|k_1|)c \\
&|k_1| = \frac{k_2 - k_o}{2T^2}, \qquad k_3 \approx k_2, \qquad \omega_2 = (k_2 - \frac{k_2-k_o}{T^2})c \\
&|k_1| \approx \frac{k_3 - k_o}{2T^2}, \qquad k_2 \approx k_3, \qquad \omega_2 = (k_3 - \frac{k_3-k_o}{T^2})c
\end{aligned} \tag{9.85}$$

respectively for Eqs. (9.82), (9.83) and (9.84). The quantity $k_o = \sqrt{2T}\omega_p$ is the cross-over wave vector, where the dispersion relation for the plasma waves intersect the vacuum dispersion relation.

From Eqs. (9.85) and (9.56) we find that the induced Raman scattering occurs in the frequency region

$$\sqrt{2T}\omega_p \leq kc \leq 2\sqrt{2T}\omega_p \tag{9.86}$$

This frequency window (in the plasma frame) corresponds to the frequencies in the pulsar frame in the range $2\sqrt{T\lambda\omega_B\Omega/\gamma_p} \leq kc \leq 4\sqrt{T\lambda\omega_B\Omega/\gamma_p}$, which is $5 \times 10^8 \mathrm{rad\,sec}^{-1} \leq kc \leq 10^9 \mathrm{rad\,sec}^{-1}$ which falls into the observed frequency range.

9.2.4 Application to Pulsars

In this section we consider the possible applications of the induced Raman scattering to the wave propagation and spectrum formation in the pulsar magnetospheres.

Scattering of the Pump Wave

There is threshold intensity of the pump wave that defines what is known as strong induced Raman scattering. The rate of induced plasmon production, which depends on the intensity of the pump wave, should exceed the rate of loss due to the various damping processes. The end result of such strong scattering is a total depletion of the initial pump wave. The critical one-dimensional photon density is determined from (9.83)

$$\int \frac{dk_1}{2\pi} \int \frac{dk_3}{2\pi} u(k_3, k_1, k_2) n_3(k_3) = \Gamma_2 \tag{9.87}$$

Linear Landau damping rate in the relativistic plasma ($T_p \gg 1$) is (Lyutikov 1997c, Chapter 7)

$$\Gamma_2 = \frac{\pi\omega_p^4}{Tkc\omega^2} \left(\gamma^3 \frac{\partial f}{\partial \gamma}\right)_{res} \tag{9.88}$$

with

$$\gamma_{res}^2 = \frac{k_0 T_p^2}{\Delta k}, \qquad k_0 c = \omega_0 = \sqrt{2T_p}\omega_p, \qquad \Delta k = k - k_0 \tag{9.89}$$

The equations are valid for $\Delta k \leq k_0$.

With a power law distribution function $f \propto \gamma^{-\alpha}$, $\alpha > 2$, we find

$$\Gamma_2 \approx \frac{\pi\omega_p}{T_p^{3/2}} \left(\frac{k_0 T_p^2}{\Delta k}\right)^{-\alpha/2+1} \tag{9.90}$$

As $\Delta k \to 0$ $\Gamma_2 \to 0$.

The threshold spectrum of the incoming radiation is then given by

$$n_3 \approx \frac{m^2 c^3 T^{-\frac{2+5\alpha}{4}}}{64\pi^2 \hbar q^2} \frac{\omega_B^2}{\omega_p^2} \left(\frac{\Delta k c}{\omega_p}\right)^{-1+\alpha/2} \tag{9.91}$$

Estimating $\Delta k \approx k_o$ we find the characteristic threshold photon density:

$$n_3^{th} \approx 10^{-2} \frac{m^2 c^3 \omega_B^2}{q^2 \hbar \omega_p^2} T^{-1-\alpha} = 2.7 \times 10^{22} \ \frac{1}{cm^2} \ B_{12} \, \lambda_5^{-1} \, P_{0.2} \, T_{10}^{-3} \, R_9^{-3} \gamma_{p,10} \tag{9.92}$$

where $B_{12} = B/10^{12}\mathrm{G}\, \lambda_5 = \lambda/10^5 \, P_{0.2} = P/0.2\mathrm{sec}\, T_{10} = T/10 \, R_9 = R/10^9\mathrm{cm}\, \gamma_{p,10} = \gamma_p/10$ and we used $\alpha = 2$. Note that this is an *upper* bound on the threshold photon density (for $k \approx 2k_o$). At the lower frequencies $k \approx k_o$ the threshold values are much lower.

While for the relativistic Gaussian-type distribution $f \propto 1/T \times \exp\{-\gamma/T\}$ the damping rate is

$$\Gamma_2 \approx \left(\frac{\omega_p}{\Delta k c}\right)^{3/2} \frac{\omega_p}{T^{3/4}} \exp\left\{-\left(\frac{2\omega_p^2 T}{\Delta k^2 \, c^2}\right)^{1/4}\right\} \tag{9.93}$$

(compare with Lominadze & Mikhailovskii 1978 Eq. (2.10)), and the spectrum of the incoming radiation is then given by

$$n_3 \approx \frac{m^2 c^3 \omega_B^2}{128\pi^2 q^2 \hbar T^{9/4} \omega_p^2} \left(\frac{\Delta k c}{\omega_p}\right)^{-3/2} \exp\left\{-\left(\frac{2\omega_p^2 T}{\Delta k^2 \, c^2}\right)^{1/4}\right\} \tag{9.94}$$

The characteristic threshold photon density is in this case

$$n_3^{th} \approx 10^{-4} \frac{m^2 c^3 \omega_B^2}{q^2 T^3 \hbar \omega_p^2} = 5 \times 10^{-5} \frac{m^2 c^3 \omega_B \gamma_p}{q^2 T^3 \hbar \Omega \lambda} = 2.7 \times 10^{20} \ \frac{1}{cm^2} \ B_{12} \, \lambda_5^{-1} \, P_{0.2} \, T_{10}^{-3} \, R_9^{-3} \gamma_{p,10} \tag{9.95}$$

(upper bound) where we used $\omega_p^2 = 2\omega_B \Omega \lambda / \gamma_p$.

For the comparable values of the temperature, i.e., for the similar dispersion of the energies of the plasma particles, the threshold in the case of a power law distribution is much larger than in the case of Maxwell-type distribution. This is due to the larger damping rate in the case of a power law distribution since there are more particles satisfying the Cherenkov resonance in this case than in the case of Maxwell-type distribution.

The estimates (9.92) and (9.95) are done for the one-dimensional photon distribution function (in $\mathbf{k}$) in the plasma frame. The photon distributions (9.92) and (9.95) are the one-dimensional distributions.

The energy flux per unit interval of frequencies is given in terms of a one-dimensional photon

distribution function as follows:

$$F(\nu)d\nu = \frac{n(\mathbf{k},\mathbf{r})c\hbar\omega d\mathbf{k}}{8\pi^3} = \frac{n(k,\mathbf{r})c\hbar\omega dk}{2\pi} = n(k,\mathbf{r})\hbar\omega d\nu \tag{9.96}$$

Where we took into account that the dispersion relation of the electromagnetic waves is almost vacuum like, so $k \approx \omega/c$.

We recall next that both three dimensional occupation numbers (which is basically three dimensional photon distribution function) $n(\mathbf{k},\mathbf{r})$ and one-dimensional photon distribution $n(k,\mathbf{r})$ (Eq. (9.80)) are relativistic invariants. It follows from Eq. (9.96) that

$$\frac{F(\nu)}{\nu} = \text{inv} \tag{9.97}$$

We note that relation (9.97) for the case of one-dimension differs from the three dimensional relation $F(\nu)/\nu^2 = \text{inv}$.

Thus, the flux in the observer frame is

$$F'(\nu') = 2\pi n(k',\mathbf{r})\hbar\nu' \text{ in erg cm}^{-2}\,\text{sec}^{-1}\,\text{Hz}^{-1} \tag{9.98}$$

We can estimate the observed flux (in Jankys) at the Earth:

$$F^{\text{obs}}(\nu') = F'(\nu')\left(\frac{R}{d_E}\right)^2 \tag{9.99}$$

where d_E is distance from the pulsar to the Earth. Using Eqs. (9.92), (9.95), (9.98) and (9.99), we find

$$F^{\text{obs}} = \begin{cases} \frac{10^{-2}}{T^{1+\alpha}} \\ \\ \frac{10^{-4}}{T^3} \end{cases} \times \frac{\pi m^2 c^3 \omega_B^* \gamma_p \nu}{q^2 \Omega \lambda}\left(\frac{R_{NS}}{d_E}\right)^2\left(\frac{R_{NS}}{R}\right) \tag{9.100}$$

for the power law and exponential distributions correspondingly.

Numerical estimates give

$$F^{\text{obs}} = \begin{cases} 30 \\ 3\times 10^{-1} \end{cases} \text{ Jy} \tag{9.101}$$

These are comparable with the fluxes observed from bright pulsars. Since the estimated threshold intensities are upper bounds, we conclude that stimulated Raman scattering may be an important factor in the formation of pulsar radio emission. Estimates for the millisecond pulsars give about an order of magnitude lower values.

The above calculations show that the radio waves propagating in the pulsar magnetosphere may be subject to strong stimulated Raman scattering. The characteristic time for the intensity variations

may be estimated from Eqs. (9.90) and (9.93) to be $t \geq 1/\omega_p$. This can account for the very fast intensity variations observed in pulsar radio emission.

Saturation of Cyclotron Instability by the Induced Raman Scattering

We assumed that the product electromagnetic waves (labeled by index 1) leave the region of resonant interaction, so we can assume that their photon densities are $n_1(k_1) \approx 0$. We are interested in the time asymptotic limit for the intensities of the transverse waves, excited by some instability mechanism with a growth rate Γ_3. Neglecting the wave convection we then find from Eqs. (9.82) and (9.84):

$$\frac{2^2 q^2 k_2^2 (2\pi)^3 \hbar\omega_2}{m^2 \omega_B^2 \left(\frac{\partial\omega_1}{\partial k_1}\right)} n_3(k_3) + \Gamma_2 n_2(k_2) = 0, \tag{9.102}$$

$$-\frac{2^2 q^2 k_2^2 (2\pi)^3 \hbar\omega_2}{m^2 \omega_B^2 \left(\frac{\partial\omega_2}{\partial k_2}\right)} n_2(k_2) + \Gamma_3 n_3(k_3) = 0 \tag{9.103}$$

Comparing Eqs. (9.87) and (9.102) we find that they are identical: the threshold intensity for the strong Raman scattering is equal to the saturation intensity. This is not a surprising fact, since in both cases it is the damping of the plasma waves that controls the electromagnetic wave intensity. In Section 9.2.4 we found that the corresponding intensities are comparable to the observed ones, so that the nonlinear saturation by the induced Raman scattering may provide observed emissivities.

We also note in this context, that at a given radius, the induced Raman scattering operates in a limited frequency range (9.56). So, if the instability that produces radio emission is intrinsically broad band (with the bandwidth of the growing mode larger than the range in which the induced Raman scattering operates), then the effects of the induced Raman scattering would produce a dip in the spectrum, corresponding to that frequency range. If, on the other hand, the instability that produces radio emission is intrinsically narrow band with the central frequency of the instability falling into the operational range of the induced Raman scattering and changing with radius to mimic the observed broadband spectrum, then the induced Raman scattering can be an effective saturation mechanism for a larger range of frequencies.

9.3 Wave Escape from Pulsar Magnetosphere

In this section we consider wave propagation and absorption in the strongly magnetized one-dimensional relativistic electron-positron plasma of a pulsar magnetosphere. Absorption coefficients at the Cherenkov, Cherenkov-drift and cyclotron resonances are calculated. We find that (i) Alfvén waves are subject to strong damping at all these resonances, (ii) high frequency ordinary and extraordinary modes may be damped on the cyclotron resonance, though circular polarization, observed in some pulsars, points to the possibility of escape of the transverse waves if they become detached from plasma due to the sharp density decrease. Both ordinary and extraordinary modes with the electric field perpendicular to the osculating plane of the curved magnetic field line may be strongly damped on the Cherenkov-drift resonance. The observed frequencies of the pulsar radio emission are then determined by the conditions of wave excitation and absorption. The spectral break observed in some pulsars may be due to the cyclotron absorption in the outer parts of pulsar magnetosphere.

In spite of a large number of works which considered wave generation and propagation in pulsar magnetosphere (Tsytovich & Kaplan 1972, Volokitin, Krasnosel'skikh & Machabeli, Arons & Barnard 1986, Barnard & Arons 1986, Lyutikov 1997a), the problem of the wave escape has not yet been resolved. The problem is complicated by the poorly constrained distribution function of plasma particles, unknown structure of the magnetic field close to the light cylinder, and the fact that there is no generally accepted theory of pulsar radio emission generation. In this work we address the possible mechanisms of the resonant absorption for the waves propagating in pulsar magnetosphere.

Previously, the wave absorption in the pulsar magnetosphere has been considered by Barnard & Arons 1986 and Mikhailovskii et al. 1982. Barnard & Arons 1986 have shown that Alfvén waves with the phase velocities not very close to the speed of light (this corresponds to small wave vectors and small frequencies) are subject to strong damping at the Cherenkov resonance as they propagate outward in the pulsar magnetosphere. At the small frequencies, where Alfvén waves are almost transverse, their resonant interactions with particles at the Cherenkov resonance (Eq. (9.104) with $s = 0\,, u_d = 0$) is ineffective, since the electric field of the waves is almost perpendicular to the particle's velocity. Mikhailovskii et al. 1982 considered damping of the high frequency electromagnetic waves at the cyclotron resonance. They concluded that the extraordinary and ordinary modes are subject to strong damping on the cyclotron resonance in the outer parts of the pulsar magnetosphere.

We analyze possible resonant absorption process (Cherenkov, cyclotron and Cherenkov-drift) on all the possible wave modes propagating in one-dimensional strongly magnetized plasma (Alfvén, ordinary and extraordinary). For the propagation of the coupled ordinary-Alfvén modes, Barnard & Arons 1986 considered the case of infinitely strong magnetic field. In this limit the high frequency ordinary mode is always superluminous and cannot interact with particles at the Cherenkov-type

resonance (with $s \leq 0$ in (9.104)). If the effects of the finite magnetic field are taken into account, the ordinary mode becomes subluminous for large frequencies and can be both excited and damped in a Cherenkov-type resonant interaction with particles.

Besides considering wave absorption at the Cherenkov resonance and cyclotron resonances we also take into account wave absorption at the Cherenkov-drift resonance (Eq. (9.104) with $s = 0$ and finite u_d). Resonant interaction of particles with *electromagnetic* waves at the Cherenkov-drift resonance may also be an important mechanism for the pulsar radio emission generation (Kazbegi et al. 1991b, Lyutikov & Machabeli 1997). We find that the subluminous waves with electromagnetic components may be subject to strong damping at the Cherenkov-drift resonance. This may be an important process for all the waves. This is the only mechanism for the absorption of the low frequency Alfvén waves. It may also result in the absorption of the extraordinary and ordinary waves at the frequencies well below the cyclotron absorption frequency.

Cherenkov-drift interaction is made possible by the curvature of the magnetic field lines. When this is taken into account, a particle propagating along the magnetic field also drifts with a velocity perpendicular to the plane of the curved field line allowing for the interaction with the electric field of the wave polarized in the direction of the particle's drift. This is a distinctive feature of a Cherenkov-drift interaction: it affects only the electric field of the wave which is perpendicular to the osculating plane of the curved magnetic field.

9.3.1 Resonant Wave-Particle Interaction

We recall, that in a curved magnetic field, with the radius of curvature much larger than any other length scale, the resonant interaction of waves and particles occurs at the resonances

$$\omega(\mathbf{k}) - k_\phi v_\phi - k_x u_d - \frac{s\omega_B}{\gamma} = 0 \tag{9.104}$$

We will distinguish the following separate cases:

(i) Cherenkov resonance ($s = 0\,, u_d = 0$),

(ii) Cherenkov-drift resonance ($s = 0\,, u_d \neq 0$),

(iii) Normal cyclotron resonance ($s > 0$),

(iv) Anomalous cyclotron-Cherenkov resonance ($s < 0$).

As we will see later, in pulsar magnetosphere drift is not important for the cyclotron-type resonance, so we did not distinguish between cyclotron resonances with and without drift.

For the resonant interaction between a particle and a wave to occur another condition (besides resonance (9.104)) should be met: there must be a nonzero component of the electric field of the wave along the particle velocity. Consequently, Cherenkov resonance (i) acts only on component of the electric field parallel to the external magnetic field. Since in the pair plasma with the same

distribution of electrons and positrons the extraordinary mode has an electric vector perpendicular to the magnetic field, it cannot be excited by the pure Cherenkov resonance (i). In contrast, when the drift of the resonant particles is taken into account, the Cherenkov-drift resonance (ii) couples the particle's velocity along the x axis to the x component of the electric field of the wave. This allows for the excitation of the transverse waves which have a nonzero x component of the electric field.

By the nature of the transition currents, the cyclotron resonance (iii) and (iv) always couples to the parts of the electric field perpendicular to the external magnetic field. It is possible to show (Lyutikov 1997b), that for the one-dimensional distribution the normal cyclotron resonance (iii) contributes to damping of the waves, while the anomalous cyclotron-Cherenkov resonance (iv) contributes to the excitation of the waves.

It is convenient to consider the resonant interaction of particles and waves on the $\omega - \mathbf{k}$ diagram. In this approach the resonance between the normal mode of the medium and a particle is seen as an intersection of the wave's dispersion curve $\omega = \omega(\mathbf{k})$ with the "particle's dispersion curve" $\omega = k_\phi v_\phi - k_x u_d + \frac{s\omega_B}{\gamma}$. We adopted this method from the hydrodynamic theory of wave interaction. We find it also useful to look at the kinetic regimes of particle interaction as well. We will use this method to illustrate the resonant interactions occurring in pulsar magnetospheric plasma.

In this section we concentrate on the wave absorption. We omit the anomalous cyclotron-Cherenkov resonance (iv) which, in one-dimensional plasma, contributes to the wave excitation only. The normal cyclotron resonance (iii) in our case always contributes to wave damping, while the net effect Cherenkov-type resonances (i) and (ii) depend on the sign of the derivative of the distribution function $\frac{\partial f_\alpha(p_\parallel)}{\partial p_\parallel}$ evaluated at the resonance $p_\parallel$. The waves are growing for $\frac{\partial f_\alpha(p_\parallel)}{\partial p_\parallel} > 0$ and are damped for the reversed sign.

We suppose that the normal modes of the medium are emitted somewhere in the pulsar magnetosphere. In that region the emission conditions for the waves excitation are assumed to hold. We are interested in the behavior of the waves as they propagate outward in the pulsar magnetosphere. We will restrict ourselves in this paper to the linear effects in wave amplitude. The nonlinear propagation effects have been considered elsewhere (Gedalin & Machabeli 1983, Machabeli 1983).

As the waves propagate outward in the pulsar magnetosphere, their dispersion will change. We assume that this change is adiabatic. For the linear waves this assumption is satisfied if the wave length is much smaller than the typical size of the inhomogeneity and if the inverse of the frequency of the waves is much smaller than the typical time scale for the change in the parameters of the plasma. For the inhomogeneity size of the order of the radius of curvature and time scale for the change in the parameters equal to the pulsar period, the adiabatic approximation is well satisfied. We also note here that the adiabatic approximation may break down near the points on the $\omega - bfk$ diagram where two dispersion curves approach each other. In a pair plasma dispersion curves of the

ordinary and Alfvén waves do approach each other for the quasi-parallel propagation near the point $\omega \approx kc = \sqrt{2}T\omega_p$. An effective wave transformation can occur near this point.

The slow change in the parameters of the plasma changes the phase speed of the waves and bring them into resonance with the particles satisfying the damping conditions for the particular wave. If the dispersion of a wave is written in the form $\omega = \omega(\mathbf{k}, \mathbf{r})$, then its evolution is described by the following equations:

$$d\omega = \frac{\partial\omega(\mathbf{k},\mathbf{r},t)}{\partial\mathbf{r}}d\mathbf{r} + \frac{\partial\omega(\mathbf{k},\mathbf{r},t)}{\partial\mathbf{k}}d\mathbf{k} + \frac{\partial\omega(\mathbf{k},\mathbf{r},t)}{\partial t}dt \tag{9.105}$$

We can find the evolution of the phase speed for the plasma normal modes. This can be done exactly for X mode and in the asymptotic limits of $kc \ll \sqrt{T_p}\omega_p$ and $kc \gg \sqrt{T_p}\omega_p$ for Alfvén and O modes. Using dispersion relations (5.74) and the radius dependence of the parameters (4.9) we find

$$\begin{aligned}
\frac{\partial v_X^{ph}}{\partial R} &= -\frac{3{v_X^{ph}}^3\omega_p^2 T_p}{\omega_B^2 R} < 0 \\
\frac{\partial v_O^{ph}}{\partial R} &= -\frac{3{v_O^{ph}}^3\omega_p^2 T_p}{\omega_B^2 R}\left(\frac{c^2\,k^2\cos^2\theta + {\omega_B}^2\sin^2\theta}{\omega^2\,R} - \frac{\left(c^2\,k^2 + {\omega_B}^2\right)\,\sin(2\,\theta)}{3\,\omega^2\,R_B}\right) \\
\frac{\partial v_A^{ph}}{\partial R} &= -\frac{v_A^{ph}}{2}\,\frac{6\,{\omega_p}^2}{{\omega_B}^2\,R} + \frac{2\,\tan\theta}{R_B} + \frac{c^2\,k^2\,\left(4\,R + 3\,R_B\,\sin(2\,\theta)\right)\,\tan\theta}{4\,{\omega_p}^2\,R\,R_B} < 0
\end{aligned} \tag{9.106}$$

which implies that the phase speed of the extraordinary mode is always decreasing as the waves propagate out in the pulsar magnetosphere. We also note that this statement will be also valid in a nondipole geometry as long as the quantity $\frac{\omega_p}{\omega_B}$ increases with radius.

The phase speed of the ordinary mode decreases if the angle of propagation is smaller than some critical angle $\theta = \frac{3\,\omega^2\,R_B}{2\,{\omega_B}^2\,R} \approx \frac{\omega^2}{\omega_B^2}$ and increases for larger angles. In the curved magnetic field even if the ordinary mode originally was propagating along magnetic field, it will develop an increasing angle, so that eventually its phase speed will start to increase and the wave will become superluminous. Thus if the ordinary mode is emitted it may leave the pulsar magnetosphere unabsorbed. The phase speed of the Alfvén mode is always decreasing as it propagates outward in a pulsar magnetosphere. As we will see in Section 9.3.2, this will result in the absorption of the Alfvén mode.

We now proceed to consider in detail the various absorption processes.

9.3.2 Absorption at the Cherenkov Resonance (i)

The resonance conditions for the interaction of waves with particles have been solved in Lyutikov 1997c. It has been shown than the resonant interaction of the Alfvén or ordinary wave with a particle depends on the parameter

$$\mu_h = \frac{2\gamma_{res}\sqrt{T_p}\omega_p}{\omega_B} \tag{9.107}$$

where it was assumed that $\gamma_{res} \gg 1$.

This criteria come from the fact that the maximum phase speed of the Alfvén wave and the minimal phase speed of the ordinary wave are equal to the Alfvén speed $v_a = c(1-\delta)$. Since the effective dispersion of the particle in the Cherenkov resonance $\omega = v_{res} k \cos\theta$, Alfvén wave can Cherenkov resonate with a particle if $\mu_h < 1$ and ordinary wave can Cherenkov resonate with a particle if $\mu_h > 1$ (see Fig. 9.4).

The absorption at the Cherenkov resonance occurs on the falling part of the distribution function. The corresponding particle velocities range from 0 to v_T. For relativistically hot plasma $v_T \approx \left(1 - 1/(2T_p^2)\right) c$. For the particles of the bulk plasma with the γ-factors in the pulsar frame of the order of γ_p the drift is not important and we can consider conventional Cherenkov resonance (i).

Alfvén Wave

We first note that the high frequency part of the Alfvén branch $\omega > \sqrt{T_p}\omega_p$ is always strongly damped on the bulk particles. There is also a possibility that the intermediate $\omega \leq \sqrt{T_p}\omega_p$ Alfvén waves are damped on the Cherenkov resonance. The low frequency Alfvén waves are not strongly affected by the Cherenkov resonance since at $\omega \ll \sqrt{T_p}\omega_p$ Alfvén waves are quasi-transverse.

In the plasma frame the absorbing particles of the bulk plasma have velocities in the range from $-v_T$ to v_T. All the forward propagating Alfvén waves with the phase velocity less than v_T will lose the component of the electric field along the external magnetic field.

Using the parameter μ_h with $\gamma_{res} = \gamma_t$ we find that the parallel component of the electric field of Alfvén waves will be strongly damped at all wave length if

$$\frac{2\sqrt{T_p}\,\gamma_t \omega_p}{\omega_B} = 2\sqrt{2T_p}\,\gamma_t \sqrt{\frac{\lambda}{\gamma_p}}\sqrt{\frac{\Omega}{\omega_B}} = 2\times 10^{-3}\left(\sqrt{\frac{T_p}{10}}\right)^{3/2}\left(\frac{\gamma_t}{10^4}\right)\left(\frac{R}{R_{NS}}\right)^{3/2} > 1 \qquad (9.108)$$

which suggests that Alfvén wave propagating in the outer region of pulsar magnetosphere $R \geq 50 R_{NS}$ are subject to the strong damping on the Cherenkov resonance (i). The damping rate for the Cherenkov absorption of the Alfvén wave is given in Table I. Estimating the typical frequency of the Alfvén waves in the plasma frame $\omega \approx \sqrt{T_p}\omega_p$, $\partial f/\partial\gamma \approx f/\gamma$ and $\theta \approx 1$ we find

$$\Gamma \approx \frac{\lambda_{res}\omega_{GJ}\gamma_{res}^2}{\sqrt{T_p\lambda}} \qquad (9.109)$$

The condition of the strong absorption, $c/\Gamma' < R_{lc}$, for the damping of Alfvén waves on the Cherenkov resonance may be written as

$$\frac{\lambda_{res}\gamma_{res}^2}{\sqrt{T_p\lambda\gamma_p}}\sqrt{\frac{\omega_B}{\Omega}} > 1 \qquad (9.110)$$

We would like to stress that condition (9.108) corresponds to the strong Cherenkov damping of the parallel component of Alfvén waves with any frequency. The low frequency Alfvén waves propagating along magnetic field are less subject to Cherenkov damping since they have the highest phase speed. It has been show in Section 9.3.2 that as the Alfvén wave propagates in a curved magnetic field its phase speed always decreases. For larger angles of propagation the potential part of the electric field also increases. This will result in a strong absorption of all Alfvén waves.

Ordinary Wave

The lowest phase speed of the ordinary wave is equal to Alfvén velocity v_a and if the thermal velocity of the plasma particles is much less than the Alfvén velocity, then the ordinary mode will not interact at the Cherenkov resonance with the particles. In the pulsar plasma the Alfvén velocity is very close to the speed of light and the thermal velocities of the particles may, at best, be comparable to it but not much larger.[2] The Cherenkov interaction of the ordinary wave with resonant particles is very sensitive to the angle of propagation. For oblique propagation, the lower phase speed part of the ordinary wave, which is most likely to be damped at the Cherenkov resonance, is quasi-transverse and, thus, almost unaffected by the Cherenkov interaction, which acts on the longitudinal part of the electric field of the wave.

The damping rate of the ordinary wave due to the Cherenkov interaction with the particles of the plasma is given in Table I. The resonant frequency in this expression has been found by Lyutikov 1997c. The Cherenkov resonance on the ordinary mode with $\mu_h \geq 1$, but not much larger, happens at

$$\omega_{res} = \begin{cases} \frac{\sqrt{2T_p}\gamma_{res}\omega_p\theta}{\sqrt{\mu_h^2-1}} & \theta \ll 1/\gamma_b \\ \omega_B\,\theta\frac{\mu_h^2+2}{\mu_h^2} & \theta \gg 1/\gamma_b \end{cases} \tag{9.111}$$

For the quasi-parallel propagation we estimate $\mu_h^2 - 1 \approx 1$. Then for $\frac{\partial f}{\partial \gamma} \approx \frac{f}{\gamma}$ we find a damping rate of the ordinary wave due to the Cherenkov interaction with the particles of the plasma:

$$\Gamma = \lambda_{res}\gamma_{res}\theta\sqrt{\frac{\Omega\omega_B}{\lambda T_p\gamma_p}}, \qquad \theta \ll 1/\gamma_{res} \tag{9.112}$$

with the γ_{res} given by the condition $\mu_h \approx 1$:

$$\gamma_{res} \approx \frac{\omega_B}{\sqrt{\gamma_t}\omega_p} \approx \sqrt{\frac{\omega_B}{\gamma_t\lambda\Omega}} = 1.2\times 10^4\left(\frac{R}{10^9\mathrm{cm}}\right)^{(-2/3)} \tag{9.113}$$

This is a very large energy for the particles in the plasma frame. The number of particles satisfying this condition is of the order of the Golreich-Julien density or less, so $\lambda_{res} \approx 1$.

[2] When comparing the velocities close to the speed of light, we compare the corresponding γ-factors $v/c \approx 1 - \frac{1}{2\gamma^2}$, thus the statement $v_1 \gg v_2$ implies $\gamma_1 \gg \gamma_2$.

Using these estimates we find that the ordinary wave is not subject to the strong damping at Cherenkov resonance (i).

9.3.3 Absorption at the Cherenkov-drift Resonance (ii)

The Cherenkov-drift resonance (ii) is important for the particles from the tail of plasma distribution and for the primary beam particles. The Cherenkov-drift excitation may be an important mechanism for the generation of pulsar radio emission (Chugunov & Shaposhnikov 1981, Lyutikov & Machabeli 1997). An important factor in the Cherenkov-drift resonance is that a resonant particle couples to the component of the electric field along the drift velocity, i.e., perpendicular to the local field lines. So that, unlike conventional Cherenkov resonance (i), Cherenkov-drift resonance (ii) affects *transverse* waves.

Since the Cherenkov-drift resonance requires a very high parallel momentum, the resonant interaction will occur on the high phase velocity waves. This implies that this resonance is always important for the extraordinary mode, while for ordinary and Alfvén modes it is important only for small angles of propagation. It is more convenient to consider the Cherenkov-drift resonance in the pulsar frame, which we will use in this section. The values in the pulsar frame will be denoted by primes. Representing the wave dispersion as

$$\omega = k' c(1-\delta'), \qquad \text{where } \delta' = \begin{cases} \frac{\omega_p'^2 T_p}{4\gamma_p^3 \omega_B^2} & \text{X mode} \\ \frac{\omega_p'^2 T_p}{4\gamma_p^3 \omega_B^2} + \frac{\gamma_p \omega_p'^2 T_p \sin^2\theta'}{k'^2 c^2} & \text{O mode} \\ \frac{\omega_p'^2 T_p}{4\gamma_p^3 \omega_B^2} - \frac{k'^2 c^2 \sin^2\theta'}{4\gamma_p \omega_p'^2 T_p} & \text{Alfvén mode} \end{cases} \tag{9.114}$$

The resonance condition (9.104) may then be written as ($s = 0$)

$$\frac{1}{2\gamma_{res}'^2} - \delta' + \frac{1}{2}\left(\psi'\right)^2 + \frac{1}{2}\left(\theta' - u_d'\right)^2 = 0 \tag{9.115}$$

where we used $v_{res} = c\left(1 - \frac{1}{2\gamma_{res}'^2} - \frac{1}{2}u_d'^2\right)$ and $\psi' = \frac{k_r'}{k_\phi'}$

An important feature of Eq. (9.115) is that it is independent of frequency. It can be simultaneously satisfied for the waves with very different phase speeds. The angular dependence of the Eq. (9.115) makes a distinction between the resonant particles with different velocities. The particles with larger velocities have a larger drift and resonate with the waves propagating at larger angles.

Cherenkov-drift resonance (ii) is important if $u_d' > \sqrt{2\delta'}$. If this condition is satisfied, then the resonant Cherenkov-drift interaction occurs for the angles $\psi' < \sqrt{2\delta'}$ and $|\theta' - u_d'| < \sqrt{2\delta'}$ (see Fig. 6.3).

Resonances	Extraordinary wave	Ordinary wave	Alfven wave
		$\omega \geq \sqrt{T_p}\omega_p$	$\omega \leq \sqrt{T_p}\omega_p$
Cherenkov (i) $(s=0,\ u_d=0)$	$\Gamma = 0$	$\Gamma = \frac{\pi}{2}\frac{\omega_{p,res}^2\gamma_{res}^3}{\omega}\sin^2\theta\left(\frac{\partial f}{\partial\gamma}\right)_{\gamma=\gamma_{res}}\quad \theta, < \frac{\omega}{\omega_B}$ $\Gamma = 0, \quad \theta > \frac{\omega}{\omega_B}$ $\omega \gg \sqrt{2T_p}\omega_p$, if $\frac{\gamma_{res}T_p\omega_p}{\omega_B} \geq 1$ $\omega \approx \sqrt{2T_p\omega_p^2 + \omega_B^2\theta^2}$, if $\frac{\gamma_{res}T_p\omega_p}{\omega_B} \gg 1$	$\Gamma = \frac{\pi}{2}\frac{\omega_{p,res}^2\gamma_{res}^3}{\omega}\sin^2\theta\left(\frac{\partial f}{\partial\gamma}\right)_{\gamma=\gamma_{res}}$ $\omega \approx \frac{\sqrt{2T_p}\omega_p}{1+\theta\gamma_{res}}$
Cherenkov-drift (ii) $(s=0,\ u_d \neq 0)$	$\Gamma = \frac{2\omega_{p,res}^2\delta}{\omega}\left(\frac{\gamma^3}{1+u_d^2\gamma^2/c^2}\frac{\partial f(\gamma)}{\partial\gamma}\right)_{\gamma=\gamma_{res}}$	$\Gamma = \frac{2\omega_{p,res}^2\delta}{\omega}\left(\frac{\gamma^3}{1+u_d^2\gamma^2/c^2}\frac{\partial f(\gamma)}{\partial\gamma}\right)_{\gamma=\gamma_{res}}$	$\Gamma = \frac{2\omega_{p,res}^2\delta}{\omega}\left(\frac{\gamma^3}{1+u_d^2\gamma^2/c^2}\frac{\partial f(\gamma)}{\partial\gamma}\right)_{\gamma=\gamma_{res}}$
Cyclotron (iii) $(s>0,\ v_{\phi,res}<0)$	$\Gamma = -\frac{\pi}{2}\frac{\omega_{p,res}^2}{\Delta\gamma\omega}$ $\omega \geq \frac{\omega_B}{2\gamma_{res}}$	$\Gamma = -\frac{\pi}{2}\frac{\omega_{p,res}^2}{\Delta\gamma\omega}$ $\omega \geq \frac{\omega_B}{2\gamma_{res}}$	$\Gamma = \frac{\pi}{2}\frac{\omega_{p,res}^2}{\Delta\gamma\omega}$ $\omega \geq \frac{\omega_B}{2\gamma_{res}}$
Cyclotron-Cherenkov (iv) $(s<0,\ v_{\phi,res}>0)$	$\Gamma = \frac{\pi}{2}\frac{\omega_{p,res}^2}{\Delta\gamma\omega}\quad \theta < \frac{\omega}{\omega_B}$ $\Gamma = 0 \quad \theta > \frac{\omega}{\omega_B}$ $\omega \approx \frac{\omega_B}{\gamma_{res}\delta}$	$\Gamma = \frac{\pi}{2}\frac{\omega_{p,res}^2}{\Delta\gamma\omega}\quad \theta < \frac{\omega}{\omega_B}$ $\Gamma = 0 \quad \theta > \frac{\omega}{\omega_B}$ $\omega \approx \frac{\omega_B}{\gamma_{res}\delta}$	$\Gamma = \frac{\pi}{2}\frac{\omega_{p,res}^2}{\Delta\gamma\omega}$ $\omega \approx \sqrt{2T_p\omega_p^2 + \omega_B^2\theta^2}$, if $\frac{\gamma_{res}\omega_p}{T_p^{3/2}\omega_B} > 0$

Table 9.3: Growth rates and corresponding resonant frequencies of waves in the kinetic approximation. All values in the table refer to the plasma frame. Negative growth rates correspond to wave absorption. The notations are the following: $\omega_{p,res}$ - plasma frequency of the resonant particles, $\Delta\gamma$ - scatter in Lorentz factor of the resonant particles.

The Cherenkov-drift absorption for the waves with $\psi' \approx 0$ and $\theta' \approx u'_d$ happens at

$$\gamma'_{res} = \frac{1}{\sqrt{2\delta'}} = \frac{\omega_B \gamma_p^{3/2}}{2\sqrt{2}\omega'_p\sqrt{T_p}} \approx 200 \left(\frac{R}{10^9 \text{ cm}}\right)^{3/2} \tag{9.116}$$

The resonance (9.116) is satisfied for the particles from the tail of plasma distribution. Since the distribution of the tail particles is of a "falling" type, the waves, or more precisely, the transverse components of the electric field of the waves, will be damped. The Cherenkov-drift resonance (ii) will result in a damping of ordinary, extraordinary and Alfvén modes with the electric field in the x direction. The waves with the electric field in the r direction will be unaffected.

The growth rate of the Cherenkov-drift absorption is given in Table I. Estimating the characteristic wave frequency in the pulsar frame as $\omega \sim \gamma_p\sqrt{T_p}\omega_p$ the condition of the strong absorption, $c/\Gamma' < R_{lc}$ may be written as

$$\frac{\lambda_t}{\gamma_t\sqrt{T_p\lambda\gamma_p}}\sqrt{\frac{\omega_B}{\Omega}} > 1 \tag{9.117}$$

where $\lambda_t = n_t/n_{GJ}$ is the multiplicity of the tail particles and we assumed that the scatter in energies of the tail particles is $\gamma_T \approx \gamma_t$.

The numerical estimates show that the left-hand side of Eq. (9.117) is of the order of unity for the assumed pulsar parameter. This implies that the Cherenkov-drift absorption may be important for the transverse waves.

An important feature of the Cherenkov-drift resonance is that emission on the primary beam particles and absorption on the tail particles can occur in the same region. Since the primary beam particles have larger energy and larger drift velocities, the waves will be emitted at larger angles and may not be absorbed on the resonance with the tail particles. As the waves propagate in the pulsar magnetosphere, the angle of propagation of the wave with respect to the local magnetic field is likely to increase and the waves will not be absorbed by the Cherenkov-drift resonance.

Thus we have shown that the Cherenkov-drift damping of the transverse electromagnetic waves on the tail particles may be important. The affected waves have a polarization perpendicular to the plane of the curved field line. It is not clear how strong this effect is. The answer to this question depends on the details of the geometry of the emission and absorption regions and on the parameters of the outflowing plasma.

9.3.4 Absorption at the Cyclotron Resonance (iii)

As we mentioned earlier, the drift velocity is unimportant for the cyclotron resonance (iii). With the drift velocity set to 0, the resonance condition in the plasma frame reads

$$1 - sign_v - \delta + sign_v\left(\frac{1}{2\gamma_{res}^2} + \frac{\theta^2}{2}\right) = \frac{s\omega_B}{kc\gamma_{res}} \tag{9.118}$$

where we introduced $sign_v = \frac{v_\phi}{|v_\phi|}$ - a sign of the particle's velocity ($sign_v = 1$ for the forward propagation), and omitted the angle ψ. The case of emission ($s < 0$) has been treated elsewhere (Machabeli & Usov 1979, Kazbegi et al. 1991b). For absorption we set $s = 1$.

From (9.118) it follows that the normal cyclotron resonance can be satisfied only if $sign_v = -1$, i.e.,on the particles streaming backwards in the plasma reference frame. All the subluminous waves with the frequency larger than

$$\omega_{min,pl} \approx \frac{\omega_B}{2T_p} \tag{9.119}$$

(in the plasma frame) will be subject to cyclotron damping.

In the pulsar frame this will correspond to the minimum frequency of

$$\omega_{min} = 2\gamma_p \omega_{min,pl} = \frac{\omega_B \gamma_p}{T_p} \approx \omega_B \tag{9.120}$$

The damping rate for the cyclotron absorption is given in Table 1. The condition for strong absorption, $c/\Gamma' < R_{lc}$, implies that for $\omega = \frac{\gamma_p \omega_B}{T_p}$ (see also Mikhailovskii et al. 1982) the waves are strongly damped if

$$\gamma_p < \lambda, \tag{9.121}$$

a condition well satisfied in the pulsar magnetosphere.

We note that the minimal frequency (9.120) at the light cylinder is $\omega_B(R = R_{lc}) = 1.4 \times 10^9$ rad sec^{-1}. This means that the waves in the typical observed window may be strongly damped. We also point out that the frequency (9.120) corresponds approximately to the frequency of the spectral break observed in some pulsars (Malofeev 1996). This break may be related to the cyclotron absorption. For almost orthogonal rotators the waves propagating at a small angle to the rotational axis may reach cyclotron absorption within the dipole magnetosphere regions. Consequently, the larger range of frequencies will be absorbed. Such pulsars (e.g., Geminga) may be observed only at low frequencies (Melikidze 1997).

The statement that the waves with frequency larger than (9.120) are strongly damped on the cyclotron resonance (iii) is based on the assumption that the dipolar geometry extends up to the light cylinder. In a real pulsar the distortion of the field lines at the light cylinder must be considerable. This may change the estimated lower frequency considerably. For example, if at some point the density of the plasma falls down considerably, the wave may get detached from plasma, become a vacuum wave and evade the cyclotron absorption. A convenient way to describe the adiabatic evolution of plasma waves is by using CMA diagrams (see Figs 5.4 and 5.5). As the wave propagates in magnetosphere, the density and magnetic field change, so that the location of the wave on the CMA diagram traces some phase curve. In order to become a vacuum wave, a particular plasma mode has to reach a line $n = 0$. If in the process of evolution this phase curve crosses a resonance,

the wave is absorbed. So that in order to become a vacuum wave the phase curve should not go through a resonance. It is clear from Figs. 5.4 and 5.5 that Alfvén wave cannot become a vacuum wave: its phase curve cannot reach the line $n = 0$ without crossing the resonance line. Ordinary and extraordinary waves, on the other hand, can become vacuum waves if the density falls fast enough.

We believe that there is observational evidence that, at some point in the magnetosphere, the transverse modes detach from plasma, thus escaping the absorption. The possible location for the location of the point where the density of the plasma drops down considerably is where the magnetic field lines cease to be dipole. The argument that lead us to the assumption that the waves detach from plasma at some point is the following. If the average streaming energies of the plasma components are different, then the transverse electromagnetic waves propagating along the field lines have circular polarization and the waves propagating with the angle to the magnetic field larger than some critical angle have linear polarization. As the waves, emitted along the field line with the circular polarization, propagate in curved magnetic field lines, they develop a finite angle the field and star splitting into the orthogonal linearlly polarized modes. The fact that we do see circular polarization in the core emission implies that the waves got detached from plasma before they acquired an angle to the magnetic field larger that the critical angle at which the polarization changes from circular to linear.

Summarizing the absorption processes in the strongly magnetized, electron-positron plasma of pulsar magnetosphere, we note that the waves may be strongly damped on the three possible resonances: Cherenkov, Cherenkov-drift and cyclotron. The conclusions are the following. Alfvén wave is always strongly damped on the Cherenkov resonances and possibly on the Cherenkov-drift resonance and cannot leave magnetosphere. Both ordinary and extraordinary waves may be damped on the Cherenkov-drift resonance. In this case Cherenkov-drift resonance affects only the ordinary and extraordinary waves with the electric field perpendicular to the plane of the curved magnetic field line. The high frequency parts of the extraordinary and ordinary wave may also be damped on the cyclotron resonances, but the observed circular polarization in the pulsar radio emission implies that the extraordinary and ordinary waves get detached from plasma, escaping absorption. In this case two orthogonal linear polarizations will be observed.

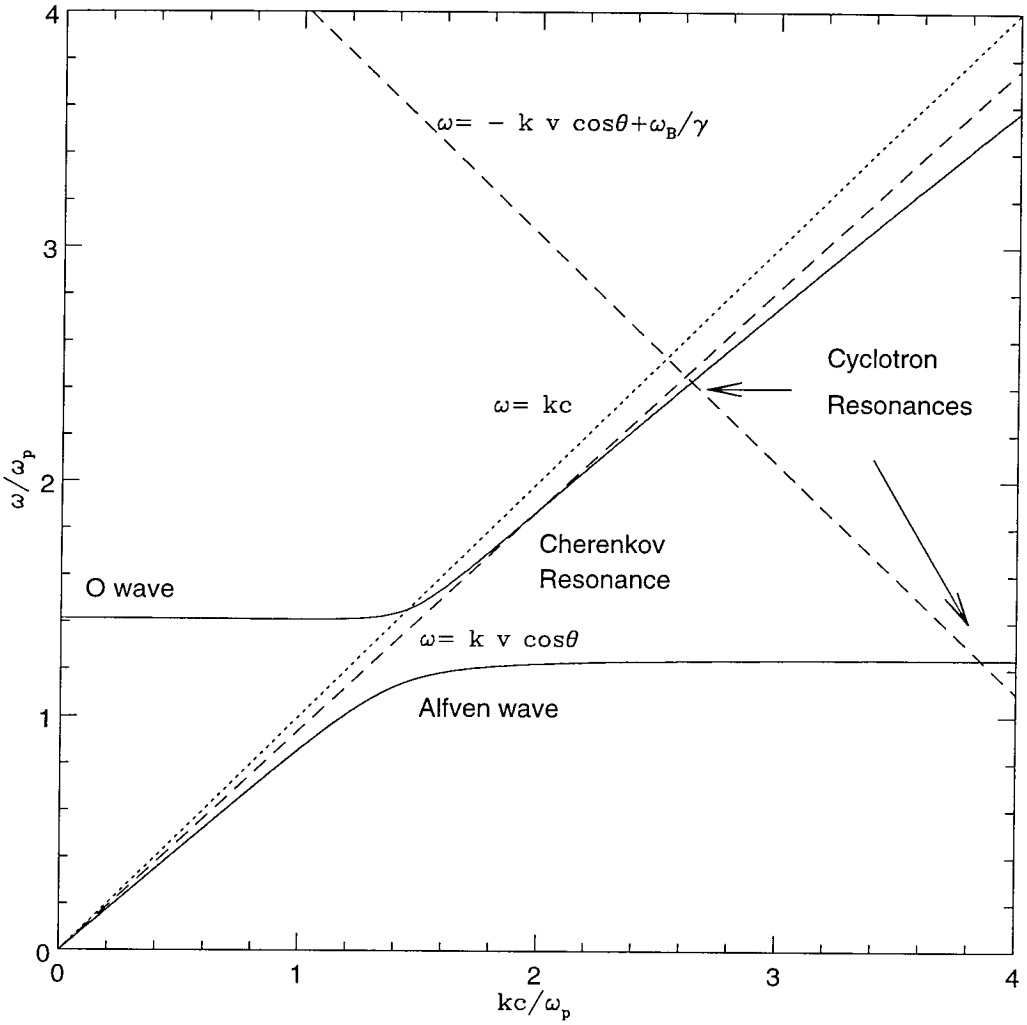

Figure 9.4: Absorption resonances on the Alfvén and Ordinary modes in the cold plasma for for $\mu > 1$. For the Cherenkov absorption the damping region is below the Cherenkov resonance line $\omega = kv\cos\theta$. For the cyclotron absorption the damping region above the cyclotron resonance line $\omega = -kv\cos\theta + \omega_B/\gamma$. For $\mu < 1$ Cherenkov resonance curve does not intersect the dispersion relation for the ordinary mode. In that case the ordinary mode is not damped on the Cherenkov resonance.

Chapter 10 Future Directions

Послушайте!
Ведь если звезды зажигают -
Значит - это кому-нибудь нужно?
Значит - кто-то хочет, чтобы они были?
Значит - кто-то называет эти плевочки
жемчужиной?

В.В. Маяковский

Listen!
You know - if they light up the stars -
That means - somebody needs them?
It means - someone wants them to be there?
It means - someone calls that spit
pearls?

V.V. Mayakovsky

In this thesis I have considered two possible pulsar emission mechanisms based on the cyclotron-Cherenkov and Cherenkov-drift instabilities. I have argued that kinetic type instabilities on electromagnetic waves are more likely candidates for the pulsar radio emission mechanism than electrostatic instabilities and have shown that the cyclotron-Cherenkov emission at the anomalous Doppler effect can account for the various observed phenomena of the core-type emission and the Cherenkov-drift emission is a likely candidate for the cone-type emission.

An important requirement of this model is that the emission is generated in the outer magnetosphere at a considerable fraction of a light cylinder radius. This is in contrast to the conventional presumption which is based upon the association of the pulse width with the angle subtended by the open field lines. In the model discussed here, the instability region is determined by the curvature of magnetic fields, which limits it to the field lines with low curvature. At this moment it is not possible to determine decisively the location and the size of the emitting regions, but interstellar scintillation observations, similar to those of (Gwinn et al. 1997), are very promising.

Another direction of research that can produce important observational evidence is the implementation of "coherent dedispersion" algorithm (e.g., Jenet et al. 1997), which allows very high

temporal or frequency resolution. Using this technique it may be possible to distinguish between "antenna" and "maser" emission mechanisms. Fine frequency structure in the fundamental emission is more likely to be found in the maser process. Unfortunately, various propagation effects in the pulsar magnetosphere and in the interstellar medium can imitate both spectral and temporal structure, complicating the interpretations.

Both cyclotron-Cherenkov and Cherenkov-drift instabilities produce characteristic polarization patterns, which can serve as tests for this model of pulsar radio emission. If the cyclotron-Cherenkov instability develops on both the primary beam and on the tail of the plasma distribution, then the effect of the switched senses of the circular polarization should be more prominent at high frequencies. A striking feature of the Cherenkov-drift instability is that it produces electromagnetic waves polarized perpendicular to the plane of the curved magnetic field line. This is orthogonal to the pattern predicted by the theories of radio emission that involve curvature emission. If, at some point, it will be possible to determine independently the relative orientation of the pulsar magnetic field and electric field in the wave, then this distinctive feature of the Cherenkov-drift instability may be used to test our model. One possibility is to assume a dipole geometry and determine the absolute position of the neutron star spin axis. However, the assumption of a dipole geometry may not be correct in the outer parts of magnetosphere, where torsion and bending of the field lines may be important.

Studies of millisecond pulsars can also provide insight into the physics of radio emission. One of the predictions of our model, though predicated on the details of the distribution function of plasma particles, is that cyclotron-Cherenkov instability does not develop in the millisecond pulsars. This implies that the amount of circular polarization observed in millisecond pulsars should be much less that in the normal pulsars.

One of the most important aspects of the pulsar emission theory, that was almost omitted in this thesis, is the relation of radiation emission to the high frequency (optical, UV, X and γ) emission. Timing observations in different spectral windows show that in some pulsars (the Crab pulsar, for example) the high frequency emission is coincident with the radio emission, which may imply that they are coming from the same location. We should note in this context that the most successful contemporary models of γ-ray emission locate the emission region in the outer magnetosphere (e.g., Romani 1996).

Turning to the theory, we note that we are still handicapped by our inability to find the global solution for the electrodynamical structure of a pulsar magnetosphere. This is a formidable problem, but probably within reach giving the growing computational power of modern computers. A serious limitation of our theory is that it is based on the *ad hoc* assumptions on the distribution function, rather than computed selfconsistently. Further development of the theory should incorporate, probably numerically, the more realistic (e.g., Arons 1981b) distribution functions for the

plasma particles and primary beam than used here. This may be an important factor for the dispersion of normal modes[1] and for the growth rates of kinetic instabilities. Finally, more detailed work on the nonlinear effects associated with the saturation processes of the cyclotron-Cherenkov and Cherenkov-drift instabilities and with the propagation effects is possible. In this thesis I discussed two possible saturation mechanisms for the cyclotron-Cherenkov instability - quasilinear diffusion and induced Raman scattering. For the induced Raman scattering I considered only a simpler case of a parallel propagation of the interacting waves. The case of oblique propagation, as well as other nonlinear processes, like wave decay and induce scattering, deserve a closer attention.

In this thesis I have presented a model for the pulsar emission that involves the application of the fundamental plasma physics concepts to the new environment of pulsar magnetospheres. The model has some striking and potentially testable observational consequences. It is hoped that even if it is contradicted by observations, the principles elucidated in this thesis will have a more general applicability and will strive to solve the long-standing puzzle of "how pulsars work."

[1]See, for example, comments on page 51 on the dependence of the plasma wave dispersion on the distribution function.

Appendix A Electromagnetic Waves in Cylindrical Coordinates

The purpose of this Appendix is to consider wave-particle interaction of the vacuum normal mode in cylindrical coordinates. As noted in Section 5.1, in the curvilinear coordinates, the electric induction is related to electric field through dielectric tensor *operator*, which involves derivatives of the electric field. This is different from the case of Cartesian coordinates, when the relation between electric field and electric induction involves algebraic relations. In this Appendix we first discuss the structure of vector waves in vacuum and in a homogeneous dielectric medium and find the conditions, when the simplifying WKB approximation may be used for wave-particle interaction in vacuum.

A.1 Vacuum Normal Modes

We expand the fundamental solutions of wave equation

$$\mathbf{curl}\,\mathbf{curl}\,\mathbf{E} - \frac{\omega^2}{c^2}\mathbf{E} = 0 \tag{A.1}$$

in terms of Fourier amplitudes

$$\mathbf{E}(\mathbf{r},t) = \sum_{\nu=-\infty}^{\nu=\infty} \int d\omega \int \frac{dk_x}{2\pi}\mathbf{E}(r,k_x,\nu,\omega)\exp\left\{-i(\omega t - \nu\phi - k_x z)\right\} \tag{A.2}$$

The wave equation (A.1) then takes the form

$$\frac{i\nu}{r^2}\frac{\partial}{\partial r}\left(rE_\phi\right) + ik_x\frac{\partial}{\partial r}E_x - \frac{k_x\nu}{r}E_\phi + \left(\frac{\nu^2}{r^2} - \left(\frac{\omega^2}{c^2} - k_x^2\right)\right)E_r = 0 \tag{A.3}$$

$$-\frac{\partial}{\partial r}\left(\frac{1}{r}\frac{\partial}{\partial r}\left(rE_\phi\right)\right) + i\nu\frac{\partial}{\partial r}\left(\frac{E_r}{r}\right) - \frac{k_x\nu}{r}E_x - \left(\frac{\omega^2}{c^2} - k_x^2\right)E_\phi = 0 \tag{A.4}$$

$$-\frac{1}{r}\frac{\partial}{\partial r}\left(r\frac{\partial}{\partial r}E_x\right) + \frac{ik_x}{r}\frac{\partial}{\partial r}\left(rE_r\right) - \left(\frac{\omega^2}{c^2} - \frac{\nu^2}{r^2}\right)E_x = 0 \tag{A.5}$$

Magnetic field is related to the electric field:

$$\mathbf{curl}\,\mathbf{E} = -\frac{1}{c}\frac{\partial\mathbf{B}}{\partial t} = i\frac{\omega}{c}\mathbf{B} \tag{A.6}$$

The amplitudes $\mathbf{E}(r, k_x, \nu, \omega)$, subject to condition of being finite at $r = 0$, are

$$\mathbf{E}^{(lt)}(r, k_x, \nu, \omega) = E^{(lt)} \left(\frac{ik_x}{\lambda} J'_\nu(\lambda r)\mathbf{e_r} - \frac{\nu k_x}{\lambda^2 r} J_\nu(\lambda r)\mathbf{e}_\phi + J_\nu(\lambda r)\mathbf{e_x} \right) \tag{A.7}$$

$$\mathbf{B}^{(lt)}(r, k_x, \nu, \omega) = \frac{\omega}{\lambda^2 c} E^{(lt)} \left(\frac{\nu J_\nu(\lambda r)}{r}\mathbf{e_r} + i\lambda J'_\nu(\lambda r)\,\mathbf{e}_\phi \right) \tag{A.8}$$

$$\mathbf{E}^{(t)}(r, k_x, \nu, \omega) = E^{(t)} \left(\frac{i\nu}{\lambda r} J_\nu(\lambda r)\mathbf{e_r} - J'_\nu(\lambda r)\mathbf{e}_\phi \right) \tag{A.9}$$

$$\mathbf{B}^{(t)}(r, k_x, \nu, \omega) = E^{(t)} \left(\frac{k_x c}{\omega} J'_\nu(\lambda r)\mathbf{e_r} + \frac{ik_x c\nu}{\lambda r \omega} J_\nu(\lambda r)\mathbf{e}_\phi - i\frac{c\lambda}{\omega} J_\nu(\lambda r)\mathbf{e_x} \right) \tag{A.10}$$

where $\lambda = \sqrt{\omega^2/c^2 - k_x^2}$, $J_\nu(\lambda r)$ are Bessel functions and $\mathbf{e_r}, \mathbf{e}_\phi, \mathbf{e_x}$ are unit vectors along the corresponding axes. A dispersion relation in cylindrical coordinates is just an equation for Bessel functions:

$$\frac{1}{r}\frac{1}{\partial r}\left(r\frac{1}{\partial r} J \right) - \left(\frac{\nu^2}{r^2} + k_x^2 - \frac{\omega^2}{c^2} \right) J = 0 \tag{A.11}$$

A.2 Waves in an Isotropic Dielectric

In a dielectric the wave equation is

$$\mathbf{curl}\,\mathbf{curl}\,\mathbf{E} - \frac{\partial^2 \mathbf{D}}{\partial t^2} = 0 \tag{A.12}$$

In an isotropic dispersive medium the relation between the electric induction $\mathbf{D}$ and electric field may be written as

$$\mathbf{D}(\omega) = \epsilon(\omega)\mathbf{E}(\omega) \tag{A.13}$$

From Eqs. (A.2) and (A.13) it follows that in a dielectric the solutions of the wave equation are

$$\mathbf{E}^{(lt)}(r, k_x, \nu, \omega) = E^{(lt)} \left(\frac{ik_x}{\hat{\lambda}^2} J'_\nu(\hat{\lambda} r)\; bfe_r - \frac{\nu k_x}{\hat{\lambda}^2 r} J_\nu(\hat{\lambda} r)\mathbf{e}_\phi + J_\nu(\hat{\lambda} r)\mathbf{e_x} \right) \tag{A.14}$$

$$\mathbf{B}^{(lt)}(r, k_x, \nu, \omega) = \frac{\omega\epsilon}{\hat{\lambda}^2 c} E^{(lt)} \left(\frac{\nu J_\nu(\hat{\lambda} r)}{r}\mathbf{e_r} + iJ'_\nu(\hat{\lambda} r)\,\mathbf{e}_\phi \right) \tag{A.15}$$

$$\mathbf{E}^{(t)}(r, k_x, \nu, \omega) = E^{(t)} \left(\frac{i\nu}{r} J_\nu(\hat{\lambda} r)\mathbf{e_r} - J'_\nu \mathbf{e}_\phi \right) \tag{A.16}$$

$$\mathbf{B}^{(t)}(r, k_x, \nu, \omega) = E^{(t)} \left(\frac{k_x c}{\omega} J'_\nu(\hat{\lambda} r)\mathbf{e_r} + \frac{ik_x \nu}{r\omega} J_\nu(\hat{\lambda} r)\mathbf{e}_\phi - i\frac{c\hat{\lambda}^2}{\omega} J_\nu(\hat{\lambda} r)\mathbf{e_x} \right) \tag{A.17}$$

where $\hat{\lambda} = \sqrt{\omega^2/c^2\epsilon - k_x^2}$.

A.2.1 Short Radial Wave Length Expansion of Vacuum Solutions

For large orders $\nu \gg 1$, argument larger than the order $\lambda r > \nu$ and not very close to it, $\lambda r - \nu \geq \nu$, we can use expansion in tangents of the Bessel functions:

$$J_\nu(\nu \sec\zeta) \approx \sqrt{\frac{2}{\pi\nu\tan\zeta}} \cos\left(\nu(\tan\zeta - \zeta) + \frac{\pi}{4}\right), \qquad \zeta \geq \nu^{-1/2} \tag{A.18}$$

In our case $\cos\zeta = \nu/(\lambda r)$.

Introducing

$$k_r^2 = \lambda^2 - \frac{\nu^2}{r^2}, \qquad k_r^2 + k_\phi^2 + k_x^2 = \frac{\omega^2}{c^2} \tag{A.19}$$

the expansion (A.18) reads

$$J_\nu(\lambda r) \approx \sqrt{\frac{2}{\pi k_r r}} \cos\left(\pm k_r r - \phi_\nu\right) \tag{A.20}$$

The limits of applicability of this expansion is that $k_r r \gg 1$ and ζ is not very small.

The normal modes in this limit are

$$\begin{aligned} \mathbf{E}^{(lt)}(\mathbf{r},t) &\propto e^{-i(\omega t - k_x x \pm k_r r)} \left(-\frac{k_x k_r}{\lambda^2}\mathbf{e}_r - \frac{k_x k_\phi}{\lambda^2}\mathbf{e}_\phi + \mathbf{e}_x\right) \\ \mathbf{E}^{(t)}(\mathbf{r},t) &\propto e^{-i(\omega t - k_x x \pm k_r r)} \left(\frac{k_\phi}{\lambda}\mathbf{e}_r - \frac{k_r}{\lambda}\mathbf{e}_\phi\right) \end{aligned} \tag{A.21}$$

A.3 WKB Solution (Short Radial Wave Length)

We can obtain solutions (A.21) of Eqs. (A.3-A.5) in the WKB limit, when the effective radial wavelength is much shorter than the characteristic scale of the problem.

Assuming that the solutions of Eqs. (A.3-A.5) have a form

$$\mathbf{E} \propto \frac{1}{\sqrt{r}} e^{iS}, \qquad \frac{\partial S}{\partial r} \gg \frac{1}{r} \tag{A.22}$$

we find

$$S = \pm \int dr \sqrt{\lambda^2 - \frac{\nu^2}{r^2}} = \pm\left(k_r r - \nu \arccos\frac{\nu}{\lambda r}\right) \tag{A.23}$$

with k_r defined by Eq. (A.19).

The "potential" term in the Schrödinger-type equation (A.11) has a characteristic scale $r_\nu = \nu/\lambda$. Solutions are exponentially decaying for smaller radii and have a wavelike structure at larger radii. The condition of applicability of the WKB approach is then $k_r r \gg \nu$, where k_r is a typical radial wave number.

The dispersion equation, which is obtained by substituting Eq. (A.22) in Eqs. (A.3-A.5), takes a form

$$\epsilon_{ij}^{(0)} E_i = 0 \tag{A.24}$$

where

$$\epsilon_{ij}^{(0)} = \begin{pmatrix} k_\phi^2 + k_x^2 - \frac{\omega^2}{c^2} & -k_r k_\phi + \frac{ik_\phi}{2r} & -k_x k_r - \frac{ik_x}{2r} \\ -k_r k_\phi - \frac{3ik_\phi}{2r} & k_x^2 + k_r^2 + \frac{3}{4r^2} - \frac{\omega^2}{c^2} & -k_x k_\phi \\ -k_x k_r + \frac{ik_x}{2r} & -k_x k_\phi & k_\phi^2 + k_r^2 - \frac{1}{4r^2} - \frac{\omega^2}{c^2} \end{pmatrix} \tag{A.25}$$

For $k_r \gg 1/r$ we can drop the complex part of the tensor $\epsilon_{ij}^{(0)}$ (which is not even Hermitian since k_r is not Killing vector). The dispersion equation $\det||\epsilon_{ij}^{(0)}|| = 0$ then gives

$$k_r^2 + k_x^2 + k_\phi^2 = \frac{\omega^2}{c^2} \tag{A.26}$$

The WKB method breaks down when the radial wave length becomes comparable to the inhomogeneity scale of the "potential." For a given radius this occurs for

$$\nu \approx \frac{\omega r}{c} \approx \frac{r}{\bar{\lambda}} = 10^8 \tag{A.27}$$

for $r = 10^9$ cm and the wave length $\bar{\lambda} = 10$ cm.

This breakdown of the WKB method may be illustrated graphically. Consider the surfaces of a constant phase of Hankel function $H_\nu^{(1)}$:

$$\phi = \arctan\left(\frac{Y_\nu(\lambda r)}{J_\nu(\lambda r)} + \frac{2\pi l}{\nu}\right), \qquad l = 0, 1, 2, ...\nu - 1 \tag{A.28}$$

(Fig. A.1).

For radii much larger than the "light cylinder" radius, $\lambda r = \nu$, the surface of a constant phase has a form of unwinding spiral with a wave length $\lambda r/\nu$. Near the light cylinder the radial wave length becomes comparable to the light cylinder radius.

From the quantum mechanical point of view, the kinetic energy, given by the derivative term in Eq. (A.11) becomes zero at the light cylinder radius. This is the classical reflection point. For larger radii the kinetic energy is real and positive: the solution of the "Schrödinger equation" (A.11) has a wavelike structure. For smaller radii the kinetic energy is complex: the solution of the "Schrödinger equation" (A.11) has exponentially decaying form, modified by the presence of the reflection point at $r = 0$.

When approaching the classical reflection point, a common approach in quantum mechanics is to use the Airy function approximation to the solutions of the "Schrödinger equation." This corresponds to the transition region in the Bessel function expansion, when relations (A.18) are no longer valid and one should use Airy function expansion. We will discuss the various regimes of the Airy function expansion in Section 6.2.1.

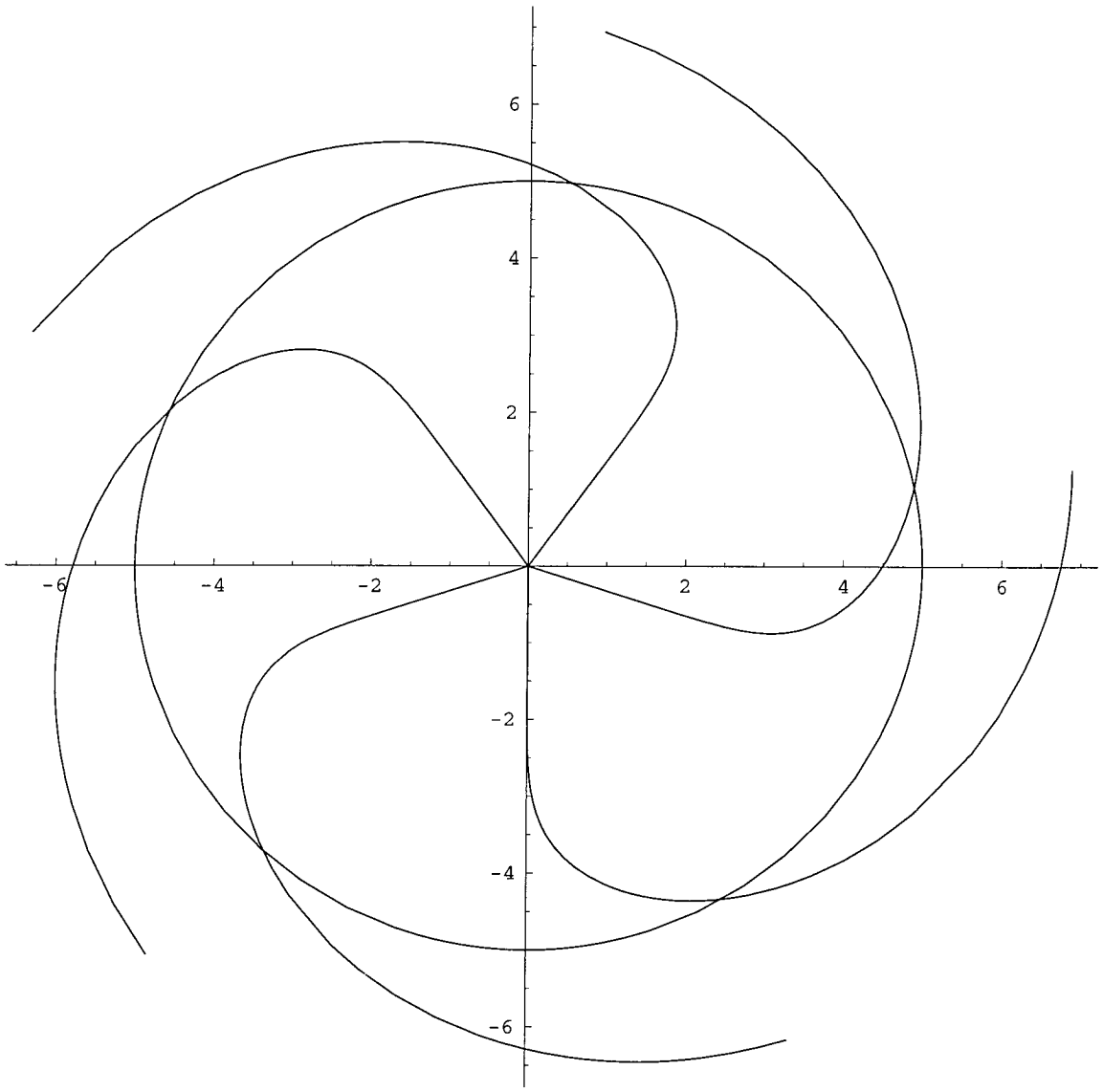

Figure A.1: Surfaces of constant phase of Hankel function $H_\nu^{(1)}$ for $\nu = 5$. Circle $\lambda r = \nu$ is an analog of a light cylinder. For radii much smaller than the light cylinder radius $\lambda r = \nu$ the rotation is similar to solid body rotation, while for the radii much larger than the light cylinder radius the surface of a constant phase has a form of unwinding spiral with a wave length $\lambda r/\nu$.

A.4 Wave-Particle Interaction in Vacuum

A considerable simplification of the wave-particle interaction in cylindrical coordinates is reached when the interaction occurs in the WKB limit, or, equivalently, when we can use the expansion in tangent for the Bessel functions. From Eq. (A.18) we find a lower limit on the azimuthal wave number:

$$\nu \geq (\lambda r)^{2/3} \approx 10^5 \tag{A.29}$$

for the observed wave length 10 cm and the curvature radius 10^9 cm. From Eqs. (A.27) and (A.29) it follows that for a given radius and given wave length cylindrical waves with azimuthal wave numbers in the range $(\lambda r)^{2/3} \leq (\lambda r)$ can be considered in the WKB limit, i.e., in the plane wave approximation.

It is possible to picture graphically the resonant and nonresonant interaction of a particle moving along the circular trajectory. The pattern in Fig. A.1 may be thought of as rotating with a frequency $\lambda c/\nu$. A particle at a given distance r_0 with a given velocity v_ϕ is rotating with an angular frequency $\Omega_\phi = v_\phi/r_0$. A resonant interaction occurs when these two frequencies are equal. In vacuum,

$$r_0 = \nu\beta_\phi\lambda \approx r_\nu\left(1 - \frac{1}{2\gamma^2}\right) \tag{A.30}$$

where $r_\nu = \nu/\lambda$ is the light cylinder radius for the mode ν. So, in vacuum, the resonance between a particle and a wave always happens inside the light cylinder.

Appendix B Field of a Single Particle in Cylindrical Coordinates

In this Appendix we show how conventional formula for the curvature or synchrotron emissivity in vacuum may be obtained in cylindrical coordinates. We calculate the spectral energy flux at infinity due to the particle executing a helical motion. We do this by finding the eigenfunction expansion of the dyadic Green's in cylindrical coordinates.

We wish to find the solutions of the vector wave equation

$$\mathbf{curl}\,\mathbf{curl}\,\mathbf{F} - \frac{\omega^2}{c^2}\mathbf{F} = \mathbf{Q} \tag{B.1}$$

where $\mathbf{F}$ is electric or magnetic field and $\mathbf{Q}$ is a source function. For a single particle source, which is a delta function in coordinates, Eq. (B.1) is an equation for the Green's function. To find Green's function we first have to find the solutions to the homogeneous equation with $\mathbf{Q} = 0$. The solutions to the homogeneous vector wave equation can be obtained from the solution of the scalar wave equation

$$\mathbf{curl}\,\mathbf{curl}\,\Psi - \frac{\omega^2}{c^2}\Psi = 0 \tag{B.2}$$

$$\Psi(\nu, k_x, \omega) = e^{i(\nu\phi + k_x x)} Z_\nu(\lambda r) \tag{B.3}$$

(Z_ν is any Bessel function) using the relations

$$\mathbf{E}^{(t)} = \mathbf{curl}(\mathbf{e}_x\Psi), \qquad \mathbf{E}^{(lt)} = \mathbf{curl}\,\mathbf{curl}\,(\mathbf{e}_x\Psi) \tag{B.4}$$

Functions (B.3) are eigenfunction for the scalar wave equation. The eigenfunction for the vector wave equation are (e.g., Eq. (6.5-6.6) of Tai 1994)

$$\mathbf{L} = \frac{1}{\lambda}\mathbf{grad}\Psi = e^{-i(\omega t - k_x x - \nu\phi)}\left(Z'_\nu \mathbf{e}_r + \frac{i\nu}{\lambda r}Z_\nu \mathbf{e}_\phi + + \frac{ik_x}{\lambda}Z_\nu \mathbf{e}_x\right) \tag{B.5}$$

$$\mathbf{M} = \frac{1}{\lambda}\mathbf{curl}(\mathbf{e}_x\Psi) = e^{-i(\omega t - k_x x - \nu\phi)}\left(i\frac{\nu}{\lambda r}Z_\nu \mathbf{e}_r - Z'_\nu \mathbf{e}_\phi\right) \tag{B.6}$$

$$\mathbf{N} = \frac{c}{\omega\lambda}\mathbf{curl}\,\mathbf{curl}(\mathbf{e}_x\Psi) = \frac{c\lambda}{\omega}e^{-i(\omega t - k_x x - \nu\phi)}\left(i\frac{k_x}{\lambda}Z'_\nu \mathbf{e}_r - \frac{k_x\nu}{\lambda^2 r}Z_\nu \mathbf{e}_\phi + Z_\nu \mathbf{e}_x\right) \tag{B.7}$$

We note that $\mathbf{curl}\mathbf{L} = 0$. $\mathbf{L}$ is an expansion in eigenfunctions of the longitudinal electric field from the point source and $\mathbf{M}$ and $\mathbf{N}$ are expansions in eigenfunctions of the transverse fields.

The orthogonality properties are (Tai 1994)

$$\int d\mathbf{r} \begin{pmatrix} \mathbf{L}^*(r,\lambda',k_x',\nu') \\ \mathbf{M}^*(r,\lambda',k_x',\nu') \\ \mathbf{N}^*(r,\lambda',k_x',\nu') \end{pmatrix} \begin{pmatrix} \mathbf{L}(r,\lambda,k_x,\nu) \\ \mathbf{M}(r,\lambda,k_x,\nu) \\ \mathbf{N}(r,\lambda,k_x,\nu) \end{pmatrix} = 2(1+\delta_{\nu,0})\pi^2 \frac{\delta(\lambda-\lambda')}{\lambda}\delta(k_x-k_x')\delta_{\nu-\nu'} \quad \text{(B.8)}$$

For the particle moving along trajectory $\mathbf{r}_0(t)$, the eigenfunction expansion of the scalar Green's function for the scalar waves equation

$$\mathbf{curl}\,\mathbf{curl}\,\Psi - \frac{\omega^2}{c^2}\Psi = -4\pi \int dt\, e^{i\omega t}\, \frac{\delta(r-r_0(t))}{r}\delta(x-x_0(t))\delta(\phi-\phi_0(t)) \quad \text{(B.9)}$$

is

$$G(r,r_0,\lambda,\nu,k_x) = i\pi\delta(\omega-\nu\Omega_\phi-k_x v_x) \begin{cases} J_\nu(\lambda r)H_\nu^{(1)}(\lambda r_0) & \text{if } r \le r_0 \\ J_\nu(\lambda r_0)H_\nu^{(1)}(\lambda) & \text{if } r \ge r_0 \end{cases} \quad \text{(B.10)}$$

This particular choice of Bessel and Hankel functions insures that the solution is regular at zero and corresponds to the outgoing wave at infinity.

The corresponding dyadic Green's functions for the vector waves equation (B.1) can be found using the relations

$$\mathcal{G}_B(\mathbf{r},\mathbf{r}_0) = \mathbf{curl}\mathcal{I}G(\mathbf{r},\mathbf{r}_0) \quad \text{(B.11)}$$

$$\mathcal{G}_E(\mathbf{r},\mathbf{r}_0) = \left(\mathcal{I} + \frac{\omega^2}{c^2}\nabla\nabla\right) G(\mathbf{r},\mathbf{r}_0) \quad \text{(B.12)}$$

where $\mathcal{I}$ is a unity matrix and $G(\mathbf{r},\mathbf{r}_0)$ is the scalar Green's function.

The eigenfunction expansion of the electric dyadic Green's function is

$$\mathcal{G}_E(r,r_0,\lambda,\nu,k_x) = i\pi(2-\delta_{\nu,0})\delta\left(\omega-k_\phi v_\phi - k_x u_d\right) \left(\mathbf{L}^*(\lambda r)\wedge\mathbf{L}(\lambda r_0) + \mathbf{M}^*(\lambda r)\wedge\mathbf{M}(\lambda r_0) + \mathbf{N}^*(\lambda r)\wedge\mathbf{N}(\lambda r_0) \right) \quad \text{(B.13)}$$

which, using relations (B.12), gives

$$\begin{aligned} \mathcal{G}_E(r,r_0,\lambda,\nu,k_x) &= i\pi(2-\delta_{\nu,0}) \Bigg(\\ &\left(H_\nu^{(1)\prime}(\lambda r)\mathbf{e}_r - \frac{i\nu}{\lambda r}H_\nu^{(1)}(\lambda r)\mathbf{e}_\phi - \frac{ik_x}{\lambda}H_\nu^{(1)}(\lambda r)\mathbf{e}_x\right) \wedge \left(J_\nu'(\lambda r_0)\mathbf{e}_r + \frac{i\nu}{\lambda r_0}J_\nu(\lambda r_0)\mathbf{e}_\phi + \frac{ik_x}{\lambda}J_\nu(\lambda r_0)\mathbf{e}_x\right) \\ &+\frac{c^2\lambda^2}{\omega^2}\left(-i\frac{k_x}{\lambda}H_\nu^{(1)\prime}(\lambda r)\mathbf{e}_r - \frac{k_x\nu}{\lambda^2 r}H_\nu^{(1)}(\lambda r)\mathbf{e}_\phi + H_\nu^{(1)}(\lambda r)\mathbf{e}_x\right) \\ &\quad\wedge\left(i\frac{k_x}{\lambda}J_\nu'(\lambda r_0)\mathbf{e}_r - \frac{k_x\nu}{\lambda^2 r_0}J_\nu(\lambda r_0)\mathbf{e}_\phi + J_\nu(\lambda r_0)\mathbf{e}_x\right) \end{aligned}$$

$$+\left(-i\frac{\nu}{\lambda r}H_\nu^{(1)}(\lambda r)\mathbf{e}_r - H_\nu^{(1)\prime}(\lambda r)\mathbf{e}_\phi\right)\wedge\left(i\frac{\nu}{\lambda r_0}J_\nu(\lambda r_0)\mathbf{e}_r - J_\nu'(\lambda r_0)\mathbf{e}_\phi\right)\quad\Bigg) \tag{B.14}$$

The first term here is just the eigenfunction expansion of the Green's dyadic for the point source.

The magnetic Green's function (the Fourier transform in ϕ, x and t) for the vector wave equation is

$$\mathcal{G}_B(r,r_0,\lambda,\nu,k_x) = i\pi(2-\delta_{\nu,0})\left(\mathbf{N}^*(\lambda r)\wedge\mathbf{M}(\lambda r_0) + \quad \mathbf{M}^*(\lambda r)\wedge\mathbf{N}(\lambda r_0)\right) \tag{B.15}$$

which, using relations (B.12), gives

$$\begin{aligned}\mathcal{G}_B(r,r_0,\lambda,\nu,k_x) &= i\pi(2-\delta_{\nu,0})\frac{c\lambda}{\omega}\Bigg(\\ &\left(-i\frac{\nu}{\lambda r}H_\nu^{(1)}(\lambda r)\mathbf{e}_r - H_\nu^{(1)\prime}(\lambda r)\mathbf{e}_\phi\right)\wedge\left(i\frac{k_x}{\lambda}J_\nu'(\lambda r_0)\mathbf{e}_r - \frac{k_x\nu}{\lambda^2 r_0}J_\nu(\lambda r_0)\mathbf{e}_\phi + J_\nu(\lambda r_0)\mathbf{e}_x\right)\\ &+\left(-i\frac{k_x}{\lambda}H_\nu^{(1)\prime}(\lambda r)\mathbf{e}_r - \frac{k_x\nu}{\lambda^2 r}H_\nu^{(1)}(\lambda r)\mathbf{e}_\phi + H_\nu^{(1)}(\lambda r)\mathbf{e}_x\right)\wedge\left(i\frac{\nu}{\lambda r_0}J_\nu(\lambda r_0)\mathbf{e}_r - J_\nu'(\lambda r_0)\mathbf{e}_\phi\right)\Bigg)\end{aligned} \tag{B.16}$$

The solution to the inhomogeneous vector wave equation (B.1) is given by the integral with a kernel given by the dyadic Green's function

$$\mathbf{F}(r,\lambda,\nu,k_x) = \int d\mathbf{r}'\mathcal{G}(r,r',\lambda,\nu,k_x)\cdot\mathbf{Q}(r',\lambda,\nu,k_x,\omega) \tag{B.17}$$

where $\mathbf{Q}(r',\lambda,\nu,k_x)$ is a Fourier transform of $\mathbf{Q}(\mathbf{r})$ and $\cdot$ denotes a scalar product.

For the particle executing the helical motion with the velocity $\mathbf{v} = \{0, v_\phi, v_x\}$, the current density is

$$\mathbf{j}(\mathbf{r}) = q\mathbf{v}\delta(\mathbf{r}-\mathbf{r}_0) \tag{B.18}$$

The Fourier transform of the current is

$$\mathbf{j}(r,\lambda,\nu,k_x,\omega) = \int dx e^{-ik_x x}\int dt e^{i\omega t}\int d\phi e^{-i\nu\phi}\mathbf{j}(\mathbf{r}) = q\mathbf{v}\delta(\omega-\nu\Omega_\phi-k_x v_x)\frac{\delta(r-r_0)}{r} \tag{B.19}$$

Using Eqs. (B.14), (B.17) and (B.19), we find the transverse component of the electric field:

$$\begin{aligned}\mathbf{E}_\perp = \pi q(2-\delta_{\nu,0})\frac{\omega}{c}\delta(\omega-\nu\Omega_\phi-k_x v_x)\Bigg(&-J_\nu'(\lambda r_0)v_\phi\left(-i\frac{\nu}{\lambda r}H_\nu^{(1)}(\lambda r)\mathbf{e}_r - H_\nu^{(1)\prime}(\lambda r)\mathbf{e}_\phi\right)\\ &-\frac{c^2\lambda^2}{\omega^2}\left(\frac{k_x\nu\Omega_\phi}{\lambda^2}-v_x\right)J_\nu(\lambda r_0)\left(-i\frac{k_x}{\lambda}H_\nu^{(1)\prime}(\lambda r)\mathbf{e}_r - \frac{k_x\nu}{\lambda^2 r}H_\nu^{(1)}(\lambda r)\mathbf{e}_\phi + H_\nu^{(1)}(\lambda r)\mathbf{e}_x\right)\Bigg)\end{aligned} \tag{B.20}$$

In the wave zone, $\lambda r \gg 1$, and for $\nu \gg 1$ this can be simplified

$$\mathbf{E}_\perp = iq\pi\sqrt{\frac{2}{\pi\lambda r}}\frac{\omega}{c}e^{i\lambda r}\delta(\omega-\nu\Omega_\phi-k_x v_x)\left(J'_\nu(\lambda r_0)v_\phi\mathbf{e}_\phi - \frac{c^2\lambda^2}{\omega^2}\left(-\frac{k_x\nu\Omega_\phi}{\lambda^2}+v_x\right)J_\nu(\lambda r_0)\left(i\frac{k_x}{\lambda}\mathbf{e}_r+\mathbf{e}_x\right)\right) \tag{B.21}$$

Similarly, we find magnetic field

$$\begin{aligned}\mathbf{B} = {} & i\pi q(2-\delta_{\nu,0})\lambda\,\delta(\omega-\nu\Omega_\phi-k_x v_x)\left(\left(-i\frac{\nu}{\lambda r}H_\nu^{(1)}(\lambda r)\mathbf{e}_r - H_\nu^{(1)\prime}(\lambda r)\mathbf{e}_\phi\right)\left(-\frac{k_x\nu}{\lambda^2 r_0}v_\phi+v_x\right)J_\nu(\lambda r_0)\right. \\ & \left.-\left(-i\frac{k_x}{\lambda}H_\nu^{(1)\prime}(\lambda r)\mathbf{e}_r - \frac{k_x\nu}{\lambda^2 r}H_\nu^{(1)}(\lambda r)\mathbf{e}_\phi + H_\nu^{(1)}(\lambda r)\mathbf{e}_x\right)J'_\nu(\lambda r_0)v_\phi\right)\end{aligned} \tag{B.22}$$

which in the limit $\lambda r \gg 1$ and $\nu \gg 1$ gives

$$\mathbf{B} = iq\pi\sqrt{\frac{2}{\pi\lambda r}}\lambda e^{i\lambda r}\delta(\omega-\nu\Omega_\phi-k_x v_x)\left(iJ_\nu(\lambda r_0)\left(\frac{k_x\nu\Omega_\phi}{\lambda^2}-v_x\right)\mathbf{e}_\phi+\left(\frac{k_x}{\lambda}\mathbf{e}_r+\mathbf{e}_x\right)J'_\nu(\lambda r_0)v_\phi\right) \tag{B.23}$$

The Pointing flux, $\mathbf{S} = c\mathbf{E}^* \times \mathbf{B}/(4\pi)$, for $r \to \infty$ is then

$$\mathbf{S} = \frac{q^2\omega}{r}\left(J'^2_\nu v_\phi^2 + \left(\frac{k_x c}{\lambda}-\frac{\omega v_x}{\lambda c}\right)^2 J_\nu^2(\lambda r_0)\right)\left(\mathbf{e}_r+\frac{k_x}{\lambda}\mathbf{e}_x\right)\delta(\omega-\nu\Omega_\phi-k_x v_x)dld\omega dk_x \tag{B.24}$$

where $dl = rd\phi$ is a unit arc length of a cylinder.

We are interested only in the radial component of the flux. Equating the Pointing flux to the emissivity, we find

$$\eta(\omega,k_x) = q^2\omega\left(J'^2_\nu v_\phi^2 + \left(\frac{k_x c}{\lambda}-\frac{\omega v_x}{\lambda c}\right)^2 J_\nu^2(\lambda r_0)\right)\delta(\omega-\nu\Omega_\phi-k_x v_x) \tag{B.25}$$

which is exactly the cyclotron emissivity per unit range $d\phi\,d\omega\,dk_x$.

Appendix C Resonant Electromagnetic Waves in the Asymptotic Regime $z \gg 1$

In this Appendix we consider resonant wave-particle interaction in a medium. We are concerned with case, when the interaction occurs "outside the light cylinder" (see Section A.3 and Fig. A.1), which corresponds to case $z > 0$ (Eq. 6.24). In particular, we show that in the limit $z \gg 1$ in cylindrical coordinates the wave-particle interaction may be described by the plane wave approximation. This fact allows a considerable simplification, when calculating the resonant terms for in the dielectric tensor (see Section 5.2).

We wish to simplify the relations (A.14-A.17) in the limit $z \gg 1$. Instead of standing waves, described by Bessel J functions, we consider propagating waves, described by Hankel $H^{(1)}$ and $H^{(2)}$ functions. For the outgoing waves, corresponding to $H^{(1)}$, we find in the limit $z \gg 1$:

$$\begin{aligned} H^{(1)} &\approx -\frac{2^{1/4}}{\sqrt{\pi}\nu^{1/3}z^{1/4}} e^{i\frac{2^{3/2}}{3}z^{3/2}+i\frac{\pi}{4}} \\ H^{(1)\prime} &\approx -i\frac{2^{3/4}z^{1/4}}{\sqrt{\pi}\nu^{2/3}} e^{i\frac{2^{3/2}}{3}z^{3/2}+i\frac{\pi}{4}} \end{aligned} \tag{C.1}$$

We next define the radial wave number

$$k_r = -i\frac{\partial \ln H^{(1)}}{\partial r} \tag{C.2}$$

Using Eqs. (C.1) and (C.2), we find

$$k_r = \frac{\sqrt{2z}\hat{\lambda}}{\nu^{1/3}} \approx \sqrt{2\delta}\hat{\lambda} \tag{C.3}$$

Introducing a notation $k_\phi = \nu/r$, the waves in the isotropic dielectric in the limit $z \gg 1$ may be written

$$\mathbf{E}^{(lt)}(\mathbf{k},\omega) = E^{(lt)}\left(-\frac{k_x k_r}{\hat{\lambda}^2}\mathbf{e_r} - \frac{k_\phi k_x}{\hat{\lambda}^2}\mathbf{e}_\phi + \mathbf{e_x}\right) \tag{C.4}$$

$$\mathbf{B}^{(lt)}(\mathbf{k},\omega) = \frac{\omega\epsilon}{\hat{\lambda}^2 c}E^{(lt)}\left(k_\phi \mathbf{e_r} - k_r\,\mathbf{e}_\phi\right) \tag{C.5}$$

$$\mathbf{E}^{(t)}(\mathbf{k},\omega) = E^{(t)}\left(k_\phi \mathbf{e_r} - k_r \mathbf{e}_\phi\right) \tag{C.6}$$

$$\mathbf{B}^{(t)}(\mathbf{k},\omega) = E^{(t)}\left(\frac{k_r k_x c}{\omega}\mathbf{e_r} + \frac{k_x k_\phi c}{\omega}\mathbf{e}_\phi - \frac{c\hat{\lambda}^2}{\omega}\mathbf{e_x}\right) \tag{C.7}$$

with $\mathbf{k} = \{k_r, k_\phi, k_x\}$ and a phase dependence $\exp\{-i(\omega t - k_r r - k_\phi \phi - k_x x\}$.

With these notations the dispersion relation is

$$k_x^2 + k_r^2 + k_\phi^2 = \frac{\omega^2 \epsilon}{c^2} \tag{C.8}$$

Relations (C.4-C.7) look similar to the relations (A.21), though they were obtained in quite a different manner. Expansions (A.21) are valid for $\lambda r - \nu \geq \nu$ with the radial wave vector defined by (A.19). Expansions (C.4-C.7) are valid for $\lambda r \approx \nu$ and $\xi \gg 1$ (the radial wave vector in this case is defined by (C.3)).

The importance of these results is that in these two limits the electromagnetic wave in cylindrical coordinates look like plane waves. This is a considerable simplification. It allows one to implement a well developed technique of Fourier transforms in considering the wave propagation.

This representation of the electromagnetic fields requires (i) the presence of a medium with the index of refraction $n > 1$, (ii) superluminal motion of the resonant particle $\delta > 1/(2\gamma^2)$, and (iii) large harmonic number $\nu > \delta^{-3/2}$.

Another important feature is that in this limit there is an additional freedom in the choice of wave polarizations in an isotropic dielectric. For example, we can introduce the polarization vector corresponding to the waves (C.4-C.7):

$$\begin{aligned} \mathbf{e}^{(t)} &= \frac{1}{\tilde{\lambda}}\{k_\phi, -k_r, 0\} = \{\sin\psi, -\cos\psi, 0\} \\ \mathbf{e}^{(lt)} &= \{-\cos\psi\sin\theta, -\sin\psi\sin\theta, \cos\theta\} \end{aligned} \tag{C.9}$$

which satisfy relations

$$\begin{aligned} \mathbf{e}^{(t)} &= \mathbf{e}_\mathbf{k} \times \mathbf{e}_x \\ \mathbf{e}^{(lt)} &= \mathbf{e}_\mathbf{k} \times \mathbf{e}^{(t)} \end{aligned} \tag{C.10}$$

The special role played by the $\mathbf{e}_x$ in defining the polarizations of the normal modes comes from the fact that in the isotropic homogeneous medium, the solutions of the vector wave equations may be chosen to be tangential to the coordinate surfaces $\mathbf{e}_x$. In the nonisotropic medium this is not true.

Alternatively, *in the limit* $z \gg 1$ we can chose the following polarizations

$$\begin{aligned} \mathbf{e}^{(t)} &= \frac{1}{k_\perp}\{-k_x, 0, k_r\} \\ \mathbf{e}^{(lt)} &= \frac{1}{kk_\perp}\{k_\phi k_r, -k_\perp^2, k_x k_\phi\} \end{aligned} \tag{C.11}$$

(see Fig. C.1). This particular choice of polarizations has an advantage that it may be related to the polarizations in the straight field line geometry.

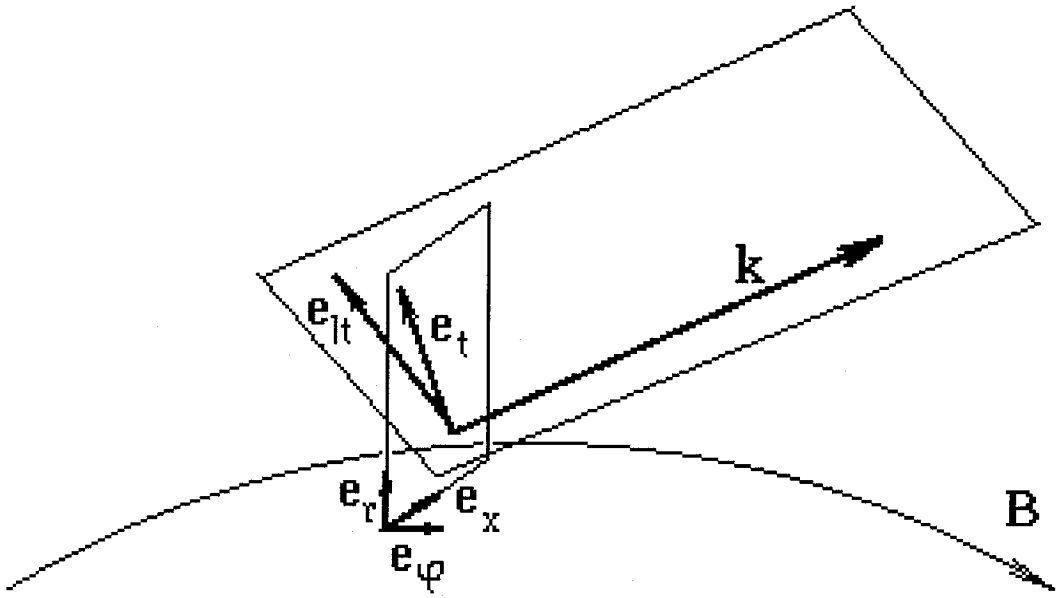

Figure C.1: Polarization of normal modes in the limit of very strong magnetic field. The electric field vector of the t-mode is in the plane $\mathbf{e_r} - \mathbf{e_x}$ and the electric vector of the lt-mode is orthogonal to $\mathbf{e}_t - \mathbf{k}$ plane.

Appendix D Relativistic Maxwellian Distribution

We seek an appropriate expression for the relativistic one-dimensional distribution. The aim of this Appendix is to define the relevant physical quantities measured in different systems. The relation obtained in the Appendix are extensively used in Chapter 5.6 when considering the properties of waves in a relativiscally hot plasma.

Relativistic covariant dispersion relations for plasma waves have been considered by Godfrey et al. 1974a, Melrose 1982 and others (see reference in Melrose 1982). The general expression for the *frame-invariant* distribution function is

$$f(\mathbf{p},\mathbf{r})^{inv} = \frac{1}{(2\pi\hbar)^3}\exp\{\mu(\mathbf{r}) - \beta p^\nu U_\nu\} \tag{D.1}$$

where μ is a chemical potential, $\beta = 1/T$), T is invariant temperature, $\mathbf{p}$ is the momentum of the particle, p^ν is a four-momentum of the particle and U_ν is four velocity of the reference frame (speed of light and particle mass are set to unity in this Appendix).

Next we define a flux four-vector:

$$N^\nu = \int \frac{d\mathbf{p}}{\gamma} p^\nu f(\mathbf{p})^{inv} = \{n(\mathbf{r},\mathbf{t}), \mathbf{j}(\mathbf{r},\mathbf{t})\} \tag{D.2}$$

An invariant density, measured in a particular frame with the four velocity U_ν, is then

$$n_o = N^\nu U_\nu = \int \frac{d\mathbf{p}}{\gamma}(p^\nu U_\nu) f(p)^{inv} \tag{D.3}$$

In particular, the invariant density in the rest frame (with $U^o_\nu = \{1,0,0,0\}$) is $n^o = N^\nu U^o_\nu$. We normalize the distribution function (D.1) to the invariant density of particles in the rest frame

$$n_o = \int \frac{d\mathbf{p}}{(2\pi\hbar)^3}\exp\{-\beta\gamma\} \tag{D.4}$$

Then, for a one-dimensional distribution $f(\mathbf{p})^{inv} = \delta(p_\perp^2) f(p)^{inv}/\pi$ (below p is a component of momentum along magnetic field)

$$f(\mathbf{p})^{inv} = \frac{n_o}{2K_1(\beta)}\exp\{-\beta p^{nu} U_{nu}\} \tag{D.5}$$

where we introduced new variables $\gamma = \cosh x$ and $\gamma_p = \cosh y$ and used a relation (Gradshtein &

Ryzhik 1980, (3.547.4))

$$\int_{-\inf}^{\inf} dx \cosh x \exp\{-\beta \cosh x\} = 2K_1(\beta) \tag{D.6}$$

The density in the frame moving with the four velocity $U_\nu = \{\gamma_p, \mathbf{v_p}\gamma_p\}$ (where $\gamma_p = 1/\sqrt{1-v_p^2}$) is

$$n = N^0 = \int d\mathbf{p} f(\mathbf{p})^{inv} = \gamma_p n_o \tag{D.7}$$

In this work we use the distribution function normalized to the *laboratory* density n

$$f(\mathbf{p}) = \frac{\delta(p_\perp^2)}{\pi} f(p), \qquad f(p) = \frac{n}{2K_1(\beta)\gamma_p} \exp\{-\beta p^\nu U_\nu\} \tag{D.8}$$

There is a natural simplification of the distribution function (D.8) in the case $\beta \gg 1$, $\gamma_p \gg 1$ (cold plasma streaming with large Lorentz factor). In this case the distribution is strongly peaked at $\gamma = \gamma_p$ so we can expand the distribution function, keeping terms up to the second order in $\gamma - \gamma_p$:

$$f(p) = \frac{n \exp\{-\beta\}}{2K_1(\beta)\gamma_p} \exp\left\{-\frac{\beta(\gamma-\gamma_p)^2}{2(\gamma_p^2-1)}\right\} = \frac{n}{\sqrt{2\pi}\Delta\gamma} \exp\left\{-\frac{(\gamma-\gamma_p)^2}{2\Delta\gamma^2}\right\} \tag{D.9}$$

where we introduced $\Delta\gamma = \sqrt{T}\gamma_p$ and used the fact that $\gamma_p \gg 1$.

In Table D.1 we give the estimates of the moments of the relativistic Maxwellian distribution. $< ... >$ implies $\int dp...f(p)/n$, where n is the noninvariant density in the laboratory frame.

The arguments of the Bessel functions in Table D.1 are $1/T_p$. When calculating moments we used a relation

$$\int_0^\infty dx\, exp(-\beta \cosh(x)) \cosh(x)^n = (-1)^n \frac{d^n K_0(\beta)}{d\beta^n} \tag{D.10}$$

The asymptotic relations for the modified Bessel functions are

$$K_\nu(x) = \sqrt{\tfrac{\pi}{2x}}\, e^{-x} \left(1 + \tfrac{4\nu^2-1}{8x}\right) \qquad x \to \infty \tag{D.11}$$

$$K_0(x) = -\ln(x), \qquad K_\nu(x) = \tfrac{1}{2}\Gamma(\nu)\left(\tfrac{x}{2}\right)^{-\nu} \qquad x \to 0 \tag{D.12}$$

	Plasma frame	Pulsar frame
Density, $< 1 >$	1	$\frac{1}{\gamma_p}$
$< \gamma >$	$\frac{K_0+K_2}{2K_1} = \begin{cases} (1+T_p/2) & \text{if } T_p \ll 1 \\ T_p & \text{if } T_p \gg 1 \end{cases}$	$\gamma_p \left(\frac{K_0+K_2}{2\,K_1} + T_p\, v_p^2\right) = \begin{cases} \gamma_p \left(1 + T_p/2 + T_p v_p^2\right) & \text{if } T_p \ll 1 \\ \gamma_p T_p \left(1 + v_p^2\right) & \text{if } T_p \gg 1 \end{cases}$
$< v >$	0	v_p
$< p >$	0	$\gamma_p v_p \frac{K_2}{K_1} = \begin{cases} \gamma_p v_p (1 + T_p/2) & \text{if } T_p \ll 1 \\ 2\,\gamma_p\, v_p\, T_p & \text{if } T_p \gg 1 \end{cases}$
$< pv >$	T_p	$\gamma_p \left(\frac{K_0+K_2}{2\,K_1} v_p^2 + T_p\right) = \begin{cases} \gamma_p \left(1 + T_p + \frac{T_p\, v_p^2}{2}\right) & \text{if } T_p \ll 1 \\ \gamma_p\, T_p \left(1 + v_p^2\right) & \text{if } T_p \gg 1 \end{cases}$
$< \frac{1}{\gamma} >$	$\frac{K_o}{K_1} = \begin{cases} (1 - T_p/2) & \text{if } T_p \ll 1 \\ \frac{\log T_p}{T_p} & \text{if } T_p \gg 1 \end{cases}$	$\frac{K_o}{\gamma_p K_1} = \begin{cases} \frac{1-T_p/2}{\gamma_p} & \text{if } T_p \ll 1 \\ \frac{\log T_p}{\gamma_p T_p} & \text{if } T_p \gg 1 \end{cases}$

Table D.1: Moments of the relativistic Maxwellian distribution

Appendix E Cutoff and Cross-Over Points for Parallel Propagation

Using streaming Maxwellian distribution it is not possible to find the exact expressions for the two important frequencies: cutoff frequency (a limit $k \to 0$ of the plasma wave dispersion) and the cross-over frequency (when the ordinary mode has a vacuum dispersion relation).

The cutoff frequency is

$$\omega^2_{cutoff} = \frac{4\pi q^2}{m_e} \int \frac{dp}{\gamma^3} f(p) = \tag{E.1}$$

and the cross-over frequency is

$$\omega^2_{cross-over} = \frac{4\pi q^2}{m_e} \int \frac{dp}{\gamma^3} \frac{f(p)}{(1-v)^2} \tag{E.2}$$

For the case of relativistic Maxwellian distribution (Eq. 5.67) the expression for the cutoff frequency may be re written as

$$\omega^2_{cutoff} = \frac{\omega_p^2}{2K_1(\beta)\gamma_p} \int \frac{dx}{\cosh^2(x+y)} \exp\{-\beta \cosh x\} \tag{E.3}$$

where $\gamma_p = \cosh y$. The corresponding integrations in the case $\beta \gg 1$ (cold plasma) may be performed using the steepest decent method. For $\beta \gg \gamma_p$ the "sharply" peaked function under integral sign in (E.3) is $\exp\{-\beta \cosh x\}$ so we can use expand around the point $x = 0$ to obtain

$$\omega^2_{cutoff} = \sqrt{\frac{\pi}{2\beta}} \frac{\exp\{-\beta\}}{2\,\gamma_p^3 2\,K_1(\beta)} = \frac{\omega_p^2}{\gamma_p^3} \text{ if } \beta \gg \gamma_p \tag{E.4}$$

where $\omega_p^2 = 4\pi q^2 n/m_e$.

For $\beta \ll 1$ (hot plasma) we can make the following approximation to the exponential function:

$$\exp\{-\beta \cosh x\} \approx \begin{cases} 1 & \text{if } \log\beta < x < -\log\beta \\ 0 & \text{otherwise} \end{cases} \tag{E.5}$$

We find then

$$\omega_{cutoff}^2 \approx \frac{n}{2K_1(\beta)\gamma_p}\int_{-\log 2\beta}^{\log 2\beta}\frac{dx}{\cosh^2(x+y)} = \begin{cases} \frac{\omega_p^2 T}{4\gamma_p^3} & \text{for } \beta\gamma_p \gg 1 \\ \frac{\omega_p^2}{T\gamma_p} & \text{for } \beta\gamma_p \ll 1 \end{cases} \tag{E.6}$$

where we used

$$\int_{-\log 2\beta}^{\log 2\beta}\frac{dx}{\cosh^2(x+y)} \approx \frac{2}{1+4\beta^2\gamma_p^2} \text{ for } \beta \ll 1 \tag{E.7}$$

An interesting consequence of Eqs. (E.4) and (E.7) is that in the case of relativistically hot plasma streaming with very large Lorentz factor, so that $\gamma_p \gg T \gg 1$, thermal motion *increases* the cutoff frequency, while for the lower streaming Lorentz factors thermal motion decreases the cutoff frequency.

The calculations of the cross-over frequency (E.2) may be done exactly:

$$\omega_{cross-over}^2 = \frac{\omega_p^2}{2K_1(\beta)\gamma_p}\int_{-\infty}^{\infty}\frac{dx}{\cosh^2 x}\frac{\exp\{-\beta\cosh(x-y)\}}{(1-\tanh x)^2} = \frac{\gamma_p(1+\beta_p)^2K_2(\beta)\omega_p^2}{2K_1(\beta)}$$
$$\approx \begin{cases} 4\gamma_p\omega_p^2 T & T \gg 1 \\ 2\gamma_p\omega_p^2 & T \ll 1 \end{cases} \tag{E.8}$$

Appendix F Conditions on the Cyclotron-Cherenkov Instability

In this Appendix we consider the development of the cyclotron-Cherenkov instability in magnetosphere of the typical pulsar. We show that the conditions on page 122 (Chapter 8) for the development of the cyclotron-Cherenkov instability are satisfied for the typical pulsar.

The conditions for the development of the cyclotron-Cherenkov instability may be easily derived for the small angles of propagation with respect to the magnetic field. Representing the wave's dispersion as

$$\omega = kc(1-\delta), \qquad \text{where } \delta = \begin{cases} \frac{\omega_p^2 T_p}{4\gamma_p^3 \omega_B^2} & \text{X mode} \\ \frac{\omega_p^2 T_p}{4\gamma_p^3 \omega_B^2} - \frac{\gamma_p \omega_p^2 T_p \sin^2\theta}{k^2 c^2} & \text{O mode} \\ \frac{\omega_p^2 T_p}{4\gamma_p^3 \omega_B^2} + \frac{k^2 c^2 \sin^2\theta}{4\gamma_p \omega_p^2 T_p} & \text{Alfvén mode} \end{cases} \tag{F.1}$$

and neglecting the drift term, the resonance condition (6.1) may then be written as

$$\frac{1}{2\gamma_{res}^2} - \delta + \frac{\theta^2}{2} = -\frac{\omega_B}{\omega\,\gamma_{res}} \tag{F.2}$$

Let us discuss the condition for the development of the cyclotron-Cherenkov instability. First we note that Eq.(F.2) requires that $\frac{1}{2\gamma_{res}^2} < \delta$ and $\frac{\theta^2}{2} < \delta$. The first is the condition that the particle is moving through plasma with the velocity faster than the phase velocity of the wave. The second condition limits the emission to the small angles with respect to magnetic field. Assuming that $\frac{1}{2\gamma_{res}^2} \ll \delta$ and $\frac{\theta^2}{2} \ll \delta$, we find from (F.2)

$$\omega = \frac{\omega_B}{\gamma_{res}\delta} = \frac{2\gamma_p^3}{\lambda T_p \gamma_{res}} \frac{\omega_B^{*2}}{\Omega} \left(\frac{R}{R_{NS}}\right)^6 \tag{F.3}$$

This resonant frequency increases with radius as R^6.

Using the upper limit on the frequencies for the relations (F.1) to hold, namely $\omega \ll \gamma_p \omega_B / T_p$. This sets the limit on δ: $\delta \gg T_p/(\gamma_p \gamma_{res})$. This condition is satisfied for the radii:

$$\left(\frac{R}{R_{NS}}\right) > \left(\frac{2\gamma_p^2 \omega_{B,NS}}{\gamma_{res}\,\lambda\Omega}\right)^{1/3} = \begin{cases} 5\times 10^2 & \text{for the beam} \\ 2\times 10^3 & \text{for the tail} \end{cases} \tag{F.4}$$

This is the radius where the resonance condition first becomes satisfied for the particles of the

primary beam and from the tail of the distribution function.

The cyclotron-Cherenkov instability growth rate is (i.e. Kazbegi et al. 1991c):

$$\Gamma = \sqrt{\frac{\pi}{2}} \frac{\omega_{p,res}^2}{\omega \, \Delta\gamma} = \sqrt{\frac{\pi}{2}} \frac{\lambda \, \lambda_{res} T_p \, \gamma_{res}}{\Delta\gamma \, \gamma_p^3} \frac{\Omega^2}{\omega_B} \tag{F.5}$$

where we have normalized the density of the resonant particles to the Goldreich-Julian density $\omega_{p,res}^2 = \lambda_{res} \, \omega_{GJ}^2$.

It follows from (F.5) that the growth rate increases with radius as R^3. Deeper in the magnetosphere the growth rate is slow and the waves are not excited. At some point the growth rate becomes comparable to the dynamic time $\Gamma/\Omega = 1$. This occurs at

$$\left(\frac{R}{R_{NS}}\right) = \left(\frac{\Delta\gamma \, \gamma_p^3}{\sqrt{\frac{\pi}{2}} \, \lambda \, \lambda_{res} T_p \, \gamma_{res}} \frac{\omega_B^*}{\Omega}\right)^{1/3} = \begin{cases} 2 \times 10^3 & \text{for the beam} \\ 1 \times 10^3 & \text{for the tail} \end{cases} \tag{F.6}$$

Using the equipartition condition (4.5) we conclude that at a given radius the growth on the tail particles is approximately the same (the higher resonant density is compensated by the higher resonant γ-factor).

Starting this radius the waves will start to grow with the growth rate increasing with radius. The highest frequency of the growing mode is determined by the condition (F.3) evaluated at the radius (F.6):

$$\omega_{max} = \begin{cases} 1 \times 10^8 \text{rad s}^{-1} & \text{for the resonance on the beam} \\ 4 \times 10^{11} \text{rad s}^{-1} & \text{for the resonance on the tail} \end{cases} \tag{F.7}$$

These estimates show, that for the chosen plasma parameters the cyclotron-Cherenkov instability always develops on the tail of the distribution function and can also develop on the particles from the primary beam. The higher density of the tail particles favors the development of the instability on the tail particles. The cyclotron-Cherenkov instability on the tail particles occurs deeper in the magnetosphere on the higher frequencies than the cyclotron-Cherenkov instability on the primary beam, which can develop further out in the magnetosphere and produce emission at the lower frequencies.

The growth rate of the cyclotron-Cherenkov instability should satisfy two other conditions: the growth length must be much less than the length of the coherent wave-particle interaction and the kinetic approximation should be valid. The coherent wave-particle interaction is limited by the curvature of the magnetic field. A particle can resonate with the waves propagating in a limited range of angles with respect to the magnetic field. As the wave propagates in a curved field, the angle that the wave vector makes with the field changes and the wave may leave the range of resonant

angles. If the range of the resonant angles is $\Delta\theta$ then the condition of a short growth length is

$$\frac{c}{\Gamma} < \Delta\theta R_B \tag{F.8}$$

For cyclotron-Cherenkov instability we can estimate $\Delta\theta \approx \sqrt{\delta}$. Then we find a condition on the radius of curvature

$$R_B > \frac{1}{\sqrt{2\pi}} \frac{c\,\Delta\gamma}{\lambda_{res}\Omega\,\gamma_{res}\delta^{3/2}} \approx \begin{cases} 10^{11}\text{cm} & \text{for the beam} \\ 5\times 10^{10}\text{cm} & \text{for the tail} \end{cases} \tag{F.9}$$

at the distance $R = 2\times 10^9$cm. The region of the cyclotron-Cherenkov instability is limited to the field lines near the central field line. The transverse size of the emission region may be estimated as $x = R^2/R_B \approx 10^8$cm. This gives an opening angle of the emission $\theta^{em_e} = x/R \approx 2^\circ$.

There is another condition that the growth rate (F.5) should satisfy, namely the condition of the kinetic approximation. In deriving the growth rate we implicitly assumed that the wave-particle interaction is described by the random phase approximation, which requires that the spread of the resonant particles satisfies the condition

$$|\mathbf{k}\delta\mathbf{v}_{res}| \gg \Gamma \tag{F.10}$$

For the particle streaming in the curved magnetic field without any gyration, this condition takes the form

$$\left| k_\parallel c\frac{\Delta\gamma}{\gamma^3} + k_x u_d \frac{\Delta\gamma}{\gamma} + \frac{s\,\omega_B \Delta\gamma}{\gamma^2} \right| \gg \Gamma \tag{F.11}$$

For the cyclotron-Cherenkov instability the last term on the left-hand side of (F.11) is dominant and the condition (F.11) becomes

$$\frac{\omega_B\,\Delta\gamma}{\gamma_{res}^2} \gg \Gamma \tag{F.12}$$

Using the growth rate (F.5), this condition may be rewritten as

$$\left(\frac{R}{R_{NS}}\right) \ll \left(\sqrt{\frac{2}{\pi}} \frac{\Delta\gamma^2\,\omega_B^{*3}\,\gamma_p^3}{\lambda_{res}\Omega^2\,\gamma_{res}^3\,\lambda T_p}\right)^{1/6} = 3\times 10^5 \tag{F.13}$$

Eq.(F.13) means that the kinetic approximation is well satisfied inside the pulsar magnetosphere.

Thus, the conditions for the development of the cyclotron-Cherenkov instability may be satisfied for the typical pulsar parameters. The waves are generated in the observed frequency range near the central field line. The radius of emission is $\approx 10^9$cm, the transverse size of the emitting region is $\approx 10^8$cm and the "thickness" of the emitting region is $\leq 10^9$cm. This may account for the core-type emission pattern.

Appendix G Grow Rate for the Cherenkov-Drift Instability

In this Appendix we calculate the growth rate for the Cherenkov-drift instability in the plane wave approximation. Originally this growth rate has been obtained by Lyutikov, Machabeli & Blandford 1997a, using the single particle emissivities. Here we give a derivation using the simplified dielectric tensor (Eq. (5.28)). The relevant components of the antihermitian part of the dielectric tensor (5.28) are Lyutikov & Machabeli 1997:

$$\begin{aligned}
\epsilon''_{xx} &= -i\frac{4\pi^2 q^2}{\omega c}\int dp_\phi u_d^2 \frac{\partial f(p_\phi)}{\partial p_\phi}\delta\left(\omega - k_\phi v_\phi - k_x u_d\right), \\
\epsilon''_{x\phi} &= -i\frac{4\pi^2 q^2}{\omega c}\int dp_\phi u_d v_\phi \frac{\partial f(p_\phi)}{\partial p_\phi}\delta\left(\omega - k_\phi v_\phi - k_x u_d\right) = \epsilon''_{\phi x}, \\
\epsilon''_{\phi\phi} &= -i\frac{4\pi^2 q^2}{\omega}\int dp_\phi v_\phi \frac{\partial f(p_\phi)}{\partial p_\phi}\delta\left(\omega - k_\phi v_\phi - k_x u_d\right).
\end{aligned} \tag{G.1}$$

The growth rate of the Cherenkov drift instability (Melrose 1978c):

$$\Gamma = \int d\mathbf{p} w(\mathbf{k},\mathbf{p})\,\hbar\mathbf{k}\cdot\frac{\partial f(\mathbf{p})}{\partial \mathbf{p}}. \tag{G.2}$$

Growth rate for the lt-mode is

$$\Gamma^{lt} = \frac{4\pi^2 q^2}{m}\int dp_\phi \left(\frac{k_\phi k_x u_d}{c k k_\perp} - \frac{v_\phi}{c}\frac{k_\perp}{k}\right)^2 \frac{\partial f(p_\phi)}{\partial p_\phi}\delta\left(\omega - k_\phi v_\phi - k_x u_d\right), \tag{G.3}$$

and growth rate for the t-mode is

$$\Gamma^{t} = \frac{4\pi^2 q^2}{m}\int dp_\phi \left(\frac{k_r u_d}{k_\perp c}\right)^2 \frac{\partial f(p_\phi)}{\partial p_\phi}\delta\left(\omega - k_\phi v_\phi - k_x u_d\right). \tag{G.4}$$

Where we chose the following polarization vectors

$$\begin{aligned}
\mathbf{e}^{\mathrm{lt}} &= \frac{1}{k k_\perp}\left\{k_\phi k_r, -k_\perp^2, k_x k_\phi\right\}, \\
\mathbf{e}^{\mathrm{t}} &= \frac{1}{k_\perp}\left\{-k_x, 0, k_r,\right\},
\end{aligned} \tag{G.5}$$

where $k_\perp = \sqrt{k_r^2 + k_x^2}$ and

$$\mathbf{k} = \left\{k_r, k_\phi, k_x\right\}. \tag{G.6}$$

The maximum growth rate for the t-mode is reached when $k_x/k_\phi = u_d/c$ and the maximum growth rate for the lt-mode is reached when $k_r = 0$. We also note, that in the excitation of both lt- and t-wave, it is the x component of the electric field that is growing exponentially.

Estimating (G.3) and (G.4) using δ-function ($\max\left[\frac{k_r}{k_\perp}\right] \approx c\sqrt{2\delta}/u_d$ and $\max[\frac{k_\phi k_x u_d}{ckk_\perp} - \frac{v_\phi}{c}\frac{k_\perp}{k}]$ $\approx \sqrt{2\delta}$), we find the maximum growth rates of the t- and lt-modes in the limit $\delta \gg 1/\gamma_{res}^2$:

$$\Gamma^t = \Gamma^{lt} \approx \frac{2\omega_{p,res}^2\delta}{\omega}\left(\frac{\gamma^3}{1+u_d^2\gamma^2/c^2}\frac{\partial f(\gamma)}{\partial\gamma}\right)_{res}, \tag{G.7}$$

where $\omega_{p,res}$ is the plasma density of the resonant particles.

We estimate the growth rates (G.7) for the distribution function of the resonant particles having a Gaussian form:

$$f(p_\phi) = \frac{1}{\sqrt{2\pi}p_t}\exp\left(-\frac{(p_\phi - p_b)^2}{2\Delta p^2}\right), \tag{G.8}$$

where p_b is the momentum of the bulk motion of the beam and p_t is the dispersion of the momentum.

Assuming in (G.7) that $u_d\gamma_b/c \gg 1$, we find the growth rates

$$\Gamma^t = \Gamma^{lt} \approx \sqrt{\frac{2}{\pi}}\frac{\omega_{p,res}^2\delta\gamma_b}{\omega\Delta\gamma^2}\frac{c^2}{u_d^2}, \tag{G.9}$$

where $\gamma_b = p_b/(mc)$, $\Delta\gamma = \Delta p/(mc)$.

Appendix H Conditions on Cherenkov-Drift Instability

In this Appendix we consider the development of the Cherenkov-drift instability in magnetosphere of the typical pulsar. We show that the conditions on page 122 (Chapter 8) for the development of the Cherenkov-drift instability are satisfied for the typical pulsar.

Since Cherenkov-drift resonance requires a very high parallel momentum, the resonant interaction will occur on the high phase velocity waves. This implies that, like cyclotron-Cherenkov resonance, Cherenkov-drift resonance is always important for the extraordinary mode, while for ordinary and Alfvén modes it is important only for small angles of propagation. We can then use the small approximation to dispersion relations for the small angles of propagation (F.1). Introducing cylindrical coordinates x , r , ϕ with r along the radius of curvature of the field line, x perpendicular to the plane of the curved field line and ϕ the azimuthal coordinate (Fig. 5.1), the resonance condition may then be written as

$$\frac{1}{2\,\gamma_{res}^2} - \delta + \frac{1}{2}\psi^2 + \frac{1}{2}\,(\theta - u_d/c)^2 = 0 \tag{H.1}$$

where we used $v_{res} = c(1 - \frac{1}{2\gamma_{res}^2} - \frac{u_d^2}{2c})$, $\theta = \frac{k_x}{k_\phi}$ and $\psi = \frac{k_r}{k_\phi}$.

We note that for the extraordinary mode, δ is independent of frequency and Eq. (H.1) becomes independent of frequency as well. This means that for the given angle of propagation, Cherenkov-drift resonance on the extraordinary mode occurs at all frequencies simultaneously. It is different from the cyclotron-Cherenkov resonance which occurs at a particular frequency. For both ordinary and Alfvén modes, δ does dependent on the frequency, so that for a given angle of propagation the Cherenkov-drift resonance occurs at a fixed frequency.

Let us now discuss the condition for the development of the Cherenkov-drift instability. First we drop the $\frac{1}{2\,\gamma_{res}^2}$ term from Eq.(H.1). This term is much smaller than δ for the radii satisfying

$$\left(\frac{R}{R_{NS}}\right) > \left(\frac{\omega_B^*\,\gamma_p^3}{\Omega\,\lambda T_p\,\gamma_b^2}\right)^{1/3} \tag{H.2}$$

which is satisfied everywhere inside the pulsar magnetosphere.

We find then that Eq. (H.1) can be satisfied for

$$\psi \le \sqrt{2\delta}, \qquad |\theta - u_d/c| \le \sqrt{2\delta} \tag{H.3}$$

Fig. 6.3 describes the emission geometry of the Cherenkov-drift instability.

From (H.3) we see that drift of the resonant particles becomes important if

$$u_d/c > \sqrt{2\delta} \tag{H.4}$$

Using the expression for δ (9.114), Eq. (H.4) gives

$$\left(\frac{R}{R_{NS}}\right) > \left(\frac{\lambda T_p \Omega\, \omega_B^* R_B^2}{c^2\, \gamma_p^3\, \gamma_b^2}\right)^{1/3} \tag{H.5}$$

At a given radius this condition may be considered as an upper limit on the curvature of the field lines

$$R_B \leq \left(\frac{c^2\, \gamma_p^3\, \gamma_b^2}{\lambda T_p \Omega\, \omega_B}\right)^{1/2} \tag{H.6}$$

Alternatively, condition (H.5) may be regarded as a lower limit on the radius from the star. In the dipole geometry the radius of curvature for the open field lines may be estimated as $R_B \geq \sqrt{\frac{Rc}{\Omega}}$. Then we find from Eq. (H.5)

$$\left(\frac{R}{R_{NS}}\right) > \left(\frac{\lambda T_p\, \omega_B^* R_{NS}}{c\, \gamma_p^3\, \gamma_b^2}\right)^{1/2} = 23 \tag{H.7}$$

In what follows we assume that the Cherenkov-drift resonance occurs in the outer parts of the pulsar magnetosphere where the typical value of the drift velocity is $u_d \approx 0.01c$.

The growth rate for the Cherenkov-drift resonance instability on the primary beam is calculated in Appendix G, Eq. G.9. Expressing the growth rate G.9 in terms of the parameters of the magnetospheric plasma, we find

$$\Gamma = \sqrt{\frac{2}{\pi}} \frac{\lambda T_p c^2}{\gamma_p^3 \Delta\gamma^2 u_d^2} \frac{\Omega^2}{\omega} \tag{H.8}$$

The growth rate (H.8) should satisfy several conditions. The first is the criteria for the fast growth: $\Gamma/\Omega > 1$. This is the requirement that the growth rate is fast enough, so that the instability have time to develop before the plasma is carried out of the magnetosphere. From (H.8) we find that the condition $\Gamma/\Omega > 1$ is satisfied for the chosen parameters and the typical frequency of emission $\omega = 5 \times 10^9$ rad $\sec^{-1}$.

The next condition that a growth rate should satisfy is that the growth length be much less than the length of the coherent wave-particle interaction (F.8). Estimating the range of resonant angles $\Delta\theta \approx \sqrt{\delta}$ and using the growth rate (H.8), this condition gives

$$R_B \geq \frac{c\,\omega}{\omega_B \Omega} \frac{\Delta\gamma^2}{\gamma_b \delta^{3/2}} \approx 10^{10}\text{cm at } R \approx 10^9\text{cm} \tag{H.9}$$

Eq.(H.9) is the lower limit on the radius of curvature of the field lines. It will restrict the emission region to the field lines closer to the central field line, where the radius curvature is large.

There is a third condition that the growth rate (H.8) should satisfy - the condition of the kinetic approximation (F.11). For the Cherenkov-drift resonance condition (F.11) gives

$$\left| k_x u_d \frac{\Delta \gamma}{\gamma} \right| \gg \Gamma \tag{H.10}$$

Estimating $k_x c \approx \omega u_d / c$ we find that this condition can be easily satisfied in the pulsar magnetosphere.

In a dipole geometry the instability occurs in the outer regions of pulsar magnetosphere with $R \approx 10^9$ cm on the field lines with radius of curvature limited both from below (by the condition of a large radius of curvature H.6) and from above (by the condition of a short growth length H.9).

Appendix I Instabilities in Millisecond Pulsars

In this Appendix we consider the development of the cyclotron-Cherenkov and Cherenkov-drift instabilities in magnetosphere of a millisecond pulsar. We show that the conditions on page 122 (Chapter 8) for the development of the Cherenkov-drift instability are satisfied for a millisecond pulsar, while the conditions for the development of the cyclotron-Cherenkov are probably not satisfied.

Here we will discuss the conditions for the development of these instabilities in a "standard" millisecond pulsar with the period $P = 5 \times 10^{-3}$ sec and the surface magnetic field $B = 10^8$ G. As a first order approximation we will assume that the other plasma parameters, i.e., the initial primary beam Lorentz factor $\gamma_b^{(0)} = 6 \times 10^7$, the primary beam Lorentz factor at the light cylinder $\gamma_b^{(0)} = 6 \times 10^6$, its scatter $\Delta\gamma = 10^2$, average streaming energy of the secondary plasma $\gamma_p = 10$, its scatter in energy $T_p = 10$ and the multiplicity factor $\lambda = 3 \times 10^5$ are the same. The light cylinder is now at a radius $R_{lc} = 2.4 \times 10^7 \text{cm} = 24\, R_{NS}$. These are very approximate assumptions. The plasma parameters in the millisecond pulsars are likely to be different from the normal pulsars. At this moment we do not understand the physics of the pair production well enough to make a quantitative distinction between normal and millisecond pulsars.

The growth rate of the cyclotron-Cherenkov instability becomes equal to the rotational frequency of the pulsar at (see (F.6))

$$\left(\frac{R}{R_{NS}}\right) = 20 \tag{I.1}$$

which is inside the light cylinder.

The approximation of the kinetic growth rate cyclotron-Cherenkov instability (F.13) requires that

$$\left(\frac{R}{R_{NS}}\right) < 3 \times 10^3 \tag{I.2}$$

which is satisfied. The condition of a short growth length (F.8) requires that

$$R_B \geq 10^9 \text{cm} \tag{I.3}$$

at the emission site of $R \approx 20\, R_{NS}$. This condition is hard to satisfy - cyclotron-Cherenkov instability does not develop in the millisecond pulsars.

For the Cherenkov-drift instability, the condition of a large drift (H.4) is now satisfied for all open magnetic field lines as well as the condition of a fast growth (H.9), and the condition of the kinetic approximation (H.10). By contrast, Cherenkov-drift instability can develop in the magnetospheres of the millisecond pulsars.

It is harder to satisfy the conditions for the development of the cyclotron-Cherenkov instability in the millisecond pulsars than in the normal pulsars. Since there is no clear distinction between core and cone-type emission for the millisecond pulsars it is possible that only Cherenkov-drift instability develops in their magnetospheres. Alternatively, different pulsars may have a substantially different plasma parameters, so that both instabilities may develop in some of them.

Appendix J Effects of Curvature Radiation Reaction on the Beam

In this Appendix we consider the effects of curvature radiation reaction on the propagation of the beam. We show, that due to the highly nonlinear dependence of the radiation reaction force on the energy of the particle, the beam becomes very cold as it propagates in the pulsar magnetosphere. This vindicates the assumed small scatter in the beam energy (see Section 4.1.1, page 23). We note here, that though the beam becomes very cold, the assumption of kinetic regime for the cyclotron-Cherenkov instability is still satisfied (Appendix F).

Consider a beam of electrons propagating in s dipole curved magnetic field. The radius of curvature on a field line near the the magnetic moment is

$$R_B = \frac{4}{3}\frac{\sqrt{R_{NS}R}}{\alpha^*} \tag{J.1}$$

Here $\alpha^* \ll \sqrt{R_{NS}/R}$ is the angle with respect to magnetic moment at which a given field line intersects the neutron star surface.

An evolution of the distribution function under the influence of the radiation reaction form is described by the equation:

$$\frac{\partial f(z,p_\phi,t)}{\partial t} + \frac{\partial}{\partial p_\phi}\left(\frac{\partial p_\phi}{\partial t} f(z,p_\phi,t)\right) = 0 \tag{J.2}$$

Eq. (J.2) can be solved by integrating along characteristics

$$\frac{\partial p_\phi}{\partial t} = -\frac{2e^2\,\gamma^4 v_\phi^3}{3c^3 R_B^2} \tag{J.3}$$

With the radius of curvature given by (J.1), Eq. (J.3) has a solution

$$\frac{1}{2}\left(\frac{\sqrt{p_\phi^2+(mc)^2}}{p_\phi^2} + \ln\left(\frac{p_\phi}{1+\sqrt{p_\phi^2+(mc)^2}}\right)\right)\Bigg|_{p_0}^{p_\phi(t)} = -\frac{3}{2}\frac{r_e\alpha^{*2}}{R_{NS}}\ln(t/t_o) \tag{J.4}$$

where $r_e = \frac{e^2}{mc^2}$ is the classical radius of an electron, $t_0 \approx R_{NS}/c$ and p_0 is the initial momentum. This equation can be solved for $p_\phi \gg mc$

$$\gamma_0(\gamma,t) = \gamma\left(1 - \gamma^3\frac{9r_e\alpha^{*2}}{8R_{NS}}\ln(t/t_0)\right)^{-1/3} \tag{J.5}$$

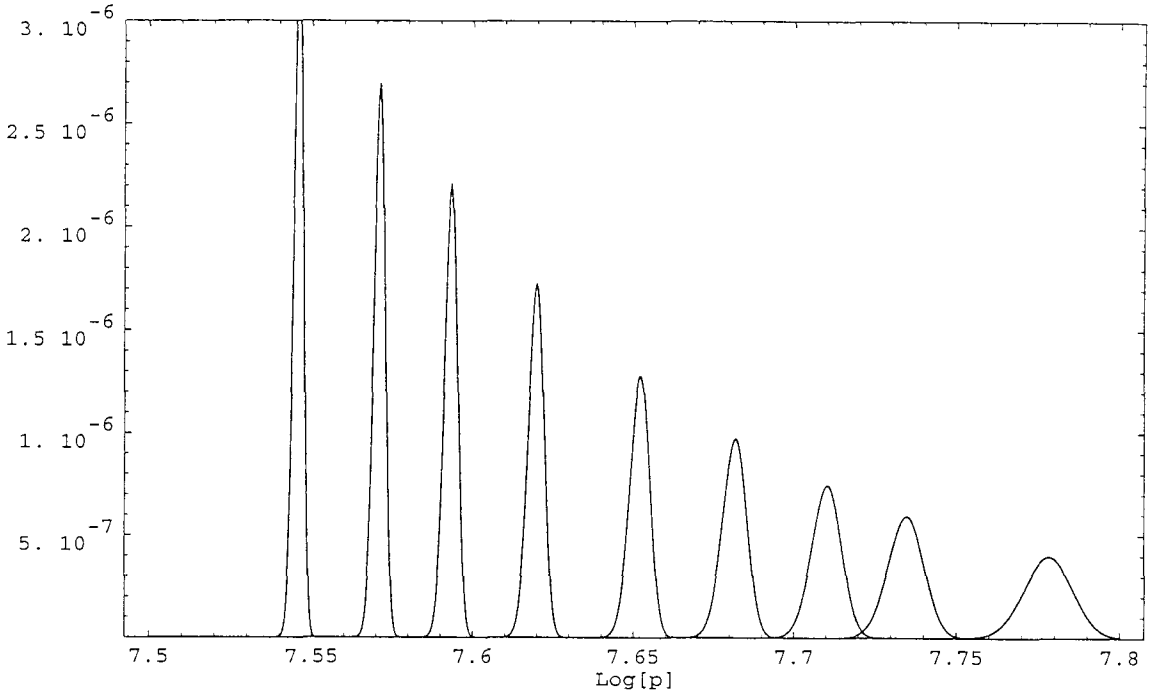

Figure J.1: Evolution of the distribution function of the primary beam due to the curvature radiation. Initial Lorentz factor of the beam is $\gamma_b = 6 \times 10^7$ and the initial scatter is $\Delta\gamma_0 = 10^6$.

Solution of the continuity equation (J.2) is then

$$f(z,\,\gamma,t) = f_0\left(\,\gamma_0(\,\gamma,t),\quad t=t_0\right)\left(\frac{\gamma}{\gamma_0(\,\gamma,t)}\right)^{-4} \tag{J.6}$$

where $f_0(\,\gamma_0, t=t_0)$ is the initial distribution function at $R = R_{NS}$.

Evolution of the distribution function is shown in Fig. J.1.

If originally the beam had a scatter in energy $\Delta\gamma_0$, then at a later moment it will have a scatter in energy given by

$$\Delta\gamma = \Delta\gamma_0\left(1+\gamma_0^3\frac{9r_e\alpha^{*2}}{8R_{NS}}\,\ln(t/t_0)\right)^{-4/3} \tag{J.7}$$

which implies that the scatter in energies of the beam may decrease much faster than its average energy.

To estimate the decrease in the average energy and in the energy scatter, we consider an evolution of the beam on the last open field line. Then $\alpha^{*2} = R_{NS}\Omega/c$ and at the light cylinder ($t = 2\pi/\Omega$) we have

$$\begin{aligned}\frac{\gamma}{\gamma_0} &= \left(1+\gamma_0^3\frac{9}{8}\frac{r_e\Omega}{c}\ln(\frac{2\pi c}{R_{NS}\Omega})\right)^{-1/3}\\ \frac{\Delta\gamma}{\Delta\gamma_0} &= \left(1+\gamma_0^3\frac{9}{8}\frac{r_e\Omega}{c}\ln(\frac{2\pi c}{R_{NS}\Omega})\right)^{-4/3}\end{aligned} \tag{J.8}$$

which may be expressed as

$$\frac{\Delta\gamma}{\gamma} = \frac{\Delta\gamma_0}{\gamma_0}\left(\frac{\gamma}{\gamma_0}\right)^3 \tag{J.9}$$

If the original beam was mildly relativistic ($\Delta\gamma_0 \approx 0.1\,\gamma_0$), then in order to reach a scatter $\Delta\gamma/\gamma \approx 10^{-4}$ the beam would have to lose about 90% of its original energy: $\gamma/\gamma_0 \approx 0.1$. Estimating (J.8), we find that the scatter in the energy of the beam on the last open field line at the light cylinder for the normal pulsars may be as small as $\Delta\gamma_{lc} = 100$. This vindicates our assumption of the chosen beam energy spread.

In the normal pulsars the cooling of the high energy beam is important for the $\gamma_0 \geq 2 \times 10^7$. In a millisecond pulsars it becomes important for the $\gamma_0 \geq 2 \times 10^6$. The cooling of the resonant particles increases growth rates of both cyclotron-Cherenkov and Cherenkov-drift instabilities. On the other hand, the kinetic approximation condition for the Cherenkov-drift instability may not be satisfied for a very small scatter in energy of the resonant particles. Unlike the cooling, the change in the average energy of the beam is normally not very important and is neglected.

Appendix K Instability on Ion Beam

In this Appendix we show that both cyclotron-Cherenkov and Cherenkov-drift instabilities do not develop on the ion beam.

If the relative orientation of rotational and magnetic axis is such that the electric field pulls up positive charges, then the primary beam may consist of ions. Since the energy of the curvature photon is independent of the mass of the particle, the critical Lorentz factor of the charge particles needed for the pair production is also independent of the mass of the particle. Ions will be accelerated to the same Lorentz factors as electrons $\gamma_b \approx 10^{6-7}$. It is possible that in approximately 50% of neutron stars the primary beam will consist of ions. In what follows, the ratio of ion and electron masses will be denoted as $\rho = m_i/m_e \approx 10^{3-4}$.

First we consider a cyclotron-Cherenkov instability on the ion beam. If the primary beam consists of ions, then the cyclotron-Cherenkov resonance at the given frequency occurs closer by a factor $\rho^{1/6} \approx 3$ (see F.4). This will increase the density of the resonant particles by ≈ 30, but the growth rate for the cyclotron-Cherenkov instability (F.5) is proportional to the squared plasma frequency of the resonant particles, which is inversely proportional to the mass of the particles. Taking into account that the condition of the kinetic instability is independent of the mass of the particle, we conclude that the cyclotron-Cherenkov instability on the ion beam does not develop due to the very small growth rate.

The growth rate of the Cherenkov-drift instability is proportional to ρ^{-3} (Eq. G.9), so the growth rate on the ion beam is many orders of magnitude smaller than the growth rate on the electron beam. Thus, we conclude that both cyclotron-Cherenkov and Cherenkov-drift instabilities do not develop on the ion beam. The pulsars with such a relative orientation of magnetic and rotational axis that the induced electric field accelerates ions can produce radio emission only at the cyclotron-Cherenkov instability on the tail particles.

Appendix L Calculation of the Radiation Reaction Force

In this Appendix we give the derivation of the expressions for the transverse and parallel parts of the work done by the radiation reaction force (Section 6.1.2, Eqs. (6.20)). We first simplify the Eq. (6.15) for the case of real polarization vectors:

$$\mathbf{f}_{RR} = -\frac{e^2}{2\,\pi^2}\sum_j \int_0^t dt' \int d\mathbf{k}\left[\frac{\mathbf{e}_j\,(\mathbf{v}'\cdot\mathbf{e}_j)}{n_j^2}\cos(\omega(t-t'))\cos(\mathbf{k}\cdot(\mathbf{R}-\mathbf{R}'))- i\,\frac{\mathbf{v}\times(\mathbf{k}\times\mathbf{e}_j)}{\omega}\sin(\omega(t-t'))\sin(\mathbf{k}\cdot(\mathbf{R}-\mathbf{R}'))\right], \tag{L.1}$$

where we used the relations

$$\begin{pmatrix} \cos(\mathbf{k}\cdot(\mathbf{R}-\mathbf{R}')) \\ \sin(\mathbf{k}\cdot(\mathbf{R}-\mathbf{R}')) \end{pmatrix} = \sum_{s,s'} J_s(\lambda)\,J_{s'}(\lambda) \begin{pmatrix} \cos\Psi_{s,s'} \\ \sin\Psi_{s,s'} \end{pmatrix} \tag{L.2}$$

The argument of the Bessel functions is $\lambda = (k\,\sin\theta\,R_\perp)$, θ is the angle of propagation with respect to magnetic field, and we introduced $\Psi_{s,s'} = (s\omega_H + k_\phi v_\phi)t - (s'\omega_H + k_\phi v_\phi)t'$. The velocity of the particle given by $\mathbf{v} = (v_\perp\cos(\omega_H\,t),\ v_\perp\,\sin(\omega_H\,t),\ v_\phi)$.

The polarization vector are: for extraordinary mode we have $\mathbf{e}^{(x)} = (0,\ 1,\ 0)$ and for the ordinary mode $\mathbf{e}^{(o)} = (\cos\theta,\ 0,\ -\sin\theta)$.

The integration over dt' may be performed using the relations

$$\begin{aligned} \int_0^t dt'\,\cos(\omega(t-t'))\,\cos(\Psi_{s,s'}(t,t'))\,) &= \pi\,\delta_{s,s'}\,\delta(\omega - s\,\omega_H - k_\phi\,v_\phi) \\ \int_0^t dt'\,\sin(\omega(t-t'))\,\sin(\Psi_{s,s'}(t,t'))\,) &= \pi\,\delta_{s,s'}\,\delta(\omega - s\,\omega_H - k_\phi\,v_\phi), \end{aligned} \tag{L.3}$$

Appendix M Calculations of the Resonant Integrals

The calculations presented in this Appendix are used in all the calculations of the kinetic growth rate of the instabilities.

$$\int dp_\phi v_\phi \frac{\partial f(p_\phi)}{\partial p_\phi} \delta(\hat{\omega}) = \frac{1}{k\cos\theta\, m_e} \left(v_\phi \gamma^3 \frac{\partial f(p_\phi)}{\partial p_\phi} \right)_{res} \tag{M.1}$$

$$\int dp_\phi \left(kv_\phi - \omega\cos\theta\right)^2 f(p_\phi)\delta\left(\omega' - \frac{\omega_B}{\gamma_b}\right) = \int dp_\phi \left(kv_\phi - \omega\cos\theta\right)^2 f(p_\phi) \frac{1}{\left| -\frac{kc\cos\theta}{m\gamma^3} + \frac{\omega_B p_\phi}{\gamma^3 mc} \right|} \delta(p_\phi - p_{res}) \tag{M.2}$$

For $\omega_B \gg kc$ this reduces to

$$\frac{\gamma^2\left(\omega\sin\theta^2 - \omega_B/\gamma\right)}{\omega_B v_\phi \cos^2\theta} f(p_\phi) \approx \left(\frac{\omega_B f(p_\phi)}{v_\phi \cos^2\theta} \right)_{res} \tag{M.3}$$

Similarly we have

$$\int dp_\phi (\omega - kv_\phi\cos\theta) f(p_\phi)\delta\left(\hat{\omega} - \frac{\omega_B}{\gamma_b}\right) = \left(\frac{\gamma f(p_\phi)}{v_\phi} \right)_{res} \tag{M.4}$$

and

$$\int dp_\phi (\omega - kv_\phi\cos\theta)^2 f(p_\phi)\delta\left(\hat{\omega} - \frac{\omega_B}{\gamma_b}\right) = \left(\frac{\omega_B f(p_\phi)}{v_\phi} \right)_{res} \tag{M.5}$$

Appendix N Phase Tracks of Particles Emitting Along Magnetic Field

In this Appendix we consider phase tracks of a single particle emitting electromagnetic waves along the magnetic field. We show that a resonant particle can lose up to half of its energy into radiation. This sets an upper limit on the effectiveness of the emission generation.

We assume that the initial transverse momentum is assumed to be zero. If there exists an initial strong wave that propagates along the magnetic field and interacts resonantly with the particle, then the emission of a single particle into this mode will be strongly amplified (by the large occupation number of the final states), so that the single particle emission into this mode will dominate over the spontaneous emission at other directions.

First we find integrals of motions. The two integrals of motion come from the following equations ($m = c = 1$ in this Appendix):

$$\Delta p_\phi = n\Delta\gamma \tag{N.1}$$

$$d(p_\perp^2) = (1 - n\beta_\phi)\, d(\gamma^2) \tag{N.2}$$

Eq.(N.1) is a consequence of the fact that the change of energy of the particle $\Delta\gamma = -\hbar\omega$ is related to the change of impulse along magnetic field $\Delta p_\phi = -\hbar\omega n$. Eq.(N.2) may be obtained by differentiating the relation

$$\gamma^2 = 1 + p_\phi^2 + p_\perp^2 \tag{N.3}$$

From Eq. (N.1) we find the first integral of motion

$$d\left(\gamma(n - \beta_\phi)\right) =, \qquad \gamma(n - \beta_\phi) = \gamma_0(n - \beta_{\phi,0}) \tag{N.4}$$

From Eq. (N.2) and using Eq. (N.4) we find the second integral of motion

$$\begin{aligned} &d\left(p_\perp^2 - \gamma^2(1 - n^2) - 2\gamma\gamma_0 n(n - \beta z, 0)\right) = 0 \\ &p_\perp^2 - p_{\perp,0}^2 = 2(\gamma - \gamma_0)\gamma_0 n(n - \beta_{\phi,0}) + (n^2 - 1)(\gamma_0^2 - \gamma^2) \end{aligned} \tag{N.5}$$

where we can use $p_{\perp,0} = 0$. Using Eqs. (N.3) and (N.5) we can parametrize the parallel momentum:

$$p_\parallel^2 - p_{\parallel,0}^2 = 2\gamma_0 n\beta_{z,0}(\gamma - \gamma_0) + (\gamma - \gamma_0)^2 n^2 \tag{N.6}$$

Eqs. (N.5) and (N.6) give a parametric dependence of $p_\perp$ and $p_\parallel$. Each phase track is specified by the choice of $\gamma_0 = 1/\sqrt{1-\beta z,0^2}$ and γ plays a role of a parameter along the phase curve.

From Eq. (N.5) we find that $p_\perp$ has a maximum at

$$\gamma^* = \frac{\gamma_0 n(n-\beta_{\phi,0})}{n^2-1}, \qquad p_\perp^* = \frac{\gamma_0(n\beta_{\phi,0}-1)}{\sqrt{n^2-1}} \tag{N.7}$$

This corresponds to the transition $n\beta_\phi = 1$. At this transition the pitch angle $\psi = p_\perp/p_\parallel = \sqrt{2\delta}$. For $\gamma > \gamma^*$ the parallel velocity of the particle is larger than the phase speed of the wave, so the particle emits waves (along the magnetic field) at the anomalous Doppler effect. For smaller Lorentz factors $\gamma < \gamma^*$ the parallel velocity of the particle is smaller than the phase speed of the wave, so the particle emits waves at the normal Doppler effect. Wave emission at the anomalous Doppler effect is accompanied by the increase in pitch angles, while wave emission at the normal Doppler effect is accompanied by the decrease in pitch angles.

Previous relations can be simplified if we take into account the $n = 1+\delta$ with $\delta \ll 1$ and assume that $\gamma_0^2 \gg 1/\delta$. Setting $\beta z, 0$ to unity we find then

$$\begin{aligned} p_\perp^2 &= (\gamma_0-\gamma)(n-1)\left(\gamma_0+\gamma-n(\gamma_0-\gamma)\right) \\ p_\parallel^2 &= \left(\gamma_0-n(\gamma_0-\gamma)\right)^2-1 \end{aligned} \tag{N.8}$$

(see Fig. (N.1)).

Next we simplified relations (N.8) and (N.7) by expanding in small $\delta = n-1$:

$$\begin{aligned} p_\perp^2 &= (\gamma_0-\gamma)\delta\left(2\gamma-\gamma_0\delta\right) \\ p_\parallel^2 &= \left(\gamma-\gamma_0\delta\right)^2-1 \\ \gamma^* &= \frac{\gamma_0}{2} \qquad p_\perp^* = \frac{\gamma_0\sqrt{\delta}}{\sqrt{2}} \end{aligned} \tag{N.9}$$

Eq. (N.9) implies that the beam cannot lose more than half of the initial energy into radiation. After losing half of the initial energy, the radiation reaction slows beam to the velocity lower than the phase velocity. If we introduce an effective parallel Lorentz factor

$$\gamma_\parallel^2 = \frac{1}{1-\beta_\parallel^2} = 1+\frac{p_\parallel^2}{\gamma_\perp^2} \tag{N.10}$$

then at the point when $\gamma = \gamma^*$ we have

$$\gamma_\parallel^* \approx \frac{1}{\sqrt{2\delta}} \tag{N.11}$$

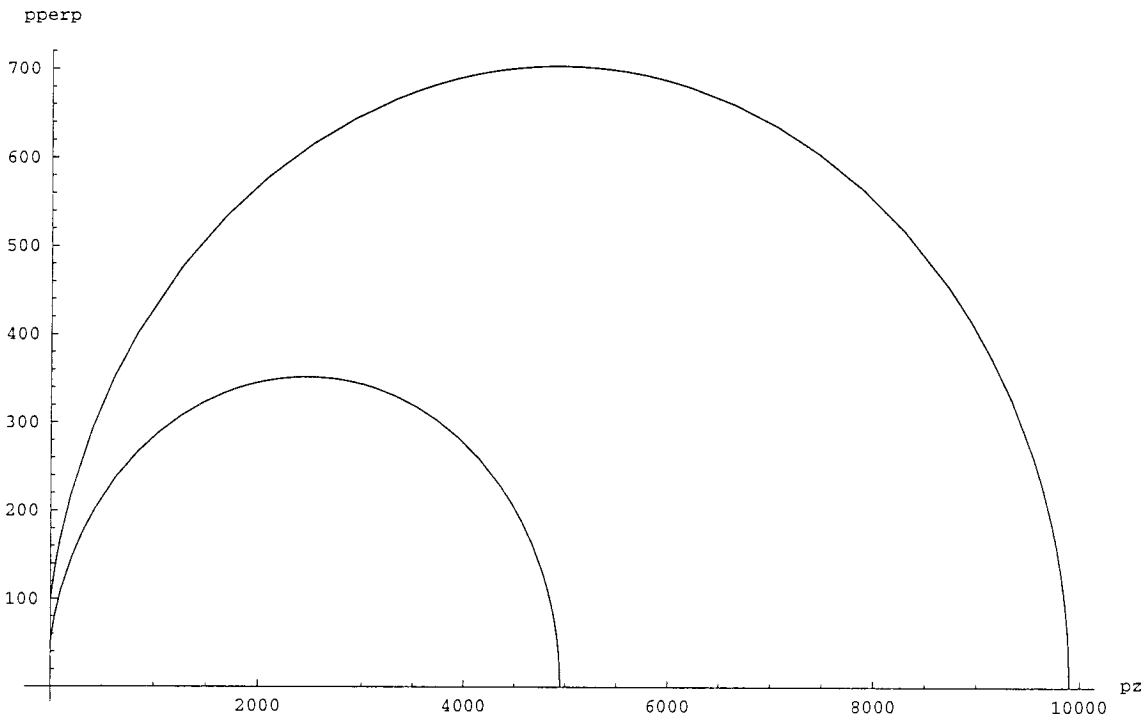

Figure N.1: Phase tracks of a resonant particle. The curves are shown for $\delta = 0.01$ and for two values of initial Lorentz factors: $\gamma_0 = 10^4$ and $\gamma_0 = 5 \times 10^3$. Initial transverse momentum is zero. The transverse momentum has maximum at $\gamma \approx \frac{\gamma_0}{2}$. For larger γ the particle emits waves at the anomalous Doppler effect which increases pitch angles, while for smaller γ the particle emits waves at the normal Doppler effect with decreasing pitch angles.

Relations (N.9) can be further simplified for $\gamma \gg \gamma_o\delta$:

$$\begin{aligned} p_\perp^2 &= 2\gamma(\gamma_0 - \gamma)\delta \\ p_\parallel^2 &= \gamma^2 - 1 - 2\gamma\gamma_0\delta \end{aligned} \tag{N.12}$$

So that the pitch angle is given by

$$\psi = \frac{p_\perp}{p_\parallel} \approx \sqrt{\frac{2\delta(\gamma_0 - \gamma)}{\gamma}} \tag{N.13}$$

REFERENCES

Ahalkatsi M. & Machabeli G. 1997, Plasm. Phys. Contr. Fus. (submitted)

Armstrong J.W., Rickett B.J. & Spangler S.R. 1995, ApJ, 443, 209

Arons J. 1981, ApJ, 248, 1099

Arons J. 1981b, in *Proc. Varenna Summ. School. & Workshop on Plas. Astr.*, ESA, p. 273

Arons J. 1983, ApJ, 266, 215

Arons J. & Barnard J.J. 1986, ApJ, 302, 120

Asseo E. 1995, Ann. NY Acad., 759, 261

Asseo E., Pellat R. & Sol H. 1983, ApJ, 266, 201

Asseo E., Pellat R. & Rosado M. 1980, ApJ, 239, 661

Asseo E., Pelletier G. & Sol H. 1990, MNRAS, 247, 529

Barnard J.J. & Arons J. 1986, ApJ, 302, 138

Barnes A. 1966, Phys. Fluids, 9, 1483

Batygin V.V. & Toptygin I.N. 1964, *Problems in Electrodynamics*, Academic Press, London

Berezhiani V.I., Tsintsadge L.N., Shukla P.K. 1992, J. Plasma Phys., **48**, 139

Benford G., Bushauer R. 1977, MNRAS, 190, 945

Beskin V.S., Gurevich A.V. & Istomin Y.N., 1983, Sov. Phys. JETF, 85, 234

Beskin V.S., Gurevich A.V. & Istomin Y.N., 1986, Astrophys. Space Sci., 146, 205

Beskin V.S., Gurevich A.V. & Istomin Y.N., 1993, *Physics of the pulsar magnetosphere*, Cambridge University Press

Blandford R.D. 1975, MNRAS, 170, 551

Blandford R.D. & Scharlemann E.T. 1976, MNRAS, 174, 59

Brodin G. & Stenflo L. 1989 J. Plasma Phys., 42, 187

Budden K. G., *The propagation of radio waves : the theory of radio waves of low power in the ionosphere and magnetosphere*, Cambridge University Press, 1985

Bushauer R. & Benford G. 1977, MANRAS, 179, 99

Case W.B. et al. 1984, J.Appl.Phys., 55, 2651

Cheng A.F. & Ruderman M.A., ApJ, 212, 800

Cheng K.S., Ho C., Ruderman M. 1986a, ApJ, 300, 500

Cheng K.S., Ho C., Ruderman M. 1986b, ApJ, 300, 522

Chian A.C.-L. & Kennel, C.F., 1983, Astroph. Space Sci., **97**, 9

Chugunov Y.V. & Shaposhnikov V.E. 1988, Astrophysika, 28, 98

Clemmow P.C. & Dougherty J.P. 1969, *Electrodynamics of Particles and Plasmas*, Addisson-Wesley Inc.

Cognard I., Shrauner J.A., Taylor J.H. &Thorsett S.E. 1996, ApJ lett., 457 (2), L81

Cordes J.M. 1981, in IAU Symposium No.95, ed. by Sieber W. and Wielebinski R., Reidel Publ., Dordrecht, 115

Cordes J.M. et al. 1990, ApJ, 349, 245

Daugherty J.K. & Harding A.K. 1983, ApJ, 273, 761

Daugherty J.K. & Harding A.K. 1996, ApJ, 458 , 278

Deich et al. 1986, ApJ 300, 540

Didenko A.N. et al. 1983, Sov. Tech. Phys. Lett., 9, 572

Dunn D.A. 1971, *Models of Particle and Moving Media*, Academic Press, NY

Egorenkov et al. 1983, Astrophysika, 19, 753

Galuzo S.Y. et al. 1982, Sov. Phys. -Tech. Phys., 52, 1681

Gedalin M.E. & Machabeli G.Z 1982, Sov. Astr. L. 8, 80

Gedalin M.E. & Machabeli G.Z 1983, Sov. J. Plas. Phys., 9, 592

Gil J.A. & Kijak J 1993, A&A, 273, 563

Ginzburg V.L. & Eidman V.Ya. 1959, Sov. Phys. JETPh, 36, 1300

Godfrey B.B. et al. 1974, IEEE Trns. Plas. Sci., v. PS-3(2), 60

Godfrey B.B. et al. 1974, IEEE Trns. Plas. Sci., v. PS-3(2), 68

Godfrey B.B. et al. 1975, Phys.Fluids, 18, 346

Goldreich P. & Keeley D.A. 1971, ApJ, 170, 463

Gradshtein I. S. & Ryzhik I.M., *Table of integrals, series, and products*, New York : Academic Press

Gurvits L.I. et al. 1987, Aust. J. Phys.,40, 847

Gwinn et al. 1997, ApJ, 483, L53

Hansen B. 1997, Ph.D. Thesis

Harding A.K., Ozernoy L.M. & Usov V.V. 1993, MNRAS, 265, 921

Harrison E.R. & Tademaru E. 1975, ApJ, 201, 447

Hewish et al. 1992. *Pulsars as Physics Laboratories*, Phil. Trans. Roy. Ast. Soc., 341, p. 1-192

Hinata S. 1976, ApJ, 203, 223

Jenet F.A. et al. 1997, Pub. Ast. Soc. Pac., 109, 707

Jenet R. & Prince T. 1997, private communication

Karpman V. & Krushkal E. 1969, Sov. Phys. JETP, 28, 277

Kates R.E. & Kaup D.J. 1992, J. Plas. Phys. **48**, 397, and reference therein.

Kazbegi A.Z. et al. 1991a, Astrophysika, 34, 433

Kazbegi A.Z., Machabeli G.Z. & Melikidze G.I 1991b, MNRAS, 253, 377

Kazbegi A.Z., Machabeli G.Z. & Melikidze G.I 1991c, Aust-J-Phys, 44, 573

Kazbegi et al. 1996, Astron. Asrophys., 309, 515

Kho T.H. & Lin A.T. 1983, Phys. Rev. A, 38, 2883

Kawamura K. & Suzuki I. 1977, ApJ, 217, 832

Kramer M. et al. 1996, A&A, 306, 867

Krishan V. 1997, Space Sci. Rev., 80, 445

Hardee P. & Rose W. 1978, ApJ, 219, 274

Landau L. D. & Lifshitz E.M. 1951, *The classical theory of fields*, Cambridge, Mass., Addison-Wesley Press

Landau L. D. & Lifshitz E.M. 1975, *Electrodynamic of Continuous Media*, Pergamon

Levinson A. & Blandford R. 1995, MNRAS, 274, 717

Litvak A.G. & Sergeev A.M., Letters to JEPT, 27, 549

Larroche O. & Pellat R. 1988, Phys. Rev. L., 61, 650

Lominadze J.G., Machabeli G.Z. & Mikhailovsky A.B. 1979, Sov. J. Plasma Phys., 5, 748

Lominadze J.G., Machabeli G.Z. & Usov V.V. 1983, Astroph.Space Sci., 90, 19

Lominadze J.G. & Mikhailovskii A.B. 1978, Sov. Phys. JETP, 49, 483

Lominadze J.G., Mikhailovsky A.B. & Sagdeev R.Z. 1979, Sov. Phys. JETP, 50(5), 927

Lorimer D.R. et al. 1995, MNRAS, 273, 411

Luo Q.H., Melrose D.B. & Machabeli G.Z. 1994, MNRAS, 268, 159

Luo Q.H. & Melrose D.B. 1992, MNRAS, 258, 616

Luo Q.H. & Melrose D.B. 1992, P.Ast.Soc.Aust., 10, 45

Lyubarskii Yu.E. 1993, Sov. Astron. Lett. 19, 208

Lyutikov M. 1997, accepted by MNRAS

Lyutikov M. 1997, Caltech preprint GRP-459

Lyutikov M. 1997, *Streaming instabilities in pulsar magnetosphere*, in progress

Lyutikov M. 1997, *Nonlinear processes in pair plasma and pulsar spectrum formation*, in progress

Lyutikov M., Blandford R.D. & Machabeli G.Z. 1997, in progress

Lyutikov M. & Machabeli G.Z. 1997, *Wave propagation in pulsar magnetosphere*, in preparation.

Lyutikov M. & Machabeli G.Z. 1997a, *Cherenkov-drift emission mechanism* , in preparation.

Lyutikov M. & Machabeli G.Z. 1997b, *Curvature-Cherenkov Radiation and Pulsar Radio Emission Generation*, in preparation.

Lyne A.G. & Ashworth M. 1983, MNRAS, 204, 519

Lyne A.G. & Manchester R.N. 1988 MNRAS, 234, 477

Malofeev V.M. 1996, in *Pulsar: Problems and Progress*, IAU Colloquium 160, eds. Johnston S., Walker M.A., Bailes M., p. 271

Mamradze P.G., Machabeli G.Z. & Melikidze G.I. 1980, Sov. J. Plasma Phys., 6, 707

Machabeli G.Z. 1983, Sov. Astron. 63, 411

Machabeli G.Z. 1995, Plasm. Phys., 37, 177

Machabeli G.Z. & Usov V.V. 1979, Sov. Astron. Lett., 5, 445

Machabeli G.Z. & Usov V.V. 1989, Sov. Astron. Lett., 15 , 393

Manchester R.N. 1996, *Pulsar: Problems and Progress*, IAU Colloquium 160, eds. Johnston S., Walker M.A., Bailes M., 193

Markwardt C.B. & Ogelman H. 1995, Nature, 375, 40

Max, C.E., Arons, J., Langdon, A.B. 1974, Phys. Rev. lett., **33**, 209

Melikidze G. 1997, in *Pacific Rim Conference on Stellar Astrophysics*, in press

Melikidze G., Pataraya A., Tsikarishvili E., Chagelishvili G. 1981, in *Intern. Conf. on Phen. in Ionized Gases*, Minsk, USSR, v. 1, 227

Melrose D.B. 1978, ApJ, 285, 577

Melrose D.B. 1978b, Aph. J., 225, 557

Melrose D.B. 1978c, *Plasma astrophysics: nonthermal processes in diffuse magnetized plasmas*, New York, Gordon and Breach

Melrose D.B. 1982, Aust. J. Phys., 35, 41

Melrose D.B. 1986, *Instabilities in space and laboratory plasmas*, Cambridge University Press

Melrose D.B. 1995, J. Astroph. Astron., 16, 137

Michel F.C. 1991, *Theory of Neutron Star Magnetosphere*, Univ. Chicago Press

Mikhailovskii A. B. 1974, *Theory of plasma instabilities*, New York, Consultants Bureau

Mikhailovski A.B. 1980, Sov. J. Plasma Phys., 6, 366

Mikhailovskii A.B. et al. 1982, Sov. Astron. Lettl 8, 369

Mikhailovskii A.B., Onischenko O.G., Tatarinov E.G. 1985, Plasma Phys. Contr. Fus. 27(5), 527

Morse P.M. & Feshbach H. 1953, *Methods of theoretical physics*, New York, McGraw-Hill

Muslimov A. & Harding A.K. 1997, ApJ, 485, 735

Nambu M. 1989, Plas.Phys.Contr. Fusion., 31, 143

Nusinovich G.S. et al. 1995, Phys. Rev. E., 52, 998

Ochelkov Y.P. & Usov V.V 1983, Asroph. Space Sci, 96, 55

Pataraya A. & Melikidze G. 1980, Astr. Space Sci., 68, 61

Rankin J.M. 1992, IAU Colloq. 128, *The magnetospheric Structure and Emission mechanisms of Radio Pulsars*, ed. T.H. Hankins, J.M. Rankin, J.A. Gill (Zelona Gora, Poland, Pedagog. Univ. Press), p. 133

Rao N.N., Shukla P.K. & Yu M.Y. 1984, Phys. Fluid. bf 27 (11), 2664

Rickett B.J. 1975, Ap.J., 197,185

Rizzato F.B. 1988, J. Plasma Phys., 40, 289

Romani R.W. 1996, ApJ, 470, 469

Romani R.W. & Yadigaroglu I.A. 1995, aj, 438, 314

Ruderman M.A & Satherland P.G. 1975, ApJ, 196, 51

Sakai J. & Kawata 1980, J. Phys. Soc. Japan, 49, 753

Schwinger J. 1976, Ann. Phys., 96, 303

Shukla P.K., Rao N.N., Anderson D., Lisak M., Wilhemsson H. 1985, Phys. Fluids, 28, 1112

Silin V.P. 1960, Sov. Phys. JETP, 11,1136

Sincell M.W. & Krolik J.H. 1992, ApJ, 395, 553

Soglasnov V.A., Popov M.V. & Kuz'min A.D. 1983, Sov. Astron., 27(2), 169

Sokolov A.A. & Ternov I.M. 1968, *Synchrotron radiation*, Pergamon Press, (1968).

Stenflo L., Shukla P.K., Yu M.Y. 1985, Asotph. Space Sci., 117

Stinebring et al. 1984, ApJ, 55, 247 ?????

Strohmayer et al. 1992, ApJ, 389, 685

Sturner S.J. & Dermer C.D. 1994, ApJ, 420, L79

Sturrock P.A. 1960, J. Appl. Phys., 31, 2052

Suvorov E.V. & Chugunov Yu.V. 1975, Astrophysika, 11, 305

Tademaru E. 1973, ApJ, 183, 625

Tai C-t. 1994, *Dyadic Green functions in electromagnetic theory*, IEEE Press

Taylor J.H. 1994, Rev. Mod. Phys., 66, 711

Thorsett S.E. 1992, IAU Colloq. 128, The magnetospheric Structure and Emission mechanisms of Radio Pulsars, ed. T.H. Hankins, J.M. Rankin, J.A. Gill (Zelona Gora, Poland, Pedagog. Univ. Press), p. 143

Tsytovich V. N. 1970, *Nonlinear effects in plasma* , New York, Plenum Press

Tsytovich V.N. & Kaplan S.A. 1972, Astrophysika, 8,411

Tsytovich V.N. & Shvartsburg A.B. 1965, Zh. Eksp. Teor. Phys. 49, 797; Sov. Phys. JETP 22, 554 (1966)

Usov V.V. 1996, in *Pulsar: Problems and Progress*, IAU Colloquium 160, eds. Johnston S., Walker M.A., Bailes M., p. 323

Volokitin A.S., Krasnosel'skikh V.V. & Machabeli G.Z. 1985, Sov. J. Plasma Phys., 11, 310

Weatherall J.C. 1994, ApJ, 428, 261

Weibel E. 1959, Phys. Rev. Lett., 2, 83

Wilson D.B. 1982, MNRAS, 200, 881

Wolszczan A. 1996, IAU Symposia 165, 187

Yadigaroglu I.A. & Romani R.W. 1995, aj, 449, 211

Yadigaroglu I.A. 1997, Ph.D. Thesis

Zheleznyakov V.V. & Shaposhnikov V.E. 1979, Aust. J. Phys., 32, 49

Zhuravlev V.I. & Popov M.V. 1990, Astronom. Zh., 67, 748